UNIVERSITY OF LEEDS

Insights into the molecular basis underlying cancer cell sensitivity to Polybia MP1 peptides

Dagmara Kobza

Submitted in accordance with the requirements for the degree of Doctor of Philosophy

September 2023

School of Chemistry

Faculty of Mathematics and Physical Sciences

University of Leeds

Supervisor: Professor Paul A. Beales

Co-supervisor: Professor Thomas A. Hughes

I confirm that the work submitted is my own and that appropriate credit has been given where reference has been made to the work of others.

Acknowledgements

"The only limits in your life are those that you set yourself" – Celestine Chua

My PhD adventure was a long journey, full of ups and downs, at which I met many people whose help, advice and support are invaluable. I would like to express my sincere gratitude to my supervisor Professor Paul A. Beales and co-supervisor Dr Thomas A. Hughes for giving me the opportunity to learn and acquire knowledge and experience in their laboratories. A million thanks for the patience, guidance and time spent with me to overcome the challenging obstacles I have encountered during my research.

I am very grateful to the University of Leeds (UoL) for the chance to undertake the doctoral degree and for awarding a Postgraduate Research Scholarship for the duration of my studies. I appreciate the support of the School of Chemistry, the School of Medicine and the Faculty of Biological Sciences at the University of Leeds for the provided resources. Special thanks to Dr Milene Volpato, Dr Arindam Pramanik, Dr Rashmi Seneviratne and Dr Marcos Arribas Perez for their support and assistance in my research work. Many thanks to Dr Andrew Booth and Dr Dede Siregar for their mentoring and support with high-throughput leakage assay. My sincerest gratitude to all lab members of the Beales and Hughes research groups for creating a positive environment. I am thankful to Prof. Thomas A. Hughes and Dr Nicola Ingram for providing cell lines for my research purpose.

I would like also to thank my family, friends and many people I met in the UK for their support and kind words.

The thesis was proof-read before submission by a third-party proof-reader. The PGR confirms that the third-party proof-reading undertaken was in accordance with the Postgraduate Researcher Proof-reading Policy.

I dedicate this thesis with love to my son Marcel,

my motivation and inspiration!

Abstract

During the past few decades, research has focused on antimicrobial peptides (AMPs) having a dual nature; they not only have bactericidal properties but may also target cancer cells. It has been proven that the mechanism of cationic AMPs is initiated by their electrostatic interaction with negatively charged membrane lipids [1]. Of note, tumour cell lipid composition differs from the non-transformed cell profile [2]. Therefore, AMPs seem to be prospective candidates to target cancer cells.

This project aimed at elucidating the structure-function relationship of the peptide Polybia-MP1 in its anticancer activity. MP1 mechanism of action underwent detailed mechanistic characterisation by applying rationally designed MP1 derivatives in systems of increasing complexity using biophysical and biological approaches. The presented work provides insights into the molecular basis underlying cell sensitivity to MP1. Chemical modifications of native structure allowed for determining amino acid residues important in MP1 activity and for identifying derivatives that displayed greater potency against cancer-like systems Testing the peptide library emphasized the interplay between charge modification, physiochemical characteristics of each residue and hydrophilic: hydrophobic face arrangement in modulating potency and specificity. GPMV formation, live cell-derived membrane platforms, although challenging and requiring optimization, facilitated studies of lipid organization indicating that variable lipid packing is a molecular determinant modulating MP1 phenomenon. Despite *in silico* transcriptomic analysis identifying prospective gene targets that might be influencing cell sensitivity to MP1, further cell viability testing failed to uncover potential molecular mechanisms. This work provides a novel insight into the role of lipid packing in the membranolytic activity of MP1 and paves new directions in the structure-function exploration of MP1.

Abbreviations

Antimicrobial peptides (AMPs) 32
Arginine (Arg) 73
Asparagine (Asn) 70
Aspartic acid (Asp) 69
Bovine serum albumin (BSA) 114
Carboxyfluorescein (CF) 85
Cardiolipin (CL) 41
Cascade blue (CB) 118
Cholesterol (Chol) 39
Critical micelle concentration (CMC) 46
Dendritic cells (DCs) 65
Diabetic foot ulcer (DFU) 65
Dioleoylphosphatidylserine (DOPS) 83
Dipalmitoylphosphatidylcholine (DOPC) 83
D-thiothreitol (DTT) 56
False discovery rate (FDR) 188
Fatty acids (FAs) 38
Fluorescein isothiocyanate (FITC) 118
General Polarization (GP) 151
Giant plasma membrane vesicles (GPMVs) 33
Giant unilamellar vesicles (GUV) 55
Glycine (Gly) 73
Glycolipids (GL) 39
Glycosphingolipids (GSL) 50
Histidine (His) 73
Host defence peptides (HDP) 65
Large unilamellar vesicles (LUV) 54
Lipopolysaccharides (LPS) 66
Lysine (Lys) 73
Multi lamellar vesicles (MLV) 54
Multiple sclerosis (MS) 65
N-ethylmaleimide (NEM) 130
Packing parameter (P) 46
Paraformaldehyde (PFA) 56
Phenylalanine (Phe) 80
Phosphocholine (PC) 39
Phosphoethanolamine (PE) 39
Phosphoglycerol (PG) 41
Phosphoinositol (PI) 41
Phosphoserine (PS) 39
Plasma membrane (PM) 41
Rheumatoid arthritis (RA) 65
Sjögren's disease (SjS) 65
Small unilamellar vesicles (SUV) 55
Sphingolipids (Sph) 41
Sphingomyelin (SM) 39
Systemic lupus erythematosus (SLE) 65
Transition temperature (Tc) 54

Contents

List of figures

List of tables

Introduction and outline

According to the World Health Organization (WHO), cancer is a leading cause of death globally, accounting for nearly 10 million deaths in 2020, signifying a need for alternatives to conventional medicine. Antimicrobial peptides (AMPs) showed a remarkable microbicidal potency and *in vitro* studies reported even anti-cancer activity against certain types of cells [3–7]. However, the mechanism of action is still not clear enough and only a few AMPs have been approved for medical treatment. This thesis focuses on investigating molecular basics underlying the membranolytic activity of Polybia MP1 and developing strategies aiming at improving cancer specificity. Due to the complexity of cell membranes, MP1 activity was tested in membrane models of increasing membrane organization. Further, the cell-derived system was optimized to study the role of lipid arrangement in cell-specific MP1 membrane lysis. These findings provide significant insight into the foundation of the MP1 mode of action and show great promise for further *in vivo* testing.

This thesis work demonstrates a systemic way to uncover the molecular basics of the membranolytic activity of Polybia MP1. It contains 5 chapters (see Figure 1 for the thesis workflow).

- The theoretical background is allocated in Chapter I. Chapter I introduces membrane science, briefly presenting the history of membrane discovery, and presents key aspects of physiochemical membrane characterisation, the concept of raft domains, and common techniques to visualise and study membrane behaviour. This part is followed, by the introduction to antimicrobial peptides showing their structural and functional diversity, classification, suspected mechanism of action and current application. This part ends with the main aims and objectives to be addressed in this thesis. The

following chapters focus on elucidating the molecular basis of the lytic activity of Polybia MP1 by the investigation of membrane models of increasing complexity;

- Chapter II attempts to identify structural determinants key to the biological relevance of MP1 and presents potent MP1 variants with higher specificity to transformed cells.
- Continuing, Chapter III demonstrates attempts for optimization protocols to produce giant plasma membrane vesicles (GPMVs), an intermediate membrane system between fully synthetic membranes and living cell membranes;
- In the following Chapter IV, GPMVs are introduced to investigate the cell membrane penetration of amphiphilic MP1 and the effect of membrane ordering by using fluorescent lipid analogues. Although membrane heterogeneity is key in the membranolytic activity of MP1, it might not be the only determinant at the molecular level driving peptide potency;
- Chapter V discusses other potential regulators of the MP1 mechanism of action that are beyond lipid organization;
- The last part summarizes the conclusions from this study and suggests further research directions in this field.

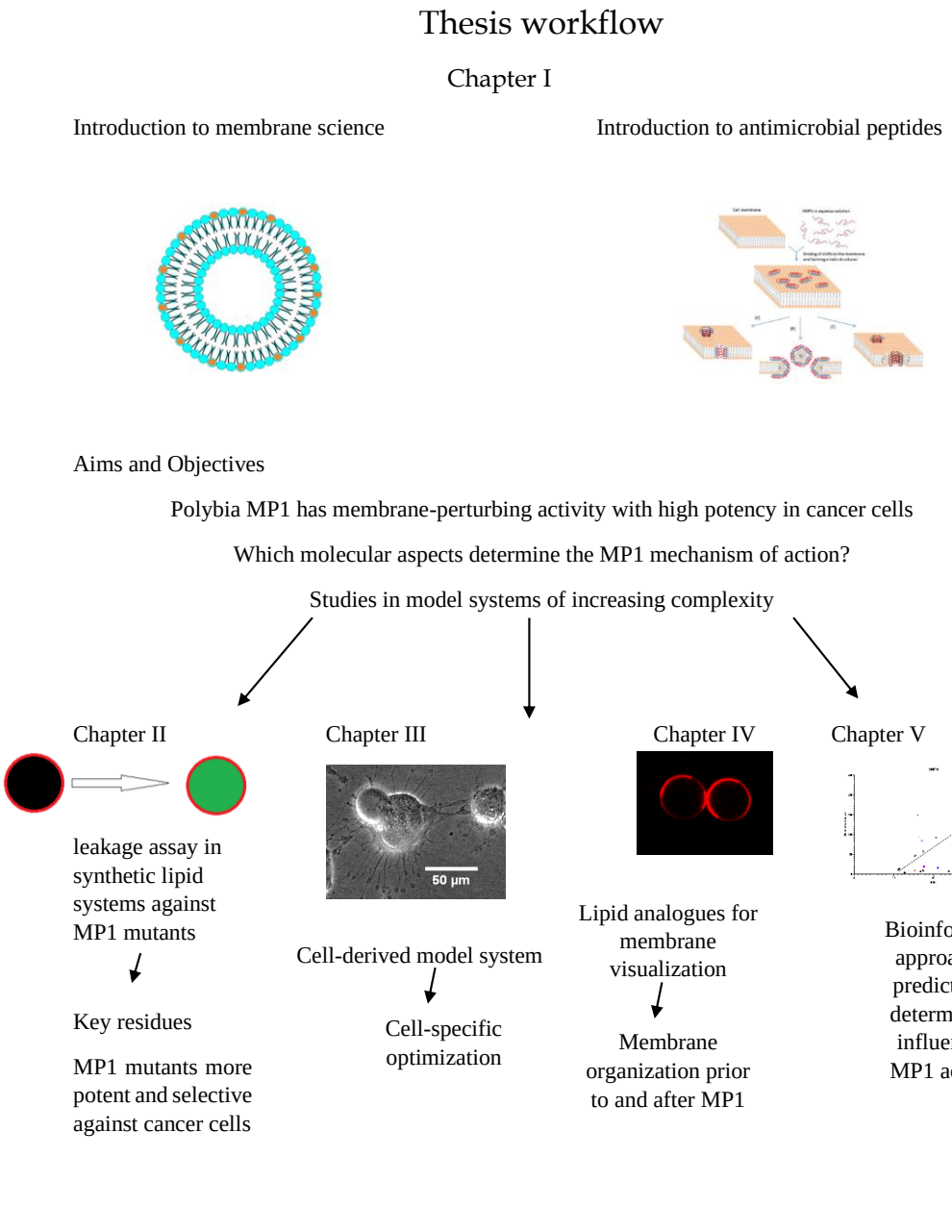

Figure 1 Thesis at a glance.

Chapter 1

Theoretical Background

Chapter 1 Theoretical background

1. Introduction to biological membranes

Most of living systems are delineated by biological membrane and its structural integrity is fundamental for cell viability and function [8]. Membranes not only define the boundary from the external environment but also construct intracellular organelles in more complex eukaryotic cells allowing spatial separation of biological processes [9]. Therefore, membranes give a shape, participate in signal transduction, store and transmit energy, provide recognition and permit cell-to-cell adhesion [10]. The unceasing progress of science allowed for a profound and extensive comprehension of cell membranes.

1.1 The importance of biological membranes: Lipid raft hypothesis.

The development of modern bio-imaging approaches has revolutionised our insight and knowledge of biological membranes from the initial model of Singer and Nicholson [11].

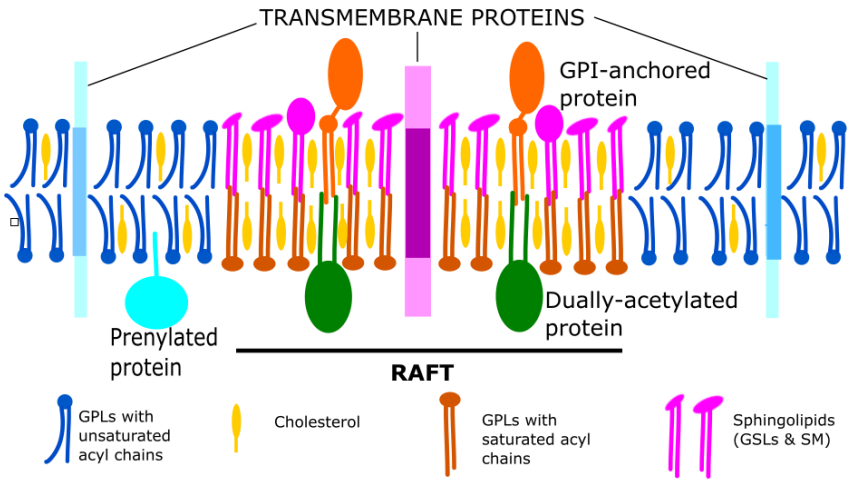

Figure 2 A simplified model of lipid rafts in cell membranes. The phospholipids (dark blue and brown) and cholesterol (yellow) are positioned in both leaflets, while

sphingolipids (purple) are exposed to the exoplasmic layer. The acyl tails of raft lipids are generally long and saturated (purple and brown) in contrast to those in non-raft domains, which are shorter and unsaturated (blue). Raft domains contain dually-acylated (green) and GPI-anchored (brown) proteins, whereas transmembrane (blue) and prenylated (green) proteins are usually non-raft-associated. Taken and modified from [12].

The hypothesis of lipid rafts emerged at the end of the 20th century proposed by Simons and Ikonen [13]. Exploring more and more functions of biological membranes, it became apparent that lipid distribution on the plasma membrane is not random and might be regulated by biophysical processes. According to Figure 2, the plasma membrane is envisaged as “a sea” of fluid-disordered phase lipids formed mainly from unsaturated lipids containing ordered microdomains enriched in saturated sphingolipids and cholesterol [14]. Raft phases are thicker and more tightly packed due to a higher degree of conformational order of acyl tails imposed by the presence of the rigid ring structure of cholesterol. Liquid-phase lipids retain lateral mobility. Furthermore, it has been suggested that these structures can bind proteins and control their mobility, functionality and localization [15].

For years the existence of lipid-mediated domains remained controversial as they couldn’t be visualised in cell membranes. The breakthrough came in the early 2000s when phase segregation was observed in membrane models derived from living cells [16]. The approximated native membrane environment and capacity of forming coexisting liquid domains render giant vesicles a decent tool to provide complementary insight into the bio-membrane organization, their physical properties and phase-mediated protein and lipid function. However, the shortcomings of giant spheres should be stressed; they only contain native cell membrane composition to some extent; their induction may result in chemical modifications of membrane

components; they lack cortical actin cytoskeleton, which provides mechanical support to a cell; they lose partially leaflet asymmetry; the extracted membrane is in the state of thermodynamic equilibrium [17]. Even though the observed phenomenon is undeniable, the raft phase seen at non-physiological conditions in giant spheres could not be taken as an equivalence to the nanoscopic dynamic organization postulated in live cells [18].

1.2 Lipid components in the membranes

Lipids have a plethora of biological roles, they are not only membrane bilayer components but also their functions include: energy source, matrix for many catalytic processes, energy transduction, hormone, vitamins, antioxidant and signal molecules [19].

As lipids exhibit a wide diversity of biological functions, only the human body may contain about 1000 major lipid species [20]. With so many different biomolecules, three major types of lipids found in bio-membranes are phospholipids, glycolipids and sterols. Variations in membrane lipid composition (possessing a range of hydrocarbon chain lengths and polar head groups) are significant factors distinguishing tissue type, cell function or progression in physiological processes. Fatty acids (FAs) are the principal building blocks of complex membrane lipids. The most abundant FAs found in mammalian membranes are (fatty acid chains are described in the format -number of carbons in the fatty acid chain: number of double bonds in the fatty acid chain): palmitic (16:0), stearic (18:0), palmitoleic (16:1), oleic (18:1), linoleic (18:2), arachidonic (20:4) and docosahexaenoic (22:6). In addition, the presence of double bonds, primarily in *cis* form, their number and location on lipid

hydrocarbon chain affect structural and dynamic properties of biological membranes [21]. Figure 3 presents common lipid membrane compositions of different origins.

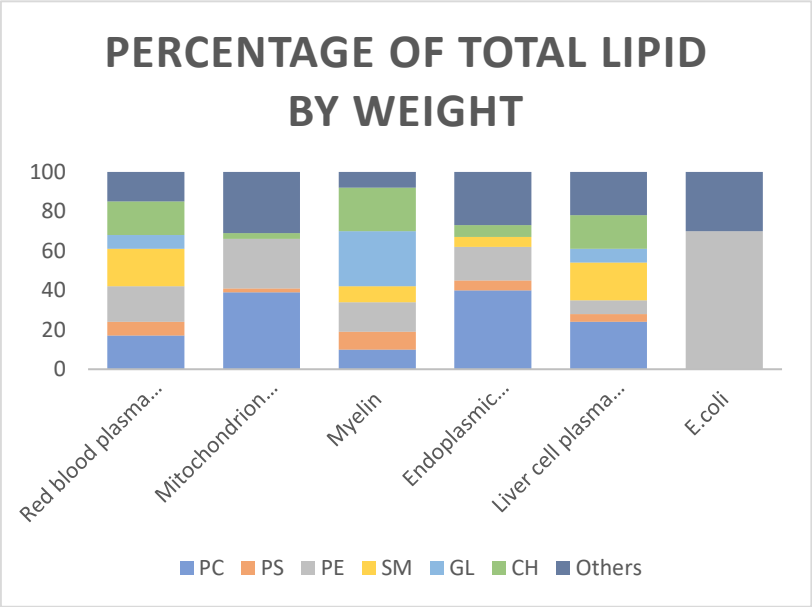

Figure 3 Membrane composition of different origins demonstrated in percentage; (PC- phosphocholine; PS- phosphoserine; PE- phosphoethanolamine; SM- sphingomyelin; GL- glycolipids; CH- cholesterol). Taken and modified from [9].

Phospholipids are the key compounds of cell membranes. Figure 4 depicts the generic chemical structure of phospholipids, defined also as glycerophospholipids. Two fatty acid tails join a negative phosphate residue by an alcohol moiety (usually a glycerol molecule)[20]. The phosphate group can be further coupled to simple organic molecules such as choline, ethanolamine, serine, inositol or glycerol. Most membrane phospholipids have an ester linkage (O-(C=O)-R, where R stands for the acyl chain, to glycerol. Esther lipids, a unique lipid family for *Archean* and individual mammalian cells, are ether-bounded (O-C-O-R) linking sidechains to the glycerol moieties.

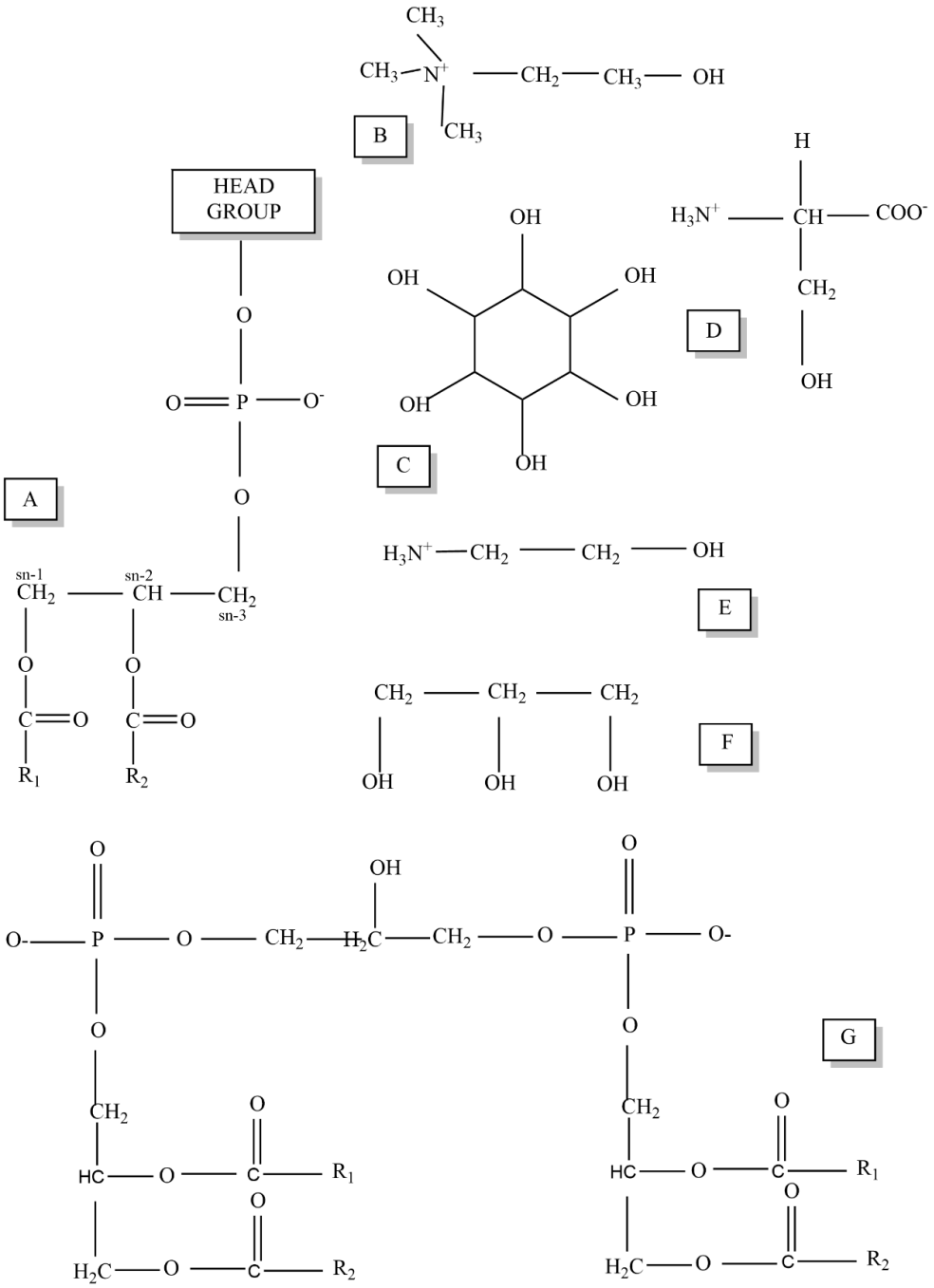

Figure 4 Chemical structure of a phospholipid with three carbons named sn-1, sn-2 and sn-3 (A). Diverse head groups can be placed at the phosphate group at the sn-3 position: choline in phosphatidylcholine (B), inositol in phosphatidylinositol (C), serine in phosphatidylserine (D), ethanolamine in phosphatidylethanolamine (E) and glycerol in phosphatidylgycerol (F). Cardiolipin is a unique phospholipid with four acyl tails (G). R1, R2 = hydrocarbon chain [19]. Drawn using ChemDraw (Revvity Signals Software, Inc. 2024).

The terminology of phospholipids stems from the polar head groups. They vary from no net charge to anions [20]. Phosphocholine (PC) and phosphoethanolamine (PE) are zwitterionic at physiological pH and phosphoserine (PS), phosphoinositol (PI) or phosphoglycerol (PG) are negatively charged and their chemical structure is seen in Figure 4. Phospholipids with a net positive charge do not occur in nature. PCs are found abundant among eukaryotes, where they play a crucial role in bilayer organization due to the propensity to adapt lamellar phase. PEs are characterized both to bacterial membranes (Gram-positive and Gram-negative bacteria) and mammalian plasma membrane (PM). A relatively small head group favours the hexagonal structure of PEs which classifies those components as membrane destabilizers. Negative-charged PS is not evenly distributed across the inner and outer leaflets of the lipid bilayer and is implicated in cell physiology. Disruption in PS organization and its excess exposure in the cytoplasmic leaflet are the hallmarks of membrane transformation in tumorigenesis [22]. A unique phospholipid, cardiolipin (CL), has a dimeric structure with four acyl tails and two phosphatidyl moieties linked to the glycerol [23]. Found abundant in the inner mitochondrial membrane, cone-shaped molecules that introduce curvature stress in the bilayer membrane [24].

A large group of membrane lipids are sphingolipids (also termed sphingosine units [25]. The exclusive feature of sphingolipids (Sph) is an amide linkage of the hydrocarbon tails to the lipid headgroup. Contrary to phospholipids, some may not contain the phosphate moiety. Sphingomyelin (SM), the leading representative of sphingolipids, is predominantly found in the nervous system particularly in the myelin sheath surrounding nerve cell axons [26]. Interestingly, Sph is recurrently co-localised with cholesterol in lipid rafts. A higher melting point of Sphs than body temperature extends the lipid bilayer rigidity [27].

Another class of membrane lipids present in biological membranes is a glycolipid [19]. Similarly to sphingomyelin, it is derived from sphingosine but also contains one or more sugar residues attached by a glycosidic bond. Cerebrosides have a single sugar as its headgroup such as galactose, which is found in the plasma membrane of neuronal cells, while those with glucose are present in the plasma membrane of non-neuronal cells [28]. Globosides have two or more sugars [20]. Gangliosides are oligosaccharides with at least one unusual anionic sugar-sialic acid [29]. Carbohydrate residues are always on the extracellular side of the membrane, which facilitates cellular recognition essential in cell-cell interactions and immune response. The affinity of water molecules to the sugar residues maintains a hydration layer close to the membrane interface. However, some sugar moieties are linked with cancer progression and function as binding sites for some types of viruses (influenza, HIV) [30]. Gangliosides are functional components of lipid rafts that regulate cell communication [31] .

The last major components of membrane lipids are sterols, found in animal, plant and fungal membranes [32]. In mammals, the most abundant sterol is cholesterol (Chol), fungal analogue is ergosterol and plant sterols are presented by β-sitosterol. One-quarter of total cholesterol in vertebrates populates in the brain and 50% of the animal plasma membrane is often composed of cholesterol [20]. However, Chol is not only an abundant structural component of the plasma membrane but also is a precursor for other bioactive molecules (vitamin D, all steroid hormones and bile salts). Chol due to

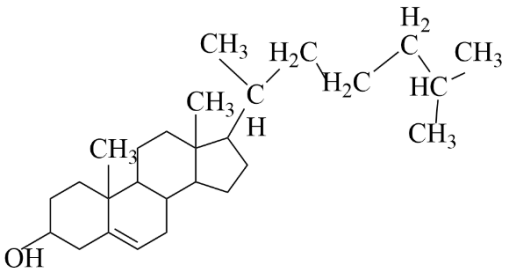

Figure 5 Chemical structure of cholesterol. Drawn using ChemDraw (Revvity Signals Software, Inc. 2024).

its distinct steroidal planar structure, does not assemble into bilayers. Rather, its steroid core aligns with the hydrophobic acyl chains and the hydrophilic hydroxyl group is exposed to the membrane interface. The planar steroid ring structure interacts through non-covalent van der Waals interaction with the hydrophobic sidechains of phospholipids having a significant effect on membrane fluidity (see Fig.5). This affinity provides mechanical strength, controls phase behaviour and supports membrane lateral organization. Overall, the greater Chol content within the lipid bilayer results in a lipid phase transformation from less condensed liquid-disordered state into the more compressed liquid-ordered lipid phase. Conversely, it has been observed that Chol incorporation into lipid gel phase, common in biological systems, increases membrane fluidity. High content of Chol is found in lipid rafts responsible for cell signalling. Thus, Chol has dual functions, it constitutes structural components of bio-membranes and regulates membrane fluidity.

1.3 Lipid composition of the cancer cell membrane

It is well known that alterations in the cell membrane have key implications in the progression of cancer, as they have a significant impact on the cell's response to its environment [33]. Altered membranes of cancer cells may change their ability to grow or even to attach and respond to surrounding cells. Moreover, alternations can influence cellular motility, aiding in invasion or metastasis [5]. Cancer is a pathological condition developed as a result of genome instability enabling replicative immortality [34]. Alternations in cell membranes are also associated with other diseases like diabetes, atherosclerosis or neurodegenerative pathologies [35, 36].

Neoplastic cells tend to modify membrane fluidity when preparing for metastasis [37–39]. This is linked with the deregulation of cholesterol metabolism in

cancer cells [33]. Overall, cholesterol regulates cell membrane rigidity and stiffness controlling their ability to deform [1,2]. In addition, higher content of cholesterol limits cell permeability and is related to the larger number of lipid rafts presented in the external leaflet of the plasma membrane [42]. On the other hand, there is evidence that cancer cell membranes are softer than non-transformed cells, which is attributed to a loss of fluid rafts forming lipids [43]. Those lipid domains are involved in key biological processes such as cell proliferation, differentiation, migration and apoptosis [44]. Lipid rafts are associated with malignant transformation, play important role in the metastatic cascade, specifically within tumor angiogenesis, cell adhesion, migration and endothelial-to-mesenchymal transition (EMT) [45]. Moreover, the cancer cell surface is greater than normal cells due to the higher number of microvilli [5]. Microvilli were commonly characterised on the surface structure of normal small intestine and govern metabolite absorption [46]. It was reported that cancer cell microvilli contain nutrient trafficking vesicles and glucose defining its metabolic capacity [47].

Dysregulation of lipid raft organization was reported to alter pathways related to malignancy such as cancer cell proliferation, migration, invasiveness or metastasis [48]. Invadopodia, actin-rich plasma membrane protrusions of tumour cells, podosome-like structures of nontransformed cells, drive adhesion and penetration of cancer cells into the underlying extracellular matrix, stroma and basal lamina (see Fig. 6). Disruption of lipid domains by depletion of membrane cholesterol using methyl-β-cyclodextrin (MβCD) prevents invadopodia formation and cancer cells expand into nearby environments, proving that lipid rafts are mandatory for invadopodia functionality in human breast cancer [49].

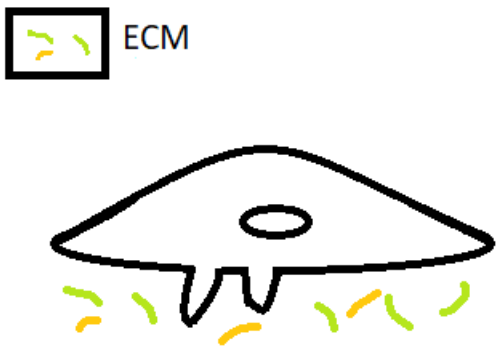

Figure 6 Schematic structure of cancer cell with invadopodia. Invasive cancer cells are thought to breach the basement membrane by specialized invadopodia, membrane protrusions. ECM: extracellular matrix. Taken and modified from [50].

Another change that occurs during tumorigenesis is an alteration in glycosylation of membrane-associated glycoproteins and glycolipids [30]. Those modifications are often caused by the activation of certain glycosyltransferases, which are responsible for catalysing the biosynthesis of glycoproteins [51]. Glycosylation is a post-translational modification of proteins. Breast cancer patients often exhibit changes in the glycosylation of mucins in the mammary gland related to a higher content of sialic acid [52]. This, in turn, is believed to contribute to a net negative charge of the cell membrane [53].

1.4 Key characterization of membrane structure and membrane organization

The cell membrane is a complex mixture of various lipids with both distinct and synergistic effects [54]. Amphiphiles are molecules capable of self-assembling in an aqueous solution if a threshold concentration called critical micelle concentration (CMC) is reached [55]. The CMC is a minimum concentration of surfactants above which they can organise into particular aggregates, determined by lipid molecular

structure (type of headgroup, sidechain, overall shape and volume, hydrophilic: hydrophobic ratio of a molecule). The self-assembly process of amphiphilic molecules occurs due to two simultaneous tendencies: hydrophobic lipid acyl tails avoid a polar environment, while hydrophilic head groups are positioned to interact favourably with the aqueous medium. To predict the structure of the aggregate we can use the packing parameter (P), which is expressed as [56]:

$$P = {}^{V}/_{AoL}$$

where *V* is the effective volume occupied by hydrophobic chains in the aggregate core; *Ao* is the effective polar head group surface area at the aggregate solution interface and *L* is the maximum effective hydrophobic tail length. The shape and size of aggregates also depend on the molecular geometry of components and the solution conditions such as temperature, pH, water content, concentration and ionic strength [57].

Kumar et al. described that upon hydration with the increase of *P* value, the amphiphiles can adapt spherical structure ($P \leq 1/3$), non-spherical (cylindrical) ($1/3 \leq P \leq 1/2$) and lamellar ($P=1$) [58]. When $1/2 \leq P \leq 1$, bilayer structures are generally formed and $P>1$ favours the aggregation to reverse hexagonal phase, reversed micellar cubic (Fd3m), reversed bicontinuous cubic (Im3m), reversed bicontinuous cubic (Pn3m) and reversed bicontinuous cubic (Ia3d) [57]. Figure 7 portrays these considerations.

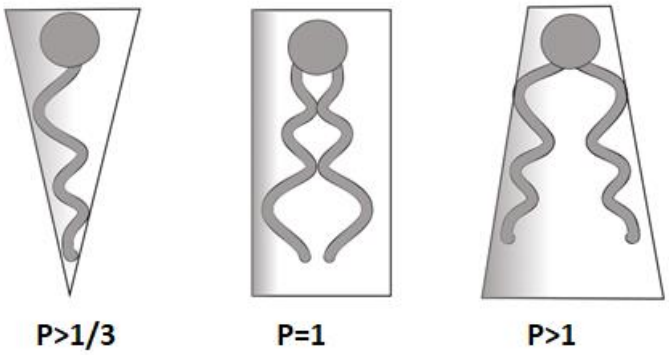

Figure 7 Amphiphilic molecule self-assembly. Illustration of the P concept and its relation to geometrical shapes. Taken and modified from [55].

Lamellar phases organize into a liquid crystalline order [59]. To reduce the energy of the system, the lipid lamellae form a bilayer in which hydrocarbon acyl chains of two leaflets face each other constructing a hydrophobic core, while polar lipid headgroups interface with water molecules. Bilayer is the prevailing organization of lipid molecules in membranes, albeit not an exclusive organisation (see Fig. 7). The key property of lamellar structure is to provide a barrier preventing from free diffusion of large solutes, constitute a platform for other non-lipid membrane components, define the shape of cells or organelles and simultaneously, protect from mechanical stress. Diverse membrane functions and related processes are specifically associated with amphiphilic non-lamellar lipid domains. The inverted hexagonal phase is specific to mitochondrial membranes introducing curvature stress in the bilayer membrane and modulating mitochondrial fusion and fission [24]. Mitochondrial fusion connects two mitochondria together, while fission divides one into two [60]. Mitochondria separate and merge to mitigate changes in energy and stress. Non-bilayer organization in membranes induces curvature strains determined by the overall concentration and distribution of these lipids in the membrane [24].

1.5 Membrane fluidity and lipid phases

Membrane lipids are capable of self-assembly and adopt principal lamellar phases: solid (also termed gel or liquid crystalline gel; L_β) and liquid (refer to the fluid, liquid crystalline or liquid disordered; L_α) [61]. They differ in the spatial arrangement and mobility of individual lipids which have an impact on membrane permeability. In the gel phase, van der Waals interactions cause highly ordered packing of the acyl tails, which are in a fully extended all-trans conformation and with a slow lateral diffusion (see Fig. 8; gel, solid phase) [62]. When the temperature increases and lipids reach their melting temperature (T_m), which depends on their type of polar head group, the length of acyl chains or the degree of unsaturation, they undergo the phase transition from gel to liquid crystalline phase. The T_m is specific to each lipid and is directly proportional to the length of fatty acids and inversely correlated to a number of unsaturated bonds in the acyl chains. Long acyl tails boost the Van der Waals interactions between carbon chains and favour ordered packing, while the decrease of melting temperature associated with a greater number of unsaturation is due to lower packing of hydrocarbon chains. At the gel-phase transition, acyl tails change from all-trans to a trans-gauche conformation. The liquid crystalline phase (L_c) is characterised by highly disordered lipid acyl tails, which experienced increased translational and rational mobility in comparison to the gel phase [63]. As a result, membrane fluidity is enhanced. In some bilayers, the intermediate phase between the gel and liquid crystalline occurs the ripple phase with characteristic curvature. In addition, in membranes containing also cholesterol and sphingolipids appear also the liquid-ordered phase [64], known also as lipid rafts (L_o) (see Theoretical background, 1.2 The importance of biological membranes: Lipid raft hypothesis). Long acyl chains of sphingolipids favour tight packing, and cholesterol, having specific H-bonding

interactions with lipids and capability to bridge the voids in lipid bilayers, expels water molecules from the highly ordered gel phase to form the liquid ordered phase [65].

Many studies have demonstrated the coexistence of gel and fluid phases in living cell membranes [66]. Figure 8 illustrates the different physical states adopted by a lipid bilayer and main phase transitions.

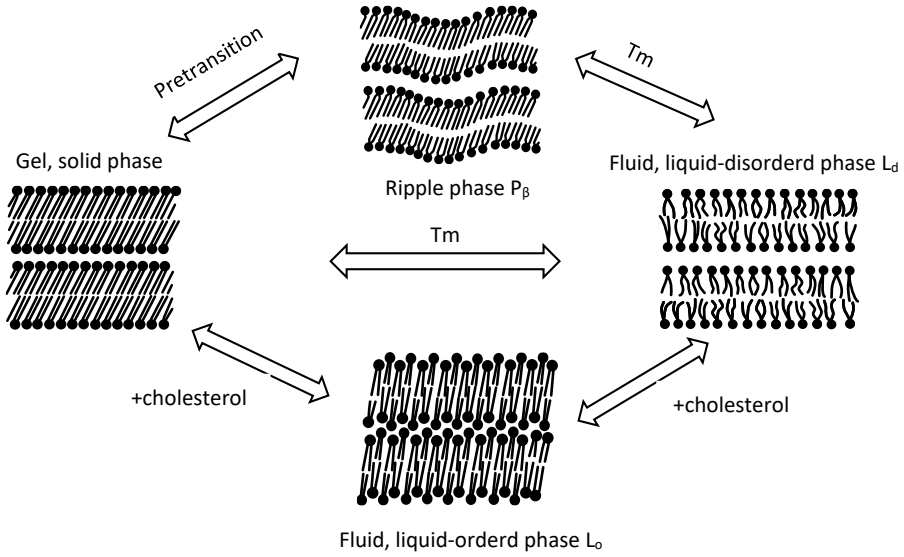

Figure 8 Different physical states adopted by a lipid bilayer, which differ in organization, membrane order and the motility of lipid molecules. Two extreme lipid phases can occur in biological membranes- gel (L_β) or fluid phases (L_d). The transition between phases occurs at specific temperature termed melting temperature (T_m). Some lipids exhibit a pretransition temperature and have additional lamellar phase, the ripple phase (P_β). When cholesterol is present, lipid bilayer can have an extra phase termed liquid-ordered phase (L_o) with characteristics of both gel and fluid lipid states. Taken and modified from [62].

1.6 Key physicochemical properties of membranes

Cell membranes are dynamic and asymmetric fluid structures that are not fixed in position. Mammalian cell structure with organelles is demonstrated on Figure 9. Lipid asymmetry specifies non-homogenous lipid composition in the exoplasmic and cytofacial leaflets of many biological membranes. The lipid asymmetry of PM is

highly preserved across eukaryotic cells [67]. In mammalian cells, the outer leaflet of PM largely consists of PC, SM and glycosphingolipids (GSL), whereas the inner leaflet is enriched in charged PE, PS and PI. Chol is present in both layers with a cell-specific distribution.

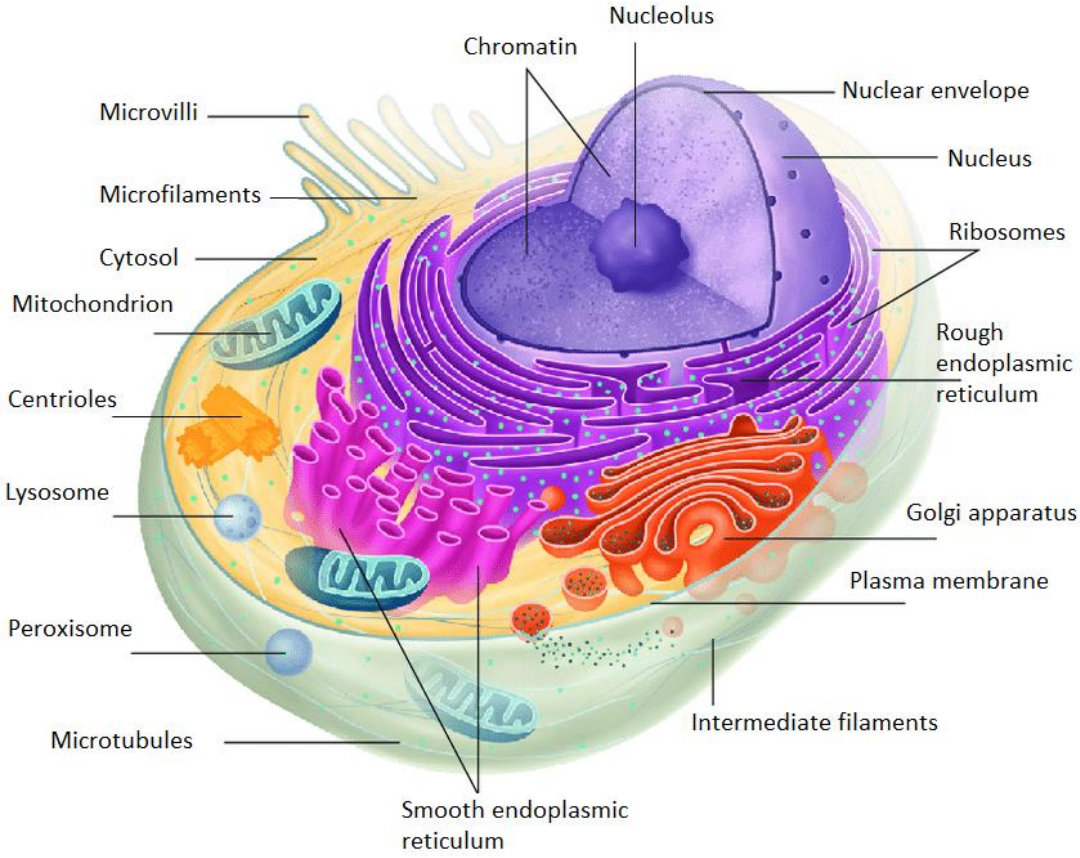

Figure 9 Structure of mammalian cell with organelles. Taken from [68].

Membrane compressibility and fluidity depend on the lipid composition (length and degree of unsaturation of fatty acids, type of polar head group or presence of sterols), temperature, pH and ionic strength. Furthermore, the local fluidity of the lipid bilayer has been shown to affect many membrane functions including passive permeability properties, signal transduction or enzyme activity [69]. Lipids and many membrane proteins are constantly in lateral motion called lateral diffusion within one

of the membrane leaflets [70]. This rapid lipid movement can lead to the formation of lipid domains and rafts. Lipids can also spontaneously rotate from one face of a membrane to the other layer in a very slow process called transverse diffusion or flip-flop, which allows lipids to maintain membrane asymmetry [70]. Lipid movement is also regulated by enzymes flippases and floppases which role is to synthesize or degrade lipids in one of the leaflets [71].

Lipid asymmetry has been investigated to have a significant function in many membrane-based processes. The loss of PS asymmetry and consequent PS exposure to the external environment activates apoptotic machinery or promotes blood clotting. Furthermore, some viruses express PS in the outer envelope to attract immune cells and induce host infection [72].

1.7 Membrane elasticity

Biological membranes determine the integrity and shapes of cells and intracellular compartments. As a result of their function, they are exposed to forces applied by molecules, such as proteins which generate changes in their structures and shapes. In 1973 German physicist Wolfgang Helfrich proposed a theoretical model of membrane elasticity which assumed that membrane resistance to deformation depends on two elastic features: stretching and bending (detailed reviewed in [73, 74]). The lipid bilayer is considered a fluid sheet with a small thickness when compared to its lateral surface dimension. The Helfrich Hamiltonian refers to the elastic contribution (per unit area) to the free energy of the membrane,

$$f_{elastic} = f_{bend} + f_{stretch}$$

where f_{bend} is the free energy per unit area as of membrane bending and $f_{stretch}$ is the free energy per unit area due to membrane stretching. As membranes are highly

resistant to stretching, the f_{strech} can be neglected. It is caused by energetically unfavourable exposure of hydrophobic hydrocarbon lipid chains to water [75]. Lipid bilayers highly resist stretching because increasing the average distance between head groups elevates exposure of the hydrophobic motifs to water molecules [75]. Therefore, the bending energy has the most significant contribution to the membrane free energy expressed as:

$$f_{elastic} = f_{bend} = \frac{1}{2} K_b (2H - C_o)^2 + K_G G$$

where the K_b and K_G are the bending modulus and Gaussian curvature modulus respectively, H represents the mean of two principal curvatures of the membrane ($H=(C_1+C_2)/2$), G is Gaussian curvature of the membrane also defines by the principal curvatures ($G=C_1C_2$) and C_o represents preferred curvature of the membrane in a relaxed state. As lipid bilayers maintain their asymmetry, the value of C_o is non-zero. On the other hand, artificial membranes composed of just one type of lipid, have identical monolayers and no spontaneous bending appears, so $C_o=0$.

$$f_{elastic} = f_{bend} = \frac{1}{2} K_b (2H)^2 + K_G G$$

In addition, the Gaussian curvature term only contributes to the alteration in free energy systems if the membrane undergoes a topological transition such as poration, fission or fusion. Therefore, the Gaussian elasticity term can be ignored and the equation of the free energy ($F_{elastic}$) of model membranes for bending at fixed topology can be described as:

$$F_{elastic} = \int f_{elastic}\, dA = 2K_b \int H^2 dA$$

where dA is the area element on the membrane. Typical values of K_b for lipid bilayers are between 10-20 k_BT. This model is relevant for membranes composed of one type

of lipids. In the case of bilayers made of a mixture of lipids, the analysis becomes more complex.

1.8 Membrane biomimetics

Due to its fundamental role and complexity, many different model systems have been created retaining essential lipid bilayer structure but simplified enough so that functions of individual components, their organization and dynamics can be assessed and visualized. Commonly used mimetic systems include lipid monolayers, lipid vesicles and supported lipid bilayers [76].

1.8.1 Lipid vesicles

The first observation of self-assembled hydrophobic lipids in an aqueous environment was made by British haematologist Alec Bangham with co-workers while testing the electron microscope in the 1960s [77]. Now those structures are known as lipid vesicles or liposomes and are characterized as small sphere-shaped structures widely used as molecular tools for investigating membrane mechanics and membrane processes [56]. Their structure is arranged similarly to biological membranes as they are composed of two lipid leaflets (Figure 10).

The great advantage of liposomes is that they can be formed with different lamellarity, size, charge and composition mimicking both prokaryotic and eukaryotic membranes. Based on lamellar structure and size, the liposomes can be classified into four main classes- unilamellar vesicles are small (20-40 nm), large (100-1000 nm) or giant (>1000nm); whereas multilamellar vesicles have several bilayers. Stable lipid vesicles from phospholipids are generated at a temperature above the gel-to-liquid crystalline transition temperature (T_c) of phospholipids related to the melting point of

the acyl chains, which is also affected by their length and degree of unsaturation and the nature of head groups [78].

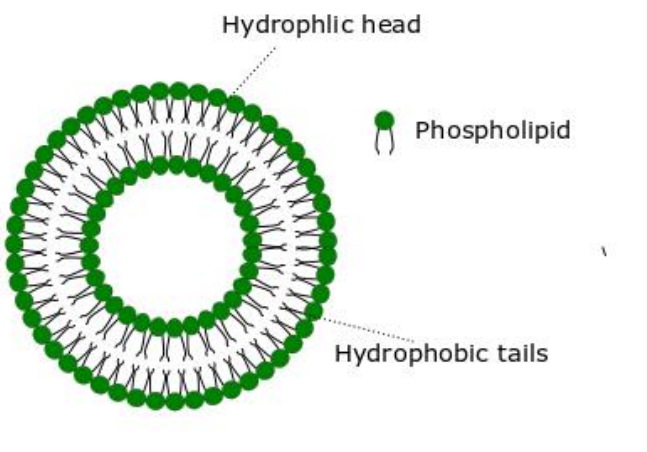

Figure 10 Schematic lipid vesicle.

According to the method of preparation, different classes of bilayer structures can be formed [78]. Multi lamellar vesicles (MLV) are created by the hydration of a dried lipid film at temperatures above the lipid phase transition. Their size can be easily reduced and homogenized with several freeze-thaw cycles. Large unilamellar vesicles (LUV) are vesicles with a size ranging between 100-1000 nm, which are formed by the extrusion of MLV through polycarbonate filters with monodisperse pore size [79]. LUVs are commonly used in fluorescence spectroscopy to study membrane permeability and fluidity. Similar in morphology and size (up to 100 μm) to native cells are giant unilamellar vesicles (GUV) often produced by the electroformation method [60]. Electroformation is a rapid and easy method which can be conducted by applying an alternating electric field in the formation chamber to induce swelling of thin lipid films on an indium tin oxide (ITO)-coated glass surface [82]. One of the advantages of using them is that they are visible under optical microscopes at the single vesicle level [81]. In addition, confocal microscopy can

provide detailed information about many biophysical features of membranes such as their fluidity, permeability or morphology. Disruption of MLVs also produced small unilamellar vesicles (SUVs), which both with LUVs have a single lipid bilayer. All these lipid vesicles are commonly utilized as membrane models not only to investigate membrane properties but also to provide suitable transport vehicles for drugs and other bioactive molecules. Thus, liposomes have been used in pharmaceutical applications as a delivery system providing targeting of particular diseased cells and liposomal drugs have reduced toxicities compared with free medicaments [83].

1.8.2 Giant plasma membrane vesicles

Despite many advantages, vesicles constructed of synthetic or purified lipids are too simplified to mimic the dynamic structure of a living cell. An alternative model system isolated directly from living cells is giant plasma membrane vesicles (GPMVs). In response to a chemical or osmotic stress, mammalian cells are capable of producing various vesicles closely mimicking the lipid and protein compositional complexity of the intact cell plasma membrane [84]. GPMVs gained importance after phase separation was observed in their membranes [16].

For vesiculation purposes, adherent cells are preferable to use as they remain attached during the process. GPMVs formation was first observed in the 1970s [85]. Cells were incubated in a buffer containing formaldehyde (PFA), D-thiothreitol (DTT) and Ca^{2+}. Chemically induced vesiculation produced nearly pure membrane vesicles with a lack of assembled cytoskeleton and nuclear material [86]. Generally, cell blebbing is a biological process occurring during cytokinesis, cell migration or apoptosis [87]. In contrast to physiological blebs, which are retracted after the reformation of an actin cortex at the bleb membrane, GPMVs fail to retract. This can

be attributed to the presence of Ca^{2+} in a vesiculation buffer. A steady influx of Ca^{2+} triggers many processes and different events dependent on Ca^{2+} thresholds occur, mainly $PI(4,5)P_2$ degradation and the loss of lipid asymmetry [17]. $PI(4,5)P_2$ is an anionic lipid regulating cellular functions including cytoskeleton dynamics [88]. Lack of $PI(4,5)P_2$ precludes the reformation of an actin cortex and as a result, blebs are formed. Elevated levels of Ca^{2+} also affect phospholipid scramblases and aminophospholipid transporters, activating and inhibiting them, respectively. Consequently, membrane asymmetry is mainly lost, at least in the case of phosphatidyl serine. Thus, cell blebbing induced by chemical vesiculation resembles apoptosis, a programmed cell death.

Producing giant plasma membrane vesicles from cells is a unique opportunity for preparing biomimetic model membranes. Currently, GPMVs are used to investigate membrane organization or processes including the mechanism of action of cell-penetrating peptides [89]. Although presenting many advantages, GPMVs also have significant limitations. Their formation is induced in the presence of PFA and DTT, which are non-specific crosslinkers and reducers, respectively. Cell incubation with chemical vesiculants leads to covalent modifications. Adaptation of this protocol is a usage of N-ethyl maleimide (NEM), instead of PFA/DTT, which blocks terminal sulfhydryl groups avoiding crosslinking [90]. Another limitation is the loss of lipid bilayer asymmetry mentioned above, typically by increased exposure of anionic PS in the outer layer. Recent studies have revealed also that GPMVs are passively permeable to hydrophilic macromolecules as large as 60 kDa as a result of shear-induced rupture of vesicles from cells [91]. Finally, cell-derived vesicles represent the cellular membrane in a state of thermodynamic equilibrium, while the living cell plasma

membrane is a dynamic structure under constant modifications including interaction with cytoskeletal components or enzyme activity.

While synthetic lipid vesicles are relatively easy to form, the production of giant plasma membrane vesicles is still challenging. Due to the complexity of living cells, there are lots of surprising events that can appear during vesiculation being impossible to predict.

2. Antimicrobial peptides: general overview

More than a century has passed since Alexander Fleming determined the antimicrobial activity of lysozyme, the first natural antibiotic identified in body fluids [92]. Since then, diverse types of molecules with antibiotic activity have been isolated from different species, and their applicability has been claimed as the most important medical breakthrough. The antimicrobial peptides (AMPs) have redefined our understanding of the fundaments underlying immunity and human disease. At present, it is known that AMPs can be found in virtually every living organism [93]. According to the Antimicrobial Peptides Database (ADP), more than 3500 peptides were classified as AMPs and have been registered up to date (https://aps.unmc.edu/) (see Figure 11). AMPs are also termed host defence peptides [94], cationic antimicrobial peptides [95], cationic amphipathic peptides [96] and α-helical antimicrobial peptides [97].

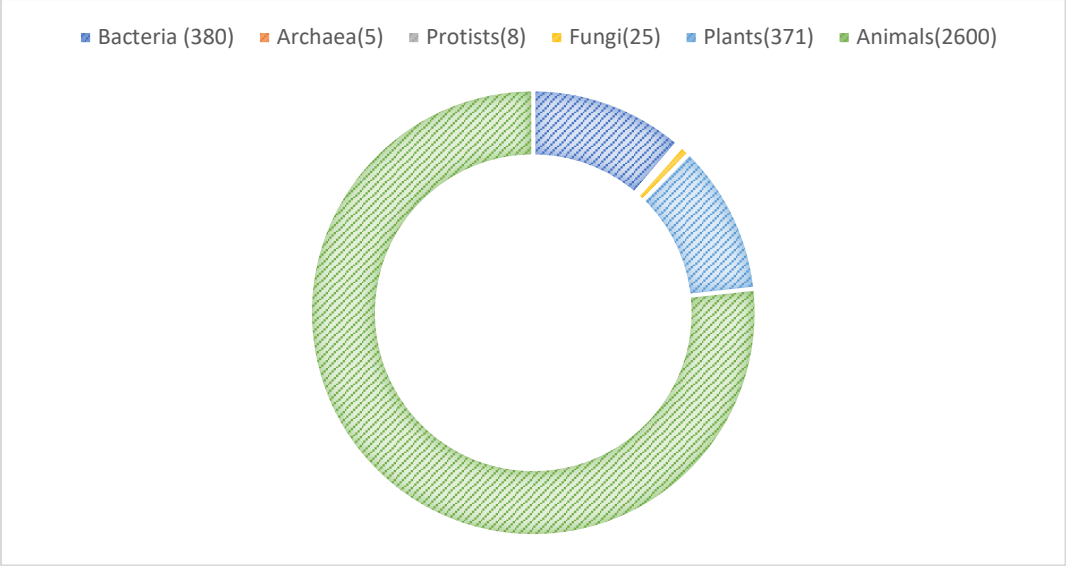

Figure 11 Sources of antimicrobial peptides (total 3569) as of July 2023 from the antimicrobial peptide database. Number obtained from https://aps.unmc.edu/, accessed on 10 July 2023.

2.1 AMPs classification system

The large diversity among AMPs led to attempts to categorise them according to their: 1) activity spectrum [98]; 2) secondary structure [99]; 3) bacterial selectivity [93]; 4) amino acid composition [3]; origin [100]. Currently, the most widely accepted classification of AMPs is the one compiled by Brogden in 2005. Amino acid composition is the key criterion used to divide peptides into 5 subclasses presented in Table 1.

Table 1 Classes of antimicrobial peptides according to Brogden [3]

Category	Unique structure/ sequence/ feature	Peptides	Origin
Anionic peptides	• Rich in Asp and Glu • Produced in mM concentration • Require Zn as a cofactor	• Dermicidin • Maximin H5	• Humans • Amphibians

Linear cationic α-helical peptides	• Lack of Cys residues • In aqueous solution are disordered, can convert into α-helix in the presence of bactericidal membranes (lipid A) or liposomes	• Cathelicidins (LL-37) • Magainins • Cecropins • Polybia MP1	• Mammalians • Amphibians • Insects • Insects
Cationic peptides enrich for specific amino acids	• Lack of Cys • Rich in Pro • Rich in Pro and Arg • Rich in Pro and Phe • Rich in His	• Abaecin • Apidaecins • Prophenin • Histatin	• Insects • Mammalians • Mammalians • Mammalians
Anionic and cationic peptides that contain cystein	• Form disulphide bonds • Adapt β-sheets as secondary structure	• Cathelicidins (protegrin) • Defensins	• Mammalians • Mammalians
Anionic and cationic peptides fragments of larger proteins	• Parts of larger proteins	• Casocidin (from casein) • Lactoferricin (from lactoferrin)	• Mammalians • Mammalians

Gramicidins, obtained from soil bacteria Bacillus brevis, are the first ever AMPs clinically used as antibiotics [1]. There are two types: gramicidin D and gramicidin S (Soviet). Gramicidin D is a linear pentadecapeptide AMP with the mixture of three types such as A (g-A), B (g-B) and C (g-C). It can adapt hetero

dimeric intertwined (double stranded) beta helix or homo dimeric single stranded helix [101]. Contrary, Gramicidin S, discovered by Russian microbiologists Gause and Brazhnikova [102], is a cyclic derivative of gramicidin which forms a ring structure and adapts β-sheet secondary structure [103].

2.2 Mechanism of action of AMPs

AMPs exert a broad spectrum of activity; therefore, it is suggested that there is no single target site or mode of action common to all peptides. Unlike antibiotics, the multi-facial nature of AMPs may prevent the development of bacteria resistance [104]. During the last decades, studies have revealed a few potential mechanisms against different types of pathogens (see [105–107] for detailed reviews). Seelig et al. divided the interaction between cationic antimicrobial peptides with lipid membranes into three thermodynamic steps: 1) the electrostatic attraction of the positively charged amino acid residues to anionic lipid head groups enhancing their concentrations on the membrane surface (additional binding between peptides with neutral net charge and non-charged lipids); 2) peptides partitioning into lipid bilayer; 3) bound peptides change their conformation induced by hydrophobic interactions [1]. The structure rearrangement and adaptation of the secondary structure is seen as a key stage in the partition process [108]. Moreover, some invading pathogens possess external cell walls, but AMPs have an ability to displace the divalent cations stabilizing the walls, which forms defects and peptides can translocate across the barrier [109].

Another factor, which is important in peptide-lipid interaction, is the peptide concentration or peptide/lipid ratio. At low ratios, AMPs lie flat on the membrane surface and only affect its thickness. Above a certain threshold, peptides begin to partition into the bilayer. In order to explain AMP’s activity, their potential

mechanisms were divided into two categories: 1) the formation of transmembrane pores (“barrel stave” and “toroidal” pore models); 2) by dissolving the membrane in the detergent-like manner (“carpet model”). These models are demonstrated in Figure 12 [105, 107].

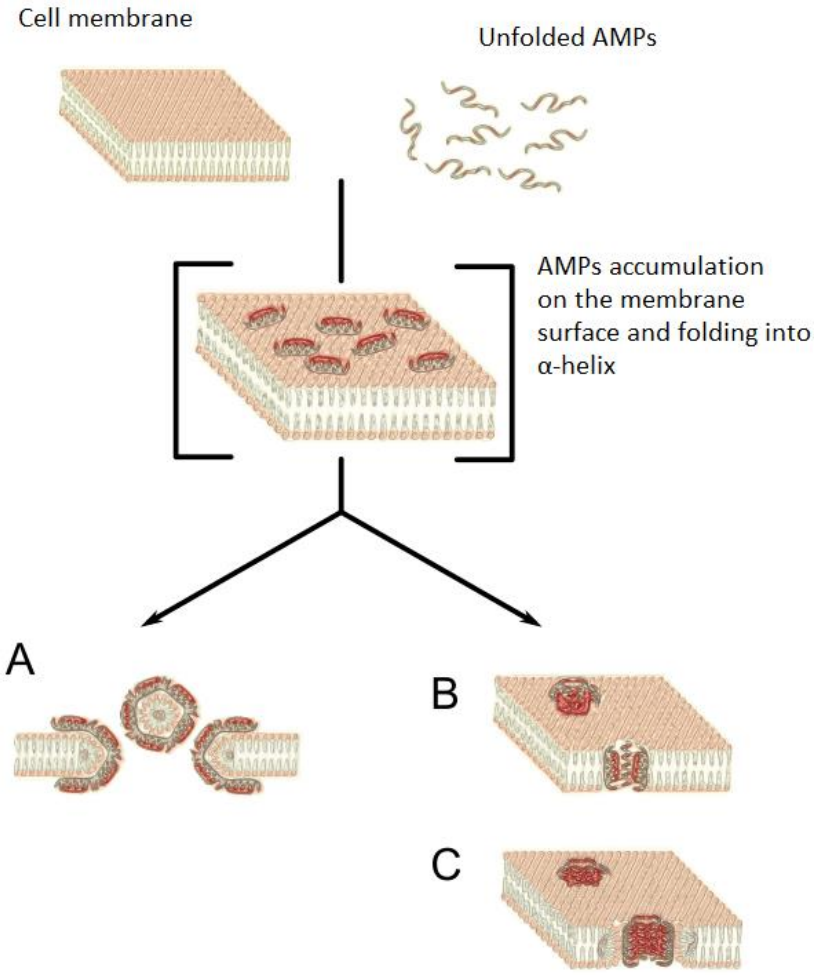

Figure 12 Schematic representation of some action mechanisms of AMPs (A)- carpet model; (B)- barrel stave model; (C)-toroidal pore model. In the “barrel-stave” model, AMPs insert within the membrane by orienting their hydrophobic face in the lipid core of the bilayer, while their water-soluble regions form the lumen of the channel. This model is unique to fungal alamethicin. The “toroidal” mechanism is another model that describes the pore formation. In this case, peptides induce the bending of lipids within the bilayer, forming a peptide-lined pore in which AMPs are associated with the lipid polar head groups. Melittin, magainins and protegrins are proposed to use a “toroidal” model. Alteration to this model is the formation of “disordered toroidal”

channels, where the peptides bind primarily to the edge of the pore and do not have a specific orientation. In comparison, in the “carpet” model AMPs fold into amphipathic conformation and accumulate on the membrane surface covering it in a carpet-like manner. When the threshold concentration is reached, peptides disrupt the bilayer in a detergent-like model, leading to its disintegration and formation of micelles. Taken and modified from [107].

One of the best studied AMPs are the family of gramicidins, g-D penetrates into the bacterial membrane leading to the cell death by the loss of solutes and ions, inhibition of respiration and genetic material synthesis, reduction in ATP or and indulgence of the transmembrane potential [110]. g-S shows greater permeability towards all the bacteria and inhibits the cell growth by disrupting cytoplasmic membrane [111]. In addition, many AMPs can affect cellular functions at low concentrations without damaging the membrane but freely translocating across the bilayer. They can interact with intracellular molecules influencing important cellular and metabolic processes such as the inhibition of DNA, RNA and protein synthesis or cytosolic enzymatic activity [3]. For instance, buforin II forms “toroidal” pores across the bacterial membrane, translocates to the cell interior and eventually, binds to nucleic acids [112]. Another AMP, nisin is capable of binding to lipid II abundant in procaryotic membranes, hindering cell wall biosynthesis, and inducing autolysis [113, 114]. Human LL-37 not only modulates immune response but creates pores across the bilayer [115].

Lately, research has focused on Polybia MP1 mechanism of action, a peptide with promising anticancer activity. The peptide was shown to have pore-forming activity [116, 117]. It is assumed that the peptide inserts into the membrane leading to membrane disruption due to the high content of hydrophobic residues and capability

to form hydrophobic interactions. MP1 is a short peptide, thus, it is proposed that it form toroidal transmembrane pores [118].

2.3 Different origin and activity spectrum of antimicrobial peptides

In the last decades, the emergence of multidrug-resistant pathogens has become one of the greatest global health issues and hence alternatives to conventional antibiotics are urgently needed. To resolve this problem, AMPs have attracted attention as promising drug candidates. Moreover, the term "antimicrobial peptides" refers to their first recognized property- they combat different pathogens. Currently, it is well-known that AMPs possess a broad spectrum of activity. Table 2 reports a summary of the different biological activities of AMPs.

Table 2 Activity spectrum of antimicrobial peptides [105, 106]

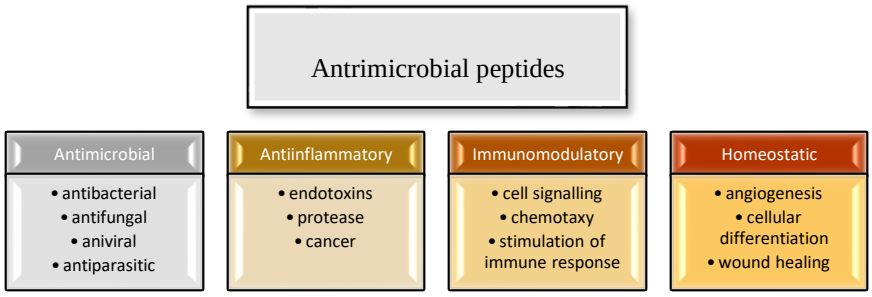

Bacterial AMPs, bacteriocins, are generated to kill other bacterial species that may compete for nutrients and the same environmental niche. In addition, they may control the colony size (so-called quorum sensing) [119].

Most AMPs reported to date are derived from eukaryotes (reviewed in detail in [106]). It is well-known that AMPs are important weapons of the immune system, constituting the first line of defence to combat pathogens. As invertebrates and plants lack adaptive immunity, AMPs play a fundamental role in their protection. They have been found in all invertebrates examined to date (in hemolymph, hemocytes and

phagocytes). Interestingly, all plant AMPs are cysteine-rich and can be found in seeds, flowers or leaves.

In comparison, vertebrate immunity consists of both an innate and adaptive immune system. AMPs are often produced by epithelial cells and can be isolated from bodily fluids such as blood, sweat, saliva and plasma. In addition, rich sources of AMPs are white blood cells, especially phagocytes, where they are in granules.

2.4 Immunomodulatory function of AMPs

The immune system is the fundamental network of biological processes that protect an organism from pathogens. AMPs have been classified as important immunity components exerting immunomodulatory properties[120]. To emphasise their immunomodulatory role, antimicrobial peptides are also called host defence peptides (HDP) [121]. AMPs resemble endogenous antibiotics and combat pathogenic bacteria, fungi, viruses and protozoa directly, or indirectly by modulating the immune response in higher organisms[122, 123]. Due to the ability to recognize chemokine receptors, cathelicidins and defensins are chemo-attractants for monocytes, neutrophils, dendritic cells (DCs), and T cells [124]. AMPs can also promote cellular differentiation of macrophages or DCs resulting in activation of adaptive immunity and can bias their polarization toward a pro-inflammatory phenotype [125, 126]. AMPs impacting antigen-presenting cells regulate the adaptive immune response (see [127] for details). Also, AMPs dysregulation in many tissues has been linked to some autoimmune or autoinflammatory diseases, namely systemic lupus erythematosus (SLE), psoriasis, rheumatoid arthritis (RA), type 1 diabetes (T1D), Sjögren’s disease (SjS), and multiple sclerosis (MS) [128].

2.5 The homeostatic capability of AMPs

It was observed that certain peptides promote tissue regeneration. Some AMPs are involved in the processes of angiogenesis and wound healing [129]. For instance, the LL-37 peptide, human cathelicidin, facilitates the proliferation of dermal cells, essential in wound restoration. LL-37 is capable of modulating angiogenesis as it has been shown to stimulate proliferation and neovascularisation, [130]. Therefore, LL-37 has been successfully applied in diabetic foot ulcer (DFU). The expression of human β-defensin (hBD)-2 was identified in human skin wounds acting as an inducer of keratinocyte cytokine production and migration [131]. Furthermore, LL-37 have been determined to promote healing at the ocular surface [132]. Some AMPs show potent wound-healing activity in other epithelial tissues such as the gut and lung [133]. Gramicidin D and S are used to treat infected wounds as well as eye, nose or throat infections [102, 110].

In addition, as invading pathogens cause inflammation, some AMPs have anti-endotoxin activity neutralizing lipopolysaccharides (LPS) and can act like anti-inflammatory agents [134].

2.6 Antimicrobial peptides as anticancer agents

Over the past few decades, the number of people suffering from cancer has arisen dramatically becoming a real worldwide issue [135]. Current methods applied in cancer treatment - chemotherapy, radiotherapy or surgical resection- have many limitations such as insufficient selectivity towards cancer cells leading to unspecific targeting of healthy cells and development of resistance to anticancer drugs [136]. As a result, there is a strong need for an effective therapy that can overcome adverse

effects caused by conventional methods. A novel class of potential therapeutics which can be implemented against both global health threats are antimicrobial peptides.

AMPs, as described above, have a wide spectrum of activity. They share common physicochemical properties: have a high content of hydrophobic residues, a net positive charge and consequently, have an amphipathic nature. Those features are fundamental in their mode of action as cationic peptides are attracted by electrostatic forces to negatively charged membranes. Likewise, the outer leaflet of PM of many cancer cells has also a high content of components with a negative charge opposite to the zwitterionic surface of non-transformed cells [137, 138]. As a result of this similarity, it is considered as a main factor of enhanced selectivity of AMPs towards malignant cells [5]. Over the years, it was proven that antimicrobial peptides are not only membrane-active agents but also target other cellular processes such as cell division, and metabolism or affect the immune system [139]. AMPs show anti-tumour mechanisms by (1) modulating the immune system, (2) inducing apoptosis or necrosis of cancer cells (both terms refer to the programmed cell death, however, during apoptosis, the affected cell actively participates in the cell death process, while in necrosis the cell death initiation is a response to adverse conditions in the cell environment [140], (3) inhibiting tumour angiogenesis to suppress its nutrition and metastasis, and (4) activating functional proteins to regulate the gene transcription and translation of tumour cells [141, 142].

Certain antimicrobial peptides exhibit a broad spectrum of cytotoxic activity towards tumour cells and, as a result, are also referred to as anticancer peptides (ACPs). Similarly to bacterial membranes, cancer cells' lipid bilayer has a strong net negative charge in the outer leaflet and the electrostatic attraction between anionic phospholipids and positively charged AMPs is believed to play an important role in

binding and disruption of cancerous cells [1–3]. The content of some anionic glycoproteins such as mucins and heparan sulfate proteoglycans may also enhance AMP–cancer cell membrane interaction [94, 143]. Cytotoxic effect on breast cancer models was reported e.g. on MCF-7, MDA-MB-435 and MDA-MB-231 cancer cell lines for peptides: lactoferricin [144], magainin II [145], peptoid 1 [146] or IW13 [147]. Magainin II was reported cytotoxic against all bladder cancer cell lines by an average IC50 of 198.1 μM [148]. Nisin, a bacteriocin and antibacterial peptide, suppressed metastatic progression of colon adenocarcinoma cells by downregulating some crucial genes [149]. Administrating AMPs in combination with chemotherapeutics showed the chemsensitizing effect- NRC-03 and NRC-07 dosing reduced the half-maximal effective concentration (EC50) of cisplatin for breast cancer cells [150]. In another study, doxorubicin combined with nisin exhibited threefold greater cytotoxicity than peptide or drug alone [151].

2.7 Polybia MP1 as a multifunctional peptide with anticancer potency

According to the antimicrobial database (http://aps.unmc.edu/AP/main.php), 276 peptides with anti-tumour properties have been discovered to date. Polybia MP1 is an example of a peptide with activity against cancer cells.

Polybia MP1 (IDWKKLLDAAKQIL) first isolated from the venom of the Brazilian wasp *Polybia paulista*, is extensively studied AMPs due to a broad anti-pathogenic spectrum and with low haemolysis to rat erythrocyte [152]. A 14-residue peptide demonstrates bactericidal activities against Gram-negative and Gram-positive bacteria without being cytotoxic and haemolytic to healthy cells (the Gram stain provides basic classification system: Gram-positive bacteria have a thick (20–80 nm) cell wall, while Gram-negative bacteria have a relatively thin (<10 nm) layer, but

harbour an additional outer membrane [153]). This peptide is cytotoxic against leukemic T lymphocytes and shows some selectivity in recognizing them [154]. MP1 showed also a selective inhibitory effect on multidrug-resistant leukemic cells, and on proliferating prostate and bladder cancer cells [116, 155]. Clinical application has not yet proceeded due to not fully explained molecular-scale mechanistic basis of Polybia-MP1 activity. However, Liu et al. synthesized polyethylenimine (F-PEI) for effective MP1 formulation and administrating MP1/F-PEI nanoparticles in mice showed prolonged lifetime within four weeks and tumour growth supression [156]. The membranolytic activity and biofilm inhibition support MP1 as a prospective alternative to conventional antibiotics [157].

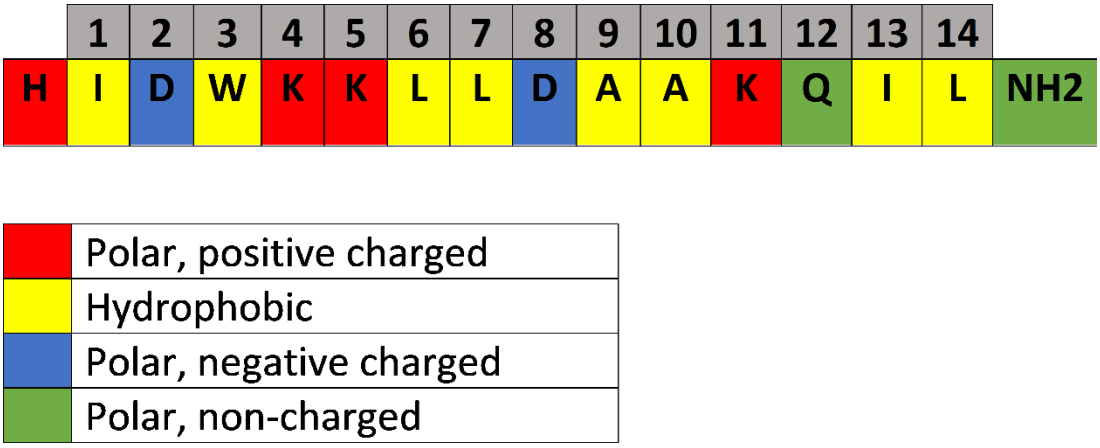

Figure 13 The primary sequence of Polybia MP1 with highlighted side chains properties.

As a member of the Mastoparan family, MP1 has a low net positive charge (+2e) due to three lysine residues, with a linear secondary structure at physiological pH (see Fig. 13). Santos et. al demonstrated a unique role of two aspartic acids (D) at positions 2 and 8 in helical stabilization and haemolysin feature [158]. MP1 in the presence of membranes was demonstrated to form an amphipathic α-helix, positioning the hydrophilic residues on one face and the hydrophobic molecules on the other. The

helix structure adaptation is a prerequisite for MP1 to exert its anti-microbial properties through membrane partitioning and the cationic face of the molecule mediates favourable ionic interactions with the negative membrane surface, while the hydrophobic face on the opposite side is key in membrane perturbation through further interaction with the apolar interior of the membrane [159]. Lately, Zhao et al. demonstrated that D-amino acid peptide analogue of MP1 promotes proteolytic stability and its antimicrobial activity remained relatively moderate [160]. Luong et al. have reported more stable and metabolically active MP1 variants by applying an advancing technology termed the "all-hydrocarbon stapling system"[161]. The inclusion of a hydrocarbon staple drastically stabilizes the secondary structure of MP1 and thereby facilitates proteolytic stability. In addition, peptide mutant with the increased net charge showed a greater inhibitory effect on *B. subtilis*, *S. aureus* and *S. epidermidis,* however exhibiting boosted cytotoxicity at the same time. The incorporation of asparagine (Arn;N) at the aspartic acid (Asp;D) position not only resulted in the increased positive net charge but also determined a higher degree of hydrophobicity. This finding indicates the important role of Asp residue at position 8 in regulating MP1 haemolytic activity [158].

The appropriate organization of hydrophobic and hydrophilic residues is essential in notably limited toxicity to non-transformed cells and, simultaneously, retained anti-cancer potency. It is believed that the origin of cancer selectivity could be caused by the intrinsic alternation in the lipid membrane composition of transformed cells specifically in lipid asymmetry. It has been proven that biomimetic membranes enriched in Chol are less susceptible to pore formation in response to MP1 [154, 158]. Furthermore, hopanoids, functional analogues of Chol, when substituting Chol, limited MP1-included poration and membrane disintegration [162]. Leice et al.

reported a synergistic role of PS and PE in facilitating the membrane-disrupting MP1 effect [118]. It has been observed that MP1 incorporates into the outer leaflet of PM and generates a hole large enough for a free leakage of intracellular contents. Continuing, MP1 was capable of forming 20-30 times bigger holes in the presence of PE. Interestingly, MP1 reaches 90% of activity in up to 1 h, while common anti-cancer therapeutics need at least 12 h to 48 h [163].

2.8 Current application of AMPs

2.8.1 Medicine

Many AMPs are capable of regulating the immune system involving cell recruitment, cell proliferation, immune response modulation, wound healing, gene expression modification or cancer cell growth inhibition [164]. α-defensins HNP-1, HNP-2, and HNP-3 displayed antiviral activity against adenovirus, human papillomavirus, herpes virus, influenza virus and cytomegalovirus. AMPs were found overexpressed in pulmonary disorders, namely idiopathic pulmonary fibrosis or acute respiratory distress syndrome [6]. Some AMPs have been tested already in the third phase of clinical trials for curing wound infections [165]. Furthermore, AMPs have been proposed as prospective agents in ophthalmology and the development of antimicrobial contact lenses could aid in overcoming microbial contamination and consequent ocular-related diseases [166].

2.8.2 AMPs and breast cancer

Breast cancer has been recently announced as a global health threat being the leading cause of cancer mortality in women across the globe [167]. The classification of breast tumours is constantly evolving and new knowledge from research is

immediately implemented into clinical practice [168]. An accurate diagnosis of the cancer subtype facilitates the introduction of the proper therapy, improves its efficacy and contributes to an increased overall patient-survival ratio.

Surgery, radiotherapy, and chemotherapy are common anti-cancer therapies, however, patients may be confronted with the side effects of the treatment later in life. The degree of cancer therapy-induced toxicity depends on the level of drug exposure and the type of DNA or structural damage [169]. Therefore, AMPs, seen as the next generation of multitask drugs, are widely tested in cancer models.

Recently, the anti-cancer effect of nisin, an AMP of bacterial origin, was evaluated against a breast model [151]. Lower cytotoxicity was observed for control non-transformed cell lines in contrast to significant selectivity against MCF-7, breast cancer cells. Furthermore, nisin was investigated to enhance the cytotoxic effect of an anticancer drug, doxorubicin potentially through destabilization of the cellular membrane or pore-formation. Another example, peptide motifs derived from bovine lactoferricin, led to 50% cell growth inhibition at a concentration of 22 μM in breast cancer cells [7]. The morphological observation using electron microscopy under the one-hour exposure of breast cancer cells to amphibian temporin-1CEa revealed profound morphological changes in both MDA-MB-231 and MCF-7 cells [170]. In addition, mass spectrometry profiling of these breast cancer cell lines revealed similar lipid profile: abundance of PC(32:1), PC(30:0), and $C_{16:1}$ and down-regulation of SM(34:0), PC(38:4), PI(38:4), $C_{18:2}$, and $C_{22:4}$ relative to control (MCF-10A breast cell line) [171].

2.9 Structure and physicochemical properties of AMPs

The evolutionary ancient peptides are considered an important first defence against invading pathogens, [172]. While a diverse range of organisms produce varied AMPs in terms of structure and sequence, evolution has conserved several common physiochemical features being pivotal in their biological activity.

Generally, AMPs are synthesized in inactive forms and under certain conditions undergo conformational changes and normally vary in length from 12 to 50 amino acids [4]. A comparison of the amino acid distribution in the N-terminal region of α-helical AMPs revealed that, independently of the following residues, glycine (Gly;G) at position 1 is predominant and its role is to prevent proteolytic cleavage by aminopeptidases [173]. Although their primary sequence is highly heterogeneous, they contain an abundance of cationic residues (lysine (Lys;K), arginine (Arg;R) or histidine (His;H)), which confer a net positive charge ranging from +2 to +13 at neutral pH [106]. Furthermore, many studies demonstrated the correlation between charge and antimicrobial activity [174]. However, an increase in positively charged residues can lead also to the loss of antimicrobial selectivity and to undesirable haemolytic activity [175]. Thus, AMPs optimal activity is reportedly between +4 to +6 which does not cause unwanted haemolytic activity [173]. It was demonstrated that a net charge above +7 is linked to the strong interaction between the peptides and phospholipid groups at the membrane [176, 177]. The electrostatic interaction prevents AMP structuring and penetration of the deeper layers of membranes. Unger at al. revealed also that peptide cyclization might promote preference to negatively charged membranes over these zwitterionic when comparing to linear analogue [178]. In addition, tryptophan (Trp;W) overrepresentation facilitates membrane anchoring [179]. Papo et al. reported an interesting observation that the replacement of one-third

of the L-amino acids of an α-helical 15 residue long AMP with D-configuration resulted in reduced haemolytic activity against human erythrocytes and enhanced solubility in water, AMPs retained full microbicidal activity and the sensitivity to enzymatic degradation was lower [180].

Another key feature is hydrophobicity. Typically AMPs have a high content of hydrophobic amino acids (up to 50% or more) [181]. Too small or too large sequence hydrophobicity can inactivate the peptide [182]. Hydrophobicity can directly influence the spectrum of biological potency, cytotoxic selectivity and it drives peptide capability of incorporating into the membrane hydrophobic core [183]. Dennison et al. associated poor solubility in polar solution with accelerated lytic activity in erythrocytes of largely hydrophobic peptidic sequences [184]. In addition, peptides with a higher content of hydrophobic residues have a greater tendency for self-aggregation when compared to those with lower hydrophobicity [185].

The physiochemical features, cationicity and hydrophobicity, allow AMPs to fold into an amphipathic secondary structure, which has two “faces”- spatially separated nonpolar residues situated on one side of the molecule and hydrophilic content on the opposite face [186]. Disrupting the amphipathic conformation of AMPs can reduce efficiency and spectrum of activity [187]. Fernández-Vidal et al. indicated amphipathic nature as a more important feature than hydrophobicity in constructing synthetic AMPs targeting certain cells [188]. A minimum length of 7-8 amino acids is required to adapt an amphipathic structure [107]. Liu et al. investigated the role of sequence length on microbicidal activity, testing a range of peptides constituting simple sequence repeats, (RW)n-NH2 (where n = 1, 2, 3, 4, or 5) [189]. The antimicrobial and haemolytic activities of variants proportionally increased along with a number of amino acid residues. An odd number of residues, particularly 11 residues

of Lys homopeptides, has been found to potentiate the inhibitory effect against Gram-positive bacteria at a concentration of 10 μM [190]. There was no cytotoxicity of 11 residues Arg homopeptides even at concentrations as high as 100 μM, however, when the peptide length reached 12, a drastic increase in specificity towards eukaryotic cells was observed. It is believed that amphiphilicity allows cationic AMPs to bind with anionic membrane lipids through electrostatic interactions [191]. The summary of structural and physiochemical determinants of AMPs activity is in below Figure 14.

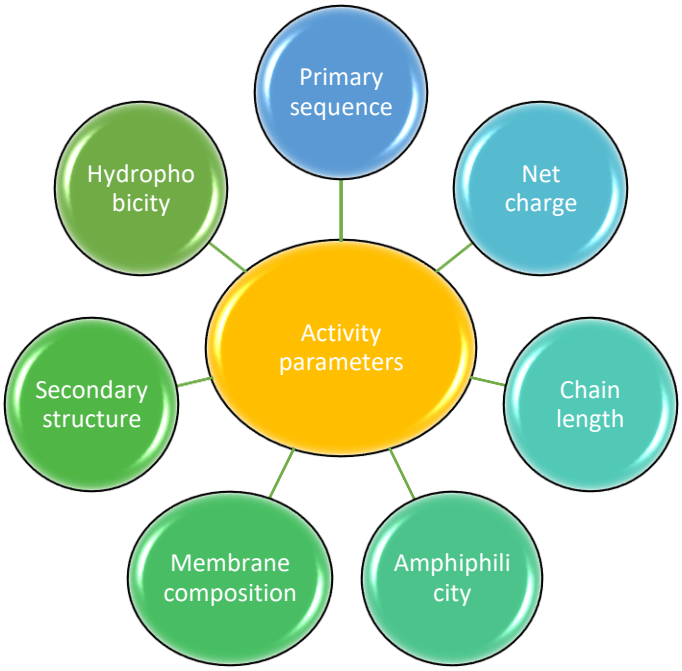

Figure 14 The interplay between structural and physicochemical determinants modulates the biological activity of AMPs [192]. Amino acid residues are fundamental building blocks of AMPs. Primary sequence of microbicidal peptides was found abundant in amino acids with charged side chains, such as Lys, Arg or His, which confer molecule a net charge. Hydrophobic residues are also greatly presented in AMPs sequence defining AMPs hydrophobicity. The content of both hydrophilic and hydrophobic residues makes molecule amphiphilicity and allows formation into secondary structure when gets activated. AMPs are triggered in the presence of pathogens, particularly sense specific membranes which are enriched in negative components. AMPs sequence varies in amino acid chain length and its determines peptide mode of action.

Aims and objectives

The overall hypothesis of the project is that the efficacy of MP1 as a membrane-lysing peptide is defined by specific elements of the sequence of MP1 itself and the constituents of the membrane upon which it is acting. Therefore, the following aims of the project are:

1) To understand the contribution of individual residues and groups of residues within MP1 to its membrane lysing action;
2) To identify MP1 derivatives with higher specificity and potency in model membrane systems;
3) To develop giant plasma membrane vesicles (GPMVs) as a model membrane system;
4) To use GPMVs and define how MP1 changes membrane properties;
5) To define how MP1 sensitivity correlates with the expression of individual genes in mammalian cancer cells, and assess whether individual genes determine sensitivity.

Results

Results

Chapter 2 Peptide mutant screening- identifying the contribution of specific key amino acid residues to the biological activity of MP1 and potent variants to biomedical application

ABSTRACT

AMPs are believed to become the next-generation therapeutics in many biomedical fields. Venom-sourced peptide, Polybia MP1, was previously reported to display not only microbicidal activity but also an inhibitory effect on proliferating cancer cells of different types. However, little is known about the molecular basis of MP1 activity. To identify the role of each amino acid residue in anticancer activity, MP1 mutants were designed and synthesized to test variations in their charge, amphiphilicity and hydrophobicity in model artificial membrane systems. Overall, studies reported that an increase in a net charge does not always correlate with enhanced potency and hydrophobicity might promote specificity against PS-enriched system. pH-responsive variants are other prospective peptides which target tumour-specific microenvironment. These findings expand the understanding of the structure-function relationship in MP1 lytic activity. Peptide mutant screening allowed for the identification of potent variants for further testing in models of increased complexity.

2.1 Introduction

AMPs prospective use has been found restricted due to: (1) adverse haemolytic activity; (2) high sensitivity to proteolysis; (3) stability in particular pH, and ion content; or (4) rising production cost. Given the potential of AMPs for managing to meet the current multidrug resistance crisis, much effort has been put into exploring AMPs mechanism of action and their rational redesign. However, design optimization should interplay between

the following five aspects: chain length, secondary structure, net charge, amphiphilicity and hydrophobicity. A site-directed mutation is one of the specific methods of natural AMPs redesign by adding, replacing or deleting one or more amino acid residues which allows for the identification of molecular determinants in peptide activity and potent variants. [186]. Migoń et al focused on aurein 1.2, the shortest naturally-sourced AMP, and correlated lesser antimicrobial activity to the different locations of aromatic rings crucial in membrane anchoring. Sajjadiyan et al. assigned phenylalanine (Phe;P) and lysine residues to play a crucial role in absorbing water molecules into the membrane [193]. Cecropin, magainin, or lactoferrin were used as AMP patterns in the template-based design method to find conservative homologous fragments [194]. Furthermore, chemical modifications such as phosphorylation, the addition of D-amino acids or unnatural amino acids (homoarginine), cyclization, halogenation, or acetylation might have a protective effect on peptides and prevent protease degradation [195]. Therefore, there are various strategies aiming at upgrading AMPs bio-activity.

Tumour-specific features are regarded as prospective factors in the design of novel therapeutics. Tumour physiology characterized by an acidic microenvironment is developing due to hypoxia and abnormal metabolism as opposed to normal tissue [196–198]. The pH-responsive peptides were already introduced, aiming at improving the selectivity based on the tumour extracellular environment [199]. Histidine modification allows peptides to undergo pH-triggered charge conversion since histidine could protonate into positive charge in the acidic microenvironment from mostly no charge in tissue at physiological state [200]. Therefore, potential cytotoxicity is overcome as the peptide activates in acidified surroundings.

Although AMPs have multiple targets, it is believed that the AMPs are electrostatically attracted to negatively charged plasma membranes of bacterial or transformed cells due to

their greater content of anionic phospholipids on the outer leaflet of the membrane. Unlike healthy cells, malignant cells lose asymmetric lipid distribution which implies an increase of anionic lipids content on the outer cell membrane which is seen in Figure 15 [201]. Of note, the extent of PS exposure on the outer leaflet differs considerably between different types of cancer cells and this variability is seen even within the same cancer type [202]. PS is investigated as a cancer biomarker for cancer imaging and therapy [22]. However, AMPs are still capable of interacting with eukaryotic membranes, typically zwitterionic, by partitioning into the hydrophobic core of lipid bilayer [203]. Hydrophobic interaction between the apolar residues of an amphipathic peptide and zwitterionic membrane phospholipids mainly drives the interaction of AMPs with mammalian cell membranes. In some cases, such as PE, better accessibility of the phosphates of the lipids to the cationic peptide, provides stronger binding relative to PC [204].

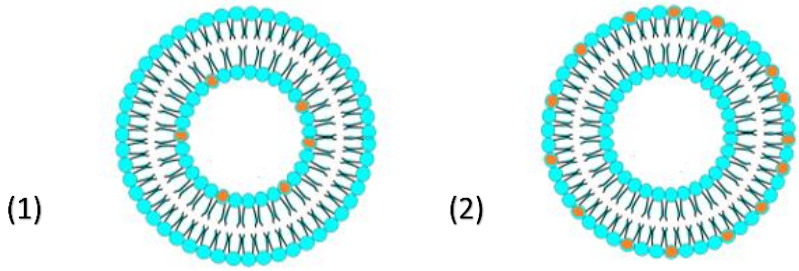

Figure 15 The schematic representation of healthy (1) and transformed (2) cell plasma membrane. Blue elements indicate uncharged phospholipid headgroups. The orange circles represent anionic lipid head groups.

The steric effect applies to the lipid headgroups organization, which induces stress on the membrane from lipid crowding interactions, and generates positive curvature strain along the peptide and the membrane bends toward the interior [205]. A high-throughput screen is widely applied to determine the effects of membrane-interacting peptides on membrane integrity [206–209]. Artificial lipid vesicles are a common choice as a model

membrane mimicking a minimal membrane system ideal for testing principal concepts. Typically, large unilamellar vesicles (LUVs) with diameters 100–1000 nm in suspension allow for monitoring the average fluorescence of the LUVs population and provide measurements of the average leakage kinetics. In addition, the simple preparation of vesicles and the availability of principal lipid membrane compounds support studies in systems of different compositions. This approach aids the investigation of changes driving lipid-associated diseases [210].

In this work, numerous design strategies are employed in order to synthesize MP1 variants to perform a comprehensive analysis of each structural element and identify peptide motifs with better therapeutic applicability. The suitable model to study membrane puncturing is the LUV lipid system which is a simple and cost-effective platform. Therefore, the incorporation of lysine and other hydrophobic residues into the hydrophilic face of a peptide was found much improving its activity. pH-triggering mutants exhibited higher potency in an acidified environment, while native MP1 was less active. Interestingly, some mutants not only displayed greater potency but also specificity in PS systems and are prospective candidates for *in vitro* testing in breast cell models. Thus, sequence ordering and physiochemical characterisation of each building block represent a unique biological signature balancing peptide action.

2.2 Materials and Methods

2.2.1 Materials

2.2.1.1 Lipid components

DOPC (1,2-dioleoyl-sn-glycero-3-phosphocholine) and DOPS (1,2-dioleoyl-sn-glycero-3-phospho-L-serine were purchased from Avanti Polar Lipids Inc (Alabaster, AL,

USA). NaCl and HEPES (4-(2-Hydroxyethyl) piperazine-1-ethanesulfonic acid, N-(2-Hydroxyethyl) piperazine-N′-(2-ethanesulfonic acid)) was obtained from Sigma Aldrich Co. (Gillingham, Dorset, UK).

2.2.1.2 Solvents

Organic solvents: chloroform ($CHCL_3$), methanol (CH_3OH), ethanol (C_2H_5OH) were used to prepare liposomes lipid stock solutions (25 mg/mL) and were obtained from Sigma Aldrich Avanti Polar Lipids with a purity >99%.

2.2.1.3 Peptides

Peptides were synthesized by the external organization Biosynthesis (Lewisville, TX, USA) using the standard solid-phase 9-fluorenylmethoxy carbonyl (Fmoc) method. Their sequences with molecular weight are presented in Table 3. Peptides underwent quality control. Observed purity was >97% judged by analitycal RP-HPLC and calculated mass was based on mass spectroscopy analysis (see Appendix 1 for a representative Certificate of analysis).

Table 3 Sequences and molecular weight of Polybia MP1 and the peptide library. Each MP1 variant is termed depending on the position of mutation- the first letter stems from the replaced amino acid, the following number is its sequence position starting from the N-terminal end and the latter letter represents incorporated residue. The peptide mutation in the amino acid sequence is marked by red

Peptide	Sequence	Molecular weight
First round of peptide mutants		
MP-1 sequence	IDWKKLLDAAKQIL	1654.02
I1A	ADWKKLLDAAKQIL	1611.94
D2A	IAWKKLLDAAKQIL	1610.01
W3A	IDAKKLLDAAKQIL	1538.89
K4A	IDWAKLLDAAKQIL	1596.93
K5A	IDWKALLDAAKQIL	1596.93

L6A	IDWKKALDAAKQIL	1611.94
L7A	IDWKKLADAAKQIL	1611.94
D8A	IDWKKLLAAAKQIL	1610.01
K11A	IDWKKLLDAAAQIL	1596.93
Q12A	IDWKKLLDAAKAIL	1596.97
I13A	IDWKKLLDAAKQAL	1611.94
L14A	IDWKKLLDAAKQIA	1611.94
K4H	IDWHKLLDAAKQIL	1662.99
K5H	IDWKHLLDAAKQIL	1662.99
K11H	IDWKKLLDAAHQIL	1662.99
A9Q	IDWKKLLDQAKQIL	1711.07
L7K	IDWKKLKDAAKQIL	1669.04
A9K	IDWKKLLDKAKQIL	1711.12
Q12K	IDWKKLLDAAKKIL	1654.07
I13K	IDWKKLLDAAKQKL	1669.04
The second round of peptide mutants		
I1W	WDWKKLLDAAKQIL	1728.08
insl	IIDWKKLLDAAKQIL	1768.18
MP1-Ac	IDWKKLLDAAKQILAc	1697.07
3K->3H	IDWHHLLDAAHQIL	1681.93
DDQKKK->6H	IHWHHLLHAAHHIL	1735.04
3K->3R	IDWRRLLDAARQIL	1739.06
A10L	IDWKKLLDALKQIL	1697.10
A10W	IDWKKLLDAWKQIL	1770.16
D2K	IKWKKLLDAAKQIL	1668.11
D8K	IDWKKLLKAAKQIL	1668.11
D2V	IVWKKLLDAAKQIL	1639.07
L6W	IDWKKWLDAAKQIL	1728.08
L6V	IDWKKVLDAAKQIL	1641.01
L7W	IDWKKLWDAAKQIL	1728.08
W3I	IDIKKLLDAAKQIL	1581.97
W3F	IDFKKLLDAAKQIL	1615.99
DDQ->3K	IKWKKLLKAAKKIL	1739.06

2.2.2 LUVs preparation

Liposomes were composed of PC or PC:PS (80:20 %mol) and encapsulated solution of 120 mM carboxyfluorescein (CF). They were prepared according to the following protocol: 25 mg/mL stock solutions in chloroform were mixed in the proper ratio (427 µL of PC and 377 µL of PC/ 97.2µL of PS) and put into round bottom flasks. Solutions were dried under a gentle flow of nitrogen and to each vial, 1 mL of CF in 10 mM HEPES (pH 7.4 or 6.5) was added. The mixture was shaken for 5-10 min at room temperature to obtain a suspension of MLVs and freeze-thawed 5 times. LUVs were formed by extruding the lipid suspension 11 times through two stacked 400nm polycarbonate filters using Avastin LF-1 extruders (Biopharma Process systems, UK). After the extrusion process, liposomes were separated from unencapsulated fluorophores by size exclusion chromatography on a Sephadex G25M column (GE Healthcare Bio-Sciences AB, Uppsala, SE). Liposomes were diluted by varying amounts on the SEC column. Vesicles were used immediately after preparation. The final lipid concentration was measured by colourimetric total phosphorus assay [211].

2.2.3 Leakage assay

Membrane-active peptides partition into membranes after reaching a threshold concentration and disrupt the lipid bilayer. Therefore, their activity depends on the peptide: lipid ratio (P:L). To test this idea the serial dilution assay was programmed for a Hamilton Microlab Star M liquid handling robot (Hamilton robotics Ltd.) during which peptides were added to CF-encapsulated LUVs in microplates (384-well black OptiPlate, PerkinElmer LAS (UK) Ltd). Peptide stock solutions were prepared fresh from lyophilised powder dissolved in the deionised water and concentration was determined by tryptophan absorbance using a Nanodrop spectrophotometer at 280 nm. CF, which is a water-soluble

fluorophore, entrapped in lipid vesicles at sufficiently high concentration, its fluorescence is almost completely quenched by the interaction between surrounding fluorophore molecules (Figure 16). Therefore, when CF release occurs, the increased level of fluorescence is used to assess peptide activity.

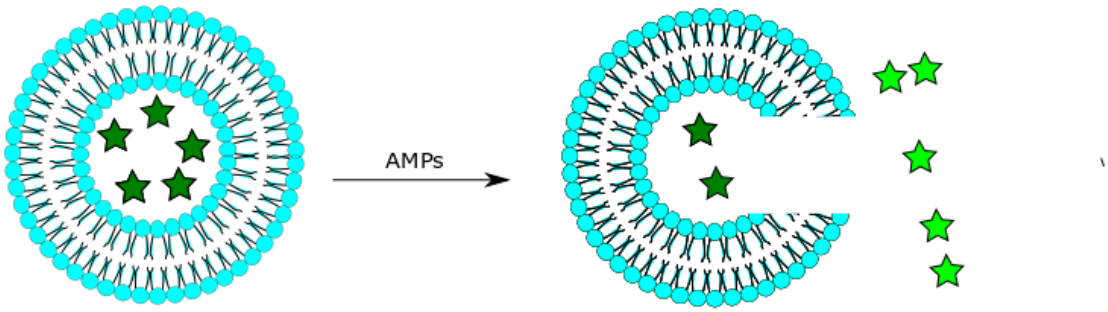

Figure 16 Illustration of the principle of lipid vesicle-based permeability assay. Dark green stars represent CF at self-quenching concentration and bright green stars reflect peptide-induced CF release which is proportional to the degree of membrane disruption.

The first column had a fixed total P:L molar ratio (1:50), but from the top to bottom rows peptide concentration (solution into HEPES buffer) decreased 1.3 times in each well in the row testing 23 peptides concentration starting with 20 μM concentration. The intensity for complete leakage was determined by adding 0.6 mM Triton X-100 to control wells containing fixed lipid concentration (1 mM). Fluorescence intensity was recorded from the final assay plate using an EnVision plate reader (PerkinElmer, Waltham, MA) equipped with a 360 nm excitation filter and a 585 nm emission filter [212]. To further compare results to experiments performed in live cell models, CF leakage was quantified in analogy to IC_{50} calculation in cell studies; the corresponding 50% leakage value was peptide concentration inducing a 50% fluorescence value of that obtained from a positive control when vesicles were treated with the detergent Triton-X 100. The curve fitting was conducted with an exponential growth function and 50% percentage leakage was obtained

from equation $y=A1*\exp(x/t1)+ y_o$ as a function of concentration using the analysis software OriginPro 9.1 (OriginLab Corporation). The carboxyfluorescein fluorescence dequenching procedure and the application of a liquid handling robot for screening of peptides were optimized by Dr Andrew Booth and Dr Dede Siregar.

2.3 Results

A number of MP1 variants were developed to expand the structure-function exploration of molecular determinants in MP1 activity. A rational peptide design approach addressed physiochemical features such as net positive charge, hydrophobicity, amphiphilicity and corresponding helical content. MP1, upon exposure to biological membranes, adapts a secondary structure and the projection of residue arrangement is illustrated in Figure 17. The membranotropic activity was studied in homogenous lipid models composed of DOPC and DOPC: POPS

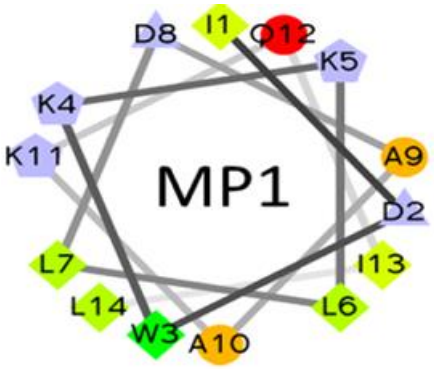

Figure 17 Helical wheel projection of Polybia MP1. Helical wheel projection is used to reflect the secondary structure of the peptide. Polybia MP1, wets activated, forms α-helix having two faces- hydrophilic and hydrophobic. Amino acid constituents are labelled by different colours reflecting different characteristics of the amino acid side chains: purple: polar, charged; red: polar, uncharged; orange: non-polar with aliphatic group; light green: non-polar with aliphatic group (more extended and with greater hydrophobicity) and dark green: non-polar with aromatic group.

2.3.1 Alanine-scan screening determines the contribution of each amino acid residue.

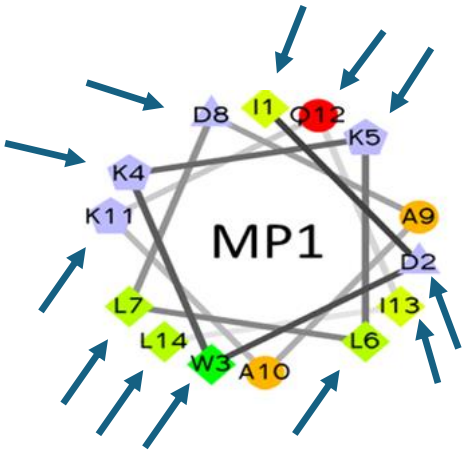

Peptide name	Sequence
MP-1	IDWKKLLDAAKQIL
I1A	ADWKKLLDAAKQIL
D2A	IAWKKLLDAAKQIL
W3A	IDAKKLLDAAKQIL
K4A	IDWAKLLDAAKQIL
K5A	IDWKALLDAAKQIL
L6A	IDWKKALDAAKQIL
L7A	IDWKKLADAAKQIL
D8A	IDWKKLLAAAKQIL
K11A	IDWKKLLDAAAQIL
Q12A	IDWKKLLDAAKAIL
I13A	IDWKKLLDAAKQAL
L14A	IDWKKLLDAAKQIA

Figure 18 Peptide mutants with sequence and helical wheel projection. Each MP1 analogue is termed depending on the position of mutation- the first letter stems from the replaced amino acid, the following number is its sequence position starting from the N-terminal end and the latter letter represents the substituted residue. The peptide mutation in the amino acid sequence is marked by red. Blue arrows on the helical wheel projection indicate substitutions.

The library of peptides with alanine substitution at each position, independently, was designed to assess the role of the side chain of each amino acid in Polybia MP1 lytic activity. Alanine, which a side chain is the smallest among all-natural amino acids, is widely used as backbone control and alanine substitution evaluates the contribution of individual amino acid side chains to the functionality of peptides or proteins [213]. Figure 18 shows peptide mutant sequences and arrows on the helical wheel projection indicate points of substitution. Peptides were dosed into CF-loaded model systems in a range of

concentrations and membranolytic potency was determined by the measurement of fluorescence intensity. The peptide activity reflects concentration (μM) inducing a 50% leakage value of that obtained from a positive control. The leakage distribution is presented in the dose-response curves and the percentage of leakage as a function of peptide concentration showed exponential profiles for peptides tested in zwitterionic (PC) and anionic (PC:PS) model lipid vesicles. The representative dose-response curves in model systems as seen in Figure 19A (PC) and Figure 19B (PC:PS). The shape of the curves indicates that after the initial lag phase, the percentage of fluorescence intensity increases at an exponential rate, then slows down and eventually reaches a plateau. It could be explained by that peptide accumulation requires a certain threshold in order to initiate puncturing activity and when it is reached, fluorescence intensity grows and achieves a plateau with system saturation.

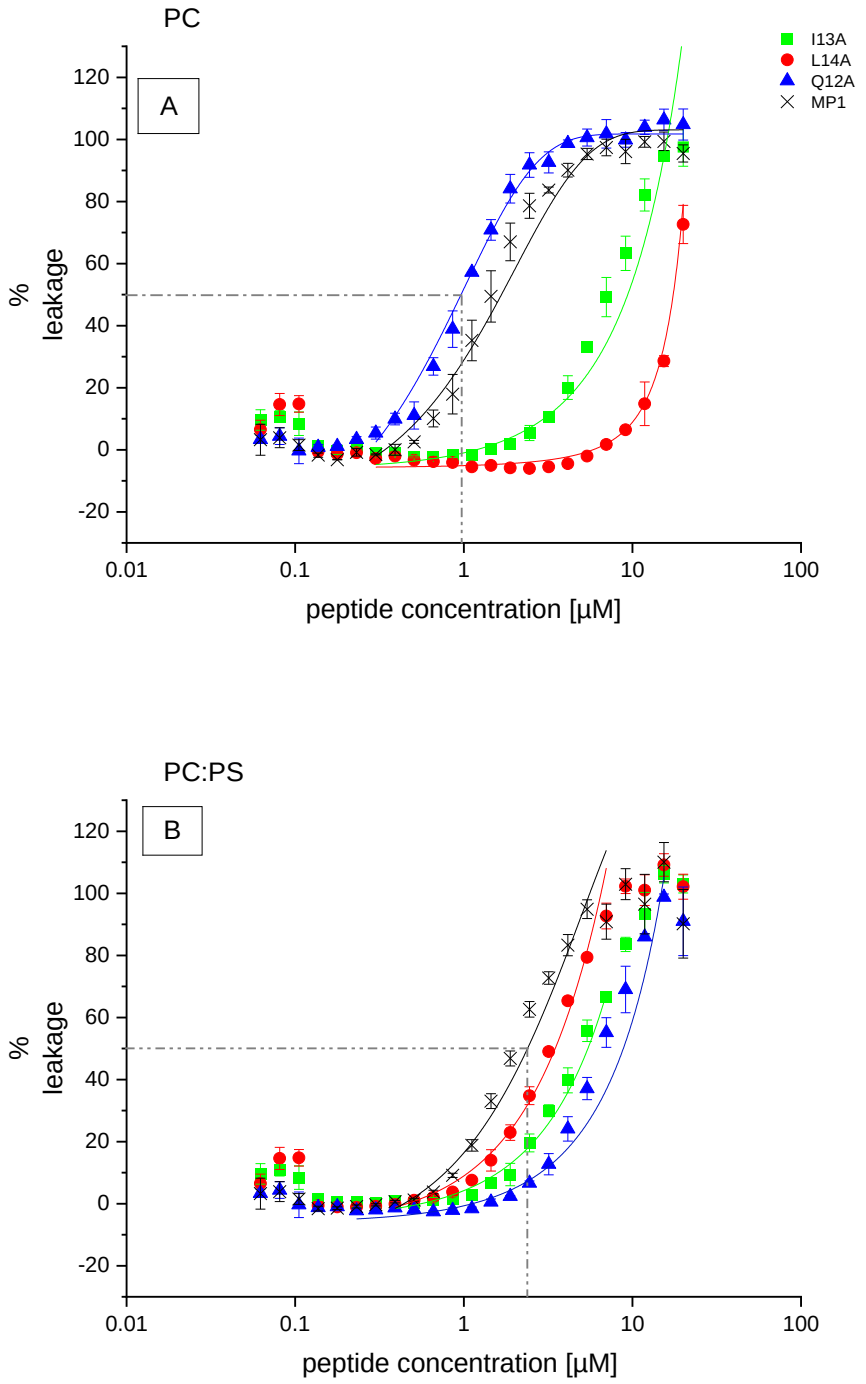

Figure 19 The representative of raw leakage assay data. I13A, L14A and Q12A mutants along with MP1 were tested in PC (A) and PC:PS (B) lipid systems. Peptide concentration is shown along the X-axis, the percentage of dye leakage of each peptide is represented on the Y-axis. The curve fitting was conducted with an exponential growth function which indicates that after the initial lag phase, the fluorescence intensity increases at an exponential rate and slows down to eventually reach a plateau. Error bars represent ±SEM from three replicate measurements.

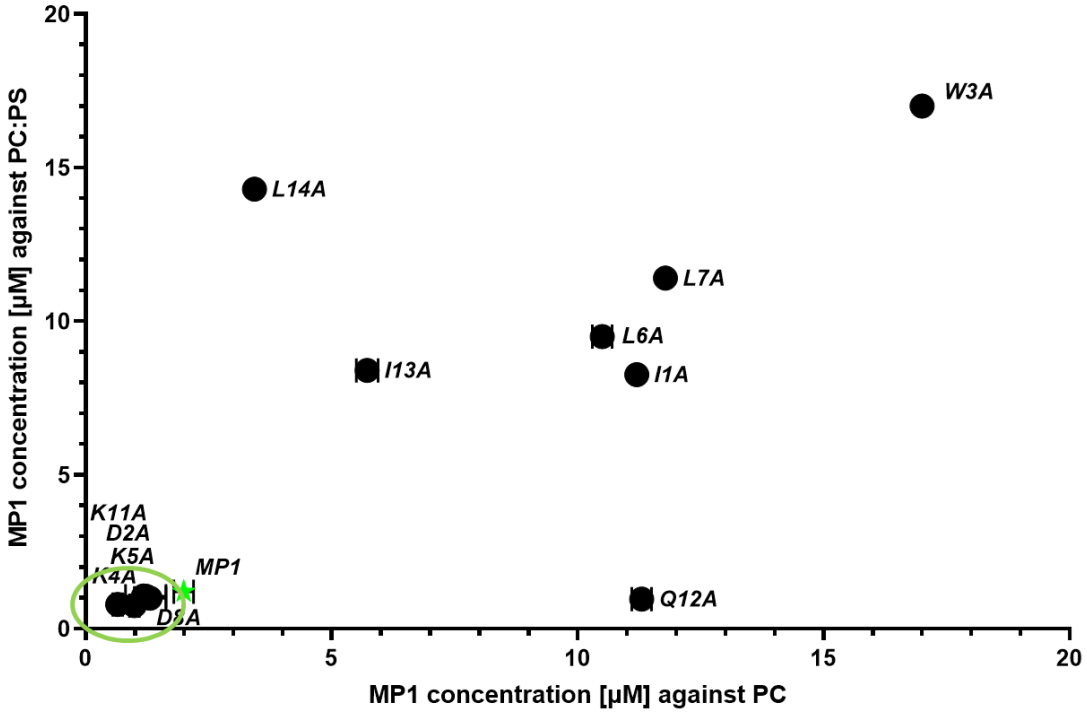

Figure 20 Leakage assay data calculated based on raw data represented in Figure 19. Each data point illustrates the concentration (µM) of peptide inducing 50% leakage (relative to CF emission spectrum after treatment with Triton X-100 performing an alanine scan against the PC **(**X-axis) and PC/PS (Y-axis) model vesicles. Green spot marks MP1 data. Green circle and surrounded peptide mutants are more potent and/ or specific relative to MP1. Error bars represent ±SEM from three replicate measurements. The raw leakage data are presented in Appendix 2.

The concentrations of peptide mutants needed to induce a 50% leakage value are demonstrated in Figure 20. The concentration range corresponds to lytic activity- more potent variants require lower concentration for leakage-inducing performance. In this study, peptide activity is termed specific when the value obtained from the PS-enriched model differs significantly from that of pure PC. Therefore, points situated above MP1

indicate MP1 derivatives less active to the native peptide -along the X-axis, in the PC system and the Y-axis, in the PC:PS model.

Substitution analysis with alanine showed that the replacement of residues situated on the hydrophilic face of peptide, namely, the aspartic acid at positions 2 and 8, lysine at 4, 5 and 11, independently, resulted in a significant enhancement in peptide activity in both neutral and anionic models. Those alternations are associated with increased hydrophobicity due to the hydrophobic nature of alanine. In addition, the aspartic acid replacement confers to a higher net charge (+3) of a variant. Likewise, lysine-substituted derivatives which are less cationic (+1) exhibited similar potency. Therefore, these amino acid residues are important in balancing peptide specificity against PS models. Their substitution with alanine led to an increase in hydrophobic content and accelerated the potency. Q12A mutant showed boosted specificity to PC:PS model, and simultaneously, its lytic capability in PC was much decreased. Glutamine (Gln;Q) at position 12 is located in the hydrophilic region of the molecule. Therefore, this residue is important for MP1 PS-specific activity. Conversely, single Ala-substitution of tryptophan, leucine and isoleucine, independently, substantially reduced peptides activity in both model systems. Tryptophan replacement resulted in the greatest activity reduction indicating its key role in MP1 activity. Modifications of the hydrophobic face of the peptide are likely to destabilize the secondary structure changing the amphipathic balance. Isoleucine substitution at position 1, as opposed to other hydrophilic face residues, led to a decrease in peptide activity. This might be associated with a hydrophobic nature of Ile. Therefore, a range of concentrations reflecting the lytic activity of these peptides suggests that each amino acid has its own contribution to the MP1 mechanism of action.

2.3.2 Charge modification does not always correlate with increased potency

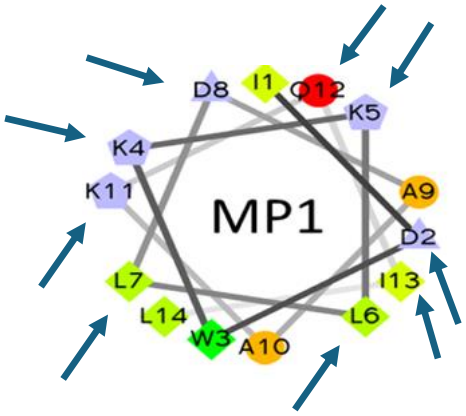

Peptide name	Sequence
MP-1	IDWKKLLDAAKQIL
L7K	IDWKKLKDAAKQIL
A9K	IDWKKLLDKAKQIL
Q12K	IDWKKLLDAAKKIL
I13K	IDWKKLLDAAKQKL
3K->3R	IDWRRLLDAARQIL
D2K	IKWKKLLDAAKQIL
D8K	IDWKKLLKAAKQIL
DDQ->3K	IKWKKLLKAAKKIL

Figure 21 Peptide mutants with sequence and helical wheel projection. Each MP1 analogue is termed depending on the position of mutation- the first letter stems from the replaced amino acid, the following number is its sequence position starting from the N-terminal end and the latter letter represents substituted residue. The peptide mutation in the amino acid sequence is marked by red. Blue arrows on the helical wheel projection indicates substitutions.

In order to investigate the role of a net charge in MP1 activity, lysine and arginine mutants were redesigned and tested in model systems which primary sequence and helical wheel projection are seen in Figure 21. Overall, Lys is more prevalent in natural venom wasps [214]. More hydrophobic Arg typically confers a tendency to haemolytic effect [215]. Although both, Lys or Arg, are positively charged at physiological pH, the p*K*a values of Arg (12.45) and Lys (10.5) are different followed by differentiating protonation states in the membrane environment. Mathematical calculations predict that Arg might retain protonation in the lipid acyl tail region of the membrane, whereas Lys appears deprotonated in the bilayer centre [216, 217]. Furthermore, Arg-rich peptides are known to have stronger interactions with membranes as a matter of the high p*K*a and hydrogen

bindings of Arg [218]. The concentrations of a panel of peptides designed for charge screening which cause 50 % leakage are demonstrated in Figure 22.

Charge modification revealed a distinct effect on peptide activity depending on the substitution position. Peptide variants, D2K, D8K, Q12K, DDQ->3K, which are charge modified at the hydrophilic face, exhibited much-increased potency than that of native MP1. However, accelerated potency is accomplished with the loss of specificity as a similar concentration inducing 50% leakage was detected in both models. Among these variants, Q12K, a peptide with Gln-to-Lys mutation, showed great specificity displaying improved activity in the leakage test. A9K variant and lysine incorporation at position 9 led to a substantial decrease in peptide activity revealing the important role of alanine. In contrast, charge incorporation into the. hydrophobic side of the MP1 resulted in a substantial decrease in membranolytic activity both in zwitterionic and anionic models. L13K MP1 derivatives were more than 10-fold less potent than unmodified MP1. Therefore, the hydrophobic content and molecule amphipaphicity modulate MP1 activity. The impaired hydrophobic face of the peptide suppresses the potency, although additional charged residue is incorporated. 3K->3R variant and lysine conversion to also positively charged arginine resulted in the loss of specificity to PC: PS models with overall increased potency. This observation might be a consequence of excessive electrostatic interaction between the guanidinium group of Arg and zwitterionic phospholipids [219].

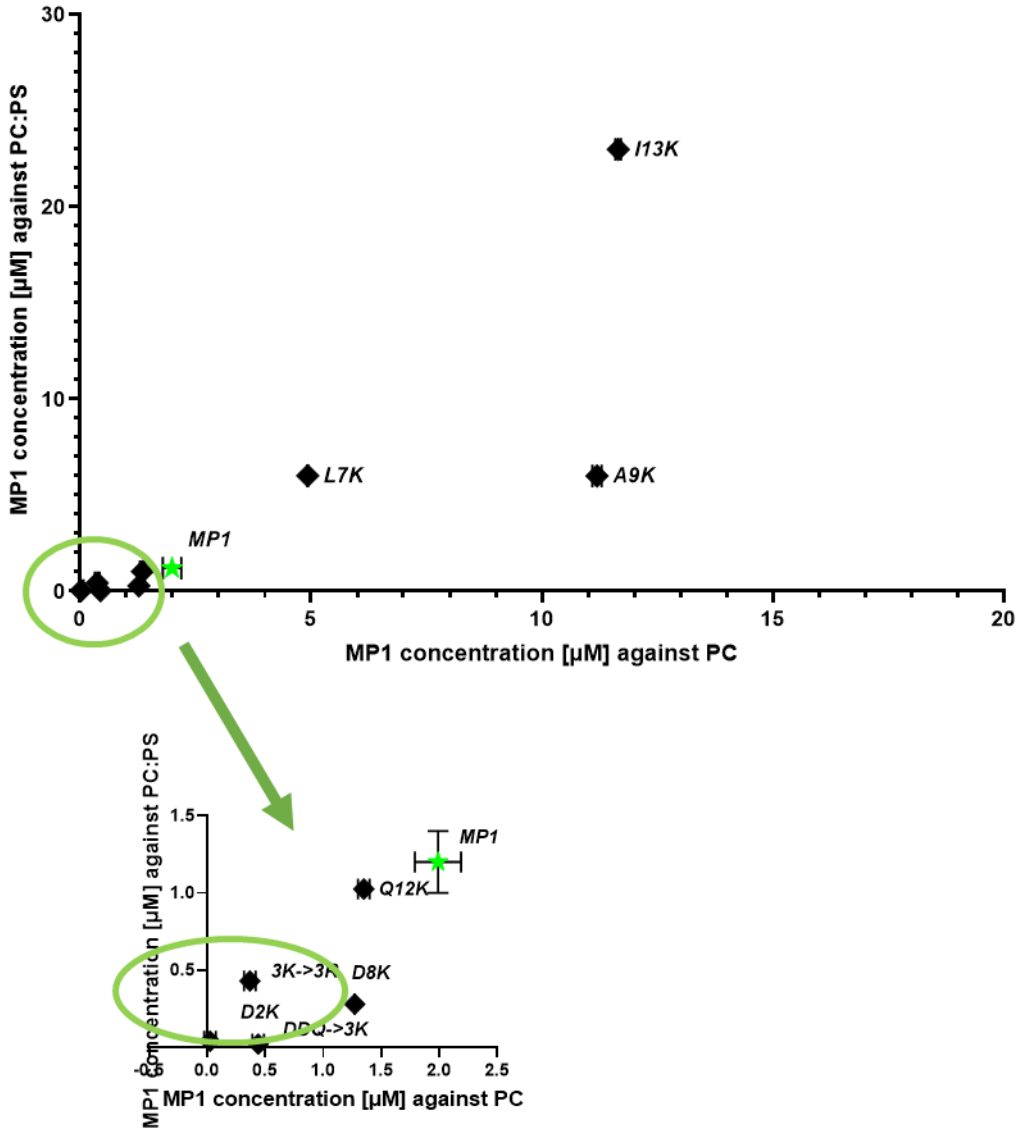

Figure 22 Leakage assay data: charge screening. Each data point stems from the concentration (µM) of peptide required to induce 50 % leakage of CF (relative CF release after Trition-100 treatment) against the PC **(**X-axis) and PC/PS (Y-axis) model vesicles. Green spot marks MP1 data. Green circle and surrounded peptide mutants are more potent and/ or specific relative to MP1. Error bars represent ±SEM from three replicate measurements. The raw leakage data are presented in Appendix 2.

2.3.3 Coiled- coil motif as another chemical modification

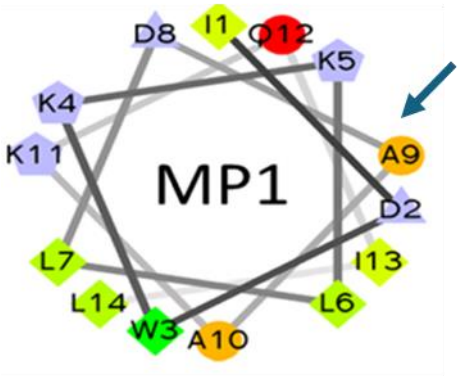

Peptide name	Sequence
MP-1	IDWKKLLDAAKQIL
A9Q	IDWKKLLDQAKQIL

Figure 23 Peptide mutants with sequence and helical wheel projection. Each MP1 analogue is termed depending on the position of mutation- the first letter stems from the replaced amino acid, the following number is its sequence position starting from the N-terminal end and the latter letter represents substituted residue. The peptide mutation in the amino acid sequence is marked by red. Blue arrows on the helical wheel projection indicates substitutions.

The A9Q variant was designed to investigate the glutamine effect, which might be crucial in promoting the association of peptides [220]. Figure 23 shows a change in primary sequence of a peptide mutant and a projection of helical wheel. Importantly, α-helices oligomerize into coiled coil, one of the best-studied protein-protein interaction motifs [221]. The formation of glutamine polar zippers was demonstrated between neighbouring β-sheets via their side-chain hydrogen bonding which aids to stabilize the structure [222]. Redesigned peptide exhibits lower potency compared to the native peptide but is highly specific to model-transformed membranes (see Figure 25). Gln side chain constitutes both an oxygen atom which can accept a hydrogen bond and a nitrogen atom which can act as a hydrogen bond donor as seen in Figure 24 [223]. Because glutamine is capable of forming

two hydrogen bonds simultaneously, a hydrogen bond network can be built between many peptides, which stabilize the cluster [224].

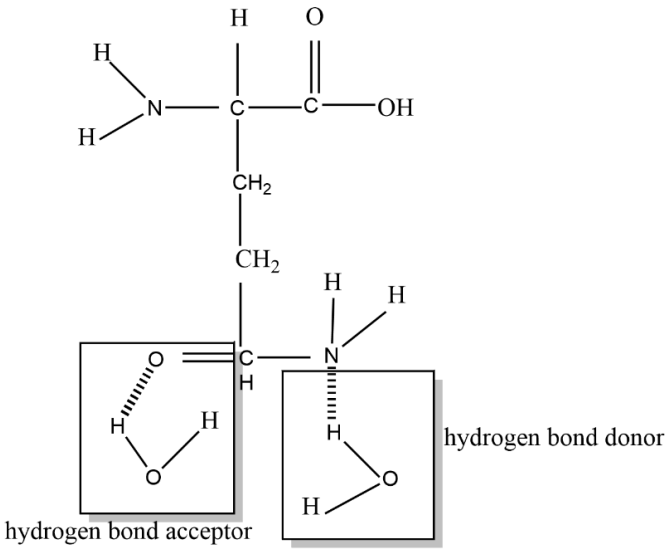

Figure 24 Examples of hydrogen bond donating and hydrogen bond accepting groups presented on glutamine residue. Drawn using ChemDraw (Revvity Signals Software, Inc. 2024).

The results suggest an important role of Gln residue in the interaction with the PS-containing system. Although Ala9 is a compound of the hydrophilic face of the peptide, alanine is a hydrophobic residue. The substitution to hydrophilic Gln broadens the polar character of the peptide and, in addition, provides potential glutamine-glutamine interaction.

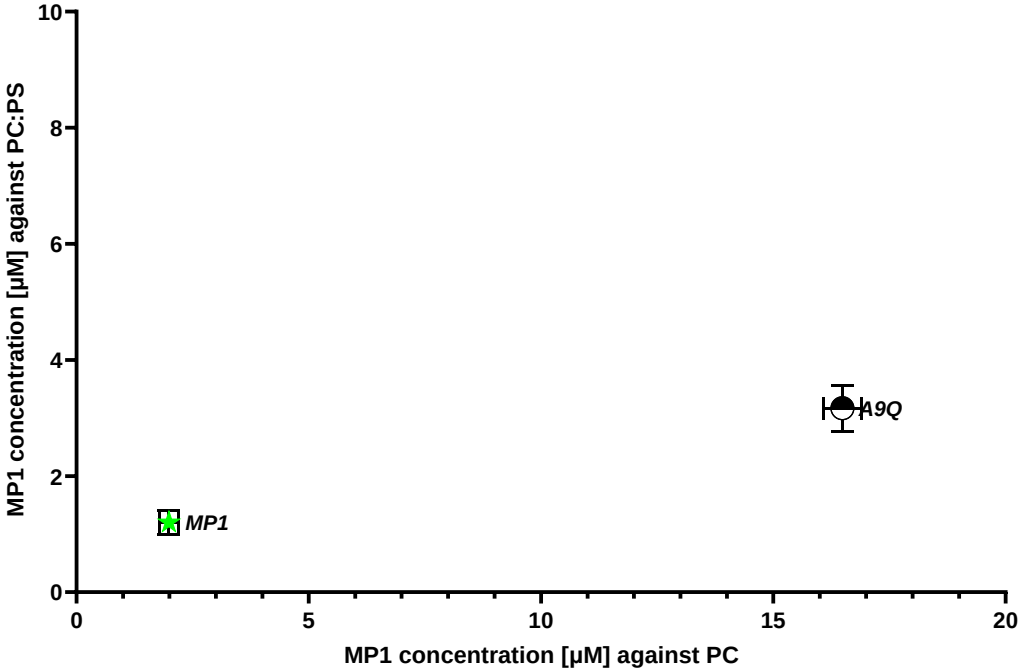

Figure 25 Leakage assay data: polar-zipper effect. Each data point stems from the concentration (µM) of peptide required to induce 50 % leakage of CF (relative CF release after Trition-100 treatment) against PC and PC:PS models. Green spot marks MP1 data.. Error bars represent ±SEM from three replicate measurements. The raw leakage data are presented in Appendix 2.

2.3.4 Tuning hydrophobicity can improve the potency and specificity

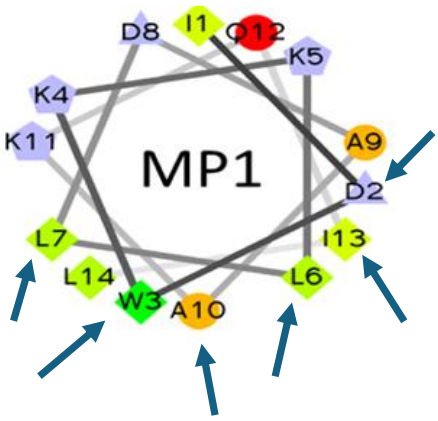

Peptide name	Sequence
MP-1	IDWKKLLDAAKQIL
I1W	WDWKKLLDAAKQIL
insl	IIDWKKLLDAAKQIL
MP1-Ac	IDWKKLLDAAKQILAc
A10L	IDWKKLLDALKQIL
A10W	IDWKKLLDAWKQIL
D2V	IVWKKLLDAAKQIL
L6W	IDWKKWLDAAKQIL
L6V	IDWKKVLDAAKQIL
L7W	IDWKKLWDAAKQIL
W3I	IDIKKLLDAAKQIL
W3F	IDFKKLLDAAKQIL

Figure 26 Peptide mutants with sequence and helical wheel projection. Each MP1 analogue is termed depending on the position of mutation- the first letter stems from the replaced amino acid, the following number is its sequence position starting from the N-terminal end and the latter letter represents substituted residue. The peptide mutation in the amino acid sequence is marked by red. Blue arrows on the helical wheel projection indicates substitutions.

As demonstrated above, hydrophobic content in the MP1 sequence is one of the key aspects determining its membrane-perturbing action. Therefore, the hydrophobicity effect was further examined by testing a series of peptide variants with modified hydrophobicity and amino acid substitutions are seen in Figure 26. The peptide concentrations inducing 50% leakage in PC and PC:PS models are shown in Figure 27.

D2V variant of aspartic acid substitution to hydrophobic valine (Val;V) showed boosted potency, alike other Asp mutants. Therefore, Asp substitution, regardless of the incorporation of hydrophobic alanine (D2A, D8A) or cationic lysine (D2K, D8K)

substantially accelerates peptide potency with the loss of specificity. Overall, L6V, L6W, L7W, A10W and A10L expressed similar effect. These mutants present alternations to the hydrophobic face of MP1. More hydrophobic residues, such as leucine, valine or tryptophan are expected to form more hydrophobic interactions which might stabilize peptide structure or facilitate lipid-peptide interaction. Interestingly, additional leucine residue incorporated into the insL mutant resulted in accelerated activity and greater capability to penetrate the PC:PS system. MP1-Ac with N-terminal acetylation exhibited slightly boosted potency with preserved specificity to PS-rich models. N-terminus acetyl group also addes hydrophobic content to the peptide motif. Thus, MP1 variants, such as MP1-Ac or insL, are promising candidates for further examination.

Ala-scan screening identified tryptophan residue substitution as substantially quenching peptide activity. However, Trp-to-Phe replacement and exchange to another aromatic amino acid residue indicated only a 2-fold drop in activity. The Trp-to-Leu mutant exhibited a 4-fold smaller activity to unmodified MP1.

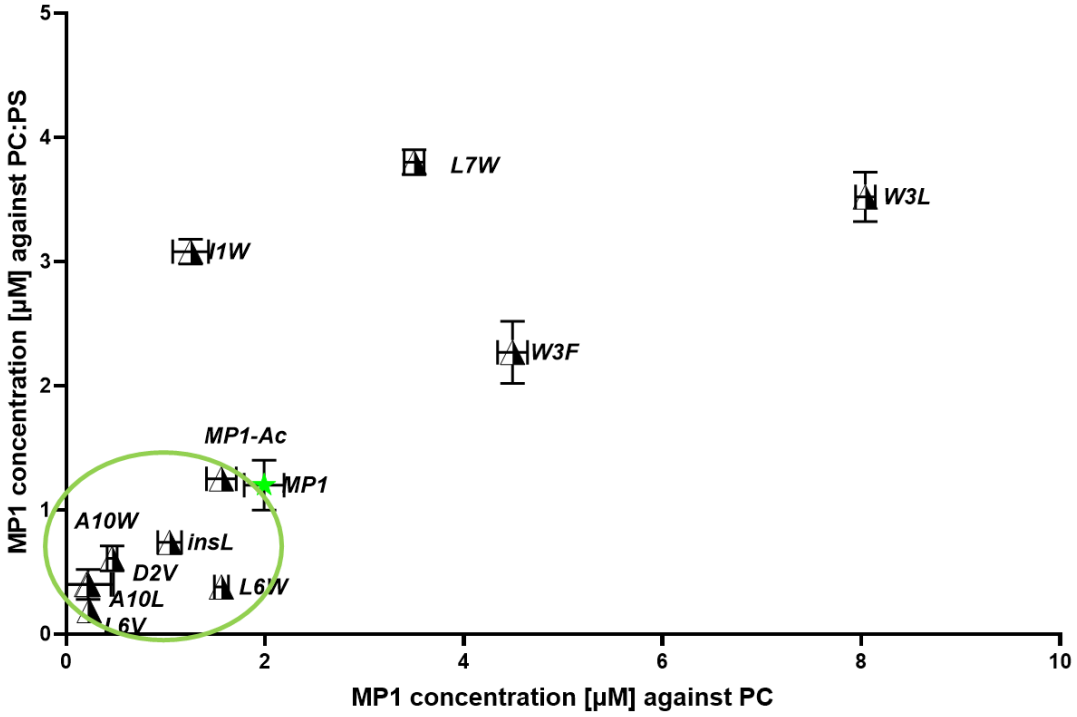

Figure 27 Leakage assay data: hydrophobicity screening. Each data point illustrates the concentration (µM) of peptide inducing 50 % leakage (relative to CF emission spectrum after treatment with Triton X-100) against PC (X-axis) and PC/PS (Y-axis) model vesicles. Green spot marks MP1 data. Green circle and surrounded peptide mutants are more potent and/ or specific relative to MP1. Error bars represent ±SEM from three replicate measurements. The raw leakage data are presented in Appendix 2.

2.3.5 pH-sensitive peptide variants to address tumour microenvironment

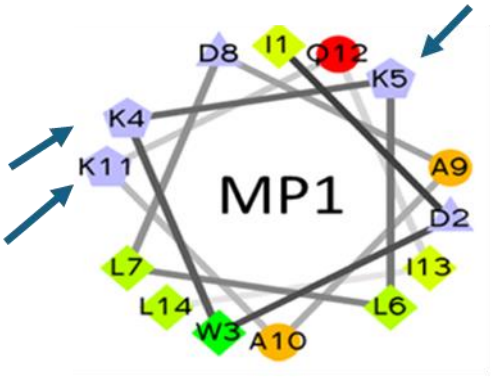

Peptide name	Sequence
MP-1	IDWKKLLDAAKQIL
K4H	IDWHKLLDAAKQIL
K5H	IDWKHLLDAAKQIL
K11H	IDWKKLLDAAHQIL
3K->3H	IDWHHLLDAAHQIL
DDQKKK->6H	IHWHHLLHAAHHIL

Figure 28 Peptide mutants with sequence and helical wheel projection. Each MP1 analogue is termed depending on the position of mutation- the first letter stems from the replaced amino acid, the following number is its sequence position starting from the N-terminal end and the latter letter represents substituted residue. The peptide mutation in the amino acid sequence is marked by red. Blue arrows on the helical wheel projection indicates substitutions.

The tumour microenvironment is often hypoxic and as a result also acidic (pH 6.5-6.9) [225]. Because of the rapid growth of the tumour, tumour cells are deprived from oxygen what leads to alter in mitochondrial oxidation. High level of glycolysis, accumulation of lactate and protons acidifies tumour microenvironment. Therefore, histidine mutants substituting lysine were redesigned to adapt pH-responsive structure, because His is protonated in an acidic environment (pKa of the side chain group is 6) and their sequence with helical wheel projection are shown in Figure 28. Figure 29 and Figure 30 present a data set obtained from a pH-mutants screening of MP1 at pH 7.4 and pH 6.5, respectively. Apart from the DDQKKK->6H mutant, H-mutants were less effective in membrane permeabilization at pH 7.4 Typically, His should not be protonated at the physiological pH. DDQKKK->6H mutant lacks charged residues (Asn and Lys) and glutamine, therefore

its hydrophilic face was significantly modified. Contrary, replacing native residues resulted in stronger potency of H-mutants at pH 6.5, giving promising direction to optimize anti-cancer therapeutics based on Polybia MP1, apart from 3K->3H mutant. K5H and K11H mutants also maintained specificity to PC:PS models. DDQKKK->6H variant was more active at pH 6.5, but not specifically.

Histidines are capable of simultaneously creating hydrogen bond to one phosphate and can interact with a Na^+ ion to coordinate another phosphate, thereby have strong interaction with membrane phospholipids. The structural arrangement is similar to that of hydrogen bonds of arginine, which modulates negative curvature in membranes required for membrane permeation processes like pore formation, therefore, the result of DDQKKK->6H and 3K->3R is analogous [226].

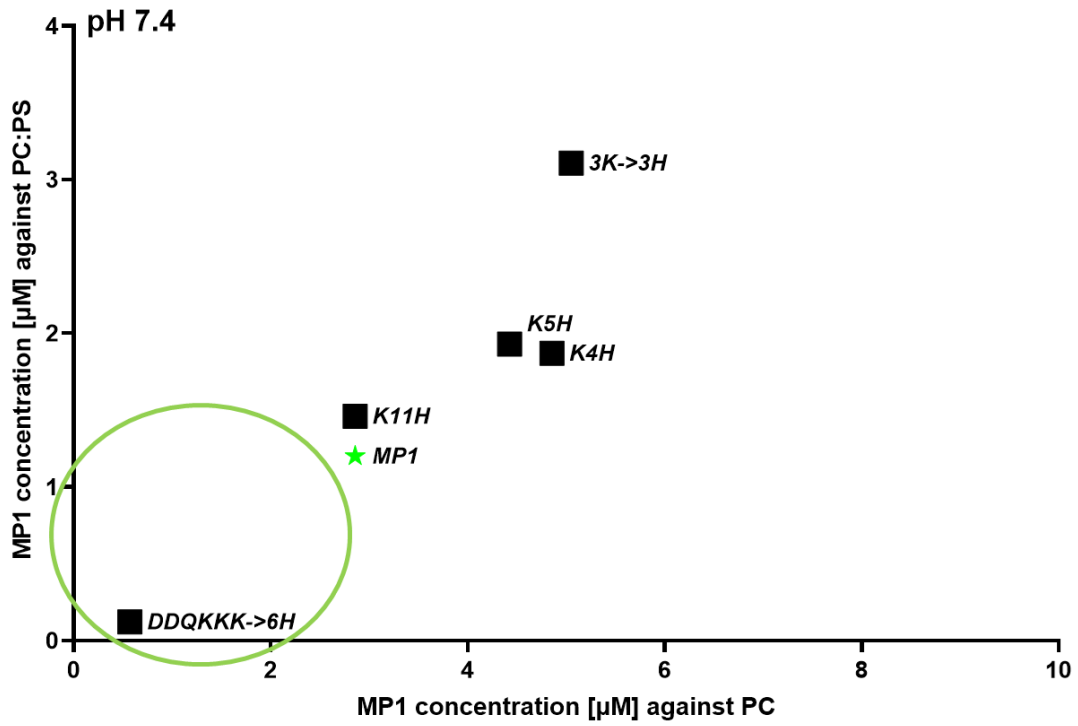

Figure 29 Leakage assay data: pH-triggering MP1 derivatives at pH 7.4. Each data point illustrates the concentration (µM) of peptide inducing 50 % leakage (relative to CF emission spectrum after treatment with Triton X-100) against PC (X-axis) and PC/PS (Y-

axis) model vesicles. Green spot marks MP1 data. Green circle and surrounded peptide mutants are more potent and/ or specific relative to MP1. No error bars are present. SEM values could not detected using Origin software. The raw leakage data are presented in Appendix 2.

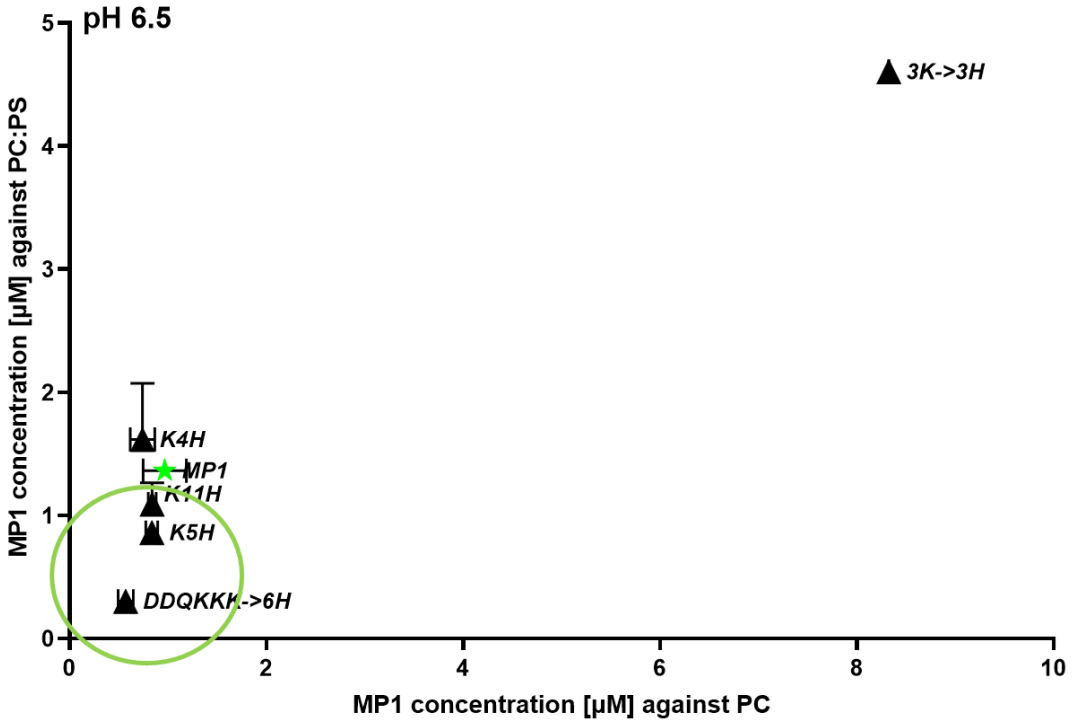

Figure 30 Leakage assay data: pH-triggering MP1 derivatives at pH 6.5. Each data point illustrates the concentration (µM) of peptide inducing 50% leakage (relative to CF emission spectrum after treatment with Triton X-100) against PC (X-axis) and PC/PS (Y-axis) model vesicles. Green spot marks MP1 data. Green circle and surrounded peptide mutants are more potent and/ or specific relative to MP1. Error bars represent ±SEM from three replicate measurements. The raw leakage data are presented in Appendix 2.

2.4 Discussion

Mastosporans, low molecular weight peptides extracted from the venom of social wasps, have been research subjects due to their broad antimicrobial activity and poor understanding of the mechanism of action [227]. The general feature of this family is sequence-specific order, INW, followed by a leucine or a lysine in the N-terminus and the C-terminus end is typically hydrophobic, with leucine being the last residue [228].

Furthermore, C-terminus might be protected by amidation and an extra hydrogen bonding has a stabilizing effect on the secondary structure [229] and prevents proteolytic degradation [98]. However, some peptidic motifs contain acidic residues in the N-terminus, in general, aspartic acid and Marqusee and Baldwin et al. explained that by increasing the helical macrodipole and providing an extra non-covalent hydrogen bonding or salt bridge between side chains might have helix stabilizing result [230].

Lately, a unique family of peptides with acidic residues in the N-terminus derived from the wasp *Polybia paulista* was introduced [152, 231]. Potent activity against Gram-positive and Gram-negative microorganisms and degranulating activity in rat mast cells are their first reported biological characteristics. Nevertheless, differentiating activities were determined in the peptides containing aspartic acid or asparagine residue in the N-terminal region. Souza observed that the peptides with IDWL in the N-terminus had lower haemolytic and degranulating properties than their parallel with asparagine, and exhibited boosted antimicrobial activity [232]. Taheri-Araghi revealed also that these peptides have varying hydrophobicities and angles of the polar faces, which are believed to synergistically modulate activity and correspond to the peptide membrane-specificity [233]. Studies conducted by Leite et al. using fluorescence measuments examined the activity of the Polybia MP1 redesigned variant, Polybia N2-MP1 and other peptides derived from Brazilian wasp, Polybia MP2 and Polybia MP3 [227]. N2-MP1 mutant with D to N substitution, as opposed to other peptides, has a slightly higher net charge,+3. Polybia N2-MP1 has been observed to, above threshold [*P*]/[*L*] values, generate a number of pores formed rapidly which was explained by the cooperative way of pore formation. Overall, peptides with varying hydrophilic and hydrophobic content of amino acid residues were shown to exhibit different affinity and lipid specificity and along with the aspartic residue in the N-terminal region are thought to lead lytic and biological

activities. The D2 residue was investigated to be an important factor modulating MP1 selectivity and its substitution to asparagine drastically increased haemolytic activity and simultaneously reduced selectivity. Zeta potential measurements showed that MP1 at low [*P*]/[*L*] ratio has a high affinity to anionic vesicles inducing vesicle aggregation at yield near the zeta potential signal inversion [234].

Huang et al. attempted to determine common sequential features for anticancer peptides using a two-step machine-learning model [235]. Analysis of amino acid frequency in ACPs vs. non-ACPs revealed the dominance of G, A, L, F, W and K residues in ACPs. Furthermore, having a positively charged sidechain, lysine occurs at the highest regularity in the peptides with anticancer activities as opposed to the anionic residues D (Asp, aspartate) and E (Glu, glutamate) occur at a much lower prevalence. Glycine and the aromatic tryptophan/phenylalanine were found over-represented at the N-terminal region of ACPs, while the C-terminus is enriched in the positively charged residue (K/R/H). It has been concluded that the cationic residue abundance might be a relevant predictor of the inhibitory effect on cancer cells [236].

Amino acid replacement is one of the chemical approaches used for the redesign, synthesis and evaluation of mutants of naturally sourced molecules which need further improvement for specific applications. Electrostatic interaction is seen as an initial step for peptide internalization into the membrane, therefore the positive charge is a key factor. D8N, another MP1 mutant carrying +3 net charge, not only was more potent to the bacteria-like membrane but also had greater affinity to zwitterionic models reflecting haemolytic tendency [161]. Luong et al. tested also the Q12K variant, where glutamine was substituted to cationic charged residue lysine. This mutation gave a promising outcome displaying a greater antimicrobial effect with minimal cytoxicity compared to the aspartic acid mutants. In this work has been concluded that the two anionic residues are irreplaceable for the

selectivity of MP1. Wang group indicated also that D8P mutation, the aspartic acid replacement to proline at position 8, resulted in higher net charge (+ 3), hydrophobic content and greater potency which may be beneficial for the anti-cancer activity of Polybia-MP1 [116]. Generally, proline residue is termed “a helix breaker” as its amino group has no free hydrogen and, therefore, cannot form the conventional intra-helical hydrogen bond [237]. Accordingly, the substitution of proline in the middle of the MP1 sequence drastically reduced membrane-penetrating potential.

The alanine scan approach presented in this work revealed that each amino acid contributes to peptide functionality. The replacement of Trp, Leu and Ile residues markedly reduced peptide activity seen as a high peptide concentration inducing 50% CF-leakage. It could be assumed that these components are important in the peptide’s internalization into the nonpolar part of the membrane, as they are localised on the hydrophobic face [238]. The alternation in a peptide net charge and the aspartic acid and lysine substitution increased the potency of peptide variants. Continuing, charge screening demonstrated a similar pattern: substitution in the hydrophilic face significantly accelerated potency, whereas modification incorporated into the hydrophobic face suppressed peptide activity. Among K-mutants, only the Q12K peptide exhibited PS-containing membrane specificity, achieved by a glutamine substitution at position 12. Surprisingly, some peptides, such as D2A, D8A, K4A, K5A or K11A had higher potency to PC model suggesting stronger hydrophobic interactions between hydrophobic face of a peptide and membrane lipid core [203].

Hydrophobicity is one of the features characteristic of the MP1 sequence. Leucine and isoleucine substitution revealed much-decreased potency with alanine or lysine replacement, whereas exchange to more hydrophobic residues improved potency. Additional leucine residue and N-terminal acetylation of a peptide also tune peptide

hydrophobicity and these modifications were identified to both accelerate potency and specificity. Another important observation is the drop in the activity of tryptophan mutants. Tryptophan is the largest aromatic amino acid with the characteristic indole functional group. The indole heterocyclic ring is known to have both hydrophilic and hydrophobic properties, thus it interacts with the water-phospholipid interface of the cell membrane and might promote the insertion of the peptide into the cell membrane [239]. Aromatic amino acids have been considered key components in AMPs structure having an ability to interact with the interfacial region of the membrane [240]. However, some studies indicated the importance of the Trp position in the sequence and the effect on peptide internalization into the membrane [241]. Cholesterol content also facilitates membrane disturbance and internalization efficacy.

A further approach for providing sequences with better cell specificity is the introduction of amino acid residues sensitive to the change in pH. Hypoxic regions of limited tissue oxygen levels, can be found in many solid tumors as a consequence of the disordered vasculature [242]. It results in a slightly acidic tumour microenvironment [243]. Histidine mutants were designed to address pH changes as histidine protonation reduces exposure of charged side chains to the hydrophobic core of the bilayer [244]. The data indicated that pH-sensitive peptides could be utilised as membrane-disrupting agents with improved potency and specificity at pH 6.5. Studies focusing on pistidines, histidine-abundant antimicrobial peptides revealed the histidine effect on the pH-dependent membrane permeabilization: histidine content and amphipathicity and their role in different directionality of membrane insertion [245]. Two homologous with three histidines (H3, H4, H11) at the same positions in N-termini but one which shows a more potent membrane disrupting effect, has a fourth histidine in the C-terminal region (H17). Neutron diffraction measurements indicated that the stronger punctuation has been linked

to the facilitated ability of the carboxyl terminus to incorporate into the membrane. Furthermore, the permeabilization efficiency of the triple-histidine peptide motif was inhibited at pH 6.0 when the conserved histidines are partially charged and H17 is mostly neutral. The neutral state of H17 is also related to pH resiliency.

Together, leakage assay analysis of MP1 derivatives revealed that each amino acid and its physiochemical characterisation are unique code balancing MP1 membrane-perturbing activity. Chemical modification and tests in model systems revealed prospective candidates for further studies and development for clinical application.

2.5 Conclusion

The current knowledge of AMPs is still not sufficient to prognose the behaviour of novel peptide sequences. The summary of alanine sequence screening and key conclusions are shown in Figure 31.These findings may expand an understanding of the MP1 structure-function relationship and advance the design of AMPs towards systemic applications.

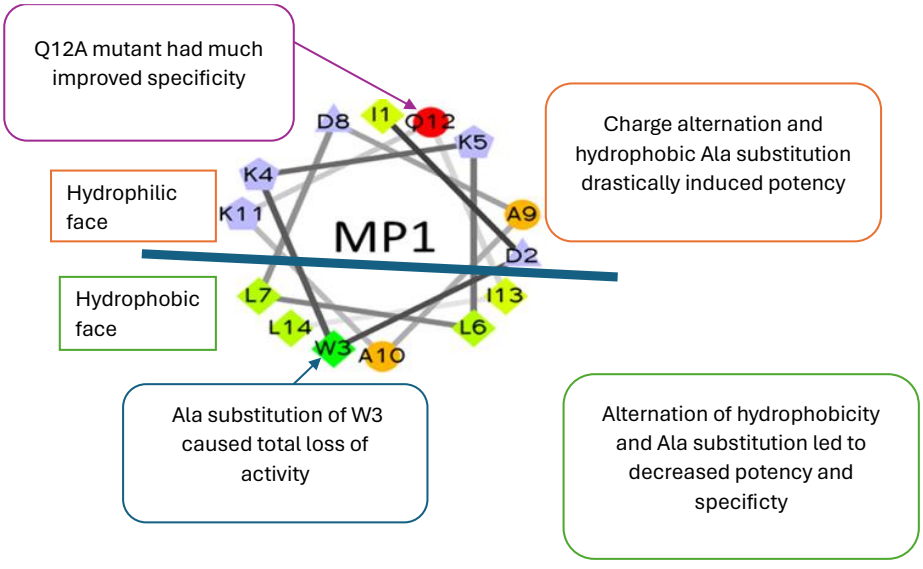

Figure 31 The summary of alanine-scan screening. Tryptophan was found inevitable to MP1 activity. Charge alternation and incorporation of apolar alanine to hydrophilic face of MP1 substantially induced peptide potency. Change in peptide hydrophobic face resulted in reduced activity. Q12A exhibited enhanced specificity relative to MP1.

Chapter 3 Investigating a cell-derived plasma membrane model system: testing different preparation protocols and characterizing membrane integrity

ABSTRACT

The cell plasma membrane is a highly dynamic and multilevel structure defining not only cell organization but also constituting a platform for diverse cell life processes. Despite the use of simple lipid vesicles, there is still a need for a cell-like model system. To study the membranotropic action of Polybia MP1 on a biological system that is an intermediate model between artificial vesicles and living cells, a search for effective conditions for isolation of mammalian and transformed cell-derived GMPVs was conducted. These vesicles are cell plasma membrane buds and, therefore comprise similar lipids and membrane structures, but lack cellular contents such as organelles. A range of cell lines that show various sensitivities to MP1 were treated in order to produce GPMVs, using protocols based on osmotic gradients or chemical vesiculation. The number and quality of GPMVs produced were assessed, demonstrating that by applying an osmotic gradient only the MCF-10 cell line produced a sufficient yield of GPMVs. Contrary to this, dithiothreitol (DTT) and paraformaldehyde (PFA) as chemical vesiculation agents effectively induced giant vesicle formation from a wide range of cell lines. Furthermore, GPMV characterization revealed that either osmotically- or chemically-induced GPMVs are permeable to a certain degree, questioning their application to study MP1-induced membrane incidents. The use of specific lipid binding dyes that respond to lipid membrane order might provide important insight into molecular principles of membrane integrity.

3.1 Introduction

The cell plasma membrane is the frontier separating the cell interior from the extracellular space [10]. The complex character and lack of specialised tools limit exploration of the underlying biology of the membrane in intact live cells. Artificial and primitive synthetic systems facilitate the exploration of the principal mechanisms likely to occur in live cells [246]. Reduced heterogeneity, controlled composition, and well-established methods for formation are undoubtedly strong points of lipid vesicles. Recent developments allow even protein reconstitution into giant vesicle systems facilitating the cell-like environment [247]. Despite improvements in reductionist approaches, the complexity of the cell environment is a key aspect of biophysical mechanisms in the cell, therefore studying systems of greater complexity would provide valuable insight into molecular basics.

The formation of membrane protrusions has been a widely explained cellular phenomenon. It has been observed that cell blebbing is a physiological process associated with the cell cycle, locomotion, spreading or even programmed death [248]. Following this finding, scientists have successfully developed methods to isolate those membrane blebs directly from adherent cell culture [85]. Due to their micron-sized, PM buds are referred to as giant plasma membrane vesicles (GPMVs). Since those membranous structures are parts of live-cell PM, GPMVs provide close-to-native protein and lipid membrane composition and organization. High-resolution imaging revealed a nearly pure yield lacking internal organelles isolated in as little as 30 minutes. Scott et. al induced vesiculation in a wide range of mammalian cultured cell lines [249]. Further investigation revealed no detectable cytoskeletal networks or any other internal cell-origin structures. Sulphhydryl-blocking agents, particularly formaldehyde and N-ethyl maleimide, are commonly used and highly effective vesiculants [16, 84, 250, 251]. Close-to-native PM

spherical extracts are attractive platforms for studying cell biophysics, lipid and protein membrane profiles, and molecular interactions based on PM or even drug delivery [252–254]. Seeking a better comprehension of the MP1 membranolytic activity, GPMVs are a prospective tool to investigate further this phenomenon. However, neglected for years, the application of PM-derived vesicles raises a number of questions. Are all types of cells capable of producing GPMVs? Do GPMVs retain the biophysical properties of the intact PM? What are the drawbacks of the formation procedure?

This section provides complementary observations and supplements to the most recent GPMVs formation protocols in which cells have been subjected to osmotic shock (a sudden change in the solute concentration, which causes a rapid change in the movement of water molecules across cell membrane) [255] and chemical treatment [84]. Herein, GMPVs are examined as a potential platform to study PM-associated events. Isolated membranous structures are visualised with lipophilic tracers and membrane integrity was investigated by incubating cell-like spheres with fluorescently labelled size-different polysaccharides. Moreover, the dynamic and subsequent influx of fluorescent probes is reported as modest as 0.6 kDa into GPMVs induced by administrating osmotic gradient (the water flow through a semipermeable membrane from a less concentrated solution into a more concentrated). As opposed, GPMVs produced upon exposure to chemicals, manifest lower permeability to macromolecules that favours their applicability in studies aiming at exploring principles of membrane-localised events.

3.2 Materials and Methods

3.2.1 Materials

3.2.1.1 Reagents

The following materials were purchased for this study from Sigma Aldrich (Sigma, St. Louis, MO): HEPES, sodium chloride (NaCl), calcium chloride ($CaCl_2$), magnesium chloride ($MgCl_2$), potassium chloride (KCl), potassium phosphate monobasic (KH_2PO_4), sodium phosphate dibasic (Na_2HPO_4), *N*-ethyl maleimide (NEM), formaldehyde (PFA), D-dithiothreitol (DTT), chloroform $(CHCL)_3$, dimethylformamide ((CH3)2NC(O)H), bovine serum albumin (BSA).

3.2.1.2 Fluorescent probes

The following materials were purchased from Invitrogen (CA, USA). The solid dyes Nile Red, DiI (1,1'-Dioctadecyl-3,3,3',3'-Tetramethylindocarbocyanine Perchlorate; $DiIC_{18}$), DiO (3,3'-Dioctadecyloxacarbocyanine Perchlorate; $DiOC_{18}$) cascade blue (CB)-10 kDa dextran and fluorescein isothiocyanate (FITC)-70 kDa dextran were dissolved in DMF. The stock solution for Nile Red and DiI was 0.5 mg/mL, whereas calcein, CB-10kDa dextran and FITC-70 kDa dextran were prepared at 1 mg/mL.

3.2.2 Cell lines

Cell lines MCF-10A, BT-474 and MDA-MB-468 were obtained from co-supervisor Prof. Thomas Hughes (School of Medicine, University of Leeds), and were originally from American Type Culture Collection (ATCC; Manassas, USA); these were subjected to confirmation of cellular identity by STR-profiling. AU-565 cells were obtained from ATCC. Immortalised human breast cancer-associated fibroblasts (LACAFs)

were obtained from co-supervisor Prof. Thomas Hughes; their collection and immortalisation have been described previously [256, 257].

MDA-MB-468 and AU-565 cells were cultured in DMEM with 10% (v/v) FBS. BT-474 cells and LACAFs were cultured in RPMI with 10% (v/v) FBS. MCF-10A cells were maintained in DMEM/F12 with Horse serum (5% v/v), Cholera toxin B subunit (0.1 µg/mL), insulin (10 µg/mL), EGF (0.02 µg/mL) and hydrocortisol (0.5 mg/mL). All cells were cultured with penicillin (100 units/ml) at 37^{o}C and in humidified 5% CO_2/air. Cells were cultured in T75 tissue culture flasks and passaged every third day. All cells were subjected to mycoplasma screening and were consistently negative.

3.2.3 Methods

3.2.3.1 GPMVs isolation: Osmotic pressure

Cell lines MCF-10A, LACAF, BT-474, MDA-MB-468 and AU-565 were seeded into 12-well plates at $5x10^4$ cells per well. Breast cancer was selected as an appropriate model to study cell sensitivity to Polybia MP1 based on Crown Bioscience (see details in Chapter 5: Materials and methods). Cells were grown for 24-48 hours (to ~70-80% confluence) before the beginning of the vesiculation process. Afterwards, based on a slightly modified method of Del Piccolo et al. [255], each well was rinsed twice with 1 mL of hypotonic PBS (1.06 mM KH_2PO_4, 2.97 mM Na_2HPO_4 and 155 mM NaCl, pH 7.4) and cells were incubated for 1 min at room temperature. The role of cell exposure to the hypotonic environment in the vesiculation process was investigated by the application of a range of differentially diluted PBS: 10%, 20%, 30% and 40%.

Then, 1 mL of vesiculation buffer was added to each well and the plate was incubated for 10h at 37^{o}C. The role of hypertonicity in the vesiculation process was examined by the application of two vesiculation buffers with different salt concentrations;

200 mM NaCl, 5 mM KCl, 0.5 mM $MgCl_2$ and 0.75 mM $CaCl_2$ buffered at pH 8.5 by 100 mM bicine (termed as buffer I)) and a second buffer was prepared with 10% increased salt concentration - 220 mM NaCl, 5.5 mM KCl, 0.55 $MgCl_2$, 0.825 mM $CaCl_2$ (buffer II). The osmolality measurements indicated 530 mOsm/kg and 650 mOsm/kg, for buffer I and buffer II, respectively. The osmolality of body fluids is normally between 275 and 290 mOsm/kg [258]. Osmolality refers to the osmotic pressure of a solution at a particular temperature, expressed as moles of solute per kilogram of solvent (osmol kg−1 or osmolal) [259]. During the vesiculation process, three representative phase-contrast images were taken every hour using IncuCyte Zoom System (Live Cell Imager, Essen Bioscience). Each condition was tested in triplicate in three independent biological experiments. From each picture, the number of cells, free vesicles, floating cells and blebbing cells were collected using ImageJ software (NIH, Maryland, USA).

3.2.3.2 GPMVs isolation: Chemical vesiculation

Cell lines MCF-10A, BT-474, MDA-MB-468 and AU-565 were seeded into 12-well plates at $5x10^4$ cells per well. These cells were grown for 24-48 hours (~70-80% confluence) before the beginning of the vesicle isolation. Following a recently updated procedure [84], each well was rinsed twice with 1mL of GPMV buffer (10 mM HEPES, 150 mM NaCl, 2 mM $CaCl_2$, pH 7.4). Then, 1mL of buffer containing vesiculation agents (2 mM, 4 mM, 6mM, 8 mM, 10 mM NEM or 25 mM PFA/2 mM DTT) in GPMV buffer was added to each well and the plate was incubated at 37^{o}C for 5 h. During the vesiculation process, three representative phase-contrast images were taken every hour using IncuCyte Zoom System (Live cell Imager, Essen Bioscience). Each condition was tested in triplicate in three independent biological experiments. From each picture, the number of cells, free vesicles, floating cells and blebbing cells using ImageJ software (NIH, Maryland, USA).

3.2.3.3 GPMVs processing

GPMVs were used immediately after isolation. For imaging experiments, GPMVs suspensions was left undisturbed for 20-30 mins to concentrate at the bottom of the tube. To remove cell debris, the GPMV supernatant was centrifuged at 100*g* for 5-10 min.

3.2.3.4 Labelling GPMVs before isolation

After reaching the proper density, cells were washed three times with 1mL of PBS. 10 µL of dye solution, Nile Red or DiI (0.5 mg/mL), were added to cells to the final concentration of 5µg/mL and incubated for 30 min at 37˚C. The solution was poured out and cells were rinsed five times with PBS to remove the unincorporated dye.

3.2.3.5 GPMVs permeability assay

Chambered coverslips, µSlides 8well (Ibidi, GmbH, Munich, Germany) were used for GPMVs observation, coated with 5% bovine serum albumin solution (10 min) and then washed with the deionized water to avoid vesicles adhesion or bursting [260]. After harvesting GPMVs, 300 µL of GPMVs suspension was pipetted from the bottom of 1mL Eppendorf into each chamber. 1 µL of fluorescein isothiocyanate -labelled 70 kDa dextran (FITC; 1 mg/mL) the green emitting with a maximum at 517 nm and 10 µL of cascade blue-labelled 10 kDa dextran (CB; 1mg/mL) the blue emitting with a maximum at 420 nm were added into GPMVs suspension. Confocal images were taken after 30 min incubation at room temperature. That time allows GPMVs to settle on the glass bottom surface. By eye, vesicles differ according to lumen brightness. To quantify a phenomenon of membrane permeation, fluorescence measurements were conducted using ImageJ software (NIH, Maryland, USA). The “relative vesicle intensity” refers to the vesicle lumen intensity ($I_{vesicle}$; representative area within the vesicle selected by the eye) relative to the

background intensity (I_{bulk}; a representative area of background area selected by the eye) and is calculated as :

relative vesicle intensity = $I_{vesicle} / I_{bulk}$

Confocal microscopy images were acquired at room temperature using model No. LSM880 (Zeiss, Jena, Germany) inverted confocal microscope equipped with 63x/1.4N.A. Oil Plan-Apochromat objective lens. The Nile Red and DiI probe was excited by a DPSS laser at 543 nm with an emission maximum at 585 nm and 565 nm, respectively, the CB was excited at 405 nm with a diode laser and emission peak at 419 nm, FITC was excited at the 488nm line of an Argon laser with an emission maximum at 517 nm.

3.3 Results

3.3.1 GPMVs isolation procedure

3.3.1.1 Osmotic vesiculation failed to generate GPMVs from cancer cell lines

First, attempts to use osmotic pressure to generate GPMVs from the MDA-MB-468, BT-474, AU-565 and MCF-10A cell lines were made. All cells were subjected to hypotonic wash followed by hypertonic buffer and GPMVs formation was monitored by the automated bright-field microscopy. The representative image of cell swelling after being subjected to hypotonic wash can be seen in Figure 32.

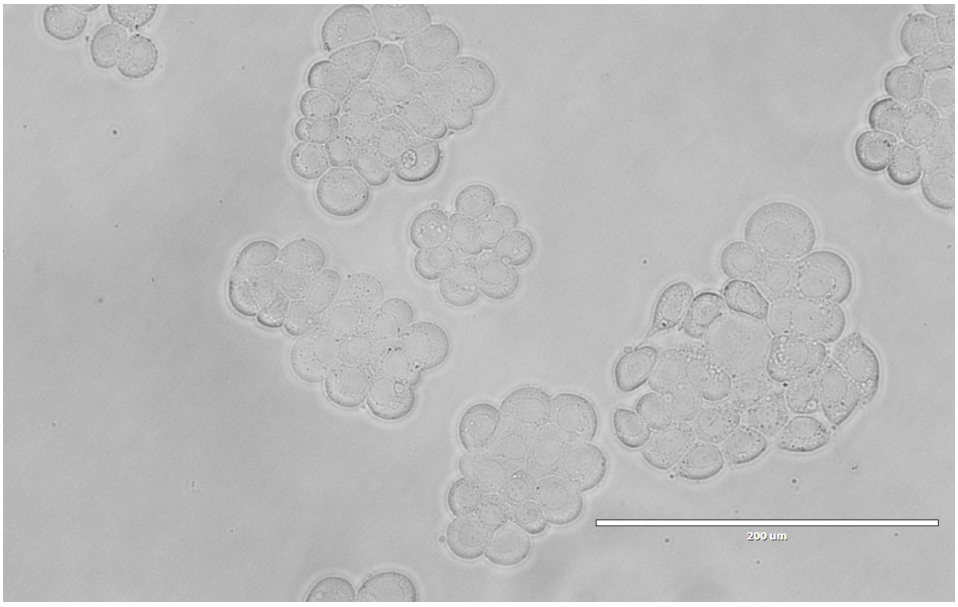

Figure 32 Representative picture of MDA-MB-468 cells subjected to hypotonic wash (10% PBS). The picture was taken using phase-contrast microscopy.

Figure 33 presents the collected variables: the number of cells, free vesicles, floating cells and blebbing cells.

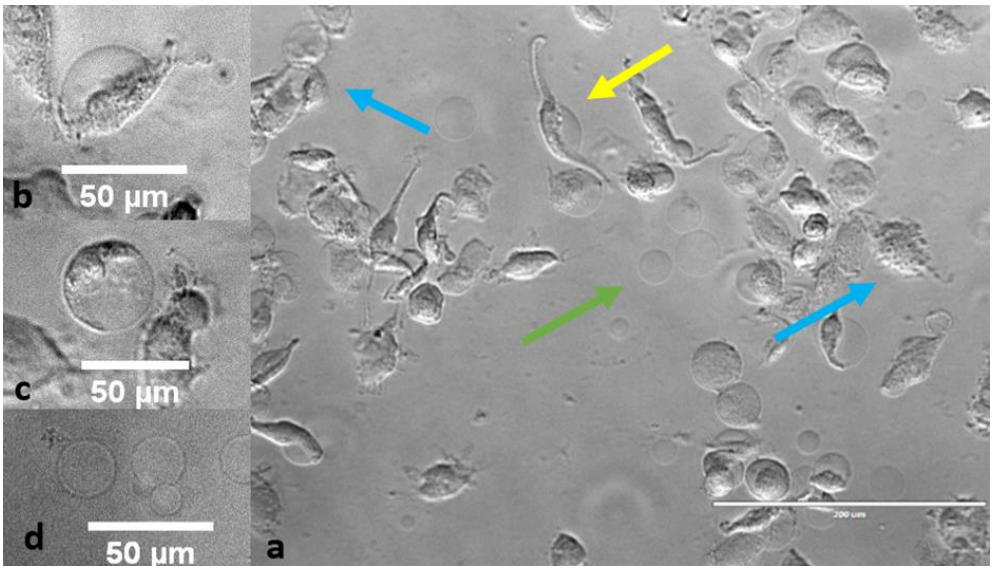

Figure 33 Representative picture of the LACAF cell line under osmotic vesiculation; (a,d) The green arrow indicates free vesicles; (a) the blue arrows mark detached cells; and (a,b) the yellow arrow shows blebbing cells (b); (c) ruptured vesicles might also contain cellular debris. The picture was taken using phase-contrast microscopy. The scale bar is (a) 200 µm and (b,c,d) 50 µm.

The number of floating cells was difficult to count exactly since floating out of the plane of focus meant that accurate identification was not always possible; therefore, rather than exact counts, floating cells were classified into ranges approximating to no floating cells, 2-10 floating cells (class “1”), 11-20 (2), 21-40 (3), 41-60 (4), >60 (5) indicated on Figure 34. In order to optimize the procedure for each cell line, a range of 8 osmotically different conditions: 4 different hypotonic buffers, each followed by 2 different hypertonic buffers; and GPMVs formation efficiency was rated at different time points from 1h to 10 h. Not only the number of released GPMVs but also the number of blebbing cells and floating detached cells expressed as a percentage of the total cell number was quantified.

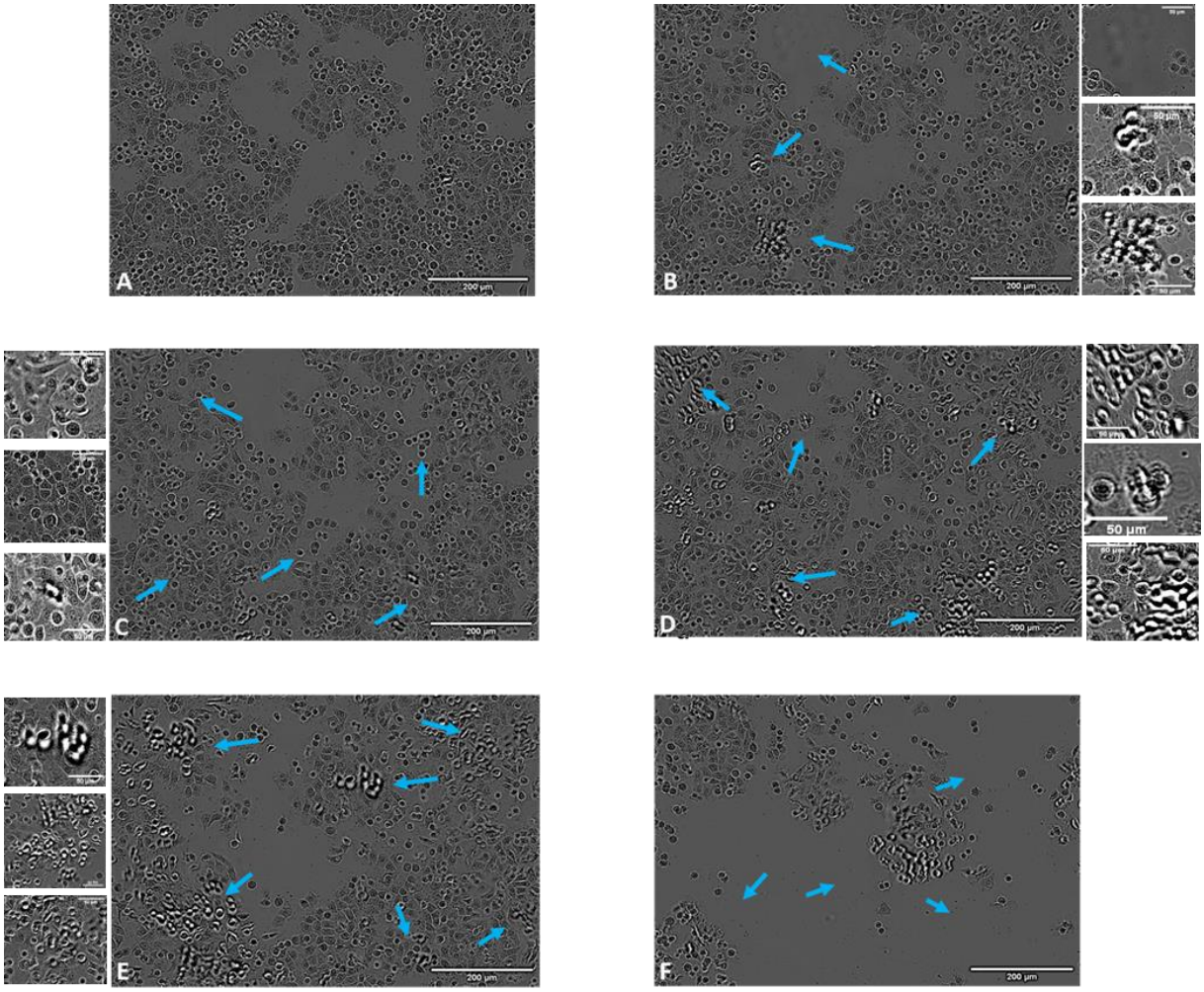

Figure 34 Representative pictures of the AU-565 cell line under chemical vesiculation using 2 mM NEM. Picture A depicts cells after the application of a vesiculation agent. The vesiculation process causes cell detachment which is difficult for counting, thus, separate classifications from 0 to 5 of floating cells were created. Each number refers to 0) no floating cells; 1)2-10 floating cells; 2)11-20; 3) 21-40; 4) 41-60; 5)60<). Pictures B, C, D, E, and F show a range of detached cells classified as 1, 2, 3, 4, and 5, respectively. The scale bar is 200 µm. Zoom images of floating cells are next to the original image and the scale bar is 50 µm.

MCF10A cells were readily budding and forming GPMVs under a range of conditions in a time-dependent manner seen in Figure 35.

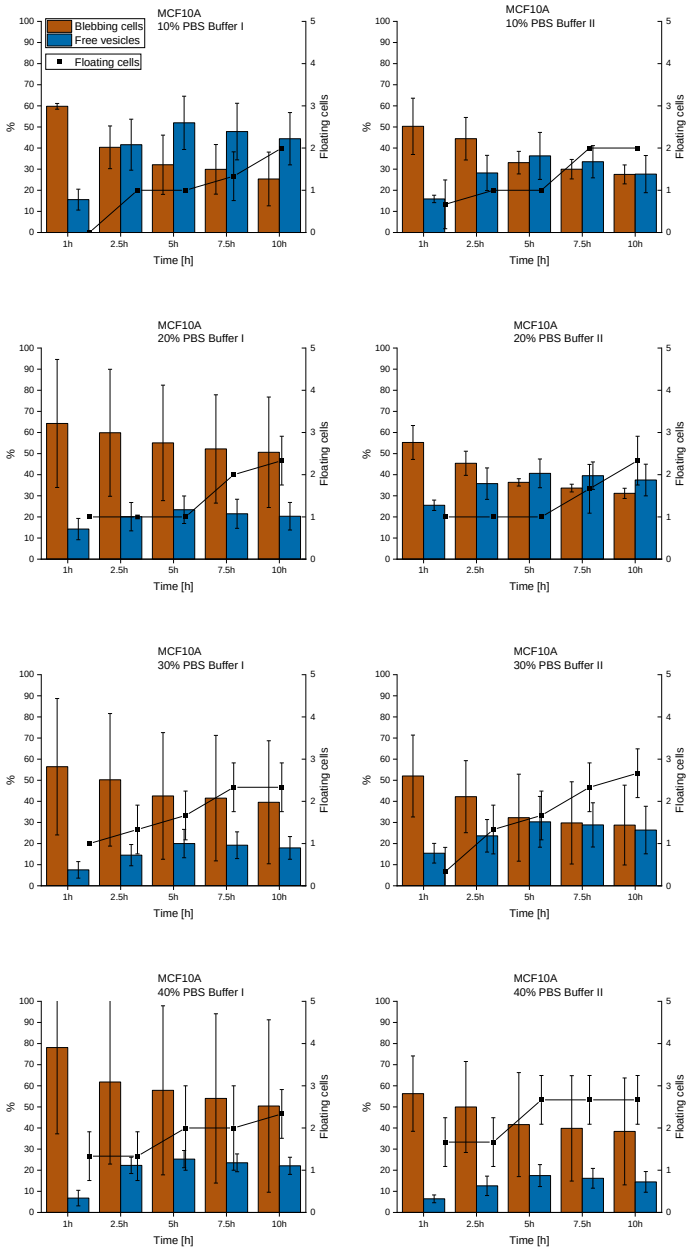

Figure 35 Osmotic formation of GPMVs in MCF-10A was successful under a range of conditions. MCF-10A cells were treated with a range of hypotonic buffers (10% PBS, 20% PBS, 30% PBS and 40% PBS), followed by a range of hypertonic buffers (buffer I and buffer II see Methods: GPMVs isolation: Osmotic pressure for buffers ingredients) and the formation of GPMVs was observed by microscopy over time, along with quantification of blebbing cells and free-floating cells. Time is shown along the X-axis, the quantity of blebbing cells (left Y-axis, orange bars), free vesicles (left Y-axis, blue bars) and floating cells (right Y-axis black line) expressed as a percentage of the total number of cells. Data represent means (with SD) of three independent experimental replicates.

However, floating cells, which can be regarded as a contaminant for the purposes of GPMVs isolation, were also present, especially at later time points, typically having a dramatic increase at the 5 h time point. Apart from 10% PBS buffer II, cell blebbing showed a time-dependent tendency to decrease. Almost 80% of cells were budding under a rinse of 40% PBS followed by buffer 1 and only 30% of vesicles constituting the total number of cells were released. Generally, buffer I generated a larger fraction of blebbing cells after cell treatment with 20%, 30% and 40% hypotonic buffers. It was shown that at a 10 h time point of GPMVs induction, a number of vesicles typically decreases, having a peak at a 5 h time point. Therefore, it was concluded that treatment with 10% PBS and buffer I was suitable for GPMVs preparation from MCF10A, with a relatively large GPMVs yield and a relatively minimal amount of cell debris. A representative image of these conditions is shown in Figure 36.

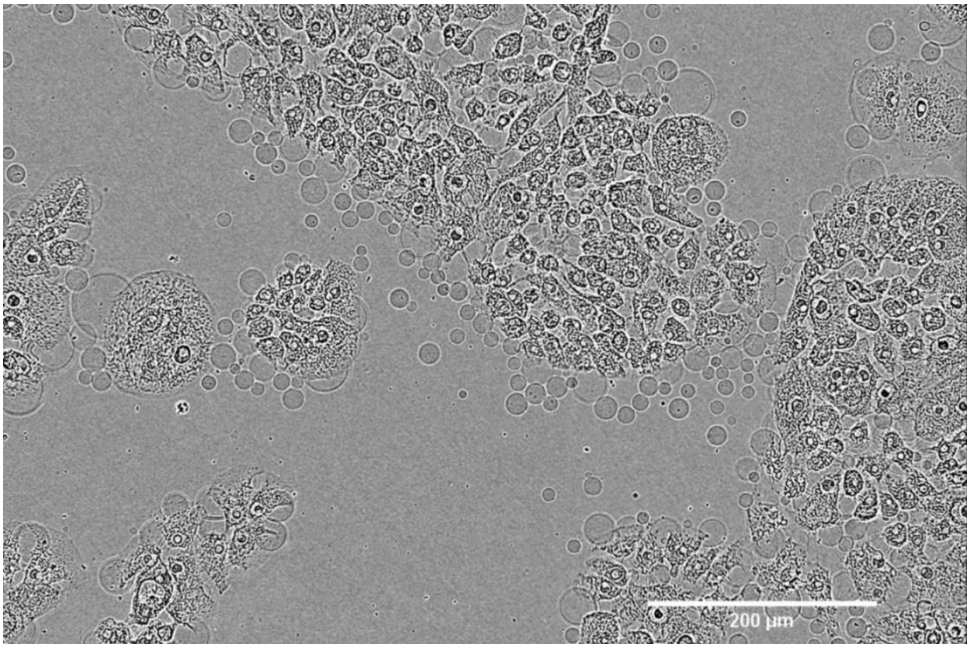

Figure 36 Representative picture of MCF10A cells under osmotic vesiculation treatment (10% PBS, buffer I). The picture was taken using phase-contrast microscopy. The scale bar is 200 µm.

The same data for the other cell types were less promising (Figure 37 – Figure 39). MDA-MB-468 cells were not budding or producing a large amount of GPMVs. 5 h incubation in vesiculation buffer usually resulted in the cell rupture by 50-80%. MDA-MB-468 cells only under specific conditions (20% PBS and buffer II) yielded a small fraction of GPMVs, but substantial cell detachment prevents GPMVs from clear visualization. Osmotic gradient induced cell blebbing of BT-474 and AU-565 cells, however, the applied physical force did not cause rupture of many GPMVs.

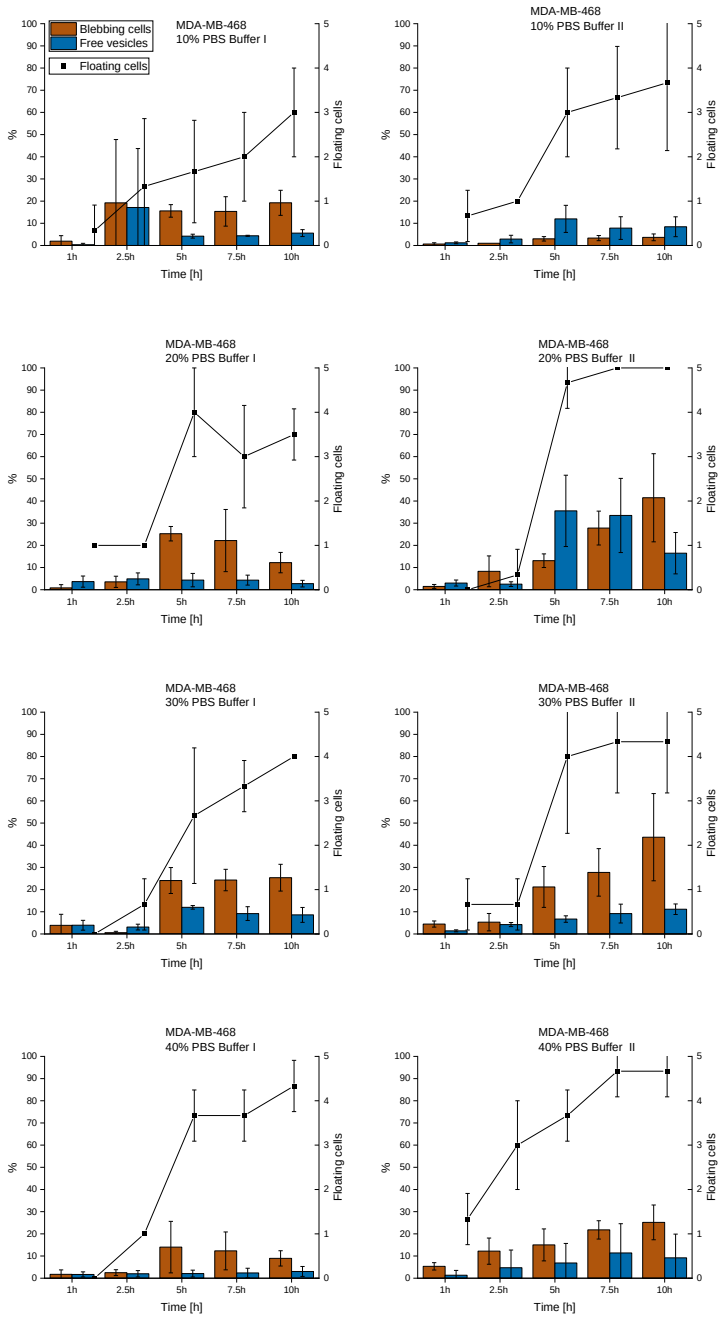

Figure 37 Osmotic formation of GPMVs in MDA-MB-468 was successful only under specific conditions. MDA-MB-468 cells were treated with a range of hypotonic buffers (10% PBS, 20% PBS, 30% PBS and 40% PBS), followed by a range of hypertonic buffers (buffer I and buffer II) and the formation of GPMVs was observed by microscopy over time, along with quantification of blebbing cells and free-floating cells. Time is shown along the X-axis, the quantity of blebbing cells (left Y-axis, orange bars), free vesicles (left Y-axis, blue bars) and floating cells (right Y-axis black line) expressed as a percentage of the total number of cells. Data represent means (with SD) of three independent experimental replicates.

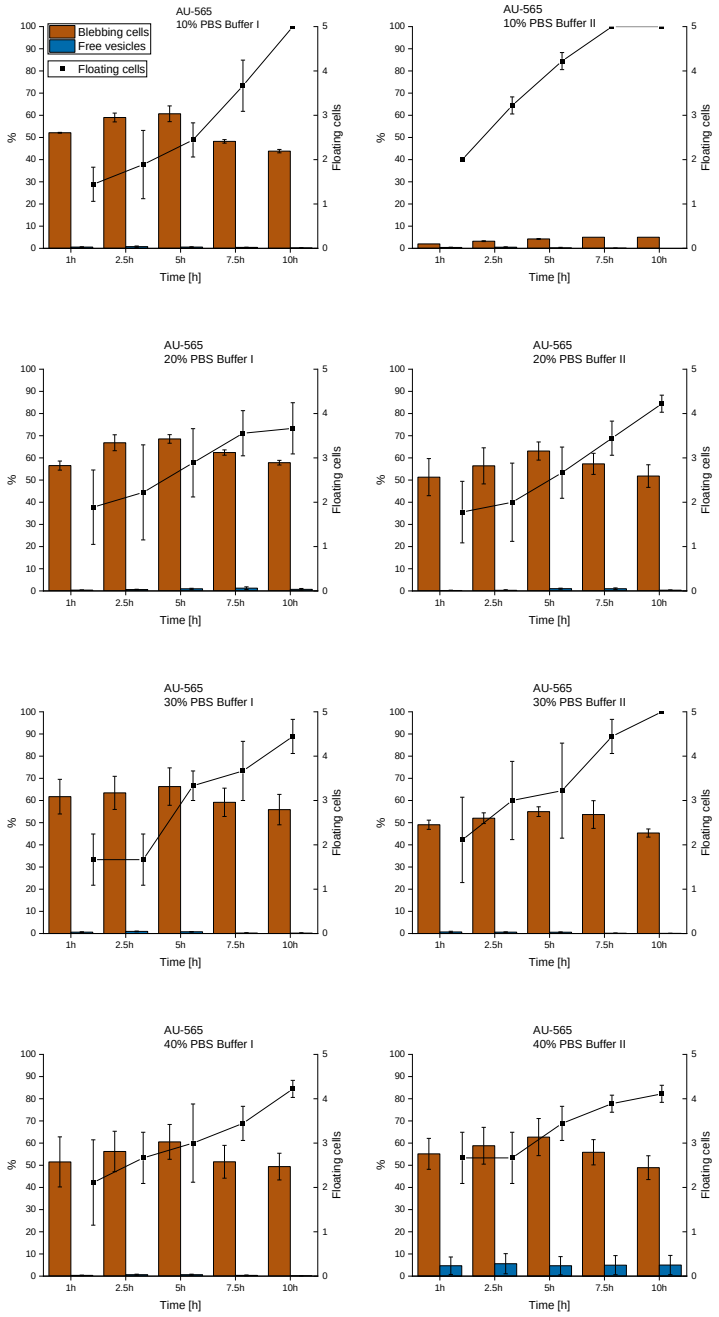

Figure 38 Osmotic formation of GPMVs in AU-565 was unsuccessful under a range of conditions. AU-565 cells were treated with a range of hypotonic buffers (10% PBS, 20% PBS, 30% PBS and 40% PBS), followed by a range of hypertonic buffers (buffer I and buffer II) and the formation of GPMVs was observed by microscopy over time, along with quantification of blebbing cells and free-floating cells. Time is shown along the x-axis, the quantity of blebbing cells (left y-axis, orange bars), free vesicles (left y-axis, blue bars) and floating cells (right y-axis black line) expressed as a percentage of the total number of cells. Data represent means (with SD) of three fully independent experimental replicates.

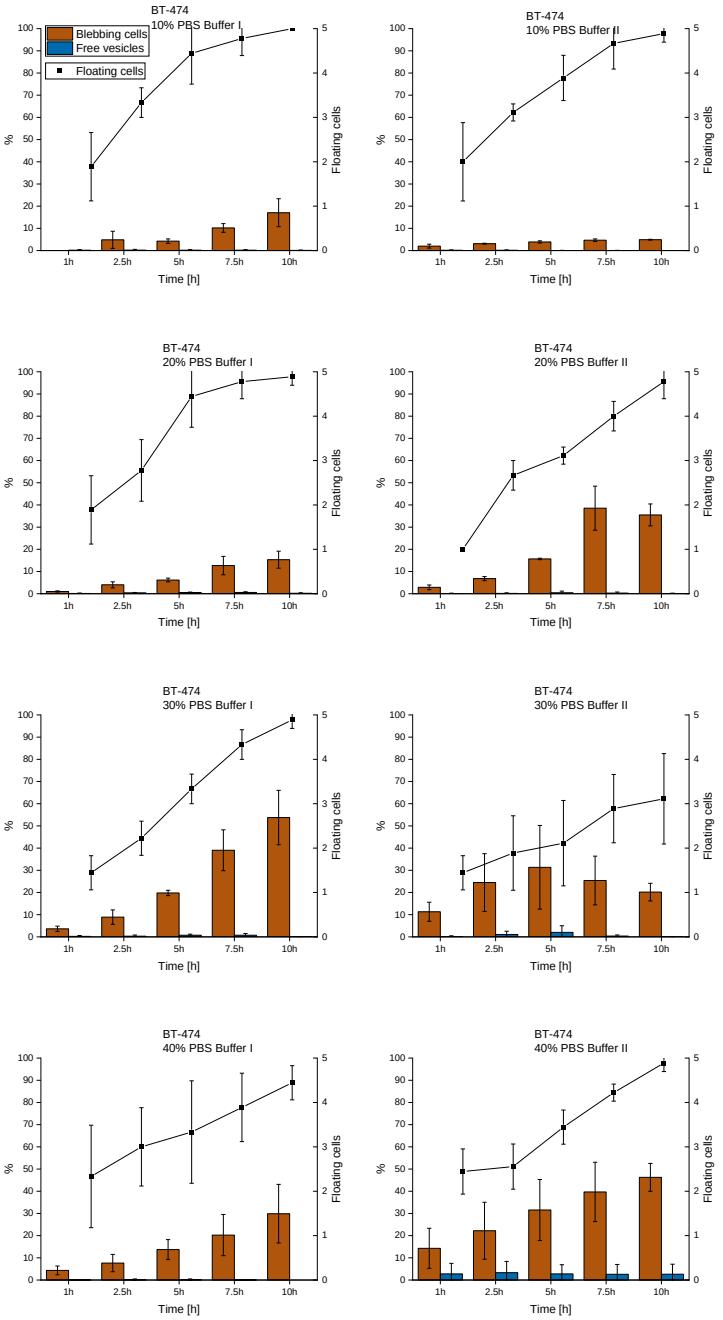

Figure 39 Osmotic formation of GPMVs in BT-474 was unsuccessful under a range of conditions. BT-474 cells were treated with a range of hypotonic buffers (10% PBS, 20% PBS, 30% PBS and 40% PBS), followed by a range of hypertonic buffers (buffer I and buffer II) and the formation of GPMVs was observed by microscopy over time, along with quantification of blebbing cells and free-floating cells. Time is shown along the x-axis, the quantity of blebbing cells (left y-axis, orange bars), free vesicles (left y-axis, blue bars) and floating cells (right y-axis black line) expressed as a percentage of the total number of cells. Data represent means (with SD) of three fully independent experimental replicates.

Overall, the results showed that only MCF-10A cells are capable of producing vesicles with a relatively small quantity of cell debris under hydrostatic pressure. Isolated membrane extracts have a spherical structure, and their size varies between 15 to 35 μm. Having produced GPMVs from at least MCF-10A cells, the attempts to separate these vesicles from the floating cells, which can be regarded as a contaminant in the GPMV suspension were conducted. Therefore, according to the Sezgin et al. protocol, GPMVs suspension was centrifuged in order to remove cellular contamination [84]. Surprisingly, no vesicles were presented in the vial after the separation procedure indicating that GPMVs were destroyed by the applied force. Also, GPMVs suspension kept in hypertonic buffer was observed to burst after 24 h from the process induction. Having failed to pellet cell debris, GPMVs cannot be transfered into a biocompatible medium.

Although the initially used LACAF cell line was replaced by MCF10A during the project progression, the phenomenon of shedding plasma membrane vesicles under osmotic pressure was captured and seen. on Figure 40.

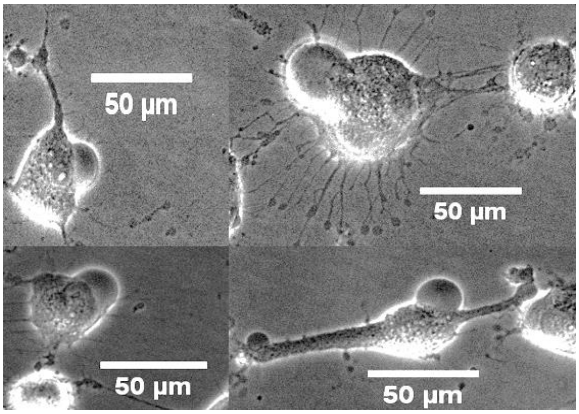

Figure 40 Representative picture of LACAF cells under osmotic vesiculation treatment (30% PBS, buffer I). The picture was taken using phase-contrast microscopy. The scale bar is 50 μm.

3.3.1.2 NEM-induced GPMVs formation fails to generate vesicles

Having failed to generate satisfactory numbers of GPMVs in the majority of cell lines under an osmotic gradient, the next aim was to test the effectiveness of chemical vesiculation. To initiate cell budding, all four cell lines were rinsed with Ca^{2+}-enriched buffer and then exposed to vesiculation agent (*N*-ethylmaleimide; NEM). NEM is a stressor agent causing cell blebbing [261]. GPMVs formation was monitored and associated cellular events: cell blebbing and cell detachment using phase-contrast microscopy. In order to optimize the procedure for each cell line, a range of different conditions was applied and GPMVs formation effectiveness was rated at different time points. The number of released GPMVs, blebbing cells and floating detached cells were quantified and expressed as a percentage of the total cell number.

Typically, at a range of NEM concentrations cell blebbing was a time-dependent process, in particular for AU-565, while for MDA-MB-468 and MCF-10A at least at very early time points. Contrary, BT-474 cells exhibited a reverse tendency as the number of budding cells gradually dropped. It might be explained by the potential progression to a floating cell. Overall, any of the cell lines were capable of GPMVs release under a range of conditions in a time-dependent manner (Figure 41 –Figure 44). Chemical vesiculation using sulfhydryl blocking agent induced cell membrane protrusions, but few vesicles were released from the membrane surface. Cell buds reach up to 10 μm in diameter, simultaneously, substantial cell detachment appeared at later time points. It has been concluded that those conditions are not suitable for GPMV preparation from MCF-10A, MDA-MB-468, BT-474 and AU-565.

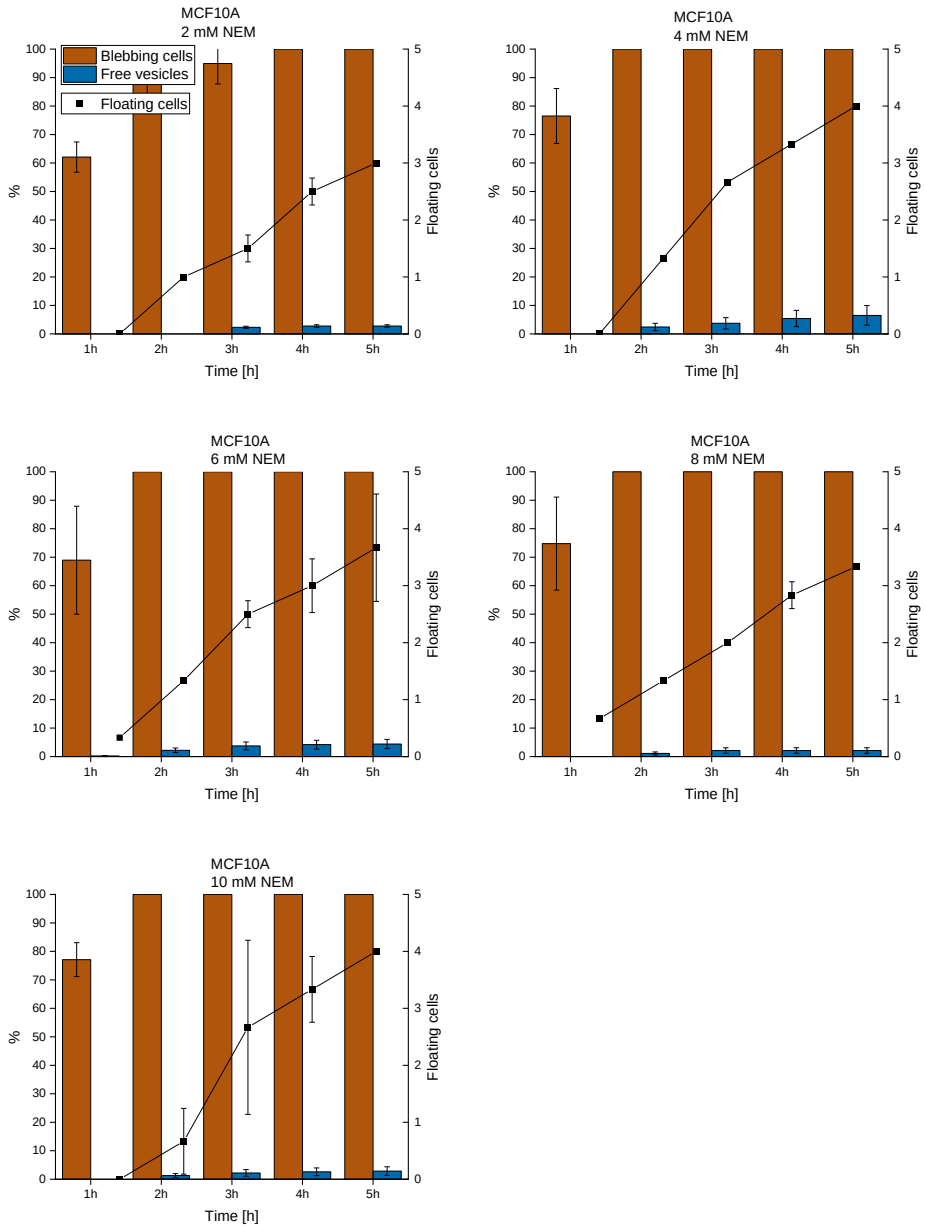

Figure 41 Chemical formation of GPMVs in MCF10A was unsuccessful under a range of conditions. MCF-10A cells were rinsed with GPMVs buffer, followed by incubation in GPMVs buffer containing NEM as a vesiculation agent and the formation of GPMVs was assessed by microscopy over time, along with quantification of blebbing cells and free-floating cells. Time is shown along the X-axis, the quantity of blebbing cells (left Y-axis, orange bars), free vesicles (left Y-axis, blue bars) and floating cells (right Y-axis black line) expressed as a percentage of the total number of cells. Data represent means (with SD) of three independent experimental replicates.

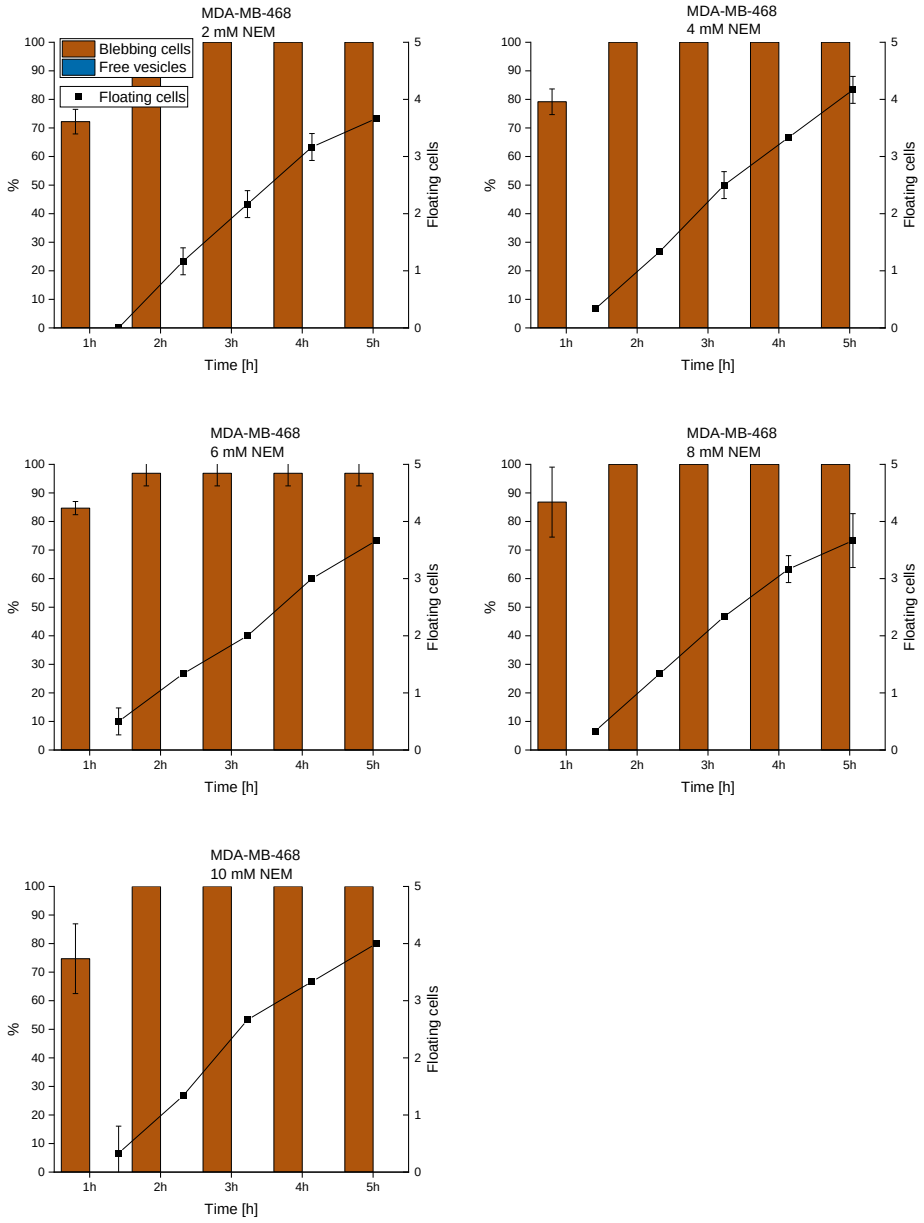

Figure 42 Chemical formation of GPMVs in MDA-MB-468 was unsuccessful under a range of conditions. MDA-MB-468 cells were rinsed with GPMVs buffer, followed by incubation in GPMVs buffer containing NEM as a vesiculation agent and the formation of GPMVs was assessed by microscopy over time, along with quantification of blebbing cells and free-floating cells. Time is shown along the x-axis, the quantity of blebbing cells (left y-axis, orange bars), free vesicles (left y-axis, blue bars) and floating cells (right y-axis black line) expressed as a percentage of the total number of cells. Data represent means (with SD) of three independent experimental replicates.

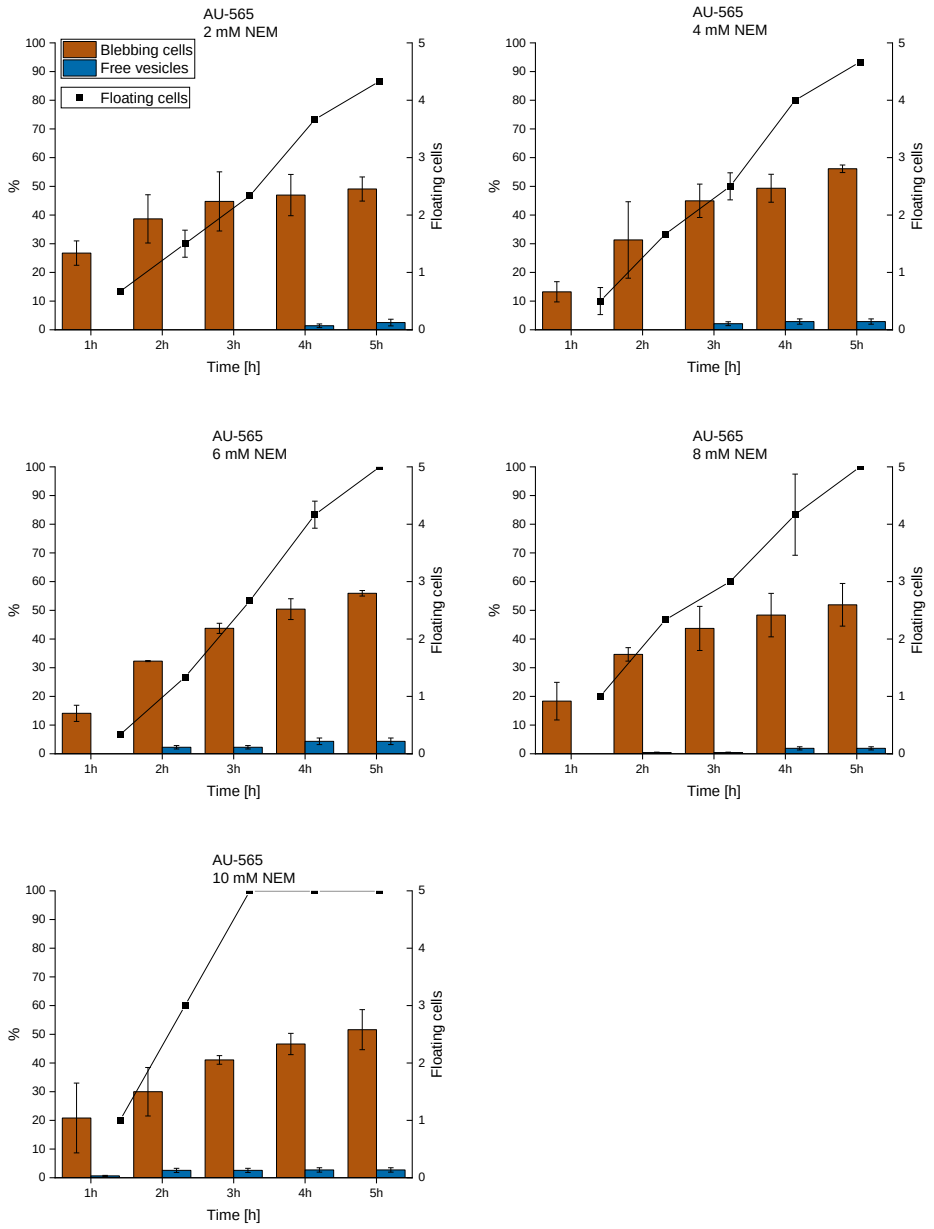

Figure 43 Chemical formation of GPMVs in AU-565 was unsuccessful under a range of conditions. AU-565 cells were rinsed with GPMVs buffer, followed by incubation in GPMVs buffer containing NEM as a vesiculation agent and the formation of GPMVs was assessed by microscopy over time, along with quantification of blebbing cells and free-floating cells. Time is shown along the X-axis, the quantity of blebbing cells (left Y-axis, orange bars), free vesicles (left Y-axis, blue bars) and floating cells (right Y-axis black line) expressed as a percentage of the total number of cells. Data represent means (with SD) of three independent experimental replicates.

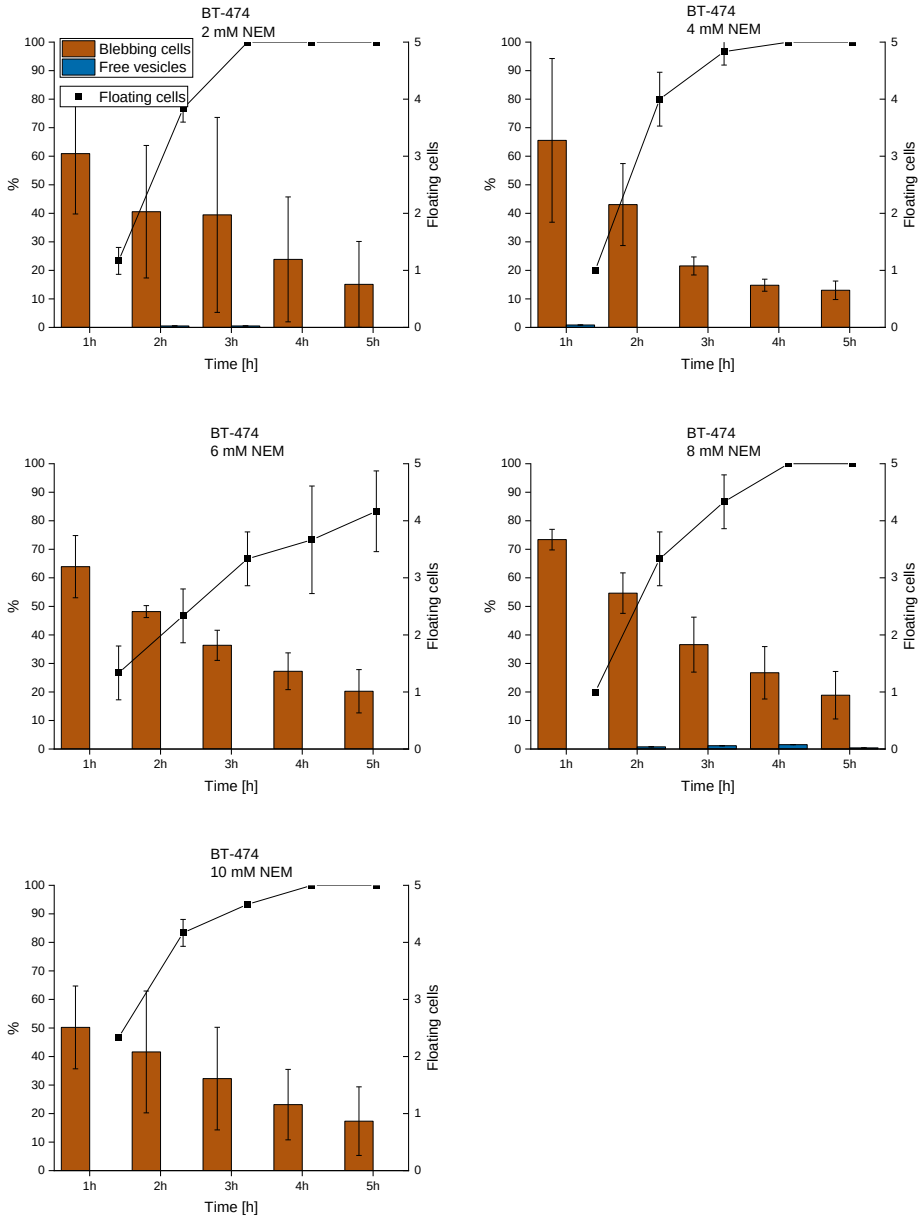

Figure 44 Chemical formation of GPMVs in BT-474 was unsuccessful under a range of conditions. Bt-474 cells were rinsed with GPMVs buffer, followed by incubation in GPMVs buffer containing NEM as a vesiculation agent and the formation of GPMVs was assessed by microscopy over time, along with quantification of blebbing cells and free-floating cells. Time is shown along the X-axis, the quantity of blebbing cells (left Y-axis, orange bars), free vesicles (left Y-axis, blue bars) and floating cells (right Y-axis black line) expressed as a percentage of the total number of cells. Data represent means (with SD) of three independent experimental replicates.

3.3.1.3 PFA and DTT induce GPMVs formation in cancer cell lines

As the data show, NEM was not an effective vesiculant for breast cell lines. Having failed to induce GPMVs by applying NEM, the next combination of paraformaldehyde (PFA) and dithiothreitol (DTT) was used to induce vesiculation. The PFA/DTT mixture induces cortex contraction and increases hydrostatic pressure, and ultimately leading to membrane blebbing [262]. Cells were washed with divalent cations-enriched buffer and then incubated with a salt solution containing 25 mM PFA and 2 mM DTT. GPMVs formation was monitored using automated bright-field microscopy. The number of released GPMVs, blebbing cells and floating detached cells were quantified and expressed as a percentage of the total cell count.

After testing and optimizing different GPMVs formation procedures, it was observed that three of the four cell lines readily released GPMVs under applied conditions in a time-dependent manner (Figure 45).

Representative images of cells under these conditions are shown in Figure 46. The procedure generated a relatively small quantity of detached cells. The only adjusted variable was the time of incubation. Sezgin et al. recommended 2 h of incubation, whereas breast cell lines require 5 h exposure to PFA and DTT [84]. GPMVs produced after exposure to PFA and DTT were smaller than those generated through osmotic force- their size range is between 0.5 µm to 15 µm. Also, it has been observed that an individual cell is capable of producing up to 10 buds The PFA/DTT method was identified to yield a substantial fraction of GPMVs from each breast cell line However, it is widely reported that PFA and DTT might incorporate membrane artefacts [84]. PFA is a cross-linker inducing cell shrinkage, while DTT is a disulfide-reducing agent which together may cause: aldehyde-induced nonspecific cross-linking of lipids and proteins; breaking of protein disulfides and thioesters; coupling of phosphatidylethanolamines to proteins [90].

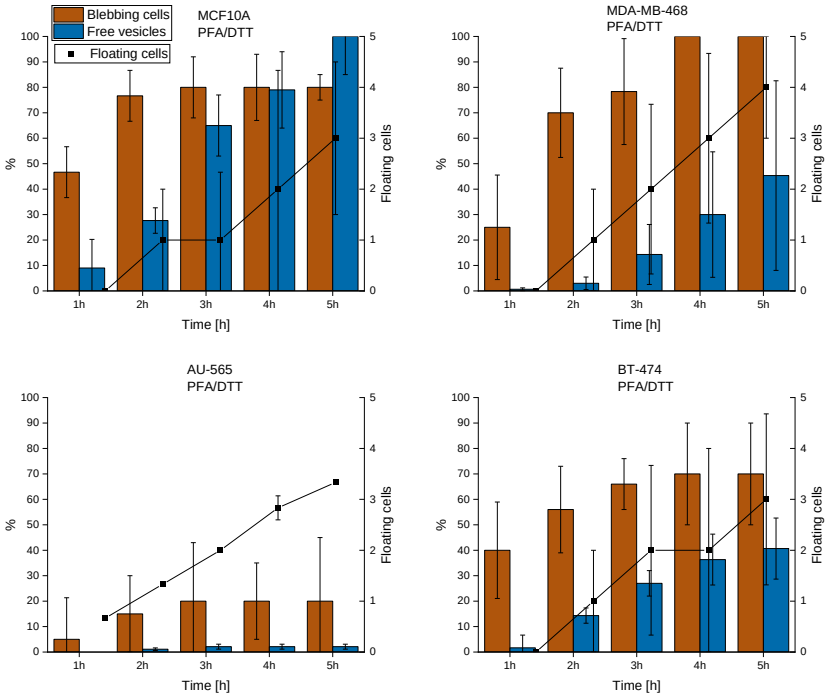

Figure 45 Chemical formation of GPMVs in three of the four cell lines was successful. Cells were rinsed with GPMVs buffer, followed by incubation in GPMVs buffer containing PFA and DTT as vesiculation agents and the formation of GPMVs was assessed by microscopy over time, along with quantification of blebbing cells and free-floating cells. Time is shown along the X-axis, the quantity of blebbing cells (left Y-axis, orange bars), free vesicles (left Y-axis, blue bars) and floating cells (right Y-axis black line) expressed as a percentage of the total number of cells. Data represent the means of three experiments.

Attempting to purify GPMVs suspension, differential centrifugation was found not to cause vesicle breaking, as opposed to vesicles which were subjected to hypertonic buffer, however, cell debris was not separated. GPMVs suspension using this vesiculation procedure can be kept for 48 h at 4˚C without substantial bursting. GPMVs cannot be transferred into a biocompatible solution.

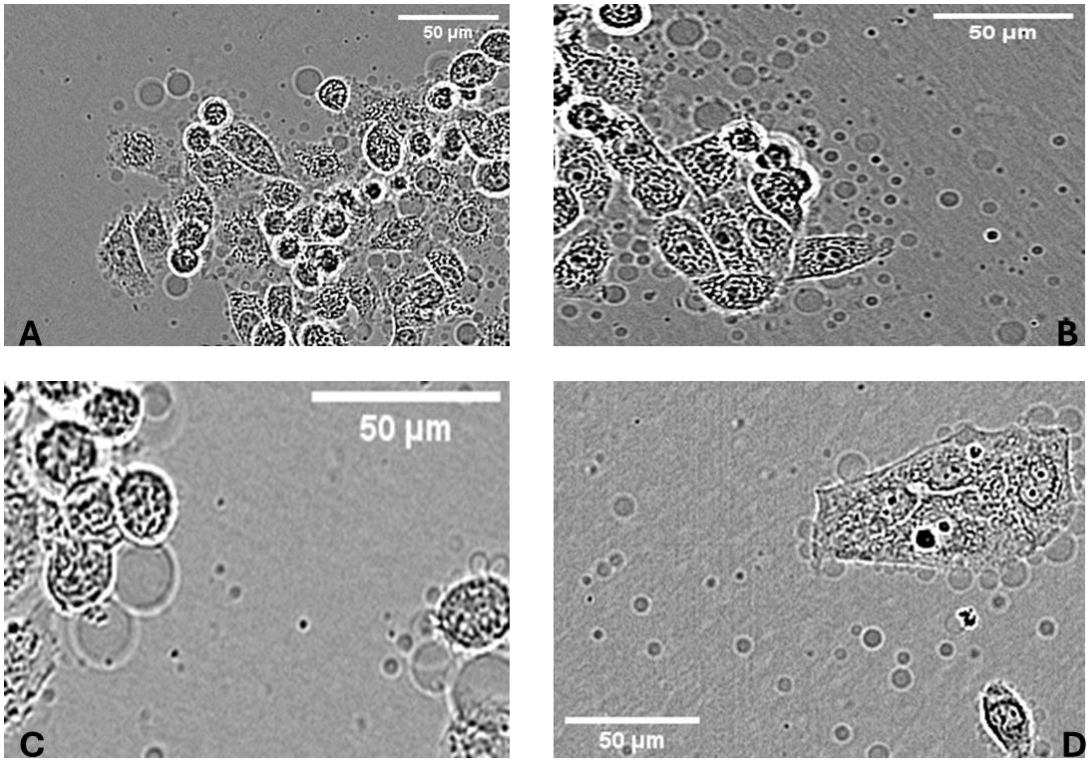

Figure 46 Representative pictures of all cell lines under chemical vesiculation using PFA and DTT: (A) MCF-10A; (B) MDA-MB-468; (C) AU-565; (D) BT-474. Pictures were taken using phase-contrast microscopy. The scale bar is 50 µm.

3.3.1.4 Membrane integrity is affected in isolated GPMVs

Having successfully isolated GPMVs by two distinct procedures, further characterization of membrane extracts was conducted. It is worth mentioning that some of the vesicles did not have spherical shapes. Knowing the limitations of applied vesiculations, such as perturbed cell biophysical properties as a consequence of cell swelling and subsequent shrinking, the incident of protein cross-linking or thioester bond cleavage, the next aim was to optimise GPMVs visualisation and to test PM integrity.

To visualise GPMVs by high-resolution fluorescence microscopy, membrane-binding lipophilic tracers were applied. Prior to the vesicle isolation, cells were incubated with Nile Red, exhibiting a deep red emission peaking at 636 nm. The initial experiments revealed poor dye incorporation into the lipid bilayer, while the larger concentration

generated high background fluorescence. An alternative approach to visualising the membrane is the use of dialkylcarbocyanine dyes. One of them, DiO, a widely applied lipid marker in GPMVs research, did not effectively label plasma cell membranes either before GPMVs isolation or at post-isolation labelling [84, 250, 263]. Another amphiphilic probe, DiI incorporated into the membrane of all types of induced GPMVs and was applied prior to GPMVs isolation. Although originated from the carbocyanine family, dyes exhibit dissimilar lateral diffusion which might explain distinct dye behaviour. Both DiO and DiI have saturated alkyl substituents (C_{18}), however DiO was previously reported to fail labelling biological samples [264].

In order to investigate membrane permeation, GPMVs were incubated with the size-different fluorophores with distinguishable emission spectra from the lipid marker, namely, cascade blue (CB) labelled 10 kDa dextran and 70 kDa dextran conjugated to fluorescein isothiocyanate (FITC). The channel detection approach allowed visualization of GPMVs permeability. The representative images captured after 30 min of confocal microscopy observation are presented in Figure 47 where the green or blue background originated from the applied fluorophores. Typically. GPMVs, seen as dark circles relative to background fluorescence, are considered “sealed”, whereas permeable spheres have bright fluorescent lumens.

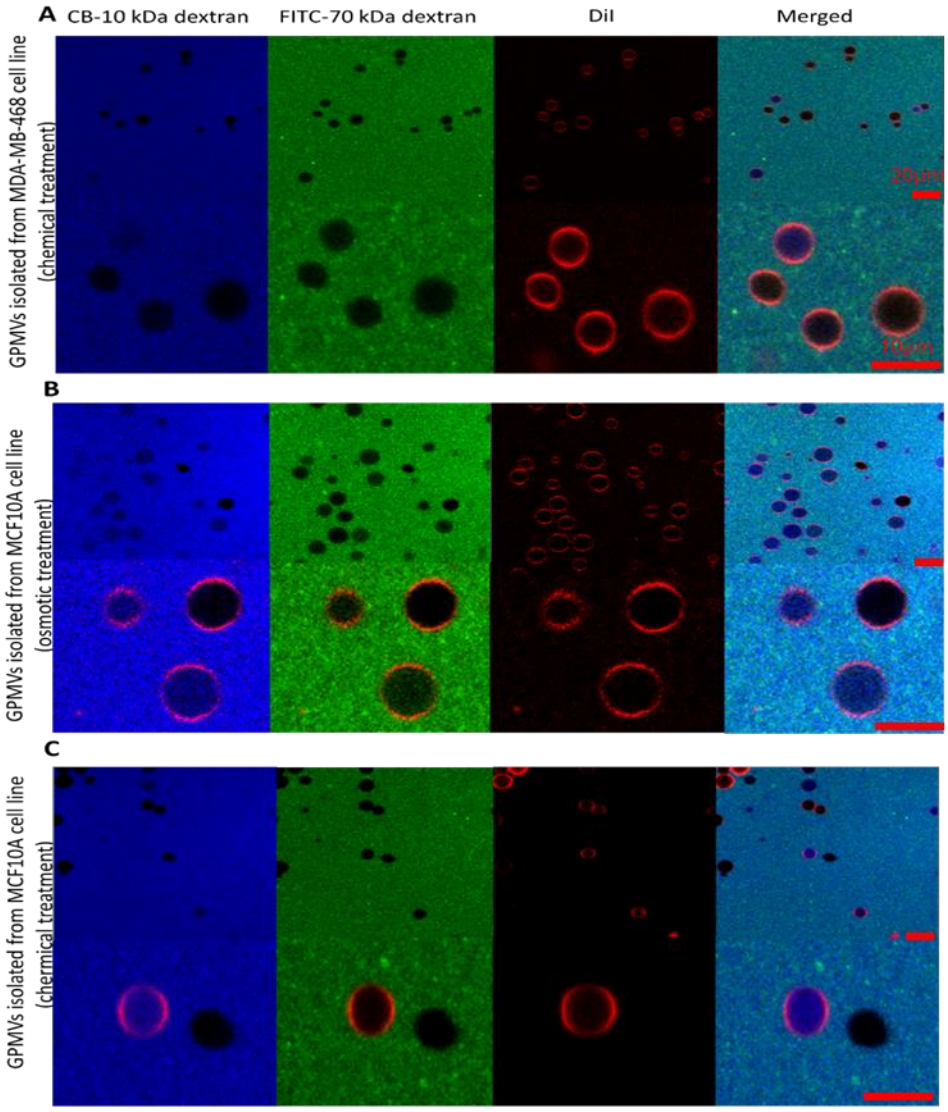

Figure 47 GPMVs membrane is permeable to solutes ranging from 10 kDa to 70 kDa. Isolated GPMVs were incubated with external Cascade blue-10 kDa dextran (CB-dextran) and fluorescein isothiocyanate - labelled 70 kDa dextran; (A) chemically induced GPMVs from MDA-MB-468 cell line; (B) osmotically induced GPVs from MCF-10A cell line; (C) chemically induced GPMVs from MCF10A cell line.

A visible accumulation of fluorescent solutes was observed inside many vesicles, however, the dye influx was heterogeneously distributed across the vesicle samples. The probe uptake was quantified after 30 min of incubation by measuring the fluorescent intensity of the GPMV lumen and the bulk fluorescence has been used as a reference.

Relative vesicle intensity equal to or above 0.7 characterizes highly permeable GPMVs. Their lumen brightness is comparable to that of a bulk solution. Due to the lack of background subtraction, relative fluorescence intensity equal or below 0.3 classifies vesicles as non-leaky.

Approximately 60 vesicles were examined to evaluate the relative fluorescence intensity in the three investigated groups: osmotically derived GPMVs from MCF10A cells and chemically-induced GPMVs from MDA-MB-468 and MCF10A cells. Figure 48A represents the permeability trends of each vesicle population in a given preparation. Overall, the total population of vesicles induced by osmotic pressure accumulated 10 kDa in the interior with a relative vesicle intensity of approx. 0.7, while permeability to 70 kDa macromolecule was heterogenous oscillating between 0.3 to 0.7 of relative fluorescence intensity. The minimal detected value was one-third of the fluorescence bulk for the incubation with FITC- 70 kDa. Unlike osmotic preparation, GPMVs produced in the response to PFA/DTT from PM of MDA-MB-468 and MCF-10A cell lines displayed a lower tendency to accumulate 70 kDa conjugated dextran above 0.3 with some individual exceptions. A range of values obtained from fluorescence measurements of 10 kDa dextran revealed a heterogeneous distribution with a relative vesicle intensity from 0.2 to 0.7. To further investigate the permeation phenomenon, size distribution was correlated to the intravesicular fluorescence intensity of chemically induced GPMVs from the MDA-MB-468 cell line and results are seen in Figure 48B and Figure 48C. Within the investigated GPMVs population, there is a size-independent variation in membrane integrity. Typically, vesicle size ranges from 3 to 8 μm and these GPMVs exhibit various permeability to both solutes. These findings are indicative of possible system permeation and that only individual vesicles preserve membrane integrity.

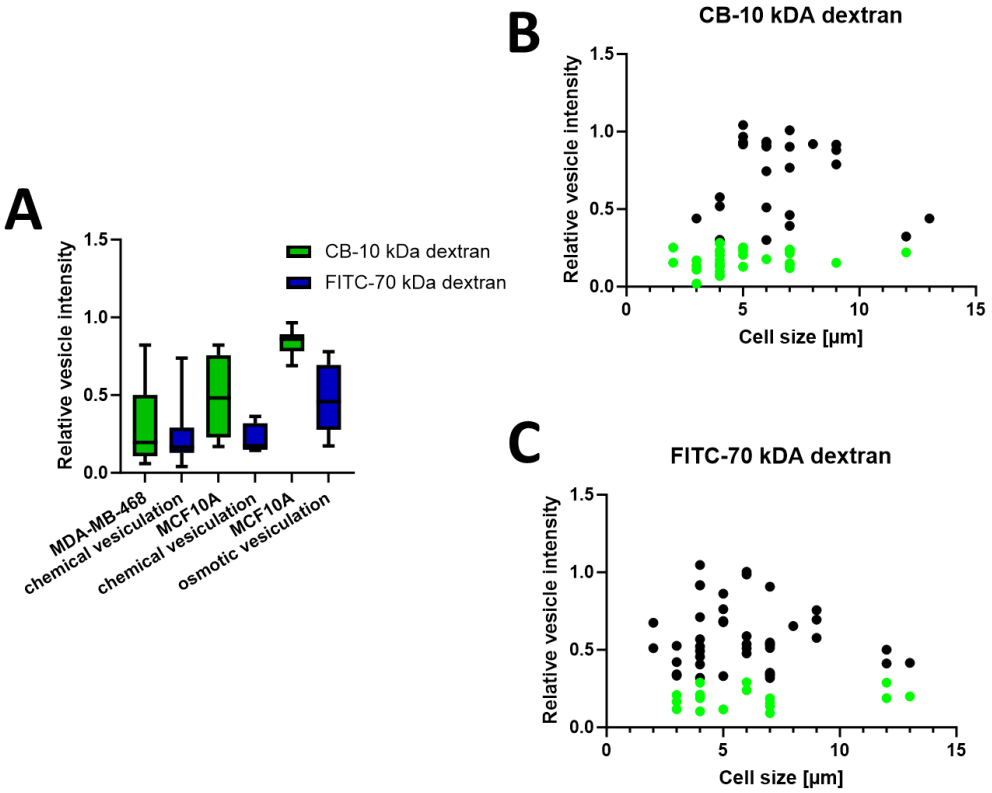

Figure 48 GPMVs membrane is permeable to solutes as large as 10 and 70 kDa. Data show an accumulation of probes in most vesicles; (A) the relative vesicle intensity is quantified and each data set represents the permeability trends of distinct vesicle populations. Results show a huge heterogeneity in GPMVs permeability. GPMVs isolated under osmotic pressure display the highest intensity profile compared to the bulk; (B, C) To further investigate the permeation phenomenon, the diameter of each vesicle was measured and correlated with the fluorescence intensity profile. Large heterogeneity seems to be size-independent. Each point represents an individual vesicle, where the X-axis indicates vesicle size (µm) and the Y-axis shows relative fluorescence intensity in a given preparation (N>60 vesicles/preparation).

3.4 Discussion

Lipid vesicles are an experimental model used to study membrane-based events [265]. The minimal system allows for minimizing complex cellular variability to uncover the principles of cell functionality [266]. Nevertheless, the plasma membrane is highly

heterogeneous, not only in terms of components but also in association with other cellular structures, and minimized systems, despite many undeniable strong points, do not mimic closely its multi-faced nature [10]. GPMVs, the live-cell-derived model system, have emerged as a prospective candidate to replace and bridge the gaps in cell membrane biophysics [254]. Herein, the search for conditions for direct isolation of vesicles from the cell PM is presented. Although reported since the 70s, there is little known about GPMVs extracted from tumour cells [85]. The straightforward procedure would facilitate studies aiming at uncovering principles of MP1-induced membranolytic activity.

3.4.1 The phenomenon of cell budding

Del Piccolo et al. developed the GPMVs formation procedure, which utilizes an osmotic chloride salt cocktail to produce giant vesicles from CHCO cells [255]. It has been observed that incubation in a hypotonic solution makes all types of cells swell, whereas only MCF-10A cells release a substantial yield of vesicles in a relatively short time (5h). This is a highly adherent cell line and among others, the only non-transformed cell line. The application of the 10-times diluted hypotonic buffer improves vesiculation. Contrastingly, it was demonstrated that hydrostatic force results in cell blebbing of BT-474, AU-565 and MDA-MB-468 cells. Notably, the major drawback of this procedure is a substantial detachment of all kinds of tested cells as a result of cell shrinkage under hypertonic conditions. Although many reports indicate the uncomplicated separation process of cell debris, it was found unachievable [84, 267–269].

Exposure of monolayer tissue culture cell line to sulphydryl blockers is an effective GPMVs formation procedure first introduced by Scott et al. almost five decades ago [85]. Initial experiments with the use of 3T3 and SV3T3 mouse embryo cells proved vesicle release into the medium after 1.5 to 2 hours at 37˚C. Here it was demonstrated that PFA,

potentiated in the presence of DTT, induces the shedding of PM vesicles. Cells require a longer incubation, up to 5 h, in order to produce a large yield of GPMVs. However, simultaneously, during the vesiculation process, a huge number of cells detach contaminating vesicle suspension. Noteworthy, many protocols recommend experimental plate shaking or rolling, which might result in higher cell debris [85, 270]. Nevertheless, the use of PFA- and DTT-based procedures has been criticized due to the high probability of non-specific protein and lipid crosslinking, cleavage of thioester bonding or specific coupling of phosphatidylethanolamines to protein [15, 90]. Optimistically, one believes that PFA at a low dose does not incorporate artefacts [271]. Here it was shown that another vesiculant, NEM, already applied to avoid PFA limitations, induced PM blebbing without vesicle budding off [84, 85].

The presented section demonstrates the benefits and drawbacks of two commonly employed GPMVs formation protocols. Vesiculation is a dose-, time-, and temperature-dependent process and for each culture cell line variable parameters ought to be optimized. The experiments confirm the effectiveness of PFA and DTT in inducing a great yield of vesicles. A summary of vesiculation procedures is presented in Table 1. Not considered before, chemical treatment is conducted at physiological pH while the hypertonic buffer which generates hydrostatic pressure has a pH of 8.5 (due to use of bicine as the buffering agent which buffering range is pH 7.6-9). Some of the membrane proteins are vulnerable to a low ratio of hydrogen ions and release protons in the process of air oxidization, which affects membrane protein interactions [272]. Another disregarded factor important to vesicle generation is the presence of divalent cations. Lack of calcium in the vesiculation buffer inhibited the process [249]. It has been reported that an influx of Ca^{2+} can cause the degradation of plasma membrane-specific phosphatidylinositol polyphosphates, which constitute the attachment points of the actin cytoskeleton to the plasma membrane [16].

Calcium and magnesium ions promote cell adhesion, thus, their optimal concentration might be of importance in preventing cell debris generation [273]. Moreover, vesicles generated in the process of apoptosis and necrosis were identified, closely resembling those produced by chemical treatment and in the consequence of applied osmotic force, respectively [274]. This finding is consistent with other observations, such as the appearance of apoptotic spikes and cell detachment, which are the hallmarks of the cell death process [275].

Here, it is shown that a large population of GPMVs has defective membrane integrity. Exposure of PM spherical extracts to a range of size-different macromolecules revealed their accumulation in the lumens. Although leakiness is highly variable, it could be assumed that GPMVs permeability is affected by the isolation procedure, however there is no size-dependent trend. Corresponding results have been reported by Skinkle [91]. It was postulated that GPMVs modulated during exposure to standardized vesiculation agents are passively permeable to macromolecules due to the formation of large transmembrane pores in the process of vesicle rupture. It has been explained that shear stress generated by bulk fluid flow mechanically forces membrane blebs to rip off and consequently, membrane perturbations are initiated and stabilized by amphiphilic proteins in the GPMVs lumen. Skinkle reported that when the shear stress is reduced, the GPMVs membrane is sealed as vesicles are released only in the “natural” process. It can be concluded that transmembrane proteins might be associated to some extent with membrane integrity. Nevertheless, regardless of the procedure, while membrane blebs are subjected to shear force, they break away from the surface in an improper manner, what might result in the loss of membrane proteins. However, it should be noted that PM contains water channels termed aquaporins, transmembrane proteins with a three-dimensional structure that constitutes a pore allowing the selective passage of water molecules [276]. Another

factor to consider, the change in lipid profile as a result of PFA and DTT exposure. Scott already reported that the vesicle's PM lipids ratio does not closely mimic that of the whole cell homogenate- PM extract surface is enriched in cholesterol, PE, PI and SM. Furthermore, one of the biophysical PM characteristics is depleted- the lipid bilayer loses its asymmetry [277]. Furthermore, Los et al. suggested that hypertonic stress might reduce membrane fluidity similarly to low-temperature exposure [278]. Membrane stability and membrane domain organization are modulated by the interactions between the plasma membrane and the actin cytoskeleton, therefore the lack of cytoskeletal components might be linked to the GPMVs leakiness [279].

Live-cell-derived systems retain cell PM composition and biophysical properties to some extent, which, undoubtedly, rank GPMVs as important tools for providing insight into cell membrane studies. Despite limitations, the close-to-native membrane model might be of use in studies aiming at uncovering the principles of membrane-associated events. Interestingly, alternative GPMVs formation procedures have been developed in recent years- vesicles can be induced upon exposure to light irradiation or a proapoptotic peptide [267, 280].

Table 4 The summary of GPMVs formation procedures- my observations to already published methods [66, 239]

CHARACTERISTICS	OSMOTIC VESICULATION	CHEMICAL VESICULATION
VESICULANTS	Hydrostatic pressure	Alkylating agents: PFA, DTT, NEM (ineffective)
pH	8.5	7.4
CELL DEBRIS	A huge inseparable amount	A huge inseparable amount
OPTIMIZATION	Required for each culture cell line	Unnecessary
EFFECTIVENESS	Vesicles formation from normal cells	Vesicles formation from all types of cells including cancer types
VESICLE YIELD	Large	Large

VESICLE SIZE	15-35 µm	0.5-15 µm
MORPHOLOGY	Spherical with some deviations	Spherical with some deviations
PERMEABILITY	Highly leaky	Heterogeneously leaky
LIMITATIONS	Ineffective, cell debris, permeable to solutes as large as 70 kDa	Cell debris, chemical artefacts, permeable to solutes as large as 70 kDa, loss of lipid asymmetry

3.5 Conclusions

This work presents testing and optimization of routinely used GPMVs preparation protocols by means of osmotic pressure and alkylating agents. The development of enhanced osmotic conditions to produce a doubled number of MCF10s-derived GPMVs revises previously published guidelines. PM vesicles were readily induced by chemical procedure, which employs PFA and DTT, a crosslinker and reducer, respectively. The membrane integrity visualization and fluorescence intensity quantification revealed the ability of solutes as large as 70 kDa to unobstructedly penetrate across the lipid bilayer accumulating in the lumen interior. However, GPMVs isolated after cell exposure to chemical agents manifested lower permeability likely due to membrane protein cross-linking. This investigation provides alternative findings to already reported GPMVs studies and their application as a model system shedding light onto not the effortless vesiculation process and not impenetrable live-cell-extracted membrane envelope. Considering peptide-induced permeability studies being challenging due to a noticeable degree of background leakiness in GPMVs, environment-sensitive membrane probes will be applied to investigate changes in membrane organisation when interacting with MP1 peptide.

Chapter 4 The heterogeneous nature of cell plasma membrane- the role of membrane lipid organization in cell response to Polybia MP1.

ABSTRACT

Artificial lipid platforms, as presented in the earlier chapters, have been employed to identify the role of membrane lipid composition in the context of Polybia MP1 lytic activity. Phosphatidylserine, a negatively charged phospholipid found abundant in the outer leaflet of the cancer cell membrane, has been recognised to facilitate the membrane-perturbing MP1 effect. This section focuses on expanding our insight into peptide: lipid interaction in GPMVs closely reflecting the heterogeneous organization of cellular membranes. By applying fluorescent lipid probes, we can observe membrane organization prior to and before MP1 treatment. This work indicates that cell-specific lipid order modulates cell response to MP1. Also, MP1 was found to induce changes in membrane packing order.

4.1 Introduction

Straightforward leakage assays testing minimal lipid platforms against a pool of MP1 variants presented in Chapter 2 demonstrated MP1 membranolytic activity in a peptide: lipid -dependent manner. Previously, Leite et al. already proved that MP1 becomes biologically active and adapts to an α-helical secondary structure when interacting with a membrane-like environment [234]. Having a reduced number of components, lipid platforms cannot sufficiently reproduce the heterogeneous and complex nature of biological membranes. The intermediate membrane model bridging synthetic platform and cell PM are GPMVs (see Chapter 3), micron-sized spheres directly harvested from cultured cells as a result of stress-induced treatment [84, 249, 255, 281]. GPMVs are

believed to retain close-to-native membrane diversity which makes them unique membrane platforms.

The biological membrane is arranged in two asymmetric layers capable of self-organizing into lateral micro- and nanodomains of various content, shapes and dynamics [44]. The coexistence of the liquid-liquid phase separation has been proven and widely investigated in GPMVs elucidating physical fundaments of the raft hypothesis in cell PM [16]. Cell-specific variables in lipid bilayer arrangement include differences in head group composition, chain lengths, degree of saturation pH or ions-enriched surroundings [282]. Investigating membrane organization requires defined imaging tools, in particular, fluorescent probes labelling the molecule of interest. Visualisation of the lipid environment by aligning fluorescent moieties to lipids and integrating these probes into PM is a standard for the optical examination of cell-like membrane systems. These fast-developing molecular probes are capable of partitioning into one of the L_o/L_d phases [283]. Correspondingly, fluorophores with saturated acyl tails preferentially co-localise with tightly packed regions, whereas unsaturated chains are found to incorporate into a disordered liquid phase [284]. Common protocols employ the polarity-sensitive fluorescent membrane probes, benefiting from the phenomenon of solvent dipolar relaxation, directly responding to a number of water molecules present at the membrane interface reflecting lipid packing [285].

Due to the reduced complexity of simple synthetic lipid membranes, the understanding of Polybia MP1 membranolytic activity is not fully elucidated. This chapter reports attempts to extend previous observations and compare lipid phase behaviour prior to and after MP1 exposure in a cell-derived model system. The lateral organization of biomimetic cell membranes was examined using commercially available fluorescent membrane probes and was investigated in the context of cell sensitivity to MP1. Studies

revealed that membrane organization is cell-specific and that MP1 modulates changes in lipid packing.

4.2 Materials and methods

4.2.1 Materials

4.2.1.1 Reagents

GPMVs were isolated using PFA/DTT agents as described in Chapter 3 following the Sezgin et al. protocol [84]. Confocal microscopy and DiI labelling were performed as indicated in Chapter 3.

4.2.1.2 Fluorescent probes

Laurdan (Cat. No D250) were purchased from Invitrogen (CA, USA). C-Laurdan (Cat. No 7273) was purchased from Tocris Bioscience (Bristol, UK). Prodan (Cat. No ab145246) was purchased from Abcam (Cambridge, UK). Probes were dissolved in DMF to 0.2 mM concentration. 8-well glass bottom chambers (Cat. No 80826) were purchased from Ibidi (USA, MS).

4.2.2 Methods

4.2.3 Membrane labelling

30 mins prior to imaging, GPMVs were labelled with Laurdan, C-Laurdan or Prodan by adding approx. 1.25µL of 0.2 mM probe solution to 50µL of GPMVs suspension at room temperature. Samples were imaged in 8-well glass bottom chambers that had been pre-coated with 200 µL of 5% BSA for 10 minutes at room temperature and thoroughly rinsed 3 times with deionised water.

4.2.4 Confocal spectral imaging

Spectral imaging of different membrane extracts was performed on a Zeiss LSM 880 confocal microscope equipped with a 32-channel GaAsP detector array at room temperature. Laser light at 405 nm was used for fluorescence excitation of Laurdan, C-Laurdan and Prodan. The lambda detection range was selected between 400-550 nm. The wavelength intervals were set to 8.9 nm to cover the whole spectrum with 32 detection channels. The images were saved in .lsm file format.

4.2.5 GP Calculation from the Spectral Images

A custom GP plug-in was used in Fiji/ImageJ (available at https://github.com/dwaithe/GP-plugin) for the analysis of acquired spectral data. This plug-in simplified the calculation of the General Polarization index through fitting wavelength intervals.

Fluorescent membrane probes are characterised by dipole moment that changes in response to excitation leading to the reorientation of solvent dipoles [286]. The energy required for adaptation decreases the fluorophore excited-state energy occurring in a more aqueous disordered lipid phase with a maximal emission peak at 490 nm (see Figure 49).

General Polarization (GP), a normalized polarity index, is a parameter indicating the ratio of fluorescence intensity in the blue-shifted (L_o phase) and red-shifted (L_d phase) spectrum, calculated as: $GP = \frac{I_{440}-I_{490}}{I_{440}+I_{490}}$,where I_x reflects the intensity at a wavelength of x nm.

Each slice of the image stack corresponds to a certain wavelength λ in respective 8.9 nm-wide intervals and the emission spectra are acquired from pre-processed images for each pixel. During processing, the spectral image stacks are integrated via Z-projection

and masked using a user-defined threshold on an 8-bit grey scale (0–256). This step allows the analysis of fluorescence-positive areas above the background. The GP plug-in applies Gaussian fit for modelling raw I_λ distribution for each pixel. The quality of the fit, determined by the R^2 measure, enters only pixels above a user-defined noise tolerance (0.0–1.0, where 1.0 is the best fitting). Finally, obtained values are normalized through division by 255 and proceed to GP calculation using Equation. GP distribution is illustrated on a spatial GP map representing the GP value for each pixel of the image and distributed on a histogram which applies a custom look-up-table (LUT) to the data. Additionally, the LUT edition provides a more vividly and distinguishably presented lipid phase state.

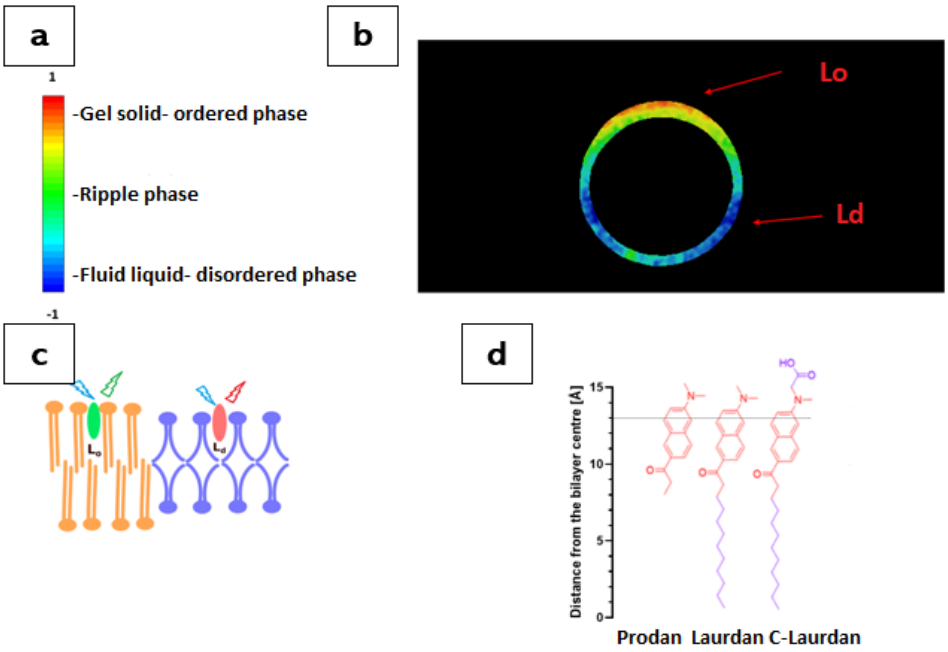

Figure 49 The polarity-sensitive dyes as indicators of lipid packing; (a) GP scale reflecting lipid order: 1 indicates ordered phase, whereas -1 reflects disorder domains; (b) GP map. Representative image of GPMV with C-Laurdan illustrating Lo and Ld phases; (c) Schematic diagram of lipid bilayer representing Lo and Ld phases and the colour response of the solvatochromic probe to the changes in the lipid order; (d) Chemical structure of Prodan, Laurdan and C-Laurdan showing their approximate bilayer locations, adapted from [17, 18]. The phospholipid bilayer of live cells is normally 30–40 Å thick [17]

4.3 Results

4.3.1 MP1-associated differential partitioning of DiI in GPMVs

First, the Dil dye was used to allow visualisation of lipids within the membrane of GPMVs both before and during their interactions with MP1. GPMVs isolated either from MDA-MB-468 or MCF-10A cells were homogenously labelled with a DiI lipid marker at the observed spatial resolution (Figure 50). The even probe distribution shows that there are no lateral heterogeneities on optically resolvable length scales indicating no cell-specific membrane characterisation. The dialkylcarbocyanine dye is well-investigated to partition into the membrane and co-localise with L_d phase [287]. Having successfully tagged GPMVs, the next aim was to characterise the MP1-induced DiI partitioning effect on the membrane. To identify MP1 concentration without being lytic but causing observable membrane-associated changes, 1-30 μM MP1 concentration was tested in a time-dependent manner (every 5 min in 30 min time scale). The empirical evaluation revealed 10 μM MP1 to generate the heterogeneous distribution of the DiI dye in GPMVs after 30 min incubation. Visible GPMVs breaking occurred at 20 and 30 μM, produced from MDA-MB-468 and MCF-10A cells, respectively.

Figure 50 represents fluorescence scanning images of GPMVs incorporating the DiI dye and its lateral organization after 10μM dosing. Although initially, GPMVs exhibited similar DiI dye lateral distribution, the membrane reorganized itself differentially as a response to MP1. MDA-MB-468 PM extracts displayed macroscopic phase separation seen as microscale domains of dye-rich and dye-depleted regions. Contrary, MCF-10A-derived model systems presented locally thicker lipid aggregates formed in the membrane surface.

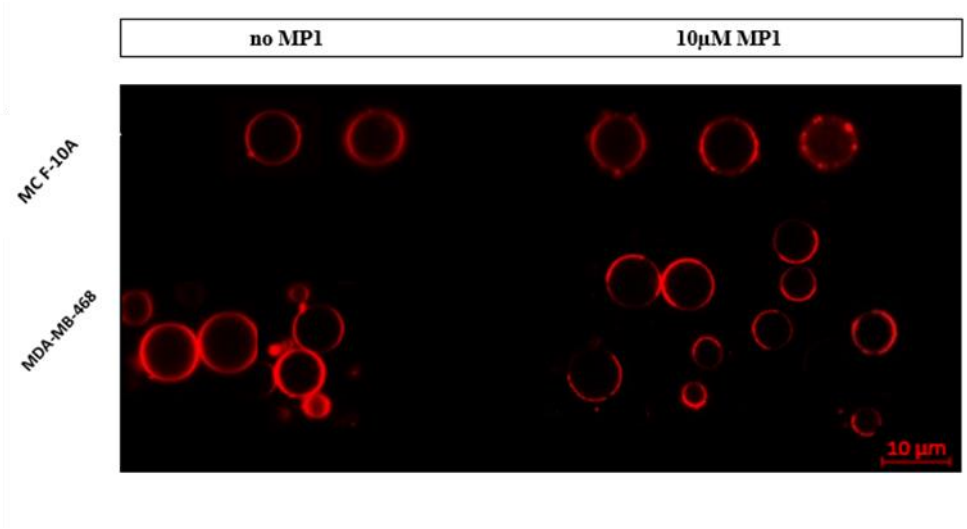

Figure 50 The representative image of GPMVs tagged with a lipid marker DiI. The top panel represents vesicles isolated from MDA-MB-468 cells and the bottom panel MCF-10A-derived model membranes prior to and after MP1 application. The scale bar is 10 μm.

4.3.2 Phase-order is cell line specific

Having observed MP1-mediated changes in lipid phase behaviour, membrane organization was next tested using the polarity sensing fluorescent analogues in the various GPMVs preparations. Breast cell models display differential sensitivity to MP1 reflected as IC50 value (Table 5). The molecular basis of the MP1-associated cell resistance might be found in the difference in order between coexisting lipid phases. The diverse packing degree was determined in all isolations and the GP index varied between particular cell subjects and dyes (Table 6).

Table 5 Cell sensitivity to Polybia MP1 expressed by the IC50 value. The IC50 defines half maximal inhibitory concentration of inhibitor causing 50% cell death and is a common indicator of resistance evaluation. A higher concentration [μM] of the IC50 indicates greater resistance to MP1 activity and higher concentration of inhibitor is needed to cause 50% cell death. The data represents MP1-associated cell screening performed by Dr Arindam Pramanik. Cell viability was determined by MTT assay. Data represent mean and ± SD from three independent measurements. MDA-MB-468 cell line was identified as highly responsive to MP1, whereas BT-474 cells are less sensitive. As indicated by the

IC50 value, MCF-10A is classified as resistant to MP1 and higher MP1 dose is needed to cause 50 % cell death.

Cell line	IC50[µM]
MDA-MB-468	23.48 ± 2.3
BT-474	50.61 ± 4.1
MCF10A	111.4 ± 9.8

Figure 51 represents a summary of spectral imaging analysis of the lipid phases in GPMVs. The ratiometric imaging displaying the GP map revealed the lipid membrane heterogeneity indicating a diverse level of hydration at the ambient temperature (Figure 51a). The ordered phases are seen as warm colours, red and orange scale, whereas less ordered lipid regions are visualised by the use of colder patterns in a green and blue scale. The average GP distribution is seen in Figure 51b, whereas Figures 51 c,d, and e demonstrate the exact values of lipid packing difference between Lo and Ld phases for Laurdan, C-Laurdan and Prodan. GPMVs labelled with Laurdan were found to display a similar pattern in GP distribution. The membrane order of PM extracted from MDA-MB-468 and BT-474 breast cancer models was overlapping beginning at -0.2 and ending at 0.2 with the maximal peak at 0. Similarly, the highest point is located approximately at 0 for MCF-10A-derived GPMVs, however, lipid ordering showed a slightly more relaxed state, mirrored in a range between -0.3 to 0.1. The average GP value was 0.017, -0.001 and -0.08 for MDA-MB-468, BT-474 and MCF-10A, respectively.

Table 6 The summary of GP measurements using a custom GP plug-in. The variables (average GP, GP distribution and the highest peak) demonstrate the average value obtained from approx. 50 GPMVs isolated from each cell line and each dye. The measurements were performed in 4-5 biological replicates

Cell line	GP distribution		The highest peak		Average GP	
	No MP1	10μM MP1	No MP1	10μM MP1	No MP1	10μM MP1
Laurdan						
MDA-MB-468	-0.2 to 0.2	-0.16 to 0.2	0.052	-0.019	0.017	-0.033
BT-474	-0.2 to 0.2	-0.25 to 0.1	-0.002	-0.005	-0.001	-0.06
MCF-10A	-0.3 to 0.15	-0.17 to 0.25	-0.07	-0.08	-0.08	-0.03
C-Laurdan						
MDA-MB-468	-0.27 to 0.2	-0.42 to 0.1	-0.031 and 0.092	0.012	-0.06	-0.15
BT-474	-0.45 to 0.2	-0.45to 0.06	-0.21	-0.3	-0.14	-0.16
MCF-10A	-0.32 to 0.005	-0.31 to 0.1	-0.25	-0.1	-0.21	-0.1
Prodan						
MDA-MB-468	-0.3 to 0.2	-0.3 to 0.23	0.018	-0.021	-0.03	-0.15
BT-474	-0.3 to 0.125	-0.43 to 0.03	-0.025	-0.017	-0.059	-0.17
MCF-10A	-0.45 to 0.01	-0.3 to 0.1	-0.11	-0.03	-0.16	-0.07

The striking difference in the variation in GP ($GP_{ordered} - GP_{disordered}$) between GPMVs derived from a range of cell lines with contrasting sensitivity to MP1 was detected with C-Laurdan. GP for MDA-MB-468, identified as the most responsive to MP1 across all screened models, was in the range of -0.27 to 0.1 with the highest peak at -0.031.

Another observable membrane lipid accumulation was at approximately 0.030. BT474 cell line, termed as mildly sensitive to MP1, exhibited a broad spectrum of proportionately distributed lipid order starting from -0.45 to 0.2 with no evident lipid phase aggregation. The striking difference was observed from GPMVs isolated from MCF-10A, the control cell standard defined as resistant to MP1. GP distribution was in a scope of -0.3 to 0 with the highest point at -0.25. The average GP value indicated -0.06, -0.14 and -0.21 for MDA-MB-468, BT-474 and MCF-10A, respectively. The average L_o:L_d ratio was significantly lower for this preparation in contrast to the samples described above.

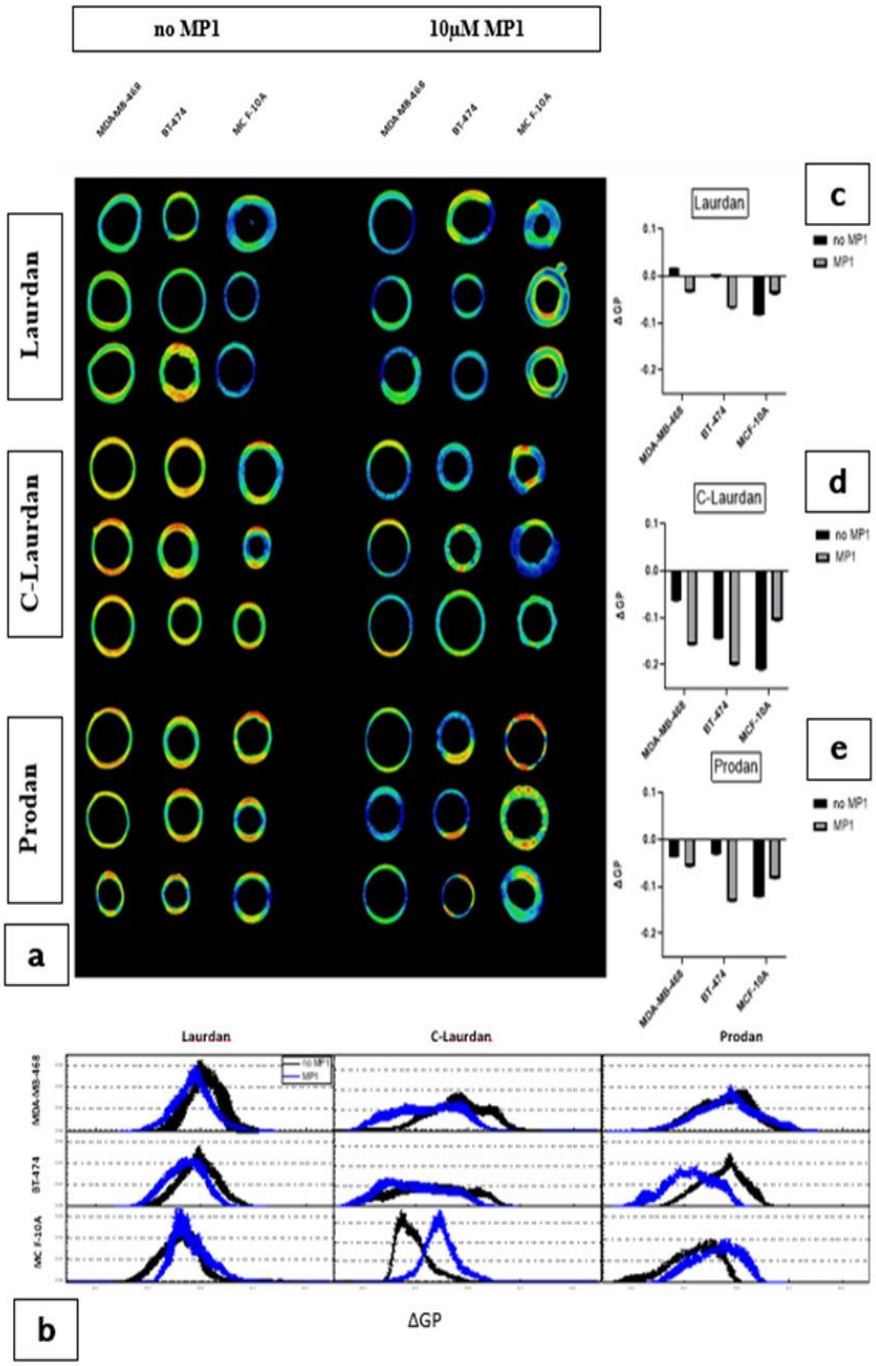

Figure 51 Spectral imaging and analysis of the lipid phases in GPMVs aiming to determine MP1-associated changes in lipid packing; (a) GP maps of three representative GPMVs for each cell line and dye. The scale bar is 10 μm; (b) GP distribution averaged from approx. 50 vesicles for each isolation condition. Variation between GPMVs is represented by the standard error of mean; (c,d,e) Lipid packing difference between Lo and Ld phases in cell-specific GPMVs plotted for Laurdan, C-Laurdan and Prodan images. Instead of having separated Lo and Ld phases, an ordered spectrum was obtained.

Prodan, another Laurdan derivative, tested with all isolations, revealed the most detectable differences in lipid packing degree. The scope of GP values of MDA-MB-468 was between -0.3 to 0.2 with the top at 0, whereas the BT474 membrane was less ordered, with the endpoint at 0.125. MCF10A measurements pointed out lipid accumulation between -0.3 to 0. The average GP index was -0.03, -0.059 and -0.16 for MDA-MB-468, BT-474 and MCF-10A, respectively.

4.3.3 MP1 tunes the order of phases in GPMVs

In order to investigate the MP1-driven effect on lipid packing, GPMVs were subjected to 10 μM MP1 treatment after labelling with the solvatochromic probes (see Figure 52a). The average GP analysis of Laurdan identified a decrease in the value to -0.033 and -0.06, for MDA-MB-468 and BT-474, respectively. The corresponding GP colour map revealed the relatively disordered lipid phase distribution expressed in darker tones. Application of C-Laurdan and Prodan in the same models revealed the consistent decrease of lipid packing difference between L_o and L_d phases (GP). C-Laurdan measurements indicated the average value of -0.15 and -0.16, whereas Prodan was -0.15 and -0.17. The left-hand emission shift of naphthalene derivatives and reduced GP are persistent for GPMVs budded from cell lines defined as sensitive to MP1.

The opposed pattern was observed for MCF-10A. In this case, MP1 generated a change in the local membrane environment seen as the right-hand spectral shift of GP distribution. GP analysis of Laurdan emission identified an increase rising to -0.03.

Similarly, C-Laurdan and Prodan measurements were raised to -0.1 and -0.07. GP map visualised more ordered lipid domains marked out as orange and red areas.

4.3.4 GP measurements of naphthalene derivatives differ across the same cell type

The application of the fluorescent polarity sensing analogues showed various GP parameters measured for one type of GPMVs and the average differences between phases (GP) for each cell line are seen in Figures 42c,d, and e. MDA-MB-468 derivatives displayed the highest lipid packing value which reflects more ordered membrane organization. Accordingly, BT-474-induced GPMVs exhibited L_o:L_d ratio at close proximity to 0. In these isolations, membrane order is more fluid and therefore loosely packed in relation to MDA-MB-468. Among all preparations, the average GP index for MCF-10A extracts is closest to -1. GP negative value suggests a large yield of disordered lipid domains with a high degree of hydration. The molecular packing of the L_d and L_o phases in the vesicles decreases ranking from MDA-MB-468> BT-474> MCF-10A. Simultaneously, according to a cell-dependent manner, GP measurement decreases in order Laurdan>Prodan>C-Laurdan.

MP1 treatment induces changes in lipid packing shown in the altered GP value. GPMVs isolated from MDA-MB-468 and BT-474 were subjected to lipid rearrangements to a less ordered state as indicated by the left-hand shift in the emission spectrum. GP distribution of MCF-10A-derived GPMVs is notably different than those of MDA-MB-468 and BT-474. Initial GP screening classified those vesicles as the least packed and the presence of MP1-induced membrane ordering was reflected as the right-hand shift of the emission spectrum.

4.4 Discussion

4.4.1 Cell-specific lipid order potentiates MP1 activity

The therapeutic potential has been attributed to Polybia MP1 because of lytic activity against particular cancer models. As presented above, breast cancer cell subtypes exhibit a diverse sensitivity to MP1 reflected in the IC50 value. Studies in cell-derived model membranes focusing on membrane organization pronounced cell-specific features for either sensitive or resistant cell types. The DiI dye partitioning in the membrane revealed no lipid clusters with differentiating order that could be optically observable. Interestingly, a detailed investigation using the fluorescent solvent relaxation technique showed cell-specific membrane organization [288]. The difference between coexisting L_d/L_o (GP) measured in GPMVs demonstrated that cell sensitivity to MP1 corresponds to lipid packing. Tested with different fluorescent analogues, lower GP correlates with cell resistance to MP1.

A literature review of membrane lipid profiling might associate GP value with specific membrane lipid components. MDA-MB-468 cells were identified with the average lipid content among other breast cancer cell lines in many lipid screenings [289–292]. Interestingly, the triple-negative breast cancer MDA-MB-468 was found to have different lipid composition in terms of C=C location and fatty acyl isomers. MDA-MB-468 cells predominantly contain PC (34:2) with isoforms of monounsaturated palmitoleic acid (C16:1) and oleic acid (C18:1) at position Δ6 and Δ8, respectively. Lipid analysis of the HER2 + BT-474 cell line revealed a dominating content of saturated acyl chains [293]. The cell membrane is enriched in diacylglycerols (32:0, 36:0), arachidonic acid (14:0), palmitic acid (16:0), and linoleic acid (20:4). In contrast, a relatively small fraction of cholesterol and 18-carbon chain fatty acids were detected in comparison to other breast cancer cell

lines. In addition, the heterogeneity of the relative abundance of PC (32:1) with monounsaturated FA (C16:1, C18:10) in BT-474 single cells was higher than that in MDA-MB-468 single cells. MCF10A cells were found with elevated levels of polyunsaturated lipids in comparison to other breast cancer cell lines [171]. Lipid species identified to be up-regulated are SM(34:0), PC(38:4), PI(38:4), linoleic acid (18:2), and adrenic acid (22:4). Levels of palmitic acid (16:0) and stearic acid (18:0) were similar to those cells of cancerous phenotypes. Both MDA-MB-468 and MCF10A cell lines have a high cholesterol content, which is suggested to play a key role in lipid-based dissimilarities between metastatic and non-metastatic cells [289]. It has been proven that cholesterol adjusts the ordering of both phases. The unsaturation degree was significantly lower in MDA-MB-468 cells when compared to MCF10A cells. Furthermore, MCF-10A cells were found enriched in lipid droplets containing unesterified cholesterol and raft proteins [294].

4.4.2 MP1 modulates changes in lipid phase behaviour in GPMVs

MP1 was reported to induce changes both in the lateral diffusion of DiI dye and GP-calculated lipid packing. Upon exposure to MP1, the MDA-MB-468 membrane system phase separated and the relatively great lipid order underwent relaxation to a rather loosely packed state. Contrarily, membrane lipids are organised into spots, which do not empirically resemble widely investigated raft domains in GPMVs isolated from the MCF-10A cell line. A relatively fluid membrane was subjected to lipid reorientation into a more ordered phase. The observed MP1-associated phenomenon provides a more in-depth understanding of MP1 lytic activity which is closely related to lipid composition and organization. Although the MDA-MB-468 cell line is composed of the common lipid species, specific C=C location or acyl tails isoforms might be attributed to MP1-induced

cell vulnerability. Furthermore, we can speculate that lipid ordering, as a response to MP1, is a cell-protective mechanism observed in the MCF-10A breast model.

4.4.3 The application of naphthalene derivatives in GPMVs

Knowing how MP1 influences the mobility of biological membranes is necessary to elucidate the MP1 mechanism of action. The application of fluorescent probes with the dipolar moment, which are positioned at various levels in the lipid bilayer, allows for a detailed investigation of lipid organization and reorientation due to surface tension. Laurdan, one of the solvatochromic dyes, exhibits an emission shift due to H-bonding as a response to the hydration level [295]. For instance, a loosely packed L_d phase promotes greater water penetration reaching the glycerol backbone of the bilayer surface and, as a consequence, the Laurdan emission spectra exhibit evident directional shift. Significantly, these spectroscopic changes are independent of the nature of the phospholipid headgroup [296]. C-Laurdan, the Laurdan derivative which differs by the presence of an additional carboxyl group, has been found to be more stable than Laurdan in the polar headgroup region of the bilayer and also much more aligned with the lipids [297]. However, the live-cell experiments revealed the rapid internalization of Laurdan and C-Laurdan to the cytoplasmic leaflet [298]. Prodan, another naphthalene analogue, having shorter hydrocarbon tails, is located closer to the lipid-water interface [299]. By employing the fluorescent solvent relaxation probes with different distributions across the lipid bilayer, we were able to investigate lipid packing prior to and after the MP1 treatment and correlate it to cell sensitivity to MP1. GP index calculations, reflecting a spectrum of ordered and disordered domains across the entire membrane, allowed the determination of lipid reorientation by measuring the spectral changes in the lipid environment. In addition, the GP map illustrates lipid domain distribution by directly visualizing GPMVs (Fig. 51a)

The application of Laurdan, C-Laurdan and Prodan is an effective method to study lipid packing at different membrane locations. Laurdan and C-Laurdan, which ought to incorporate similarly in-between acyl tails, presented different parameters. Laurdan, across all cell-specific isolations, exhibited analogues emission spectra. The data suggest that, although Laurdan reflects differences in lipid packing, due to flip-flop diffusion, it might not sense accurately changes in the lipid environment. C-Laurdan, despite being structurally similar to Laurdan, demonstrated more disordered phase behaviour across samples. Furthermore, it indicated broader spectra of lipid order in MDA-MB-468 and BT-474, whereas the MCF=10A spectrum was complementary to Laurdan. Prodan, being situated on the membrane surface in close proximity to phospholipids, displayed dissimilar order to Laurdan and C-Laurdan. Overall, all dyes were distributed in a cell-dependent manner. Those with initially relatively low GP values were forming ordered domains after MP1 treatment.

As mentioned above, MP1 activity is tension-related, thus it causes localised-dependent different lipid reorientation. The increased surface area due to lipid: peptide interaction causes a decrease in the local lipid density at the headgroup surface. Simultaneously, lipid density increases in the mid-plane of the bilayer indicating interdigitation of the acyl chains of the opposing lipid layers Laurdan and C-Laurdan which moieties are more aligned with lipids. Lipid interdigitation is speculated to drive the formation of membrane micro-domains [59]. Moreover, changes in lipid order parameters modulated with tension are smaller in the headgroup region and larger near the end point of acyl tails. By applying a range of position-different dyes in the bilayer we are able to investigate changes in membrane organization either on the membrane surface or in the interior of the lipid bilayer.

4.4.4 GPMVs to study membrane organization

GPMVs derived from different cancer cell subtypes allowed for determining cell-specific lipid packing. We can observe and quantify the actual response to MP1, which appears to be different even within the same cancer type. Although GPMVs provide a more comprehensive understanding of lipid: peptide interaction than artificial vesicles, the system does not reflect the exact membrane dynamics.

The isolation procedure for GPMVs could substantially affect membrane behaviour and phase-separation properties. PFA/DTT mixture is known to generate protein cross-linking, which is believed to stabilise phase separation [90]. Furthermore, DTT strongly impacts GPMVs transition temperature [300]. Exposure to DTT alters the lipid packing due to the depalmitoylation effect of DTT [15]. Palmitoylan was investigated to regulate the functionality of raft phases [261].

Apart from lipid rafts, a novel type of membrane domain was speculated to reside in the PM. Studies in erythrocytes and kidney cells lacking cortical networks revealed increased diffusion of membrane proteins [301, 302]. Kusumi et al. reported that skeletal filaments interact with integrated membrane proteins forming nanoscopic assemblies[303]. GPMVs are produced due to cytoskeleton disruption which indicates another disparity to the intact PM.

4.5 Conclusions

Although MP1 exhibits a therapeutic potency against breast cancer subtypes, little is known about the exact mechanism of action. GPMVs which are close-to-native membrane platforms provide more detailed insight into lipid: peptide interaction in the MP1 membranolytic activity. Here I propose fluorescent solvent relaxation probes as a sufficient tool to study membrane organization. Those dyes which directly sense

membrane motion allow for obtaining a spectrum of lipid packings for L_o/L_d phases. This work shows that the lipid order correlates to cell sensitivity to MP1. The more disordered system the more resistant cell to MP1. Utilizing probes which incorporate the different membrane layers detect changes occurring either in the phospholipid region or hydrophobic core. When incubated with MP1, ΔGP for GPMVs obtained from MDA-MB-468 and BT-474 experienced a left-hand shift in the emission spectrum, whereas MCF-10A displayed a right-hand shift. The differentiating response to the MP1 indicates cell membrane mechanisms involved in the peptide: lipid interaction. Models more sensitive to MP1 become less packed, while modulated resistance to MP1 is linked to more ordered lipid packing. Changing experimental conditions, for instance, testing cholesterol-deprived membrane models induced by cyclodextrin could explore the role of cholesterol in defining the membrane ordering.

Chapter 5 Analysis of the molecular mechanisms of cell sensitivity to MP1 using bioinformatic and functional approaches

ABSTRACT

The fast-advancing molecular techniques allow for determining in-depth principles of key biochemical pathways within an individual cell. Gathering massive information instantaneously, public data sets are available sources of *in silico*-constructed metabolic networks. Polybia MP1 screening in a panel of cancer cell types determined that cell sensitivity to MP1 is a cell-specific feature. Therefore, to investigate whether cell sensitivity is defined by molecular determinants, bioinformatics approaches were used to predict which genes might be correlating with cell survival. The regression approach screened out a significant list of hub genes ranking the top ten targets. The gene-silencing technique evaluates prediction in the MP1-resistant cell line with a relatively high expression of gene targets. Statistical analysis of cell proliferative capacity shows a significant change accomplished with the knockdown of Indian hedgehog signalling molecule gene (*IHH*) suggesting a need for further investigation of the MP1 activity.

5.1 Introduction

Cell-specific lipid order, as presented in Chapter 4, is shown as one of the potential factors driving cell sensitivity to MP1 activity. The presented results led to the conclusion that the more disordered the initial membrane organization, the more resistant cell line to MP1. Having discovered such an important aspect associated with MP1, we can speculate that certain metabolic pathways might play a role in the cell response. However, a single cell is a living unit of a multidimensional network system, and due to its complexity, investigating the functionality of each compound would be highly unlikely to proceed by

manual experimentation. Traditional research tests typically one or a few genes targets at a time. Recently bioinformatic analysis has become a common approach to perform multiple analyses with the application of many variables [304–306]. This high-throughput method is capable of generating a list of gene candidates based on analytical approaches. One of them, regression analysis is a statistical technique used for determining the relationship between a single dependent variable and one or more independent predictor variables [307]. Linear models provide a high prediction accuracy when the formulation reflects the interfering relationship of variables captured using a line [308]. However, not all correlations fit standard linear modelling, hence non-linear strategies can be applied to identify any other relationships that do not fit in line In contrast, the gene-annotation enrichment analysis allows us to determine biological pathways linked to groups of genes of interest. Notably, numerous public gene expression data sets are available of published and unpublished data.

In this section, *in silico* attempts are presented to identify molecular determinants associated with cell responsiveness to MP1. The applicability of the multilayer bioinformatic strategy allowed the screening of multiple variables under a range of statistical conditions. The regression method was employed to find significant variations of gene expression across a range of cell lines characterised by the differential sensitivity to MP1. Additional non-linear testing ranked them through the custom-designed scoring identifying those genes which might modulate MP1 activation under particular expression levels. Furthermore, over-representation analysis (ORA) identified genes with related functionality from lists of gene candidates, providing details of metabolic networks that are probable to affect MP1 membranolytic activity. The role of the top ten gene targets in MP1-associated cell response selected in the combinational approach was evaluated by the gene silencing technique and quantified by cell viability.

5.2 Materials and methods

5.2.1 Cell-line datasets

Polybia MP1 50% inhibitory concentrations were determined in 64 cancer cell lines using CellTiter-Glo luminescent cell viability assay performed by Crown Bioscience (Project No.: E3782-U1801). Crown Bioscience is a global research organization providing high-quality *in vivo*, *in vitro*, and *ex vivo* quantification of the efficacy and pharmacological profile of the drug candidate(s). The culture medium was supplemented with 10-20% FBS and purchased from GIBCO or Sigma, USA. Cells were cultured at a temperature of 37 ˚C, 5% CO_2 and 95% humidity. Polybia MP1 was applied in a range of concentrations starting from 316 μM with 3.16-fold serial dilutions to achieve 9 dose levels and incubated for 48h before measurement of cell survival using CellTiterGlo. This cell viability assay is a method of determining the number of viable cells in culture based on quantitation of the ATP present, an indicator of metabolically active cells. The IC50 absolute values were calculated according to the dose-response curves and are presented in the table below (Table 7).

Whole transcriptome gene expression data were found and downloaded from The Cancer Cell Line Encyclopaedia (https://sites.broadinstitute.org/ccle/) for 54 out of 64 cell lines used in the IC50 MP1 screening, as indicated in Table 7.

Table 7 A panel of 64 cell lines used in the IC50 screening of Polybia MP1. ✓ indicates cell lines which gene sets data were used in the bioinformatic analysis

No.	Cell line	IC50 [μM]	Tissue origin	Transcriptome data
1	CCRF-CEM	31.24	Blood	
2	HL-60	10.57		✓
3	K-562	19.52		✓

4	Molt-4	53.21		
5	RPMI 8226	23.1		✓
6	A-172	50.24	Brain&Nerves	✓
7	LN-229	22.24		✓
8	M059K	37.28		✓
9	SF268	25.26		✓
10	SH-SY5Y	21.45		
11	U251	29.9		✓
12	U-87 MG	32.28		✓
13	AU565	20.51	Breast	✓
14	BT-20	25.13		✓
15	BT-474	50.61		
16	BT-549	27.48		✓
17	CAL-120	42.23		✓
18	Hs 578T	34.26		✓
19	MCF7	30.53		✓
20	T47D	56.78		
21	SK-BR-3	32.98		✓
22	Caco-2	57.89	Colorectum	
23	COLO 205	67.89		
24	DLD-1	45.68		
25	HCT 116	30.62		✓
26	HCT-15	32.14		✓

27	HT-29	67.02		✓
28	LoVo	65.02		✓
29	LS 174T	45.67		
30	SW620	65.7		
31	786-O	20.3	Kidney	✓
32	A498	24.33		✓
33	ACHN	30.71		✓
34	UO.31	25.46		✓
35	A549	38.62	Lung	✓
36	A-427	26.5		✓
37	Calu-3	33.48		✓
38	DMS 114	45.47		✓
39	NCI-H226	22.73		✓
40	NCI-H23	23.72		✓
41	NCI-H460	18.39		✓
42	NCI-H522	29.69		✓
43	SHP-77	45.67		
44	Caov-3	47.86	Ovary	✓
45	IGR-OV1	78.9		
46	OVCAR-3	76.67		
47	OVCAR-4	24.53		✓
48	OVCAR-5	45.78		
49	OVCAR-8	24.72		✓

50	SK-OV-3	44.13		✓
51	SW626	34.45		
52	AsPC-1	32.73	Pancreas	✓
53	BxPC-3	24.93		✓
54	Capan-1	64.74		✓
55	Capan-2	41.3		✓
56	PANC-1	55.44		✓
57	DU 145	18.85	Prostate	✓
58	PC-3	34.82		✓
59	Malme-3M	30.72	Skin	✓
60	RPMI-7951	34.78		
61	SK-MEL-2	56.78		✓
62	SK-MEL-28	19.03		
63	SK-MEL-5	14.95		✓
64	SR		Thymus	

5.2.2 Bioinformatic workflow

In silico analysis was employed to construct predictive models for genes potentially associated with MP1-related cell sensitivity (see Figure 52). Dr Dapeng Wang combined the IC50 dataset and the gene expression dataset of 54 cell lines. First, the transcriptome dataset was cleaned to remove genes regarded as ‘not expressed’, providing 22,939 genes identified in all screened cell lines. Next, a linear fitting of MP1 sensitivity (IC50 values) to the expression of every individual gene was plotted indicating if it is a positive or

negative relationship. Any correlation was tested for estimating whether to accept or reject them utilizing the criteria: $p < 0.05$ meaning the test is controlled to have a probability equal to or less than 0.05. Performing high-throughput analysis and having thousands of statistical tests simultaneously requires correction for multiple tests to avoid the appearance of false discoveries. Thus, the Benjamini-Hochberg correction ("B+H") or the Bonferroni correction was applied, which controls the procedure under the assumption of independence of p-values. Benjamini-Hochberg limits the False Discovery Rate (FDR), Bonferroni procedure controls family-wise error rate (FWER).

Based on the linear regression, Prof. Paul Beales designed a statistical approach aiming at capturing any non-linear trends that might have been omitted by the linear regression analysis. Four predictor variables were defined: gene expression positive correlation, gene expression negative correlation, IC50 positive correlation and IC50 negative correlation. The 6 top/bottom cell lines ranked by the MP1 sensitivity (the IC50) were evaluated to being in the top or bottom quartile (top/bottom 13) of the gene expression ranking and consistently, the top/bottom 6 gene expressions were matched to the ranked list of MP1 sensitivity. Each gene with an estimated B+H p-value was scored under a range of predictor variables and the resulting value reflects the fitting level to each variable (positive/negative correlation fitting). By subtracting the sum of positive correlations and the sum of negative correlations we receive the final count in a scope from 0 to 16, where 16 displays the greatest probability of relationship incident.

Another way to analyse the large number of gene datasets is to subdivide them into functional groups of known biological pathways. The over-representative analysis allows for determining significantly enriched or depleted groups of genes which are stronger candidates than any free-standing individual gene in the raw list of the significant targets.

Prof. Thomas Hughes performed enrichment analyses using GO [309] and KEGG [310] available at http://www.webgestalt.org.

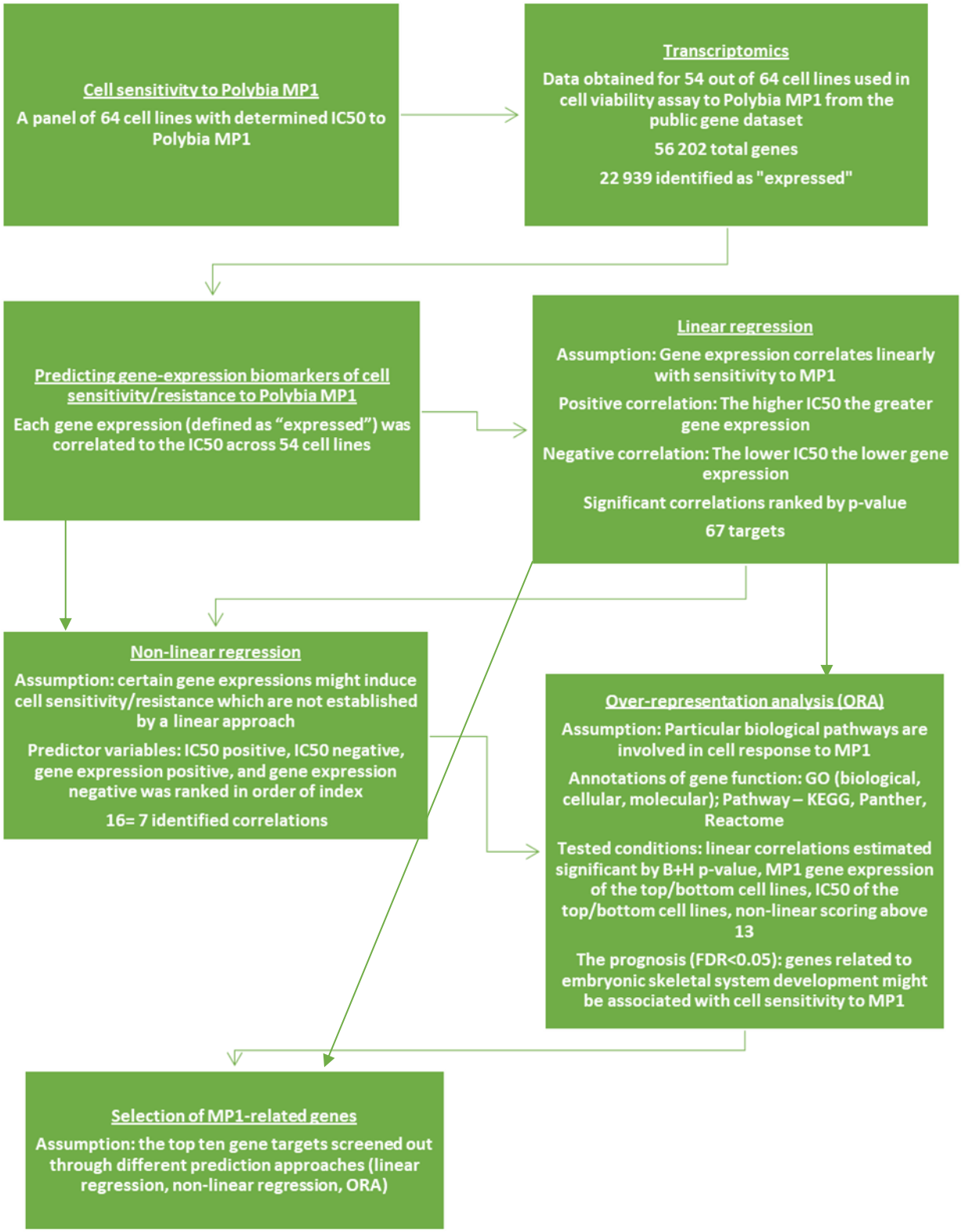

Figure 52 Schematic diagram of the bioinformatic workflow. First, cell line drug sensitivity data and gene expression data were combined and transformed. Data sets were used to build predictive models of MP1-associated cell sensitivity. The aim was to identify

a group of 10 genes whose gene expression levels were predictive of the IC50 values of the drug but were also biologically plausible as causative of MP1 sensitivity.

5.2.3 Cells

HT-29 cells were obtained from Dr Nicola Ingram (School of Medicine, University of Leeds) and cultured as monolayers in 75cm^2 flasks in RPMI-1640 (Thermofisher; Waltham, USA), supplemented with 10% FCS (Sigma; St Louis, USA) and 1% penicillin/streptomycin (final concentrations 100 U/ml and 100µg/ml) (Thermofisher; Waltham, USA). Cells were grown at 37˚C in humidified 95% air/5% CO_2. Cell line identity was confirmed using STR profile (Leeds Genomic Service) and cultures were consistently Mycoplasma negative (MycoAlert; Lonza; Basel, Switzerland).

5.2.4 Cell transfection

Transfection of siRNAs was performed using siPORT™ *NeoFX*™ Transfection Agent (Cat. No: AM4510, Thermo Fisher Scientific, Inc., Waltham, MA, USA) according to the manufacturer's protocol. A total of 6×10^3 cells were seeded into 96-well plates and transfected at 30-40% confluency the next day with 30 nM final concentration of siRNA (*Silencer*™ Select Negative Control Cat. 4390843, HOXA6, Cat. 4392420, ID: s223863; HOXB5, Cat. 4331182, ID: Hs00357820_m1; BMP4, Cat. 4331182, ID: Hs00370078_m1; PLA2G16, Cat. 4331182, ID: Hs00912734_m1; IHH, Cat. 4331182, ID: Hs00745531_s1; PDE4C, Cat. 4392420, ID: s10195 FAAH, Cat. 4392420, ID: s4961 LIPG, Cat. 4392420, ID: s17963; NCOR2 Cat. 4392420, ID: s18467 and KLF5, Cat. 4392420, ID: s2115, Thermo Fisher Scientific, Inc., Waltham, MA, USA) using 0.5 µl siPORT™ *NeoFX*™ Transfection Agent. At 24h or 48h post-transfection, cells were processed for further analysis.

5.2.5 Cell viability assay

To determine the drug resistance of HT-29 cells to Polybia-MP1, cells were treated with various concentrations of Polybia MP1 (0, 20, 40 or 67 μM) for 24 h Following incubation, 200μL of 0.5 mg/ml 3-(4,5-dimethylthiazol-2-yl)-2,5-diphenyltetrazolium bromide (MTT) solution reagent was added to each well and incubated for 4 h. The purple-blue MTT formazan precipitate was dissolved in 200 μl of isopropanol. The absorbance was determined using a microplate reader at 490 nm (BertholdTech Mithras, Driver Version: 1.05, (1.0.5.0), S/N: 42-6037, Embedded Version: 1.17). Cell viability was determined relative to the control cells.

5.2.6 Analysis of gene expression

A total of 1×10^6 cells were seeded into 6-well plates and were harvested 24 and 48 h after transfection. Total RNA extraction was performed using the Qiagen RNeasy kit (Qiagen, Cat. No. 74104) according to the manufacturer's instructions. RNA concentration was measured using Nanodrop 1000 (Thermo Fisher Scientific, Waltham, MA). Single-strand cDNA was synthesized from 2μg of total RNA using a High-Capacity cDNA Reverse Transcription Kit (Applied Biosystems Life Tech, Thermo Scientific Cat. No. 4368814). A parallel tube without RT (RT-negative control) was included in the RT reactions as the control for DNA contamination. mRNA expression was analyzed using Taqman™ Fast Advanced Mastermix (Thermo Fisher, Paisley, Cat. No. 4444557) and Taqman ® Gene expression assays (BMP4 Cat. No. 4331182, ID: Hs00370078_m1; IHH Cat. No. 4331182, ID: Hs00745531_s1; HOXB5 Cat. No. 4351372, ID: Mm01307012_m1; PLA2G16 Cat. No. 4351379, ID: C__64003733_10) for qPCR on 96 well QuantStudio Flex 7 (Applied Biosystems Life Tech, Thermo Scientific). Amplification was carried out in a 10 μl volume (5 μL master mix, 0.25 μL TaqMan probe,

2 μL cDNA (5-fold dilution) and 2.75 μL distilled water) for 40 cycles. The relative gene expression was normalized to GAPDH (Cat. No. 4333764T) and data analyses were performed using the comparative CT method [311]. All experiments were conducted in technical triplicates and are presented as mean ± SEM of three or more independent replicates. The real-time PCR conditions were as follows: 95 ºC initial template denaturation (20s) and 40 cycles of 95ºC denaturation (1s) and 60ºC anneal/extension (20s).

5.2.7 Statistics analysis

Statistical analysis was performed using GraphPad Prism 9 (GraphPad Software, Inc.). Experiments were performed at least in triplicate, and data are presented as the standard error of the mean (SEM). ANOVA and non-linear test were used to compare differences between multiple groups. Data with *P* values lower than 0.05 were accepted as statistically significant.

5.3 Results

5.3.1 Various *in silico* approaches signify a list of potential MP1 sensitivity biomarkers

The first aim was to use linear regression to compare MP1 sensitivity in a large panel of cells lines (using the IC50 values) to the expression levels of each individual gene within those cell lines and estimate whether expression correlates with sensitivity. Dr Dapeng Wang employed *in silico* statistical methods to investigate potential relationships of approximately 22,939 transcripts across 54 cell lines to MP1 IC50 values and defined the probability of any relationship by calculating p-values. The application of p-value Benjamini-Hochberg corrections decreased the false discovery rate and determined 67

significant genes, presented in Table 9. The more stringent Bonferroni correction, which relies on the Family Wise Error Rate (FWER), was also used indicating 2 significant genes – HOXB5 and RP11-120K24.3 (Table 8).

Table 8 The list of gene targets identified by linear regression performed by Dr Dapeng Wang. The probability of each relationship was determined by p-value ($p<0.05$). Additional p-value corrections decreased the number of targets to 67 by Benjamini-Hochberg correction ("B+H") and to 2 by Bonferroni correction ("B")

				Gene expression		
	Gene name	p-value (B+H)	p-value (B)	Mean	Min.	Max.
1	HOXB5	0.005893978	0.005894	4.000179	0	32.7004
2	RP11-120K24.3	0.009523023	0.019046	0.190052	0	1.91672
3	GIPC2	0.015948305	0.0812449	0.815575	0	10.0477
4	IHH	0.015948305	0.1116381	0.632631	0	7.99594
5	HOXA-AS3	0.015948305	0.0641827	0.338162	0.001861	1.99429
6	HOXA6	0.015948305	0.0587945	1.365679	0	9.62216
7	HOXB6	0.015948305	0.1018459	4.309282	0.002789	30.6795
8	HOXB-AS3	0.017622613	0.1409809	2.43402	0.005182	22.2024
9	HOXA11-AS	0.019351666	0.2297903	1.792378	0.003264	20.7645
10	BMP4	0.019351666	0.1858104	22.11665	0.032345	205.024
11	RP11-927P21.2	0.019351666	0.23222	0.128108	0	1.05279
12	CTD-2619J13.3	0.019351666	0.21553	0.215068	0	1.01297
13	TRIM15	0.021119172	0.2745492	1.473861	0.006543	13.0644
14	NYNRIN	0.02271355	0.3179897	1.140616	0.001028	13.5942

15	RP11-465B22.8	0.023299897	0.3702251	1.995769	0	18.2831
16	GRHL3	0.023299897	0.3960982	1.063143	0.0022	8.55922
17	PIGHP1	0.023299897	0.3887392	0.437023	0.098329	1.46651
18	TRIM31-AS1	0.023739488	0.4729256	0.388134	0	4.01418
19	TRIM10	0.023739488	0.4637691	0.221739	0	1.93517
20	KLF5	0.023739488	0.4747898	20.64211	0.38211	120.991
21	MFSD4	0.0274898	0.8875132	0.372528	0.018131	1.72238
22	CAPN8	0.0274898	0.9766116	1.212071	0	16.5137
23	AC013268.5	0.0274898	0.5985171	0.764083	0	5.34552
24	AC112229.7	0.0274898	0.718472	0.88277	0	5.65825
25	MIR3131	0.0274898	0.6153374	0.09026	0	1.81795
26	SOWAHB	0.0274898	0.8213321	0.970124	0.002838	6.18469
27	CCAT1	0.0274898	0.8251335	2.531172	0	26.6536
28	ZNF214	0.0274898	0.861714	0.467555	0	1.83594
29	PLA2G16	0.0274898	0.9773201	19.3153	0.068602	173.12
30	LIPT2	0.0274898	0.8394108	1.53028	0.27673	5.25302
31	COLCA2	0.0274898	0.9496434	1.003399	0	15.4654
32	AL163953.2	0.0274898	0.6471672	0.15595	0	2.31066
33	AKAP13	0.0274898	0.9996038	5.041096	0.148604	12.6758
34	LYSMD4	0.0274898	0.7411407	2.164001	0.792809	7.1727
35	HOXB-AS4	0.0274898	1	0.590997	0	10.016
36	PDE4C	0.0274898	0.886255	0.267777	0.007932	5.9344
37	AC008982.2	0.0274898	0.6969289	1.314509	0.204846	4.51002
38	CHDH	0.029092799	1	2.550008	0.004237	17.1759

39	HOTTIP	0.033167725	1	0.595893	0	9.90996
40	TTC22	0.0334018	1	1.06172	0	8.51889
41	RP11-112J3.16	0.0334018	1	0.899586	0	3.84964
42	RP11-255B23.4	0.034202135	1	1.41268	0	16.9563
43	RP13-122B23.8	0.034202135	1	0.079068	0	1.34261
44	LIPG	0.034202135	1	3.899724	0.006701	27.0147
45	FAAH	0.037151676	1	3.143243	0.031408	13.2097
46	RP1-170O19.20	0.037151676	1	0.343801	0	3.28071
47	C11orf53	0.037151676	1	0.1395	0	3.77672
48	MIR192	0.037757451	1	0.173648	0	2.28576
49	GPX2	0.037757451	1	30.74659	0.082623	428.571
50	RP11-299G20.2	0.037757451	1	0.367222	0.020177	2.56265
51	RP11-304L19.3	0.037757451	1	0.539041	0	2.78267
52	CTB-39G8.3	0.037757451	1	0.952089	0	5.81128
53	HOXB-AS2	0.037757451	1	0.418716	0	3.07969
54	SLCO1B7	0.041663846	1	0.197151	0	3.09088
55	ZCCHC14	0.041663846	1	6.773401	1.24501	17.8292
56	RSPH1	0.041663846	1	1.261919	0	10.4959
57	S100A5	0.041774401	1	0.586057	0	5.40881
58	AC004067.5	0.041774401	1	0.399253	0.066988	1.28005
59	HOTAIRM1	0.041774401	1	5.345099	0.015928	37.017

60	RP11-395P17.3	0.041774401	1	2.816606	0.136243	23.2651
61	MUC5AC	0.041774401	1	3.061643	0.002651	71.5586
62	CAPN12	0.041774401	1	0.434857	0.012848	4.21834
63	FLNB-AS1	0.042753887	1	1.105893	0.026555	5.00763
64	UGT1A13P	0.046527967	1	0.041399	0	1.04555
65	NPFFR1	0.046527967	1	0.075314	0	1.54028
66	RP11-304L19.1	0.046527967	1	0	8.44229	
67	C15orf62	0.049713663	1	0.27829	7.77492	

Next, acquired gene expression to the IC50 relationships was tested using non-linear regression analysis under different predictor variables to express the irregular scientific nature. Prof. Paul Beales designed various probability-based strategies and examined the top/bottom ranked cell lines by cell sensitivity to MP1 (IC50) scoring each gene according to the matching signature to each predictor variable. Four variables were determined: gene expression positive correlation, gene expression negative correlation, IC50 positive correlation and IC50 negative correlation. 6 cell lines from the top/bottom MP1 sensitivity scanning were evaluated to fit the top or bottom quartile (top or bottom 13) of the gene expression ranking and line up by a score reflecting consistency with a negative or positive correlation. Simultaneously, the top/bottom 6 gene expression was matched to the ranked list of MP1 sensitivity. Next, each relationship was estimated numerically by subtracting the negative correlation from the positive correlation value obtaining a score between 0 and 16. Overall, this strategy estimates that the higher the magnitude of the score the more likely that there is a correlation. The maximal response

variable was 16 and 7 gene targets gained the greatest scoring. Following, 12 gene candidates were under 15 score and 25 achieved 14 points. Table 9 presents gene expressions with a non-linear link to cell sensitivity with a score ≤14. The expression of a particular gene may work like an on-off switch for MP1 sensitivity, which can be seen when above a certain threshold expression level, the IC50 value decreases drastically, while below the threshold, it expresses a different higher IC50 value. Furthermore, both regression analyses revealed many overlapping gene targets suggesting the close assumptions in searching for MP1 sensitivity predictors.

Table 9 Gene targets that might be influencing sensitivity to MP1 identified by non-linear regression analysis. The maximal prediction score is 16. The below table presents genes with scores above 14

Gene name	Prediction score
RP11-276H7.2	16
LRRC49	16
CEP89	16
SIPA1L3	16
AC026806.2	16
RN7SL566P	16
KIF3B	16
CCDC24	15
MTMR11	15
LINC00886	15
TCTEX1D2	15
MYO6	15

HOTAIRM1	15
C10orf12	15
PDX1	15
THAP10	15
ACE	15
C19orf55	15
CNOT3	15
RP11-276H7.3	14
SPOPL	14
INPP1	14
FBXO36	14
NGEF	14
PLXNB1	14
CHDH	14
ABLIM2	14
ZBED3	14
UBTD2	14
HOXA-AS3	14
C11orf49	14
AP003068.18	14
PGM2L1	14
CAPN5	14
NCOR2	14
EFNB2	14
VKORC1	14

PLCD3	14
SAMD4B	14
ZNF837	14
C20orf195	14
B3GALT5	14
RP5-1158E12.3	14
FGF13	14

5.3.2 Analysis of over-representation of functional gene classes within the candidate list

Having a list of gene candidates selected by linear and non-linear strategy, over-representation analysis (ORA) was applied to identify the groups of particular genes with known or suspected biological relevance, which are more prevalent in a set of variables of interest than would be expected by chance [312]. Prof. Thomas Hughes analysed a list of gene candidates which came out significant in linear regression and non-linear strategy designed by Prof. Paul Beales seeking significantly over-represented genes using functional databases: gene ontology and pathways (KEGG, Reactome and Panther). Furthermore, the enrichment analysis might indicate certain biological pathways involved in MP1 sensitivity and, more importantly, by altering the expression of a single gene, the expression of a number of different individual genes could also be affected. Any pathway-related gene would be a stronger candidate than any free-standing individual gene in the raw list of significant outcomes. GO analysis signified embryonic development pathway with the false discovery rate (FDR) <0.05 presenting BMP4, GRLHL3, HOXA6, HOXB5, HOXB6 and IHH with potential importance in MP1 resistance (see Table 10).

Table 10 Gene candidates determined to be involved in the metabolic pathways identified in the bioinformatic search. The metabolic pathways used are GO, KEGG and Reactome.

DATABASE	BIOLOGICAL FUNCTION	FDR	GENES
GO	embryonic skeletal system dev, skeletal system morphogenesis, pattern specification process, embryonic organ development	<0.05	BMP4, GRHL3, HOXA6, HOXB5, HOXB6, IHH
REACTOME	mitochondrial fatty acid beta-oxidation of unsaturated fatty acids	0.007	HADHA, HADHB
GO	cell-cell junction	0.012	ACTN4, AHNAK, CDC42EP4, CGN, CYTH2, DDX58, EPB41L3, EPHA2, ESAM, FGF13, NHS, PPL, SHROOM3, SIPA1L3
KEGG	Phosphatidylinositol signalling system	1	INPP1, INPP5A, PLCD3
GO	Lipase activity	0.14	FAAH, LIPG, PLA2G16
GO	carboxylic ester hydrolase activity	1	CAPN12, CAPN8

5.3.3 Prioritization of candidate genes

The aim was to select approximately 10 genes identified in these analyses to study further, potentially using cell-based approaches. The overall selection strategy was based

on three predictive models: linear regression, non-linear approach and the functional enrichment analysis. Genes with statistical significance by $p<0.05$ (Bonferoni correction, B+H correction) were gathered and supplemented with those from the non-linear scoring. Another criterion was the function and cellular location of the gene products encoded by the genes; a function/location of specific interest was the plasma membrane, given the fact that this is site at which MP1 acts. As presented in Chapter 4, cell MP1 sensitivity might be rooted in the local lipid composition. In addition, genes playing a crucial role in lipid metabolism were considered. Having a list of top-ranked genes, ten of them were selected as general biomarkers and/or mediators of the sensitivity of cell lines to MP1 (Table 11). The diverse function of these genes included transcription regulation, cell signalling, lipid biosynthesis/metabolism and tumorigenesis. Considering different gene ranks and limited experimental resources, ten targets seem to be an appropriate choice for down-stream testing.

Table 11 Gene candidates identified in the signature score ranking

Gene	Function	Localisation	Scoring (max. 16)	p-value (B+H correction)	Expression in cancer
Linear regression with Bonferoni correction					
HOXB5	Transcription factor	Nucleus, cytosol	10	0.0058	Enhanced (endometrial cancer) Detected in many[313]
HOXA6	Transcription factor	Nucleus	12	0.015	Low tissue specificity Detected in many[314]
Linear regression with B+H correction					
IHH	Secreted signalling molecule; calcium ion binding; patched binding	Plasma membrane,	12	0.015	Enhanced (colorectal cancer) Detected in many[315]

		extracellular space			
BMP4	Growth factor activity (secreted ligand of the TGF-beta)	Extracellular space	13	0.019	Low cancer specificity Detected in all[321]
PDE4C	Hydrolyzes the second messenger cAMP	Extracellular space, cell projection	10	0.027	Low cancer specificity Detected in many[317]
PLA2G16	N-acyltransferase activity; phospholipase activity	Cytosol, plasma membrane, peroxisome, ER	11	0.027	Low cancer specificity Detected in all[318]
LIPG	Phospholipase and triglyceride lipase activities; secreted	Extracellular region	10	0.034	Enriched (thyroid cancer) Detected in many[319]
FAAH	Hydrolysis of a number of primary and secondary fatty acid amides	Cytosol, plasma membrane	8	0.037	Enhanced (prostate cancer) Detected in all[320]
Non-linear regression scoring					
NCOR2	Transcriptional corepressor	Nucleus	14	0.333	Low cancer specificity Detected in all[321]

5.3.4 Selection of cell model with which to test whether identified genes impact on MP1-sensitivity

A suitable cell model was selected to evaluate the accuracy of predictive genes which might regulate cell response to MP1. Expression of selected genes was plotted as a function of the IC50 across 54 cell lines. Figure 53 presents plots for each gene correlated with twenty cell lines determined with the highest gene expression in order from least to greatest. HOXB5, HOXA6, BMP4, IHH, LIPG, PLA2G16, PDE4C and KLF5 expression levels positively correlated with the IC50, whereas NCOR2 and FAAH expression does

not seem to correlate with MP1 sensitivity. The linear regression does not reflect fluctuating gene expression level, thus certain drug doses what might stimulate genes to work like “on-off” switch to MP1 sensitivity. Having analysed all graphs, it was noted that HT-29 cells expressed all of the 10 genes at detectable levels, and furthermore, HOXB5, BMP4, HOXA6, IHH, KLF5 and PLA2G16 were expressed at the relatively high levels in this cell line (see position of HT-29 highlighted on the plots of Figure 53). HT-29 is a human colorectal adenocarcinoma cell line characterised by a relative resistance to MP1; the IC50 value is 67 μM [322]. Relatively higher expression of selected gene targets in the relatively resistant HT-29 cells suggested that those genes might be influencing cell sensitivity to MP1, and also – in practical terms – defined that these genes were potentially suitable for experimental siRNA-mediated knock-down.

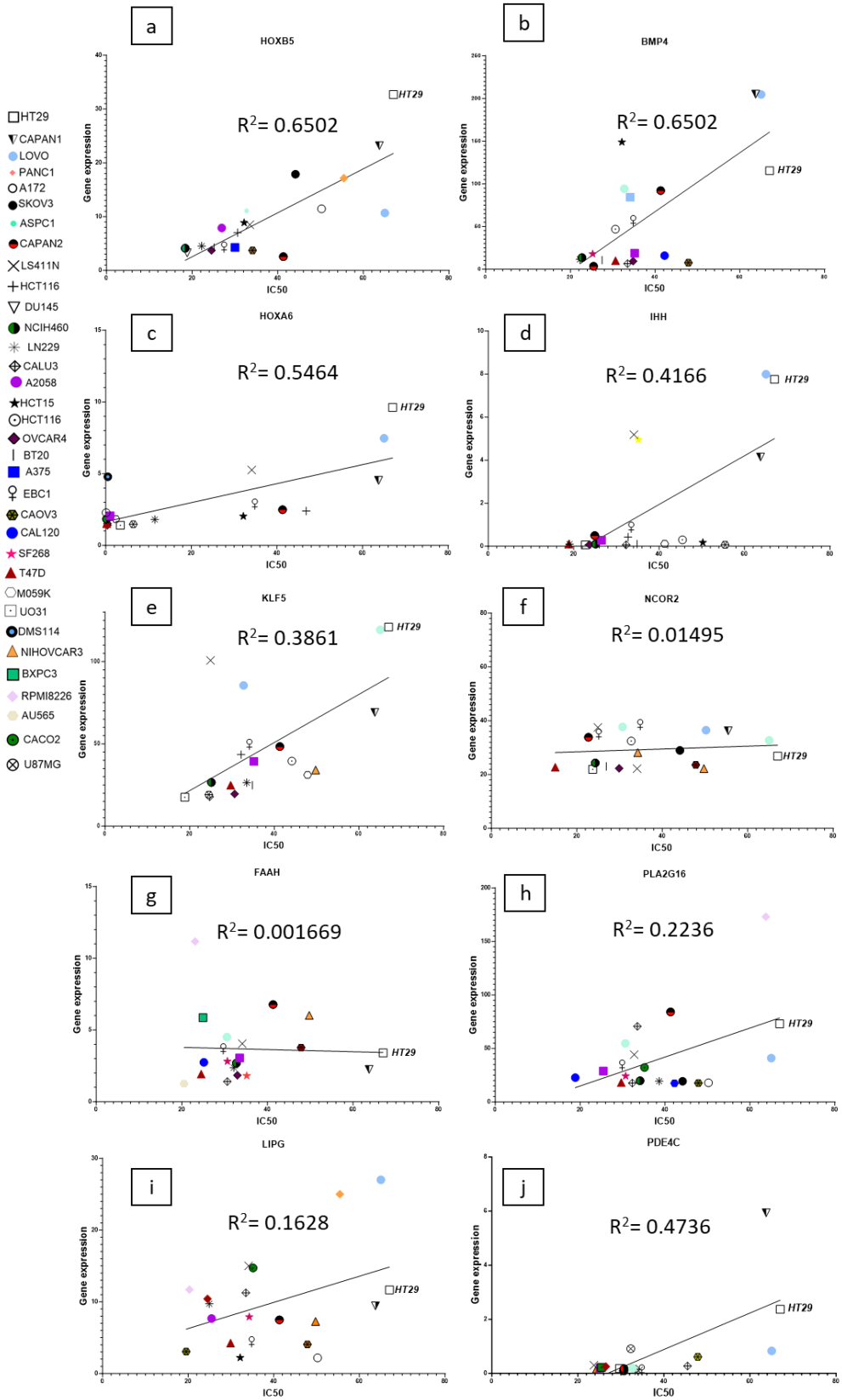

Figure 53 Relationships between IC50 values for MP1 and each gene expression: (a)HOXB5, (b)BMP4, (c)HOXA6, (d)IHH, IKLF5, (f)NCOR2, (g) FAAH, (h)PLA2G16, (i) LIPG and (j) PDE4C.

5.3.5 siRNA knockdown has a slight effect on MP1 cytotoxicity

Knockdown experiments were to be performed for those 10 gene targets in the HT-29 cell line. First, it was necessary to validate that siRNA-mediated knock-down was effective in this cell line. Accordingly, total RNA was isolated from HT-29 cells transfected for 24 h or 48 h with non-silencing siRNA and PLA2G-16-targeting siRNA. Relative fold differences in mRNA levels compared to scrambled siRNA treated are shown on Figure 54. The 0.7 fold change reflects successful gene knockdown. Therefore, qPCR validation confirmed that transfection of HT-29 cells effectively limited the expression of the targeted genes.

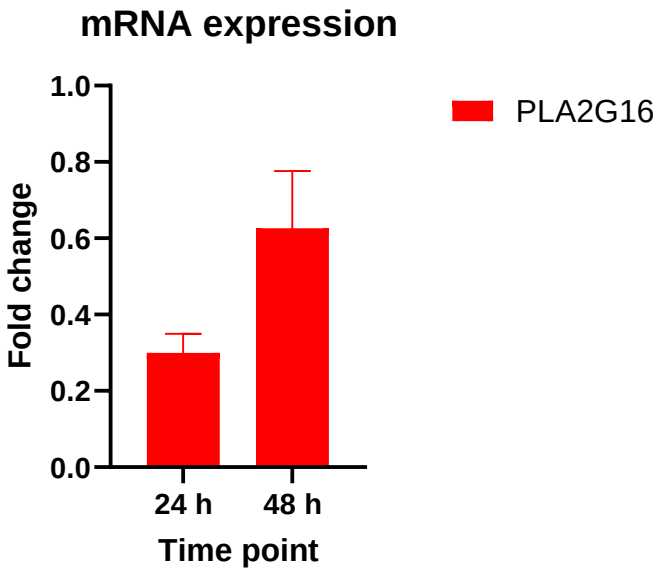

Figure 54 HT-29 cells were transfected with siRNA or control siRNA. 24 h and 48 h after transfection qPCR was performed to assess relative expression of PLA2G16 mRNA. Data represent 1 biological experiment with SD of technical triplicates.

Having validated the gene knockdowns, the influence of each gene on MP1 sensitivity was conducted. Next, HT-29 cells were transfected either with control non-targeting siRNA sequences or with siRNAs targeting the specific genes of interest. 24 h or

48 h later, cells were then treated with a range of 0, 20, 40 or 67 μM of MP1, and cell survival/proliferation was assessed by MTT assays after a further 24h. Data are presented in two groups – initially for 4 target genes (Figure 55) and then for the remaining 6 target genes (Figure 56). In both cases the data are analysed in two ways. Firstly, survival/proliferation is shown relative to the control transfected cells that were not treated with MP1(Figure 55 A and B, Figure 56 A and B). From these, it is possible to see the dose response in the control transfected cells, and the variation from this in the specific gene siRNA samples. Secondly, data were analysed within each dose of MP1, comparing the control transfected to the specific knock-downs; in this analysis absolute inhibition of survival/proliferation is hidden, allowing easier focus on relative differences between siRNAs (Figure 55 C and D, Figure 56 C and D). Apart from 48 h transfection of HOXA6, PDE4C, LIPG, FAAH, NCOR2 and KLF5, relative survival to control without MP1 dosing confirmed that 67 μM MP1 dose inhibited cell growth by 50%. Alternation in cell survival under MP1 dosing of 48-hr transfected cells might relate to the transfection agent effect. Statistical analysis revealed that only the knockdown of *IHH* (48h transfection) in combination with 40 μM MP1 had a significant effect on cell survival compared to control. Knockdown of other gene targets treated at a range of MP1 doses did not significantly alter MP1 sensitivity.

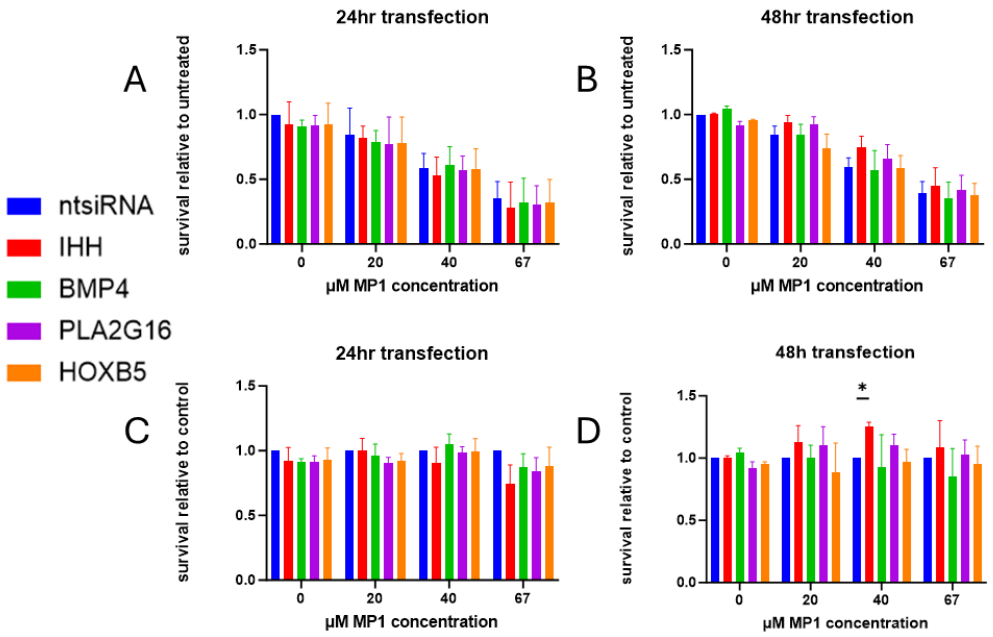

Figure 55 HT-29 cells were transfected with siRNA or control siRNA for 24 h and 48 h cells and then were treated with 20, 40 and 67 µM doses of Polybia MP1 or with vehicle control for 24 h. Relative survival was determined using MTT assays. Data are presented in two separate plots: Figure A and B present cell survival relative to untreated (vehicle control) and Figure C and D show cell survival relative to control at each dose, of 3 biological repeats showing error bars representing ± SEM of 8 replicate wells. Differences between targeted siRNA and scrambled siRNA were tested using ANOVA and non-linear regression; *indicates $p<0.05$

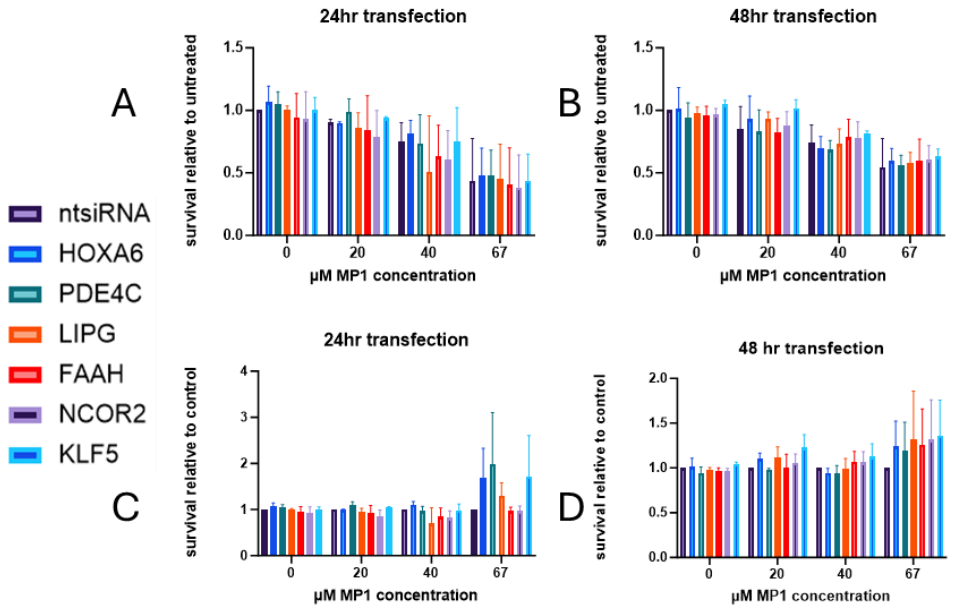

Figure 56 HT-29 cells were transfected with siRNA or control siRNA for 24 h and 48 h cells and then were treated with 20, 40 and 67 μM doses of Polybia MP1 or with vehicle control for 24 h. Relative survival was determined using MTT assays. Data are presented in two separate plots: Figure A and B present cell survival relative to untreated (vehicle control) and Figure C and D show cell survival relative to control at each dose, of 3 biological repeats showing error bars representing ± SEM of 8 replicate wells. Differences between targeted siRNA and scrambled siRNA were tested using ANOVA and non-linear regression; *indicates $p<0.05$

5.4 Discussion

5.4.1 Predicting cell response to Polybia MP1 based on gene-expression biomarkers of sensitivity learned from cell lines

The traditional scientific research study typically investigates one gene or a few genes at a time. In the contrary, high-throughput genomic, proteomic and bioinformatics screening approaches are alternative technologies that allow simultaneous detection of the changes and regulation of genome-wide genes under certain biological conditions. Those high-throughput platforms usually generate large data using the biological knowledge

accumulated in public databases. There is a wide range of *in silico* tools to determine drug responses at different sensitivity and resistance levels for various therapeutic agents. The common are regression models [307], random forest models [323], neural networks [324] or support vector machine (SVM) models [325]. Furthermore, in the last years, the number of enrichment tools remarkably increased facilitating the functional analysing of large datasets [305]. Before applying any novel therapeutic, it is necessary to understand the molecular mechanism that drives it. In this respect, it is highly unlikely to perform all of the required assays testing the behaviour of the single molecule. Finding the biological systems that interact with a drug and display changes at the transcriptome level provide a strong indication that a certain application is truly beneficial. Since testing multiple model systems has been crucial to identifying overlapping similarities, bioinformatics become an indispensable tool.

Predictive models for Polybia MP1 were built using data on gene expression and drug sensitivity (IC_{50}) from 54 cell lines. Regressions and pathway analyses of gene expression were employed to identify genes that are potentially up- and down-regulated in cell lines characterised by varied sensitivity to MP1. Many IC50-gene expression level interactions were determined uncovering several potential MP1-gene associations. The most accurate gene signatures based on the expression of multiple genes to predict key responses for Polybia MP1 are HOXB5, HOX6, BMP4, IHH, FAAH, LIPG, PLA2G16, PDE4C, KLF5 and NCOR2.

5.4.2 The effect of gene knockdown on MP-1 treated cell survival

In silico multiple testing guided the selection of genes for siRNA screening. The live-cell model system was applied to evaluate the prognostic accuracy of the designed statistical models. Gene knockdown was performed in the HT-29 cell line being a relatively

MP1 resistant (IC50 67μM) characterised by a relatively high expression of chosen gene targets. Testing a data-driven assumption, *IHH* knockdown resulted in increased cell survival compared to control at the 40 μM MP1 dose. This is inconsistent to the assumption that gene knockdown of gene with positive correlation to MP1 sensitivity in the MP1 resistant model would result in cell sensitization to MP1 treatment.

IHH is one of the protein ligands in the mammalian hedgehog signalling pathway, essential in bone growth and differentiation [326]. It has been indicated that IHH expression highly correlates with the advancement of malignancy. Furthermore, its expression is induced during mechanical stress [327]. The Hedgehog signalling regulates cholesterol metabolism and homeostasis[328].

Testing 10 out of 67 survival-associated genes and metabolic pathways, bioinformatic prediction cannot be explicitly admitted or failed as a prospective tool to find MP1-related gene signatures. The initial knockdown screening demonstrated potential *IHH* involvement in cell resistance mechanism to MP1, however, gene silencing of multiple targets might reveal a synergistic effect. In addition, apart from gene targets signified by the computational method, worth investigating are proteins of membrane repair pathways that might be relevant to MP1 sensitivity.

5.4.3 Resistance factors to membrane-active peptides and potential targets

Despite that targeting the cell membrane allowed cell-penetrating peptides to overcome the development of resistance, there are still some cell self-protecting strategies [218]. When peptides accumulate on the membrane surface, they might undergo degradation due to aminopeptidase activity [329]. Hence, elevated activity of the extracellular peptidases, biosynthesis pathways or transport, suggests a potential target.

Interestingly, studies in HT-29 cells revealed eight cell-surface peptidases [330]. Furthermore, as specified in Chapter 4, membrane composition, in particular, negative lipids facilitate peptide-lipid interaction. Flippases and flopases are enzymes modelling lipid organization across the lipid bilayer [331]. Rapid membrane reshaping and altered enzymes activity is another potent determinant of cell resistance. According to HT-29, the colorectal cancer cell membrane has a relatively low surface expression of PS [332]. Cells are also capable of expelling drugs in endogenous transporters [333].

5.5 Conclusions

Motivated by the public availability of informative data resources, *in silico* model for predicting MP1 response data was designed. Noteworthy, none of the statistical methods is perfectly suitable for this prediction. *IHH* coding gene was found to slightly modify HT-29 cell response to MP1, but the finding requires further investigation. IHH protein is localised in the cell membrane, where displays autoproteolysis and cholesterol transferase activity. Although various statistical models were applied to identify multiple interacting genomic features testing each cell line's sensitivity to MP1, there is still a need for comprehensive models searching for the global cellular response to drugs.

Conclusions

One in six deaths worldwide is cancer-related and there were around 20 million new cancer cases in 2020 [334]. Cancers arise as a conseqence of many changes in the behavior of cells, one of which is cell survival beyond normal limits, or acquired capability to baypass cell death [34]. Typically, changes in the expression of key genes defined as oncogenes or tumour suppressors can lead to loss of cell cycle control and relatively unrestrained cell growth [335]. The conventional treatment strategies involve surgical intervention, radiation and chemotherapy [336]. These regimes, especially chemotherapy drugs, affect the cell cycle often at the specific stages of mitosis or DNA replication [337]. Unfortunately, chemotherapy can also be 'cytotoxic' to normal dividing cells and their therapeutic applicability relies on a larger fraction of cell kill in cancer cells as opposed to normal cells [338]. Toxicities fluctuate in terms of the specific drug, dose, schedule of administration and any patient-associated factors, which are known or unknown [339]. Although medical approaches are constantly improving, new therapeutic strategies with greater specificity and lower toxicity with a relatively smaller number of co-incident side effects have become a focus of anticancer research [340]. So far, numerous bioactive peptides have been detected to have therapeutic anti-cancer properties that hold great promise for cancer treatment in the future [341]. A great number of them have been also classified as antimicrobial peptides, naturally secreted by living organisms and compounds of the first line of immune defence with microbicidal activity [342]. These bioactive agents were already thoroughly characterised and depicted in the literature and are now applied in many various sectors such as agriculture, food industry and medicine [343]. Out of interest, AMPs were under consideration in the recent SARS-CoV-2 pandemic as novel antiviral molecules to counteract COVID-19 disease [344].

Chapter 1 extensively reviews the most recent developments in the field of cell membrane biophysics, followed by an introduction to the AMPs and their characterisation. Wide-spectrum activity, diverse origin sourced in nature, low probability of development of resistance, and rapid killing activity, outweigh the disadvantages of these peptides over conventionally applied pharmaceuticals [345]. AMPs are also considered immunomodulators, anti-inflammatory agents and antioxidants and, thus, the multifaceted mechanism of action should be thoroughly explored prior to the implementation of AMPs to commercial sale [6]. Specifically, AMPs are evolutionary conserved short amino acid sequences varying in structure and bio-functionality [3]. Although displaying an inhibitory effect on a broad range of pathogens, AMPs have similar biophysical characteristics: due to the presence of charged residues, peptides carry typically a positive net charge and contain a notable proportion of hydrophobic amino acids and eventually conform amphiphilic structure in contact with the membrane-like environment [181]. Therefore, AMPs exert their activity by interacting with biological membranes. The membranolytic activity is thought to be greatly impacted by lipid cell composition, however, the mechanism of membrane penetration is still a matter of debate [346].

Biological membranes are complex dynamic structures serving as platforms for various cellular processes [59]. For a long time, their nature was a big puzzle as there were no adequate research tools available [347]. The lipid bilayer constitutes the principal scaffolding of any cell membrane with embedded proteins. Phospholipids are the most abundant membrane lipids, which are also amphipathic. Nowadays much simplified artificial model systems are used to explore cell membrane fundaments. One of them, giant plasma lipid vesicles, cell-derived systems which maintain the compositional complexity of biological membranes have been utilized as a new toolbox for membrane investigation [84]. In recent years, GPMVs gained much attention in the field of liquid-liquid phase

separation in the plasma membrane [16]. The organization of eukaryotic membranes remained not fully understood as coexisting liquid domains cannot be directly visualized in living cells by light microscopy [348]. The observation of these structures and validation of the raft hypothesis has become feasible using GPMVs [349].

This work reports a systematic investigation of molecular elements determining the membranotropic activity of Polybia MP1 searched in a sequence of MP1 itself, the lipid organization of the membrane and within the transcriptomic profile of the target cells. MP1 is a representative of AMPs displaying a dual nature: antimicrobial and anticancer against a diverse range of targets [116]. Recent studies in synthetic membrane models have brought to light its lytic potency against PS-enriched systems [117, 159, 350]. Therefore, to address the in-depth lack of understanding structure-function relationship of Polybia MP1 in anticancer activity, a list of project aims is outlined below:

1. To understand the contribution of individual residues and groups of residues within MP1 to its membrane lysing action, using artificial model membranes;
2. To identify MP1 derivatives with higher specificity and potency towards the membrane models;
3. To develop giant plasma membrane vesicles as a model membrane system;
4. To define how MP1 changes membrane properties using a cell-derived model system;
5. To define how MP1 sensitivity correlates with expression of individual genes in mammalian cancer cells, and determine whether individual genes determine sensitivity using knock-down approaches.

A range of experimental approaches was applied to address those specific aims: starting from a chemical modification of short peptide motifs, leakage assays based on fluorescence

spectroscopic measurements in synthetic models, mammalian cell culture, confocal laser scanning microscopy, *in silico* transcriptomic analysis and molecular tools such as gene silencing technique.

The first and second aims were addressed in Chapter 2. A number of chemical modifications were applied in order to study the contribution of individual or grouped amino acid residues and to identify MP1 analogues with greater potency than native MP1. Amino acid substitutions altered also primary physiochemical properties of MP1 and provided insight into the role of the net charge, hydrophilic and hydrophobic content and its ratio and consequent molecule amphipathicity in its mechanism of action. The result showed that: (1) Trp residue substitution, in alanine scan screening, significantly quenched peptide activity, however, further studies and incorporation of another aromatic residue, Phe and hydrophobic Ile maintained membrane puncturing activity; (2) Leu and Ile situated at the hydrophobic face of the peptide are important modulators in MP1 activity; (3) all of the 14 residues are required in membrane-lysing activity; (4) increasing the net charge of molecules does not always correlate to the facilitated activity ;(5) pH-sensitive peptides could be utilised as therapeutic agents as mutants directly sense cancer-related microenvironment; (6) overall alternation of the hydrophobic side of the MP1 aiming at increasing molecule hydrophobicity boosted potency and specificity in some cases; (7) the majority of variants displaying greater potency than MP1, simultaneously, loses specificity to PS-enriched systems; (8) therefore, rational redesigning of MP1 for optimal balance across principal physiochemical characterisation, cationicity, hydrophobicity and amphiphilicity, is crucial in MP1 activity. Overall, alanine-scan screening is a simple and widely applied method to probe chains of amino acids, their structure and function [351]. Contrary to Ala mutants tested in the simplified model system, Torres et al. performed a similar investigation of Polybia CP in order to examine *in vitro* biological activity to check

the inhibition efficacy of different bacteria strains [352]. Like MP1, 12-residue Polybia CP was isolated from the venom of Brazilian wasp and was reported to be potent against Gram-positive bacteria [152]. Threonine, glycine and serine are sequence-specific amino acid residues characterising venom peptide and only one positively charged Lys residue occurs in the sequence. This approach allows for the thorough identification of chemical modification effects directly in biological systems based on MIC assay (minimal inhibitory concentration). MIC refers to the lowest concentration of drug to inhibit growth [353]. Continuing, circular dichroism spectroscopy measurements and molecular dynamics simulations were performed to study the effect of side chains on peptides secondary structure. Overall, these techniques provide important insight into molecule helicity and therefore, relationships between helical content and activity can be directly drawn. Stability is a typical concern limiting the translation of AMPs into the clinical phase. One of the undesired effects, the haemolytic activity of AMPs is inevitably associated with a high affinity to zwitterionic membranes [345]. A major challenge in the AMPs field is rational redesign for efficient modulation of membrane interaction while minimizing the risk of erythrocyte membrane lysis, therefore Torres et al. examined the haemolytic activity of peptides to verify their translatability prior to *in vivo* assays. In addition, CP mutants were exposed to fetal bovine serum (FBS) protease to investigate protease-mediated degradation. Similar studies were performed in order to elucidate the structure-function relationship of Aurein 1.2 [354]. Apart from already described biological methods, the hydrophobicity of peptides and their self-assembly were explored using reversed-phase chromatography. Additional insight into the role of hydrophobicity in peptide self-association capability can expand comprehension of peptide biological activity. Zamora-Carreras et al. conducted an Ala-scan screening of Lys-rich BP100 peptide by using solid-state ^{15}N and ^{2}H NMR to estimate and refine the orientation in model systems [355].

Peptide concentration and the lipid spontaneous curvature were determined to influence helix orientation. The peptide insertion was found deeper along with increasing spontaneous curvature of the lipids.

The third aim was addressed in Chapter 3. As shown in the peptide screening section, minimal membrane systems allow for quantitative characterization of peptide potency and specificity in zwitterionic and anionic lipid platforms. Thus, principal membrane alternation differing cancer cells to normal tissue was investigated. Well-controlled composition is the main advantage of lipid systems, however, the native cell environment is much more complex. Therefore GPMVs, cell-derived PM platforms which retain molecular richness with lipid and protein composition close to the intact cell, were proposed to expand understanding of MP1 membranotropic activity. Testing different vesiculation protocols, results showed that: (1) GPMV formation is a dose-, time-, and temperature-dependent process which requires cell-specific optimisation in order to increase vesicle yield; (2) it is almost impossible to avoid the generation of undesired cell debris, and, therefore, obtain a pure GPMVs suspension; (3) the application of osmotic gradient induces substantial GPMVs yield from healthy cell model; (4) PFA and DTT are potent agents inducing membrane buds and their rupture in both cancer and non-transformed cell lines; however, GPMVs incubation with size-different probes revealed that|: (5) GPMVs display heterogeneous permeability to solutes as large as 70 kDa and as a consequence, there is a need for reasonable use of GPMVs as membrane model. Accordingly, this work is the first to attempt to optimize GPMV formation by osmotic method and chemical vesiculation of breast cell lines and to evaluate the membrane integrity of generated vesicles. The analogue phenomenon was reported by Skinkle et al.[91]. It was observed that PFA and DTT-induced GPMVs are passively permeable to hydrophilic solutes as large as 40 kDa and explained by the relatively large pore formation

by rupture of vesicles from cells. Sarabipour and colleagues attempted to characterize differences between osmotically induced and PFA/DTT vesicles revealing that soluble proteins are retained within the chemically induced vesicles and that soluble proteins of molecular weight up to 210 kDa are not found inside the GPMVs induced via osmotic pressure [356].

Despite the limitations of the cell-derived membrane system, GPMVs were further tested to explore the membrane penetration of amphiphilic MP1 at the single vesicle level demonstrated in Chapter 4. The coexistence of the liquid-liquid phase separation has been already investigated in GPMVs elucidating the physical principles of the lipid raft hypothesis in cell PM [16]. The use of solvatochromic probes, which sense changes in lipid order in the plasma membrane is a powerful tool enabling the development of lipid raft research [298]. These fluorescent molecules take advantage of the phenomenon of solvent dipolar relaxation, which corresponds to a number of water molecules present at the membrane interface reflecting lipid packing [285]. Therefore, testing GPMVs membrane organization prior to and after exposure to MP1 indicated that: (1) GPMVs are a suitable model to study membrane lipid packing; (2) the application of Laurdan, and its derivatives are an effective method to study lipid packing at different membrane locations; (3) the difference between coexisting L_d/L_o (ΔGP) shows that cell sensitivity to MP1 corresponds to lipid packing, lower GP correlates with cell resistance; (4) MP1 modulates changes in lipid phase behaviour in GPMVs, however, vesicles derived from a cell line classified as sensitive to MP1 undergo observable phase-separation, while GPMVs isolated from resistant MCF-10A cell line organised into spots not empirically resembling raft domains; (5) lipid phase rearrangement observed in the MCF-10A breast model might be a cell-protective mechanism against MP1. Accordingly, it could be assumed that lipid membrane organization underlies the molecular basis of MP1 cell specificity. This work first presents

the MP1-driven phenomenon, however, the influence of other antimicrobial peptides on lipid ordering has been widely reported. Recently, Almeida and collaborators observed that the amphipathic peptide RW9 induced lipid re-packing in GPMVs tagged with di-4-ANEPPDHQ, Laurdan derivative, increasing membrane disordering [357]. Säälik et al. reported the phase preference of MAP, pAntp and Transportans, cell-penetrating peptides observing high affinity to the L_d phase indicated by the colocalization with the annexin V-positive domains or in the presence of Laurdan [89]. In addition, Steinkühler and colleagues extended the use of C-Laurdan along with molecular rotors to study the elastic properties of PM in GPMVs which are decoupled from the mechanical influence of cytoskeletal network. Thus, Laurdan and its analogues are commonly applied to study membrane organization.

Already employed and demonstrated techniques allowed for determining side chains important in peptide activity and a key role of lipid bilayer arrangement in cell response to MP1. Continuing, Chapter 5 attempted to identify molecular mechanisms of cell sensitivity to MP1 using bioinformatic and functional approaches addressing the final aim. The preliminary *in silico* investigation into cell sensitivity to MP1 based on the transcriptomic cell profiles followed by gene knockdown technique showed that: (1) statistical strategies are capable of selecting significant relationships between gene expression and the cell sensitivity (the IC50 value); (2) ORA analysis and biological analysis are useful tools for eliminating genes that might be retrieved due to their overexpression for example in cancer tissue or drawing gene networks pronouncing gene correlations or mutual pathways which might play a role in cell response to MP1; (3) however, siRNA transfection is an efficient technique for gene silencing, statistical analysis revealed that only *IHH* knockdown allowed for increased cell survival ratio under 40 µM MP1 dose; (4) none of the strategies is perfectly suitable for the prediction of cell significant molecular determinants to MP1

response. Having found that cell sensitivity correlates with membrane organization (see Chapter 4), therefore, other potential gene targets could be involved in regulating membrane order. Prior to the administration of any novel drug, it is conditional to understand the molecular mechanism and know its potential side effects. Martinez-Hernandez et al. reported *in silico* investigation of the relationships of the peptide-specific features (amino acid composition, physicochemical properties, sequence motifs and sequence homology) with selectivity towards healthy and cancer cell models [358]. Bioinformatic analysis was also applied to identify therapeutic targets of glioblastoma [359]. Transcriptomic analysis along with samples obtained from patients with their RNA-sequencing allows for predicting sensitivity to anticancer drugs [360, 361].

With all those findings, it could be concluded that the presented work provides insights into the molecular basis underlying cell sensitivity to Polybia MP1 peptides. Some of the redesigned MP1 derivatives displayed great potency against PS-enriched systems, hence, they have the potential to be used for *in vivo* applications. So far, variable lipid packing, and phase separation emerged as important molecular determinants driving cell-specific MP1 phenomenon. Undoubtfully, it could not be seen without GPMVs use. No other model reflects native cell membrane composition, therefore, attempts to remove cell debris and chemical reagents should be intensified. A variety of cells are capable of producing GPMVs and, despite their permeability, giant vesicles are important tools addressing the long-standing question of the roles of lipid domains, for instance in cell entry of HIV or SARS-CoV-2 [362, 363]. Prior to experimental work, a choice of cell line for vesiculation should be considered carefully to avoid a great amount of cell debris and procedure conditions should be accurate to omit any inconsistency.

Future perspectives

Polybia MP1 is considered one of the shortest antimicrobial peptides with great therapeutic potential, a low probability of haemolytic activity but high susceptibility to proteolytic degradation [116]. Attempts to improve MP1 potency for specific applications are presented in this work. In detail, the modified peptide Q12K, which has non-charged residue glutamine at position 12 changed to cationic lysine, displays an overall +3 net charge and showed higher specificity to PS-containing vesicles than native MP1. This modification was already reported, however, in addition peptide variant was also stabled by using an emerging technology termed "all-hydrocarbon stapling" [161]. A unique cross-linking system was found effective in stabilizing helical structures of short peptide motifs [364]. Therefore, this approach is another possibility for redesigning MP1 analogues with enhanced potency and proteolytic stability. Other approaches worth considering to improve the native peptide activity are: hybridization, cyclization, fragmentation, multimerization, and conjugation [365].

Evidencing the phenomenon of phase separation in GPMVs revolutionalised membrane research. These studies employed vesicles induced by osmotic pressure and a mixture of DTT and PFA [84, 255]. It has been reported that PFA/DTT reagents incorporate changes in the lipid phase which might potentially modulate differences in mechanical properties [366]. The artefacts induced by DTT can affect membrane bending rigidity and, consequently, membrane response to MP1. Importantly, cell culture conditions can have either similar effect on mechanical resistance. Local cell density and time in the culture were also reported to influence the membrane composition of adherent cells. Steinkühler et al. correlated initial cell density and GPMV bending rigidity indicating a trend for a stiffer phenotype at higher cell confluency. Growth conditions and asynchrony of the cell cycle can modulate the phase transition temperature of GPMVs at varied

confluency [367]. Therefore, an additional step in the GPMVs isolation procedure should be incorporated to optimize their formation with respect to consistent growth behaviour and phase separation.

There are various extraction conditions for GPMV isolation. Calmidazolium is another vesiculation agent which does not correlate with a strong cross-linking of membrane components as induced by PFA/DTT [250]. Another GPMVs preparation method is the nanomaterial-assisted strategy during which cells are incubated with carboxylfullerenes followed by light irradiation [267]. Authors postulate high vesicle yield and purity, hence those strategies might be further tested in order to optimize protocols for breast cell lines. Continuing GPMVs characterization, it has been observed that cells cultured with GPMVs encapsulated with fluorescent dextran displayed some fluorescence [269]. Based on this finding, it has been assumed that GPMVs loaded with cargo can fuse with cells and pass the cargo. Therefore, GPMVs might be used as a delivery system with specific optimization, even for MP1. Effective GPMV loading with curcumin, an anti-inflammatory drug, was already reported using flow cytometry analysis [267]. Before GPMVs are applied as carriers, the resistance of giant vesicles in the variable physiological conditions in the human body should be determined. Therefore, GPMVs could be investigated at varied cell culture conditions together with the influence of isolation chemicals under MP1 treatment.

Interestingly, GPMVs are applied as starting material and their homogenization for the preparation of monodisperse nano plasma membrane vesicles (nPMVs) extrusion through filter membranes with pore sizes up to 400 nm [368]. In addition, size exclusion chromatography or dialysis is used to purify GPMV yield and to remove the PFA and DTT-containing buffer for further experiments [369]. nPMVs are seen as a prospective source

for developing EV-based pharmaceutical therapeutics, hence these findings might direct further GPMV research.

Lipid asymmetry is a fundamental characteristic of PM in animal cells and disturbance of its maintenance is linked to many cellular functionalities [370]. Loss of phospholipid asymmetry has been accomplished through apoptosis, blood coagulation, cell fusion and more importantly, tumorigenesis [277]. There is growing evidence suggesting the apoptotic nature of GPMVs [269]. A drop of Annexin V, which was shown to interact specifically with PS, can detect apoptosis by targeting the loss of PM asymmetry by the use of flow cytometry [371].

Domain-dependent cell response to MP1 could be further investigated by using more advanced techniques such as AFM. Alternatively, there is a possibility of applying Pro12A, another Laurdan analogue with an attached anchor group composed of sulfonate charged group and dodecyl alkyl chain [298]. As recently published, Pro12A is characterized by more effective binding to the exoplasmic membrane layer, therefore, it shows higher susceptibility to monitor changes in the lipid environment. Another strategy, lipidomic studies on the sensitive and resistant cell lines to MP1 might indicate differences in lipid composition and link them to cell response. Furthermore, lipidomic investigation on GPMVs could reveal the effect of the isolation procedure on the membrane.

Affinity photolabeling is a novel approach to studying non-covalent interactions between molecules, as well as specific membranotropic peptides [372]. Jiao et al. investigated a mode of action of insertion, a cell-penetrating peptide, which was photo-labelled with different moieties [373]. Conversely, membrane models with incorporated photoreactive lipids are another advancement in probing hydrophobic bondings between proteins and phospholipids in membranes [374]. The idea is to theoretically obtain precious geometrical information on the platforms composed of the interacting peptide and the

membrane with the photoreactive lipid. Therefore, it is highly likely to monitor exactly which amino acid residue(s) are in close proximity to the lipid photoprobe. Alamethicin, Gramicidin A and Magainin are some of the AMPs family members investigated in photosensitive lipid systems. Alamethicin, a peptide isolated from the fungus *Trychoderma viride* has been proven to partially insert in the lipid bilayer through the N-terminus [375]. In 1998, researchers focused on an amphibian-derived magainin 2 showing that along with the increased peptide-to-lipid ratio, photolabeling yield escalated in membranes enriched with negative lipids [376]. Furthermore, a time-course experiment exhibited fast (less than 30 s) and stable (over 30 min) peptide insertion. Gramicidin A is reported to form an ion channel in membranes with the two N-termini located near the centre of the bilayer [377]. N-terminal valine substitution to electron rich tryptophan, which is reactive towards carbenes, increased twice photolabeling and evidenced that the photo tag was therefore in the middle of the two layers. Therefore, photolabeling either peptide or membrane is another prospective method to investigate structure-function exploration of MP1.

Further tests in cholesterol-deprived conditions could indicate the role of sterol structure role in defining the membrane order [378]. As already reported, cholesterol depletion was performed by cyclodextrins, which activate cholesterol exchange [48]. GPMVs isolated from cholesterol-depleted cells were described as softer in contrast to stiffer cholesterol-enriched systems, thus cholesterol role and raft domain formation capability could determine MP1 membrane perturbing efficiency.

The transcriptomic analysis presented in this work, followed by gene knock-down, was not efficient in determining the molecular basis of MP1 cell response. Other approaches to expand studies are: the use of different cell lines, gene knock-down of multiple targets at once or knock-down validation at the protein level. The best results

could be obtained by the RNA-sequencing method which allows for investigation of mRNA levels prior to and after cell exposure to MP1.

Bibliography

1. Seelig J (2004) Thermodynamics of lipid–peptide interactions. Biochim Biophys Acta BBA - Biomembr 1666:40–50. https://doi.org/10.1016/j.bbamem.2004.08.004

2. Preta G (2020) New Insights Into Targeting Membrane Lipids for Cancer Therapy. Front Cell Dev Biol 8:. https://doi.org/10.3389/fcell.2020.571237

3. Brogden KA (2005) Antimicrobial peptides: pore formers or metabolic inhibitors in bacteria? Nat Rev Microbiol 3:238–250. https://doi.org/10.1038/nrmicro1098

4. Jenssen H, Hamill P, Hancock REW (2006) Peptide Antimicrobial Agents. Clin Microbiol Rev 19:491–511. https://doi.org/10.1128/CMR.00056-05

5. Hoskin DW, Ramamoorthy A (2008) Studies on anticancer activities of antimicrobial peptides. Biochim Biophys Acta 1778:357–375. https://doi.org/10.1016/j.bbamem.2007.11.008

6. Guaní-Guerra E, Santos-Mendoza T, Lugo-Reyes SO, Terán LM (2010) Antimicrobial peptides: general overview and clinical implications in human health and disease. Clin Immunol Orlando Fla 135:1–11. https://doi.org/10.1016/j.clim.2009.12.004

7. Jafari A, Babajani A, Sarrami Forooshani R, et al (2022) Clinical Applications and Anticancer Effects of Antimicrobial Peptides: From Bench to Bedside. Front Oncol 12:819563. https://doi.org/10.3389/fonc.2022.819563

8. Nieh M-P, Heberle FA, Katsaras J (2019) Characterization of Biological Membranes: Structure and Dynamics. Walter de Gruyter GmbH & Co KG

9. Alberts B, Johnson A, Lewis J, et al (2002) Molecular Biology of the Cell, 4th ed. Garland Science, https://doi.org/10.1093/aob/mcg023

10. Cuevas J (2015) Structure and Function of Membranes. Reference Module in Biomedical Sciences. Elsevier, p B9780128012383053204

11. Singer SJ, Nicolson GL (1972) The fluid mosaic model of the structure of cell membranes. Science 175:720–731. https://doi.org/10.1126/science.175.4023.720

12. Waheed AA, Freed EO (2009) Lipids and Membrane Microdomains in HIV-1 Replication. Virus Res 143:162–176. https://doi.org/10.1016/j.virusres.2009.04.007

13. Simons K, Ikonen E (1997) Functional rafts in cell membranes. Nature 387:569–572. https://doi.org/10.1038/42408

14. Owen D, Gaus K (2013) Imaging lipid domains in cell membranes: the advent of super-resolution fluorescence microscopy. Front Plant Sci 4: https://doi.org/10.3389/fpls.2013.00503

15. Levental I, Grzybek M, Simons K (2010) Greasing their way: lipid modifications determine protein association with membrane rafts. Biochemistry 49:6305–6316. https://doi.org/10.1021/bi100882y

16. Baumgart T, Hammond AT, Sengupta P, et al (2007) Large-scale fluid/fluid phase separation of proteins and lipids in giant plasma membrane vesicles. Proc Natl Acad Sci U S A 104:3165–3170. https://doi.org/10.1073/pnas.0611357104

17. Keller H, Lorizate M, Schwille P (2009) PI(4,5)P2 Degradation Promotes the Formation of Cytoskeleton-Free Model Membrane Systems. ChemPhysChem 10:2805–2812. https://doi.org/10.1002/cphc.200900598

18. Veatch SL, Cicuta P, Sengupta P, et al (2008) Critical fluctuations in plasma membrane vesicles. ACS Chem Biol 3:287–293. https://doi.org/10.1021/cb800012x

19. Berg JM, Tymoczko JL, Stryer L (2002) There Are Three Common Types of Membrane Lipids. Biochem 5th Ed, ISBN 9780716730514

20. Stillwell W (2016) An Introduction to Biological Membranes: Composition, Structure and Function. Elsevier, ISBN 9780444637727

21. Martinez-Seara H, Róg T, Pasenkiewicz-Gierula M, et al (2007) Effect of Double Bond Position on Lipid Bilayer Properties: Insight through Atomistic Simulations. J Phys Chem B 111:11162–11168. https://doi.org/10.1021/jp071894d

22. Kaynak A, Davis HW, Kogan AB, et al (2022) Phosphatidylserine: The Unique Dual-Role Biomarker for Cancer Imaging and Therapy. Cancers 14:2536. https://doi.org/10.3390/cancers14102536

23. Paradies G, Paradies V, Ruggiero FM, Petrosillo G (2019) Role of Cardiolipin in Mitochondrial Function and Dynamics in Health and Disease: Molecular and Pharmacological Aspects. Cells 8:728. https://doi.org/10.3390/cells8070728

24. Basu Ball W, Neff JK, Gohil VM (2018) The role of nonbilayer phospholipids in mitochondrial structure and function. FEBS Lett 592:1273–1290. https://doi.org/10.1002/1873-3468.12887

25. Jelinek R (2018) Membranes: From Biological Functions to Therapeutic Applications. Walter de Gruyter GmbH & Co KG, ISBN: 9783110453690

26. Merrill AH, Sweeley CC (1996) Chapter 12 - Sphingolipids: metabolism and cell signalling. In: Vance DE, Vance JE (eds) New Comprehensive Biochemistry. Elsevier, pp 309–339

27. Contreras F-X, Sot J, Alonso A, Goñi FM (2006) Sphingosine Increases the Permeability of Model and Cell Membranes. Biophys J 90:4085–4092. https://doi.org/10.1529/biophysj.105.076471

28. Kishimoto Y (1983) Ceramides and Cerebrosides. In: Lajtha A (ed) Metabolism in the Nervous System. Springer US, Boston, MA, pp 179–199

29. Yu RK, Tsai Y-T, Ariga T, Yanagisawa M (2011) Structures, biosynthesis, and functions of gangliosides—An overview. J Oleo Sci 60:537–544

30. Zhang M, Gaschen B, Blay W, et al (2004) Tracking global patterns of N-linked glycosylation site variation in highly variable viral glycoproteins: HIV, SIV, and HCV envelopes and influenza hemagglutinin. Glycobiology 14:1229–1246. https://doi.org/10.1093/glycob/cwh106

31. Sonnino S, Mauri L, Chigorno V, Prinetti A (2007) Gangliosides as components of lipid membrane domains. Glycobiology 17:1R-13R. https://doi.org/10.1093/glycob/cwl052

32. Dufourc EJ (2008) Sterols and membrane dynamics. J Chem Biol 1:63–77. https://doi.org/10.1007/s12154-008-0010-6

33. Hendrich AB, Michalak K (2003) Lipids as a target for drugs modulating multidrug resistance of cancer cells. Curr Drug Targets 4:23–30. https://doi.org/10.2174/1389450033347172

34. Hanahan D, Weinberg RA (2000) The Hallmarks of Cancer. Cell 100:57–70. https://doi.org/10.1016/S0092-8674(00)81683-9

35. Estes RE, Lin B, Khera A, Davis MY (2021) Lipid Metabolism Influence on Neurodegenerative Disease Progression: Is the Vehicle as Important as the Cargo? Front Mol Neurosci 14:788695. https://doi.org/10.3389/fnmol.2021.788695

36. Poznyak A, Grechko AV, Poggio P, et al (2020) The Diabetes Mellitus–Atherosclerosis Connection: The Role of Lipid and Glucose Metabolism and Chronic Inflammation. Int J Mol Sci 21:1835. https://doi.org/10.3390/ijms21051835

37. Alves AC, Ribeiro D, Nunes C, Reis S (2016) Biophysics in cancer: The relevance of drug-membrane interaction studies. Biochim Biophys Acta BBA - Biomembr 1858:2231–2244. https://doi.org/10.1016/j.bbamem.2016.06.025

38. Yang F, Chen G-X (2018) Production of extracellular lysophosphatidic acid in the regulation of adipocyte functions and liver fibrosis. World J Gastroenterol 24:4132–4151. https://doi.org/10.3748/wjg.v24.i36.4132

39. Zhao Z, Hao D, Wang L, et al (2019) CtBP promotes metastasis of breast cancer through repressing cholesterol and activating TGF-β signaling. Oncogene 38:2076–2091. https://doi.org/10.1038/s41388-018-0570-z

40. Gracià RS, Bezlyepkina N, Knorr RL, et al (2010) Effect of cholesterol on the rigidity of saturated and unsaturated membranes: fluctuation and electrodeformation analysis of giant vesicles. Soft Matter 6:1472–1482. https://doi.org/10.1039/B920629A

41. Lei K, Kurum A, Kaynak M, et al (2021) Cancer-cell stiffening via cholesterol depletion enhances adoptive T-cell immunotherapy. Nat Biomed Eng 5:1411–1425. https://doi.org/10.1038/s41551-021-00826-6

42. Hryniewicz-Jankowska A, Augoff K, Biernatowska A, et al (2014) Membrane rafts as a novel target in cancer therapy. Biochim Biophys Acta 1845:155–165. https://doi.org/10.1016/j.bbcan.2014.01.006

43. Händel C, Schmidt BUS, Schiller J, et al (2015) Cell membrane softening in human breast and cervical cancer cells. New J Phys 17:083008. https://doi.org/10.1088/1367-2630/17/8/083008

44. Brown DA, London E (2000) Structure and Function of Sphingolipid- and Cholesterol-rich Membrane Rafts. J Biol Chem 275:17221–17224. https://doi.org/10.1074/jbc.R000005200

45. Greenlee JD, Subramanian T, Liu K, King MR (2021) Rafting Down the Metastatic Cascade: The Role of Lipid Rafts in Cancer Metastasis, Cell Death, and Clinical Outcomes. Cancer Res 81:5–17. https://doi.org/10.1158/0008-5472.CAN-20-2199

46. Ren J, Hamada J, Okada F, et al (1990) Correlation between the Presence of Microvilli and the Growth or Metastatic Potential of Tumor Cells. Jpn J Cancer Res Gann 81:920–926. https://doi.org/10.1111/j.1349-7006.1990.tb02668.x

47. Han X, Ma L, Gu J, et al (2021) Basal microvilli define the metabolic capacity and lethal phenotype of pancreatic cancer. J Pathol 253:304–314. https://doi.org/10.1002/path.5588

48. Zidovetzki R, Levitan I (2007) Use of cyclodextrins to manipulate plasma membrane cholesterol content: evidence, misconceptions and control strategies. Biochim Biophys Acta 1768:1311–1324. https://doi.org/10.1016/j.bbamem.2007.03.026

49. Maja M, Mohammed D, Dumitru AC, et al (2022) Surface cholesterol-enriched domains specifically promote invasion of breast cancer cell lines by controlling invadopodia and extracellular matrix degradation. Cell Mol Life Sci 79:417. https://doi.org/10.1007/s00018-022-04426-8

50. Schoumacher M, Goldman R, Louvard D, Vignjevic D (2010) Actin, microtubules, and vimentin intermediate filaments cooperate for elongation of invadopodia. J Cell Biol 189:541–56. https://doi.org/10.1083/jcb.200909113

51. Aubrey M (2002) Glycans in Cell Interaction and Recognition. CRC Press, ISBN 9789058230522

52. Burchell JM, Mungul A, Taylor-Papadimitriou J (2001) O-Linked Glycosylation in the Mammary Gland: Changes that Occur During Malignancy. J Mammary Gland Biol Neoplasia 6:355–364. https://doi.org/10.1023/A:1011331809881

53. Dennis JW (1991) N-linked oligosaccharide processing and tumor cell biology. Semin Cancer Biol 2:411–420

54. Doktorova M, Symons JL, Zhang X, et al (2023) Cell Membranes Sustain Phospholipid Imbalance Via Cholesterol Asymmetry. 2023.07.30.551157

55. Marques EF, Silva BFB (2013) Surfactant Self-Assembly. In: Tadros T (ed) Encyclopedia of Colloid and Interface Science. Springer, Berlin, Heidelberg, pp 1202–1241

56. Findenegg GH (1986) J. N. Israelachvili: Intermolecular and Surface Forces (With Applications to Colloidal and Biological Systems). Academic Press, London, Berichte Bunsenges Für Phys Chem 90:1241–1242. https://doi.org/10.1002/bbpc.19860901226

57. Huang Y, Gui S (2018) Factors affecting the structure of lyotropic liquid crystals and the correlation between structure and drug diffusion. RSC Adv 8:6978–6987. https://doi.org/10.1039/C7RA12008G

58. Kumar VV (1991) Complementary molecular shapes and additivity of the packing parameter of lipids. Proc Natl Acad Sci 88:444–448. https://doi.org/10.1073/pnas.88.2.444

59. Yeagle PL (2004) The Structure of Biological Membranes. CRC Press, New York , https://doi.org/10.1201/9781420040203rk,

60. Liu YJ, McIntyre RL, Janssens GE, Houtkooper RH (2020) Mitochondrial fission and fusion: A dynamic role in aging and potential target for age-related disease. Mech Ageing Dev 186:111212. https://doi.org/10.1016/j.mad.2020.111212

61. Nagle JF, Tristram-Nagle S (2000) Structure of lipid bilayers. Biochim Biophys Acta 1469:159–195

62. Lewis RNAH, McElhaney RN (2012) The mesomorphic phase behavior of lipid bilayers. In: Yeagle, P. L. (Ed.), The Structure of Biological Membranes, 3rd ed., CRC Press, New York, pp. 23–26

63. Pabst G, Amenitsch H, Kharakoz DP, et al (2004) Structure and fluctuations of phosphatidylcholines in the vicinity of the main phase transition. Phys Rev E 70:021908. https://doi.org/10.1103/PhysRevE.70.021908

64. Quinn PJ, Wolf C (2009) The liquid-ordered phase in membranes. Biochim Biophys Acta BBA - Biomembr 1788:33–46. https://doi.org/10.1016/j.bbamem.2008.08.005

65. M'Baye G, Mély Y, Duportail G, Klymchenko AS (2008) Liquid Ordered and Gel Phases of Lipid Bilayers: Fluorescent Probes Reveal Close Fluidity but Different Hydration. Biophys J 95:1217–1225. https://doi.org/10.1529/biophysj.107.127480

66. van Meer G, Voelker DR, Feigenson GW (2008) Membrane lipids: where they are and how they behave. Nat Rev Mol Cell Biol 9:112

67. Fadeel B, Xue D (2009) The ins and outs of phospholipid asymmetry in the plasma membrane: roles in health and disease. Crit Rev Biochem Mol Biol 44:264–277. https://doi.org/10.1080/10409230903193307

68. Davies K, Meimaridou E (2020) Biological basis of child health 1: understanding the cell and genetics. Nurs Child Young People 32:. https://doi.org/10.7748/ncyp.2020.e1047

69. Nicolson GL (2014) The Fluid—Mosaic Model of Membrane Structure: Still relevant to understanding the structure, function and dynamics of biological membranes after more than 40years. Biochim Biophys Acta BBA - Biomembr 1838:1451–1466. https://doi.org/10.1016/j.bbamem.2013.10.019

70. Berg JM, Tymoczko JL, Stryer L (2002) Lipids and Many Membrane Proteins Diffuse Rapidly in the Plane of the Membrane. Biochem 5th Ed

71. Sakuragi T, Nagata S (2023) Regulation of phospholipid distribution in the lipid bilayer by flippases and scramblases. Nat Rev Mol Cell Biol 24:576–596. https://doi.org/10.1038/s41580-023-00604-z

72. Morizono K, Chen ISY (2014) Role of Phosphatidylserine Receptors in Enveloped Virus Infection. J Virol 88:4275–4290. https://doi.org/10.1128/JVI.03287-13

73. Beales PA, Ciani B, Cleasby AJ (2015) Nature's lessons in design: nanomachines to scaffold, remodel and shape membrane compartments. Phys Chem Chem Phys 17:15489–15507. https://doi.org/10.1039/C5CP00480B

74. Campelo F, Arnarez C, Marrink SJ, Kozlov MM (2014) Helfrich model of membrane bending: From Gibbs theory of liquid interfaces to membranes as thick anisotropic elastic layers. Adv Colloid Interface Sci 208:25–33. https://doi.org/10.1016/j.cis.2014.01.018

75. Janmey PA, Kinnunen PKJ (2006) Biophysical properties of lipids and dynamic membranes. Trends Cell Biol 16:538–546. https://doi.org/10.1016/j.tcb.2006.08.009

76. Chan Y-HM, Boxer SG (2007) Model membrane systems and their applications. Curr Opin Chem Biol 11:581–587. https://doi.org/10.1016/j.cbpa.2007.09.020

77. Bangham AD (1983) Introduction," Liposomes: An Historical Perspective,". Liposomes Ostro MJ Ed 1–25

78. Gregoriadis G (1991) Overview of liposomes. J Antimicrob Chemother 28:39–48. https://doi.org/10.1093/jac/28.suppl_B.39

79. Mui B, Chow L, Hope MJ (2003) Extrusion technique to generate liposomes of defined size. Methods Enzymol 367:3–14. https://doi.org/10.1016/S0076-6879(03)67001-1

80. Angelova MI, Soléau S, Méléard Ph, et al (1992) Preparation of giant vesicles by external AC electric fields. Kinetics and applications. In: Helm C, Lösche M, Möhwald H (eds) Trends in Colloid and Interface Science VI. Steinkopff, pp 127–131

81. Wesołowska O, Michalak K, Maniewska J, Hendrich AB (2009) Giant unilamellar vesicles - a perfect tool to visualize phase separation and lipid rafts in model systems. Acta Biochim Pol 56:33–39

82. Witkowska A, Jablonski L, Jahn R (2018) A convenient protocol for generating giant unilamellar vesicles containing SNARE proteins using electroformation. Sci Rep 8:9422. https://doi.org/10.1038/s41598-018-27456-4

83. Akbarzadeh A, Rezaei-Sadabady R, Davaran S, et al (2013) Liposome: classification, preparation, and applications. Nanoscale Res Lett 8:102. https://doi.org/10.1186/1556-276X-8-102

84. Sezgin E, Kaiser H-J, Baumgart T, et al (2012) Elucidating membrane structure and protein behavior using giant plasma membrane vesicles. Nat Protoc 7:1042–1051. https://doi.org/10.1038/nprot.2012.059

85. Scott RE (1976) Plasma membrane vesiculation: a new technique for isolation of plasma membranes. Science 194:743–745. https://doi.org/10.1126/science.982044

86. Scott RE, Maercklein PB (1979) Plasma membrane vesiculation in 3T3 and SV3T3 cells. II. Factors affecting the process of vesiculation. J Cell Sci 35:245–252

87. Charras GT, Coughlin M, Mitchison TJ, Mahadevan L (2008) Life and Times of a Cellular Bleb. Biophys J 94:1836–1853. https://doi.org/10.1529/biophysj.107.113605

88. Gericke A, Leslie NR, Lösche M, Ross AH (2013) PI(4,5)P2-Mediated Cell Signaling: Emerging Principles and PTEN as a Paradigm for Regulatory Mechanism. Adv Exp Med Biol 991:85–104. https://doi.org/10.1007/978-94-007-6331-9_6

89. Säälik P, Niinep A, Pae J, et al (2011) Penetration without cells: Membrane translocation of cell-penetrating peptides in the model giant plasma membrane vesicles. J Controlled Release 153:117–125. https://doi.org/10.1016/j.jconrel.2011.03.011

90. Levental I, Grzybek M, Simons K (2011) Raft domains of variable properties and compositions in plasma membrane vesicles. Proc Natl Acad Sci 108:11411. https://doi.org/10.1073/pnas.1105996108

91. Skinkle A, Levental I (2019) Cell-derived plasma membrane vesicles are permeable to hydrophilic macromolecules. Biophysics J118(6):1292-1300. https://doi.org/ 10.1016/j.bpj.2019.12.040

92. Tan SY, Tatsumura Y (2015) Alexander Fleming (1881–1955): Discoverer of penicillin. Singapore Med J 56:366–367. https://doi.org/10.11622/smedj.2015105

93. Papo N, Shai Y (2003) Can we predict biological activity of antimicrobial peptides from their interactions with model phospholipid membranes? Antimicrob Pept II 24:1693–1703. https://doi.org/10.1016/j.peptides.2003.09.013

94. Riedl S, Zweytick D, Lohner K (2011) Membrane-active host defense peptides – Challenges and perspectives for the development of novel anticancer drugs. Chem Phys Lipids 164:766–781. https://doi.org/10.1016/j.chemphyslip.2011.09.004

95. Bradshaw JP (2003) Cationic Antimicrobial Peptides. BioDrugs 17:233–240. https://doi.org/10.2165/00063030-200317040-00002

96. Groenink J, Walgreen-Weterings E, Hof W van 't, et al (1999) Cationic amphipathic peptides, derived from bovine and human lactoferrins, with antimicrobial activity against oral pathogens. FEMS Microbiol Lett 179:217–222. https://doi.org/10.1111/j.1574-6968.1999.tb08730.x

97. Huang Y, Huang J, Chen Y (2010) Alpha-helical cationic antimicrobial peptides: relationships of structure and function. Protein Cell 1:143–152. https://doi.org/10.1007/s13238-010-0004-3

98. Andreu D, Rivas L (1998) Animal antimicrobial peptides: An overview. Pept Sci 47:415–433. https://doi.org/10.1002/(SICI)1097-0282(1998)47:6%3C415::AID-BIP2%3E3.0.CO;2-D

99. Hancock REW, Lehrer R (1998) Cationic peptides: a new source of antibiotics. Trends Biotechnol 16:82–88. https://doi.org/10.1016/S0167-7799(97)01156-6

100. Novel alternatives to antibiotics: bacteriophages, bacterial cell wall hydrolases, and antimicrobial peptides - Parisien - 2008 - Journal of Applied Microbiology - Wiley Online Library. https://onlinelibrary.wiley.com/doi/full/10.1111/j.1365-2672.2007.03498.x. Accessed 13 Aug 2019

101. Burkhart BM, Gassman RM, Langs DA, et al (1998) Heterodimer formation and crystal nucleation of gramicidin D. Biophys J 75:2135–2146. https://doi.org/10.1016/S0006-3495(98)77656-8

102. Gause GF, Brazhnikova MG (1944) Gramicidin S and its use in the Treatment of Infected Wounds. Nature 154:703–703. https://doi.org/10.1038/154703a0

103. Llamas-Saiz AL, Grotenbreg GM, Overhand M, van Raaij MJ (2007) Double-stranded helical twisted β-sheet channels in crystals of gramicidin S grown in the presence of trifluoroacetic and hydrochloric acids. Acta Crystallogr D Biol Crystallogr 63:401–407. https://doi.org/10.1107/S0907444906056435

104. Peschel A, Sahl H-G (2006) The co-evolution of host cationic antimicrobial peptides and microbial resistance. Nat Rev Microbiol 4:529–536. https://doi.org/10.1038/nrmicro1441

105. Hansen PR (2017) Antimicrobial Peptides: Methods and Protocols. Humana Presshttps://doi.org/10.1007/978-1-4939-6737-7

106. Kumar P, Kizhakkedathu JN, Straus SK (2018) Antimicrobial Peptides: Diversity, Mechanism of Action and Strategies to Improve the Activity and Biocompatibility In Vivo. Biomolecules 8:. https://doi.org/10.3390/biom8010004

107. Bahar AA, Ren D (2013) Antimicrobial Peptides. Pharmaceuticals 6:1543–1575. https://doi.org/10.3390/ph6121543

108. Wimley WC, White SH (1996) Experimentally determined hydrophobicity scale for proteins at membrane interfaces. Nat Struct Biol 3:842–848. https://doi.org/10.1038/nsb1096-842

109. Lam NH, Ma Z, Ha B-Y (2014) Electrostatic modification of the lipopolysaccharide layer: competing effects of divalent cations and polycationic or polyanionic molecules. Soft Matter 10:7528–7544. https://doi.org/10.1039/C4SM01262C

110. Wishart DS, Knox C, Guo AC, et al (2008) DrugBank: a knowledgebase for drugs, drug actions and drug targets. Nucleic Acids Res 36:D901–D906. https://doi.org/10.1093/nar/gkm958

111. Katsu T, Kobayashi H, Fujita Y (1986) Mode of action of gramicidin S on *Escherichia coli* membrane. Biochim Biophys Acta BBA - Biomembr 860:608–619. https://doi.org/10.1016/0005-2736(86)90560-2

112. Kobayashi S, Chikushi A, Tougu S, et al (2004) Membrane translocation mechanism of the antimicrobial peptide buforin 2. Biochemistry 43:15610–15616. https://doi.org/10.1021/bi048206q

113. Bierbaum G, Sahl HG (1987) Autolytic system of Staphylococcus simulans 22: influence of cationic peptides on activity of N-acetylmuramoyl-L-alanine amidase. J Bacteriol 169:5452–5458

114. Breukink E, Wiedemann I, van Kraaij C, et al (1999) Use of the cell wall precursor lipid II by a pore-forming peptide antibiotic. Science 286:2361–2364. https://doi.org/10.1126/science.286.5448.2361

115. Lee C-C, Sun Y, Qian S, Huang HW (2011) Transmembrane Pores Formed by Human Antimicrobial Peptide LL-37. Biophys J 100:1688–1696. https://doi.org/10.1016/j.bpj.2011.02.018

116. Wang K, Zhang B, Zhang W, et al (2008) Antitumor effects, cell selectivity and structure–activity relationship of a novel antimicrobial peptide polybia-MPI. Peptides 29:963–968. https://doi.org/10.1016/j.peptides.2008.01.015

117. Alvares DS, Ruggiero Neto J, Ambroggio EE (2017) Phosphatidylserine lipids and membrane order precisely regulate the activity of Polybia-MP1 peptide. Biochim Biophys Acta BBA - Biomembr 1859:1067–1074. https://doi.org/10.1016/j.bbamem.2017.03.002

118. Bueno Leite N, Aufderhorst-Roberts A, Sergio Palma M, et al (2015) PE and PS Lipids Synergistically Enhance Membrane Poration by a Peptide with Anticancer Properties - ScienceDirect. https://www.sciencedirect.com/science/article/pii/S0006349515007687. Accessed 27 Aug 2019

119. Rossi LM, Rangasamy P, Zhang J, et al (2008) Research advances in the development of peptide antibiotics. J Pharm Sci 97:1060–1070. https://doi.org/10.1002/jps.21053

120. Pahar B, Madonna S, Das A, et al (2020) Immunomodulatory Role of the Antimicrobial LL-37 Peptide in Autoimmune Diseases and Viral Infections. Vaccines 8:517. https://doi.org/10.3390/vaccines8030517

121. Bowdish DME, Davidson DJ, Lau YE, et al (2005) Impact of LL-37 on anti-infective immunity. J Leukoc Biol 77:451–459. https://doi.org/10.1189/jlb.0704380

122. Zanetti M (2004) Cathelicidins, multifunctional peptides of the innate immunity. J Leukoc Biol 75:39–48. https://doi.org/10.1189/jlb.0403147

123. Hancock REW, Sahl H-G (2006) Antimicrobial and host-defense peptides as new anti-infective therapeutic strategies. Nat Biotechnol 24:1551–1557. https://doi.org/10.1038/nbt1267

124. Yang D, Chertov O, Oppenheim JJ (2001) Participation of mammalian defensins and cathelicidins in anti-microbial immunity: receptors and activities of human defensins and cathelicidin (LL-37). J Leukoc Biol 69:691–697. https://doi.org/10.1189/jlb.69.5.691

125. Davidson DJ, Currie AJ, Reid GSD, et al (2004) The cationic antimicrobial peptide LL-37 modulates dendritic cell differentiation and dendritic cell-induced T cell polarization. J Immunol Baltim Md 1950 172:1146–1156. https://doi.org/10.4049/jimmunol.172.2.1146

126. van der Does AM, Beekhuizen H, Ravensbergen B, et al (2010) LL-37 directs macrophage differentiation toward macrophages with a proinflammatory signature. J Immunol Baltim Md 1950 185:1442–1449. https://doi.org/10.4049/jimmunol.1000376

127. Liang W, Diana J (2020) The Dual Role of Antimicrobial Peptides in Autoimmunity. Front Immunol 11:

128. Zhang C, Yang M (2020) The Role and Potential Application of Antimicrobial Peptides in Autoimmune Diseases. Front Immunol 11:859. https://doi.org/10.3389/fimmu.2020.00859

129. Patrulea V, Borchard G, Jordan O (2020) An Update on Antimicrobial Peptides (AMPs) and Their Delivery Strategies for Wound Infections. Pharmaceutics 12:E840. https://doi.org/10.3390/pharmaceutics12090840

130. Koczulla R, von Degenfeld G, Kupatt C, et al (2003) An angiogenic role for the human peptide antibiotic LL-37/hCAP-18. J Clin Invest 111:1665–1672. https://doi.org/10.1172/JCI200317545

131. Niyonsaba F, Ushio H, Nakano N, et al (2007) Antimicrobial peptides human beta-defensins stimulate epidermal keratinocyte migration, proliferation and production of proinflammatory cytokines and chemokines. J Invest Dermatol 127:594–604. https://doi.org/10.1038/sj.jid.5700599

132. Kolar SS, McDermott AM (2011) Role of Host-Defence Peptides in Eye Diseases. Cell Mol Life Sci CMLS 68:2201–2213. https://doi.org/10.1007/s00018-011-0713-7

133. Di Meglio P, Perera GK, Nestle FO (2011) The multitasking organ: recent insights into skin immune function. Immunity 35:857–869. https://doi.org/10.1016/j.immuni.2011.12.003

134. Rosenfeld Y, Shai Y (2006) Lipopolysaccharide (Endotoxin)-host defense antibacterial peptides interactions: Role in bacterial resistance and prevention of sepsis. Biochim Biophys Acta BBA - Biomembr 1758:1513–1522. https://doi.org/10.1016/j.bbamem.2006.05.017

135. Arnold M, Karim-Kos HE, Coebergh JW, et al (2015) Recent trends in incidence of five common cancers in 26 European countries since 1988: Analysis of the European Cancer Observatory. Eur J Cancer Oxf Engl 1990 51:1164–1187. https://doi.org/10.1016/j.ejca.2013.09.002

136. Mansoori B, Mohammadi A, Davudian S, et al (2017) The Different Mechanisms of Cancer Drug Resistance: A Brief Review. Adv Pharm Bull 7:339–348. https://doi.org/10.15171/apb.2017.041

137. Desai T, Toombs J, Minna J, et al (2016) Identification of lipid-phosphatidylserine (PS) as the target of unbiasedly selected cancer specific peptide-peptoid hybrid PPS1. Oncotarget 7:. https://doi.org/10.18632/oncotarget.8929

138. Fei W, Yan J, Wu X, et al (2023) Perturbing plasma membrane lipid: a new paradigm for tumor nanotherapeutics. Theranostics 13:2471–2491. https://doi.org/10.7150/thno.82189

139. Hancock REW, Haney EF, Gill EE (2016) The immunology of host defence peptides: beyond antimicrobial activity. Nat Rev Immunol 16:321–334. https://doi.org/10.1038/nri.2016.29

140. Fink SL, Cookson BT (2005) Apoptosis, Pyroptosis, and Necrosis: Mechanistic Description of Dead and Dying Eukaryotic Cells. Infect Immun 73:1907–1916. https://doi.org/10.1128/IAI.73.4.1907-1916.2005

141. Wu D, Gao Y, Qi Y, et al (2014) Peptide-based cancer therapy: Opportunity and challenge. Cancer Lett 351:13–22. https://doi.org/10.1016/j.canlet.2014.05.002

142. Ma R, Wong SW, Ge L, et al (2020) In Vitro and MD Simulation Study to Explore Physicochemical Parameters for Antibacterial Peptide to Become Potent Anticancer Peptide. Mol Ther Oncolytics 16:7–19. https://doi.org/10.1016/j.omto.2019.12.001

143. Raman K, Kuberan B (2010) Chemical Tumor Biology of Heparan Sulfate Proteoglycans. Curr Chem Biol 4:20–31. https://doi.org/10.2174/187231310790226206

144. Furlong SJ, Mader JS, Hoskin DW (2006) Lactoferricin-induced apoptosis in estrogen-nonresponsive MDA-MB-435 breast cancer cells is enhanced by C6 ceramide or tamoxifen. Oncol Rep 15:1385–1390

145. Anghel R, Jitaru D, Bădescu L, et al (2013) The Cytotoxic Effect of Magainin II on the MDA-MB-231 and M14K Tumour Cell Lines. BioMed Res Int 2013:831709. https://doi.org/10.1155/2013/831709

146. Huang W, Seo J, Willingham SB, et al (2014) Learning from Host-Defense Peptides: Cationic, Amphipathic Peptoids with Potent Anticancer Activity. PLoS ONE 9:e90397. https://doi.org/10.1371/journal.pone.0090397

147. Prabha N, Sannasimuthu A, Kumaresan V, et al (2020) Intensifying the Anticancer Potential of Cationic Peptide Derived from Serine Threonine Protein Kinase of Teleost by Tagging with Oligo Tryptophan. Int J Pept Res Ther 26:75–83. https://doi.org/10.1007/s10989-019-09817-3

148. Lehmann J, Retz M, Sidhu SS, et al (2006) Antitumor activity of the antimicrobial peptide magainin II against bladder cancer cell lines. Eur Urol 50:141–147. https://doi.org/10.1016/j.eururo.2005.12.043

149. Norouzi Z, Salimi A, Halabian R, Fahimi H (2018) Nisin, a potent bacteriocin and anti-bacterial peptide, attenuates expression of metastatic genes in colorectal cancer cell lines. Microb Pathog 123:183–189. https://doi.org/10.1016/j.micpath.2018.07.006

150. Hilchie AL, Doucette CD, Pinto DM, et al (2011) Pleurocidin-family cationic antimicrobial peptides are cytolytic for breast carcinoma cells and prevent growth of tumor xenografts. Breast Cancer Res BCR 13:R102. https://doi.org/10.1186/bcr3043

151. Avand A, Akbari V, Shafizadegan S (2018) In Vitro Cytotoxic Activity of a Lactococcus lactis Antimicrobial Peptide Against Breast Cancer Cells. Iran J Biotechnol 16:e1867. https://doi.org/10.15171/ijb.1867

152. Souza BM, Mendes MA, Santos LD, et al (2005) Structural and functional characterization of two novel peptide toxins isolated from the venom of the social wasp Polybia paulista. Peptides 26:2157–2164. https://doi.org/10.1016/j.peptides.2005.04.026

153. Mai-Prochnow A, Clauson M, Hong J, Murphy AB (2016) Gram positive and Gram negative bacteria differ in their sensitivity to cold plasma. Sci Rep 6:38610. https://doi.org/10.1038/srep38610

154. dos Santos Cabrera MP, Arcisio-Miranda M, Gorjão R, et al (2012) Influence of the Bilayer Composition on the Binding and Membrane Disrupting Effect of Polybia-MP1, an Antimicrobial Mastoparan Peptide with Leukemic T-Lymphocyte Cell Selectivity. Biochemistry 51:4898–4908. https://doi.org/10.1021/bi201608d

155. Wang K, Yan J, Zhang B, et al (2009) Novel mode of action of polybia-MPI, a novel antimicrobial peptide, in multi-drug resistant leukemic cells. Cancer Lett 278:65–72. https://doi.org/10.1016/j.canlet.2008.12.027

156. Li G, Lei Q, Wang F, et al (2019) Fluorinated Polymer Mediated Transmucosal Peptide Delivery for Intravesical Instillation Therapy of Bladder Cancer. Small Weinh Bergstr Ger 15:e1900936. https://doi.org/10.1002/smll.201900936

157. Wang K, Yan J, Dang W, et al (2014) Dual antifungal properties of cationic antimicrobial peptides polybia-MPI: membrane integrity disruption and inhibition

of biofilm formation. Peptides 56:22–29. https://doi.org/10.1016/j.peptides.2014.03.005

158. dos Santos Cabrera MP, Costa STB, de Souza BM, et al (2008) Selectivity in the mechanism of action of antimicrobial mastoparan peptide Polybia-MP1. Eur Biophys J 37:879–891. https://doi.org/10.1007/s00249-008-0299-7

159. Alvares DS, Fanani ML, Ruggiero Neto J, Wilke N (2016) The interfacial properties of the peptide Polybia-MP1 and its interaction with DPPC are modulated by lateral electrostatic attractions. Biochim Biophys Acta BBA - Biomembr 1858:393–402. https://doi.org/10.1016/j.bbamem.2015.12.010

160. Zhao Y, Zhang M, Qiu S, et al (2016) Antimicrobial activity and stability of the D-amino acid substituted derivatives of antimicrobial peptide polybia-MPI. AMB Express 6:122. https://doi.org/10.1186/s13568-016-0295-8

161. Luong HX, Kim D-H, Lee B-J, Kim Y-W (2017) Antimicrobial activity and stability of stapled helices of polybia-MP1. Arch Pharm Res 40:1414–1419. https://doi.org/10.1007/s12272-017-0963-5

162. Alvares DS, Monti MR, Ruggiero Neto J, Wilke N (2021) The antimicrobial peptide Polybia-MP1 differentiates membranes with the hopanoid, diplopterol from those with cholesterol. BBA Adv 1:100002. https://doi.org/10.1016/j.bbadva.2021.100002

163. Hilchie AL, Sharon AJ, Haney EF, et al (2016) Mastoparan is a membranolytic anti-cancer peptide that works synergistically with gemcitabine in a mouse model of mammary carcinoma. Biochim Biophys Acta BBA - Biomembr 1858:3195–3204. https://doi.org/10.1016/j.bbamem.2016.09.021

164. de la Fuente-Núñez C, Silva ON, Lu TK, Franco OL (2017) Antimicrobial peptides: Role in human disease and potential as immunotherapies. Pharmacol Ther 178:132–140. https://doi.org/10.1016/j.pharmthera.2017.04.002

165. Björn C, Noppa L, Näslund Salomonsson E, et al (2015) Efficacy and safety profile of the novel antimicrobial peptide PXL150 in a mouse model of infected burn wounds. Int J Antimicrob Agents 45:519–524. https://doi.org/10.1016/j.ijantimicag.2014.12.015

166. Khan SA, Lee C-S (2020) Recent progress and strategies to develop antimicrobial contact lenses and lens cases for different types of microbial keratitis. Acta Biomater 113:101–118. https://doi.org/10.1016/j.actbio.2020.06.039

167. Wilkinson L, Gathani T (2022) Understanding breast cancer as a global health concern. Br J Radiol 95:20211033. https://doi.org/10.1259/bjr.20211033

168. Nascimento RGD, Otoni KM (2020) Histological and molecular classification of breast cancer: what do we know? Mastology 30:e20200024. https://doi.org/10.29289/25945394202020200024

169. van den Boogaard WMC, Komninos DSJ, Vermeij WP (2022) Chemotherapy Side-Effects: Not All DNA Damage Is Equal. Cancers 14:627. https://doi.org/10.3390/cancers14030627

170. Wang C, Tian L-L, Li S, et al (2013) Rapid Cytotoxicity of Antimicrobial Peptide Tempoprin-1CEa in Breast Cancer Cells through Membrane Destruction and Intracellular Calcium Mechanism. PLOS ONE 8:e60462. https://doi.org/10.1371/journal.pone.0060462

171. He M, Guo S, Li Z (2015) In situ characterizing membrane lipid phenotype of breast cancer cells using mass spectrometry profiling. Sci Rep 5:11298. https://doi.org/10.1038/srep11298

172. Hancock REW, Scott MG (2000) The role of antimicrobial peptides in animal defenses. Proc Natl Acad Sci U S A 97:8856–8861

173. Tossi A, Sandri L, Giangaspero A (2000) Amphipathic, α-helical antimicrobial peptides. Pept Sci 55:4–30. https://doi.org/10.1002/1097-0282(2000)55:1

174. Hong SY, Park TG, Lee K-H (2001) The effect of charge increase on the specificity and activity of a short antimicrobial peptide. Peptides 22:1669–1674. https://doi.org/10.1016/S0196-9781(01)00502-2

175. Dathe M, Nikolenko H, Meyer J, et al (2001) Optimization of the antimicrobial activity of magainin peptides by modification of charge. FEBS Lett 501:146–150. https://doi.org/10.1016/S0014-5793(01)02648-5

176. Tossi A, Scocchi M, Skerlavaj B, Gennaro R (1994) Identification and characterization of a primary antibacterial domain in CAP18, a lipopolysaccharide binding protein from rabbit leukocytes. FEBS Lett 339:108–112. https://doi.org/10.1016/0014-5793(94)80395-1

177. Pasupuleti M, Schmidtchen A, Malmsten M (2012) Antimicrobial peptides: key components of the innate immune system. Crit Rev Biotechnol 32:143–171. https://doi.org/10.3109/07388551.2011.594423

178. Unger T, Oren Z, Shai Y (2001) The Effect of Cyclization of Magainin 2 and Melittin Analogues on Structure, Function, and Model Membrane Interactions: Implication to Their Mode of Action. Biochemistry 40:6388–6397. https://doi.org/10.1021/bi0026066

179. Chen F, He ZH, Xia XC, et al (2006) Molecular and biochemical characterization of puroindoline a and b alleles in Chinese landraces and historical cultivars. TAG Theor Appl Genet Theor Angew Genet 112:400–409. https://doi.org/10.1007/s00122-005-0095-z

180. Papo N, Oren Z, Pag U, et al (2002) The consequence of sequence alteration of an amphipathic alpha-helical antimicrobial peptide and its diastereomers. J Biol Chem 277:33913–33921. https://doi.org/10.1074/jbc.M204928200

181. Powers J-PS, Hancock REW (2003) The relationship between peptide structure and antibacterial activity. Peptides 24:1681–1691. https://doi.org/10.1016/j.peptides.2003.08.023

182. Chen Y, Guarnieri MT, Vasil AI, et al (2007) Role of Peptide Hydrophobicity in the Mechanism of Action of α-Helical Antimicrobial Peptides. Antimicrob Agents Chemother 51:1398–1406. https://doi.org/10.1128/AAC.00925-06

183. Yount NY, Bayer AS, Xiong YQ, Yeaman MR (2006) Advances in antimicrobial peptide immunobiology. Biopolymers 84:435–458. https://doi.org/10.1002/bip.20543

184. Dennison SR, Wallace J, Harris F, Phoenix DA (2005) Amphiphilic alpha-helical antimicrobial peptides and their structure/function relationships. Protein Pept Lett 12:31–39. https://doi.org/10.2174/0929866053406084

185. Yin LM, Edwards MA, Li J, et al (2012) Roles of Hydrophobicity and Charge Distribution of Cationic Antimicrobial Peptides in Peptide-Membrane Interactions. J Biol Chem 287:7738–7745. https://doi.org/10.1074/jbc.M111.303602

186. Nguyen LT, Haney EF, Vogel HJ (2011) The expanding scope of antimicrobial peptide structures and their modes of action. Trends Biotechnol 29:464–472. https://doi.org/10.1016/j.tibtech.2011.05.001

187. Giangaspero A, Sandri L, Tossi A (2001) Amphipathic alpha helical antimicrobial peptides. Eur J Biochem 268:5589–5600. https://doi.org/10.1046/j.1432-1033.2001.02494.x

188. Fernández-Vidal M, Jayasinghe S, Ladokhin AS, White SH (2007) Folding amphipathic helices into membranes: amphiphilicity trumps hydrophobicity. J Mol Biol 370:459–470. https://doi.org/10.1016/j.jmb.2007.05.016

189. Liu Z, Brady A, Young A, et al (2007) Length Effects in Antimicrobial Peptides of the (RW)n Series. Antimicrob Agents Chemother 51:597–603. https://doi.org/10.1128/AAC.00828-06

190. Guzmán F, Marshall S, Ojeda C, et al (2013) Inhibitory effect of short cationic homopeptides against gram-positive bacteria. J Pept Sci Off Publ Eur Pept Soc 19:792–800. https://doi.org/10.1002/psc.2578

191. Fidai S, Farmer SW, Hancock REW (1997) Interaction of Cationic Peptides with Bacterial Membranes. In: Shafer WM (ed) Antibacterial Peptide Protocols. Humana Press, Totowa, NJ, pp 187–204

192. Shagaghi N, Palombo E, Clayton A, Bhave M (2018) Antimicrobial peptides: biochemical determinants of activity and biophysical techniques of elucidating their functionality. World J Microbiol Biotechnol 34:. https://doi.org/10.1007/s11274-018-2444-5

193. Sajjadiyan Z, Cheraghi N, Mohammadinejad S, Hassani L (2017) Interaction of aurein 1.2 and its analogue with DPPC lipid bilayer. J Biol Phys 43:127–137. https://doi.org/10.1007/s10867-016-9438-z

194. Fjell CD, Hiss JA, Hancock REW, Schneider G (2011) Designing antimicrobial peptides: form follows function. Nat Rev Drug Discov 11:37–51. https://doi.org/10.1038/nrd3591

195. Zhong C, Zhu N, Zhu Y, et al (2020) Antimicrobial peptides conjugated with fatty acids on the side chain of D-amino acid promises antimicrobial potency against multidrug-resistant bacteria. Eur J Pharm Sci Off J Eur Fed Pharm Sci 141:105123. https://doi.org/10.1016/j.ejps.2019.105123

196. Otero-Albiol D, Carnero A (2021) Cellular senescence or stemness: hypoxia flips the coin. J Exp Clin Cancer Res 40:243. https://doi.org/10.1186/s13046-021-02035-0

197. Donohoe DR, Collins LB, Wali A, et al (2012) The Warburg Effect Dictates the Mechanism of Butyrate Mediated Histone Acetylation and Cell Proliferation. Mol Cell 48:612–626. https://doi.org/10.1016/j.molcel.2012.08.033

198. Geng H-W, Yin F-Y, Zhang Z-F, et al (2021) Butyrate Suppresses Glucose Metabolism of Colorectal Cancer Cells via GPR109a-AKT Signaling Pathway and Enhances Chemotherapy. Front Mol Biosci 8:634874. https://doi.org/10.3389/fmolb.2021.634874

199. Chang L, Wu X, Ran K, et al (2023) One New Acid-Activated Hybrid Anticancer Peptide by Coupling with a Desirable pH-Sensitive Anionic Partner Peptide. ACS Omega 8:7536–7545. https://doi.org/10.1021/acsomega.2c06766

200. Makovitzki A, Fink A, Shai Y (2009) Suppression of human solid tumor growth in mice by intratumor and systemic inoculation of histidine-rich and pH-dependent host defense-like lytic peptides. Cancer Res 69:3458–3463. https://doi.org/10.1158/0008-5472.CAN-08-3021

201. Zwaal RFA, Comfurius P, Bevers EM (2005) Surface exposure of phosphatidylserine in pathological cells. Cell Mol Life Sci CMLS 62:971–988. https://doi.org/10.1007/s00018-005-4527-3

202. Vallabhapurapu SD, Blanco VM, Sulaiman MK, et al (2015) Variation in human cancer cell external phosphatidylserine is regulated by flippase activity and intracellular calcium. Oncotarget 6:34375–34388

203. Matsuzaki K (2009) Control of cell selectivity of antimicrobial peptides. Biochim Biophys Acta BBA - Biomembr 1788:1687–1692. https://doi.org/10.1016/j.bbamem.2008.09.013

204. von Deuster CIE, Knecht V (2012) Antimicrobial selectivity based on zwitterionic lipids and underlying balance of interactions. Biochim Biophys Acta BBA - Biomembr 1818:2192–2201. https://doi.org/10.1016/j.bbamem.2012.05.012

205. Schmidt NW, Wong GCL (2013) Antimicrobial peptides and induced membrane curvature: geometry, coordination chemistry, and molecular engineering. Curr Opin Solid State Mater Sci 17:151–163. https://doi.org/10.1016/j.cossms.2013.09.004

206. Rausch JM, Wimley WC (2001) A High-Throughput Screen for Identifying Transmembrane Pore-Forming Peptides. Anal Biochem 293:258–263. https://doi.org/10.1006/abio.2001.5137

207. Palacios-Ortega J, Rivera-de-Torre E, Gavilanes JG, et al (2020) Evaluation of different approaches used to study membrane permeabilization by actinoporins on model lipid vesicles. Biochim Biophys Acta BBA - Biomembr 1862:183311. https://doi.org/10.1016/j.bbamem.2020.183311

208. Krauson AJ, He J, Wimley WC (2012) Determining the mechanism of membrane permeabilizing peptides: Identification of potent, equilibrium pore-formers. Biochim Biophys Acta 1818:10.1016/j.bbamem.2012.02.009. https://doi.org/10.1016/j.bbamem.2012.02.009

209. Al Nahas K, Fletcher M, Hammond K, et al (2022) Measuring Thousands of Single-Vesicle Leakage Events Reveals the Mode of Action of Antimicrobial Peptides. Anal Chem 94:9530–9539. https://doi.org/10.1021/acs.analchem.1c03564

210. Ventura R, Martínez-Ruiz I, Hernández-Alvarez MI (2022) Phospholipid Membrane Transport and Associated Diseases. Biomedicines 10:1201. https://doi.org/10.3390/biomedicines10051201

211. King EJ (1932) The colorimetric determination of phosphorus. Biochem J 26:292–297

212. Weinstein JN, Blumenthal R, Klausner RD (1986) Carboxyfluorescein leakage assay for lipoprotein-liposome interaction. In: Methods in Enzymology. Elsevier, pp 657–668

213. Morrison KL, Weiss GA (2001) Combinatorial alanine-scanning. Curr Opin Chem Biol 5:302–307. https://doi.org/10.1016/S1367-5931(00)00206-4

214. Lee SH, Baek JH, Yoon KA (2016) Differential Properties of Venom Peptides and Proteins in Solitary vs. Social Hunting Wasps. Toxins 8:32. https://doi.org/10.3390/toxins8020032

215. Cutrona KJ, Kaufman BA, Figueroa DM, Elmore DE (2015) Role of Arginine and Lysine in the Antimicrobial Mechanism of Histone-derived Antimicrobial Peptides. FEBS Lett 589:3915–3920. https://doi.org/10.1016/j.febslet.2015.11.002

216. Yoo J, Cui Q (2010) Chemical versus mechanical perturbations on the protonation state of arginine in complex lipid membranes: insights from microscopic pKa calculations. Biophys J 99:1529–1538. https://doi.org/10.1016/j.bpj.2010.06.048

217. Gleason NJ, Vostrikov VV, Greathouse DV, Koeppe RE (2013) Buried lysine, but not arginine, titrates and alters transmembrane helix tilt. Proc Natl Acad Sci U S A 110:1692–1695. https://doi.org/10.1073/pnas.1215400110

218. Li J, Koh J-J, Liu S, et al (2017) Membrane Active Antimicrobial Peptides: Translating Mechanistic Insights to Design. Front Neurosci 11:73. https://doi.org/10.3389/fnins.2017.00073

219. Yang S-T, Shin SY, Lee CW, et al (2003) Selective cytotoxicity following Arg-to-Lys substitution in tritrpticin adopting a unique amphipathic turn structure. FEBS Lett 540:229–233. https://doi.org/10.1016/s0014-5793(03)00266-7

220. Kokona B, Rosenthal ZP, Fairman R (2014) Role of the coiled-coil structural motif in polyglutamine aggregation. Biochemistry 53:6738–6746. https://doi.org/10.1021/bi500449a

221. Fletcher JM, Bartlett GJ, Boyle AL, et al (2017) N@a and N@d: Oligomer and Partner Specification by Asparagine in Coiled-Coil Interfaces. ACS Chem Biol 12:528–538. https://doi.org/10.1021/acschembio.6b00935

222. Wang M, Wang J, Zhou P, et al (2018) Nanoribbons self-assembled from short peptides demonstrate the formation of polar zippers between β-sheets. Nat Commun 9:5118. https://doi.org/10.1038/s41467-018-07583-2

223. Shimoni L, Glusker JP (1995) Hydrogen bonding motifs of protein side chains: Descriptions of binding of arginine and amide groups: Hydrogen bonding motifs of protein side chains. Protein Sci 4:65–74. https://doi.org/10.1002/pro.5560040109

224. Thøgersen L, Schiøtt B, Vosegaard T, et al (2008) Peptide Aggregation and Pore Formation in a Lipid Bilayer: A Combined Coarse-Grained and All Atom Molecular Dynamics Study. Biophys J 95:4337–4347. https://doi.org/10.1529/biophysj.108.133330

225. Muz B, de la Puente P, Azab F, Azab AK (2015) The role of hypoxia in cancer progression, angiogenesis, metastasis, and resistance to therapy. Hypoxia 3:83–92. https://doi.org/10.2147/HP.S93413

226. Xian W, Hennefarth MR, Lee MW, et al (2022) Histidine Mediated Ion Specific Effects Enable Salt Tolerance of a Pore Forming Marine Antimicrobial Peptide. Angew Chem Int Ed Engl 61:e202108501. https://doi.org/10.1002/anie.202108501

227. Leite NB, da Costa LC, dos Santos Alvares D, et al (2011) The effect of acidic residues and amphipathicity on the lytic activities of mastoparan peptides studied by fluorescence and CD spectroscopy. Amino Acids 40:91–100. https://doi.org/10.1007/s00726-010-0511-9

228. Piek T N (1986) Pharmacological biochemistry of Vespid venom. Venom of Hymenoptera. London: Academic Press

229. Sforça ML, Oyama Sérgio, Canduri F, et al (2004) How C-Terminal Carboxyamidation Alters the Biological Activity of Peptides from the Venom of the Eumenine Solitary Wasp. Biochemistry 43:5608–5617. https://doi.org/10.1021/bi0360915

230. Marqusee S, Baldwin RL (1987) Helix stabilization by Glu-...Lys+ salt bridges in short peptides of de novo design. Proc Natl Acad Sci 84:8898–8902. https://doi.org/10.1073/pnas.84.24.8898

231. de Souza BM, da Silva AVR, Resende VMF, et al (2009) Characterization of two novel polyfunctional mastoparan peptides from the venom of the social wasp

Polybia paulista. Peptides 30:1387–1395. https://doi.org/10.1016/j.peptides.2009.05.008

232. Souza BM de [UNESP (2006) Estrutura e função de mastoparanos dos venenos de vespas. Aleph x, 143 f.

233. Taheri-Araghi S, Ha B-Y (2007) Physical Basis for Membrane-Charge Selectivity of Cationic Antimicrobial Peptides. Phys Rev Lett 98:168101. https://doi.org/10.1103/PhysRevLett.98.168101

234. Leite NB, dos Santos Alvares D, de Souza BM, et al (2014) Effect of the aspartic acid D2 on the affinity of Polybia-MP1 to anionic lipid vesicles. Eur Biophys J 43:121–130. https://doi.org/10.1007/s00249-014-0945-1

235. Huang K-Y, Tseng Y-J, Kao H-J, et al (2021) Identification of subtypes of anticancer peptides based on sequential features and physicochemical properties. Sci Rep 11:13594. https://doi.org/10.1038/s41598-021-93124-9

236. Tyagi A, Kapoor P, Kumar R, et al (2013) In Silico Models for Designing and Discovering Novel Anticancer Peptides. Sci Rep 3:2984. https://doi.org/10.1038/srep02984

237. Chakrabarti P, Chakrabarti S (1998) C--H...O hydrogen bond involving proline residues in alpha-helices. J Mol Biol 284:867–873. https://doi.org/10.1006/jmbi.1998.2199

238. Cantisani M, Finamore E, Mignogna E, et al (2014) Structural Insights into and Activity Analysis of the Antimicrobial Peptide Myxinidin. Antimicrob Agents Chemother, Sep;58(9):5280-90. https://doi.org/ 10.1128/AAC.02395-14

239. Strøm MB, Svendsen JS, Rekdal (2000) Antibacterial activity of 15-residue lactoferricin derivatives: Antibacterial lactoferricin derivatives. J Pept Res 56:265–274. https://doi.org/10.1034/j.1399-3011.2000.00770.x

240. Galdiero S, Russo L, Falanga A, et al (2012) Structure and orientation of the gH625-644 membrane interacting region of herpes simplex virus type 1 in a membrane mimetic system. Biochemistry 51:3121–3128. https://doi.org/10.1021/bi201589m

241. Khemaissa S, Walrant A, Sagan S (2022) Tryptophan, more than just an interfacial amino acid in the membrane activity of cationic cell-penetrating and antimicrobial peptides. Q Rev Biophys 55:e10. https://doi.org/10.1017/S0033583522000105

242. Al Tameemi W, Dale TP, Al-Jumaily RMK, Forsyth NR (2019) Hypoxia-Modified Cancer Cell Metabolism. Front Cell Dev Biol 7:. https://doi.org/10.3389/fcell.2019.00004

243. Justus CR, Dong L, Yang LV (2013) Acidic tumor microenvironment and pH-sensing G protein-coupled receptors. Front Physiol 4:. https://doi.org/10.3389/fphys.2013.00354

244. Hitchner MA, Santiago-Ortiz LE, Necelis MR, et al (2019) Activity and characterization of a pH-sensitive antimicrobial peptide. Biochim Biophys Acta Biomembr 1861:182984. https://doi.org/10.1016/j.bbamem.2019.05.006

245. Mihailescu M, Sorci M, Seckute J, et al (2019) Structure and Function in Antimicrobial Piscidins: Histidine Position, Directionality of Membrane Insertion, and pH-Dependent Permeabilization. J Am Chem Soc 141:9837–9853. https://doi.org/10.1021/jacs.9b00440

246. Chan Y-HM, Boxer SG (2007) Model Membrane Systems and Their Applications. Curr Opin Chem Biol 11:581–587. https://doi.org/10.1016/j.cbpa.2007.09.020

247. Litschel T, Schwille P (2021) Protein Reconstitution Inside Giant Unilamellar Vesicles. Annu Rev Biophys 50:525–548. https://doi.org/10.1146/annurev-biophys-100620-114132

248. Charras GT (2008) A short history of blebbing. J Microsc 231:466–478. https://doi.org/10.1111/j.1365-2818.2008.02059.x

249. Scott RE, Perkins RG, Zschunke MA, et al (1979) Plasma membrane vesiculation in 3T3 and SV3T3 cells. I. Morphological and biochemical characterization. J Cell Sci 35:229–243

250. Levental KR, Levental I (2015) Isolation of Giant Plasma Membrane Vesicles for Evaluation of Plasma Membrane Structure and Protein Partitioning. In: Owen DM (ed) Methods in Membrane Lipids. Springer New York, New York, NY, pp 65–77

251. Sedgwick A, Olivia Balmert M, D'Souza-Schorey C (2018) The formation of giant plasma membrane vesicles enable new insights into the regulation of cholesterol efflux. Exp Cell Res 365:194–207. https://doi.org/10.1016/j.yexcr.2018.03.001

252. Zartner L, Garni M, Craciun I, et al (2021) How Can Giant Plasma Membrane Vesicles Serve as a Cellular Model for Controlled Transfer of Nanoparticles? Biomacromolecules 22:106–115. https://doi.org/10.1021/acs.biomac.0c00624

253. Podkalicka J, Blouin CM (2020) GPMVs as a Tool to Study Caveolin-Interacting Partners. In: Blouin CM (ed) Caveolae: Methods and Protocols. Springer US, New York, NY, pp 81–88

254. Sezgin E (2022) Giant plasma membrane vesicles to study plasma membrane structure and dynamics. Biochim Biophys Acta BBA - Biomembr 1864:183857. https://doi.org/10.1016/j.bbamem.2021.183857

255. Del Piccolo N, Placone J, He L, et al (2012) Production of Plasma Membrane Vesicles with Chloride Salts and Their Utility as a Cell Membrane Mimetic for Biophysical Characterization of Membrane Protein Interactions. Anal Chem 84:8650–8655. https://doi.org/10.1021/ac301776j

256. Verghese ET, Shenoy H, Cookson VJ, et al (2011) Epithelial–mesenchymal interactions in breast cancer: evidence for a role of nuclear localized β-catenin in carcinoma-associated fibroblasts. Histopathology 59:609–618. https://doi.org/10.1111/j.1365-2559.2011.03917.x

257. Tiernan JP, Perry SL, Verghese ET, et al (2013) Carcinoembryonic antigen is the preferred biomarker for in vivo colorectal cancer targeting. Br J Cancer 108:662–667

258. Brinkman JE, Dorius B, Sharma S (2023) Physiology, Body Fluids. In: StatPearls. StatPearls Publishing, Treasure Island (FL)

259. Poolman B, Van der heide T (2003) CHAPTER 13 - STRUCTURE AND FUNCTION OF OSMOREGULATED ABC TRANSPORTERS. In: Holland IB, Cole SPC, Kuchler K, Higgins CF (eds) ABC Proteins. Academic Press, London, pp 263–275

260. Ritz S, Eisele K, Dorn J, et al (2010) Cationized albumin-biocoatings for the immobilization of lipid vesicles. Biointerphases 5:FA78–FA87. https://doi.org/10.1116/1.3494039

261. Levental I, Lingwood D, Grzybek M, et al (2010) Palmitoylation regulates raft affinity for the majority of integral raft proteins. Proc Natl Acad Sci 107:22050–22054. https://doi.org/10.1073/pnas.1016184107

262. Thone MN, Kwon YJ (2020) Extracellular blebs: Artificially-induced extracellular vesicles for facile production and clinical translation. Methods 177:135–145. https://doi.org/10.1016/j.ymeth.2019.11.007

263. Chiang P-C, Tanady K, Huang L-T, Chao L (2017) Rupturing Giant Plasma Membrane Vesicles to Form Micron-sized Supported Cell Plasma Membranes with Native Transmembrane Proteins. Sci Rep 7:15139. https://doi.org/10.1038/s41598-017-15103-3

264. Balice-Gordon RJ, Chua CK, Nelson CC, Lichtman JW (1993) Gradual loss of synaptic cartels precedes axon withdrawal at developing neuromuscular junctions. Neuron 11:801–815. https://doi.org/10.1016/0896-6273(93)90110-D

265. Sarkis J, Vié V (2020) Biomimetic Models to Investigate Membrane Biophysics Affecting Lipid–Protein Interaction. Front Bioeng Biotechnol 8:

266. Chatterjee SN, Agarwal S (1988) Liposomes as membrane model for study of lipid peroxidation. Free Radic Biol Med 4:51–72. https://doi.org/10.1016/0891-5849(88)90011-1

267. Liu Q, Bi C, Li J, et al (2019) Generating Giant Membrane Vesicles from Live Cells with Preserved Cellular Properties. In: Research. https://spj.sciencemag.org/research/2019/6523970 https://doi.org/10.34133/2019/6523970

268. Pae J, Liivamägi L, Lubenets D, et al (2016) Glycosaminoglycans are required for translocation of amphipathic cell-penetrating peptides across membranes. Biochim Biophys Acta BBA - Biomembr 1858:1860–1867. https://doi.org/10.1016/j.bbamem.2016.04.010

269. Zemljič Jokhadar Š, Klančnik U, Grundner M, et al (2018) GPMVs in variable physiological conditions: could they be used for therapy delivery? BMC Biophys 11:1. https://doi.org/10.1186/s13628-017-0041-x

270. Cohen S S, Ushiro H, Chinkers M A Native 170,000 Epidermal Growth Factor Receptor-Kinase Complex from Shed PlasmaMembrane Vesicles. J Biol Chem. 1982 Feb 10;257(3):1523-31

271. Klockenbusch C, Kast J (2010) Optimization of Formaldehyde Cross-Linking for Protein Interaction Analysis of Non-Tagged Integrin β 1. J Biomed Biotechnol 2010:1–13. https://doi.org/10.1155/2010/927585

272. Hobbs GA, Gunawardena HP, Campbell SL (2014) Biophysical and Proteomic Characterization Strategies for Cysteine Modifications in Ras GTPases. Methods Mol Biol Clifton NJ 1120:75–96. https://doi.org/10.1007/978-1-62703-791-4_6

273. Fuhrmann A, Li J, Chien S, Engler AJ (2014) Cation Type Specific Cell Remodeling Regulates Attachment Strength. PLOS ONE 9:e102424. https://doi.org/10.1371/journal.pone.0102424

274. Barros LF, Kanaseki T, Sabirov R, et al (2003) Apoptotic and necrotic blebs in epithelial cells display similar neck diameters but different kinase dependency. Cell Death Differ 10:687–697. https://doi.org/10.1038/sj.cdd.4401236

275. Syed Abdul Rahman SN, Abdul Wahab N, Abd Malek SN (2013) In Vitro Morphological Assessment of Apoptosis Induced by Antiproliferative Constituents from the Rhizomes of Curcuma zedoaria. Evid-Based Complement Altern Med ECAM 2013:257108. https://doi.org/10.1155/2013/257108

276. Alleva K, Chara O, Amodeo G (2012) Aquaporins: Another piece in the osmotic puzzle. FEBS Lett 586:2991–2999. https://doi.org/10.1016/j.febslet.2012.06.013

277. Kakuda S, Suresh P, Li G, London E (2022) Loss of plasma membrane lipid asymmetry can induce ordered domain (raft) formation. J Lipid Res 63:100155. https://doi.org/10.1016/j.jlr.2021.100155

278. Los DA, Murata N (2004) Membrane fluidity and its roles in the perception of environmental signals. Biochim Biophys Acta BBA - Biomembr 1666:142–157. https://doi.org/10.1016/j.bbamem.2004.08.002

279. Fais S, Luciani F, Logozzi M, Parlato S, Lozupone F. (2000) Linkage between cell membrane proteins and actin-based cytoskeleton: the cytoskeletal-driven cellular functions. Histol Histopathol 539–549. https://doi.org/10.14670/HH-15.539

280. Lauster D, Vazquez O, Schwarzer R, et al (2015) Potential of Proapoptotic Peptides to Induce the Formation of Giant Plasma Membrane Vesicles with Lipid Domains. ChemBioChem 16:1288–1292. https://doi.org/10.1002/cbic.201500045

281. Holowka D, Baird B (1983) Structural studies on the membrane-bound immunoglobulin E-receptor complex. 1. Characterization of large plasma membrane vesicles from rat basophilic leukemia cells and insertion of amphipathic fluorescent probes. Biochemistry 22:3466–3474. https://doi.org/10.1021/bi00283a025

282. Krok E, Batura A, Chattopadhyay M, et al (2022) Lateral organization of biomimetic cell membranes in varying pH conditions. J Mol Liq 345:117907. https://doi.org/10.1016/j.molliq.2021.117907

283. Klausner RD, Wolf DE (1980) Selectivity of fluorescent lipid analogues for lipid domains. Biochemistry 19:6199–6203. https://doi.org/10.1021/bi00567a039

284. Mesquita RM, Melo E, Thompson TE, Vaz WL (2000) Partitioning of amphiphiles between coexisting ordered and disordered phases in two-phase lipid bilayer membranes. Biophys J 78:3019–3025

285. Klymchenko AS, Kreder R (2014) Fluorescent probes for lipid rafts: from model membranes to living cells. Chem Biol 21:97–113. https://doi.org/10.1016/j.chembiol.2013.11.009

286. Demchenko AP (2010) The concept of λ-ratiometry in fluorescence sensing and imaging. J Fluoresc 20:1099–1128. https://doi.org/10.1007/s10895-010-0644-y

287. Baumgart T, Hunt G, Farkas ER, et al (2007) Fluorescence probe partitioning between Lo/Ld phases in lipid membranes. Biochim Biophys Acta 1768:2182–2194. https://doi.org/10.1016/j.bbamem.2007.05.012

288. Hutterer R, Parusel ABJ, Hof M (1998) Solvent Relaxation of Prodan and Patman: A Useful Tool for the Determination of Polarity and Rigidity Changes in Membranes. J Fluoresc 8:389–393. https://doi.org/10.1023/A:1020532817530

289. Nieva C, Marro M, Santana-Codina N, Rao S, Petrov D, Sierra A. The lipid phenotype of breast cancer cells characterized by Raman microspectroscopy: towards a stratification of malignancy. PLoS One. 2012;7(10):e46456.

290. Li Z, Cheng S, Lin Q, et al (2021) Single-cell lipidomics with high structural specificity by mass spectrometry. Nat Commun 12:2869. https://doi.org/10.1038/s41467-021-23161-5

291. Jones D, Valli A, Haider S, et al (2018) 3D Growth of Cancer Cells Elicits Sensitivity to Kinase Inhibitors but Not Lipid Metabolism Modifiers. Mol Cancer Ther 18:molcanther.0857.2018. https://doi.org/10.1158/1535-7163.MCT-17-0857

292. Cheng S, Zhang D, Feng J, et al (2023) Metabolic Pathway of Monounsaturated Lipids Revealed by In-Depth Structural Lipidomics by Mass Spectrometry. Research 6:0087. https://doi.org/10.34133/research.0087

293. Robinson MA, Graham DJ, Morrish F, et al (2015) Lipid analysis of eight human breast cancer cell lines with ToF-SIMS. Biointerphases 11:02A303. https://doi.org/10.1116/1.4929633

294. Galbiati F, Razani B, Lisanti MP (2001) Emerging Themes in Lipid Rafts and Caveolae. Cell 106:403–411. https://doi.org/10.1016/S0092-8674(01)00472-X

295. Jay AG, Hamilton JA (2017) Disorder Amidst Membrane Order: Standardizing Laurdan Generalized Polarization and Membrane Fluidity Terms. J Fluoresc 27:243–249. https://doi.org/10.1007/s10895-016-1951-8

296. Pokorna S, Olżyńska A, Jurkiewicz P, Hof M (2013) Hydration and Mobility in Lipid Bilayers Probed by Time-Dependent Fluorescence Shift. In: Mély Y, Duportail G (eds) Fluorescent Methods to Study Biological Membranes. Springer, Berlin, Heidelberg, pp 141–159

297. Barucha-Kraszewska J, Kraszewski S, Ramseyer C (2013) Will C-Laurdan Dethrone Laurdan in Fluorescent Solvent Relaxation Techniques for Lipid Membrane Studies? Langmuir 29:1174–1182. https://doi.org/10.1021/la304235r

298. Danylchuk DI, Sezgin E, Chabert P, Klymchenko AS (2020) Redesigning solvatochromic probe Laurdan for imaging lipid order selectively in cell plasma membranes. Anal Chem 92:14798–14805. https://doi.org/10.1021/acs.analchem.0c03559

299. Krasnowska EK, Gratton E, Parasassi T (1998) Prodan as a Membrane Surface Fluorescence Probe: Partitioning between Water and Phospholipid Phases. Biophys J 74:1984–1993. https://doi.org/10.1016/S0006-3495(98)77905-6

300. Gerstle Z, Desai R, Veatch SL (2018) Giant Plasma Membrane Vesicles: An Experimental Tool for Probing the Effects of Drugs and Other Conditions on Membrane Domain Stability. Methods Enzymol 603:. https://doi.org/10.1016/bs.mie.2018.02.007

301. Sheetz MP, Schindler M, Koppel DE (1980) Lateral mobility of integral membrane proteins is increased in spherocytic erythrocytes. Nature 285:510–512. https://doi.org/10.1038/285510a0

302. Sako Y, Kusumi A. (1995) Barriers for lateral diffusion of transferrin receptor in the plasma membrane as characterized by receptor dragging by laser tweezers: fence versus tether. J Cell Biol 129:1559–1574

303. Kusumi A, Sako Y, Yamamoto M (1993) Confined lateral diffusion of membrane receptors as studied by single particle tracking (nanovid microscopy). Effects of calcium-induced differentiation in cultured epithelial cells. Biophys J 65:2021–2040. https://doi.org/10.1016/S0006-3495(93)81253-0

304. Cui H, Lan X, Lu S, et al (2017) Bioinformatic prediction and functional characterization of human KIAA0100 gene. J Pharm Anal 7:10–18. https://doi.org/10.1016/j.jpha.2016.09.003

305. Huang DW, Sherman BT, Lempicki RA (2009) Bioinformatics enrichment tools: paths toward the comprehensive functional analysis of large gene lists. Nucleic Acids Res 37:1–13. https://doi.org/10.1093/nar/gkn923

306. Al Taweraqi N, King RD (2022) Improved prediction of gene expression through integrating cell signalling models with machine learning. BMC Bioinformatics 23:323. https://doi.org/10.1186/s12859-022-04787-8

307. Palmer PB, O'Connell DG (2009) Regression Analysis for Prediction: Understanding the Process. Cardiopulm Phys Ther J 20:23–26

308. Liu C, Wang W (2017) Contextual Regression: An Accurate and Conveniently Interpretable Nonlinear Model for Mining Discovery from Scientific Data. 210997

309. Ashburner M, Ball CA, Blake JA, et al (2000) Gene Ontology: tool for the unification of biology. Nat Genet 25:25–29. https://doi.org/10.1038/75556

310. Kanehisa M, Goto S (2000) KEGG: Kyoto Encyclopedia of Genes and Genomes. Nucleic Acids Res 28:27–30

311. Medrano G, Guan P, Barlow-Anacker AJ, Gosain A (2017) Comprehensive selection of reference genes for quantitative RT-PCR analysis of murine extramedullary hematopoiesis during development. PloS One 12:e0181881. https://doi.org/10.1371/journal.pone.0181881

312. Pomyen Y, Segura M, Ebbels TMD, Keun HC (2015) Over-representation of correlation analysis (ORCA): a method for identifying associations between variable sets. Bioinformatics 31:102–108. https://doi.org/10.1093/bioinformatics/btu589

313. Wang J, Lei C, Shi P, et al (2021) LncRNA DCST1-AS1 Promotes Endometrial Cancer Progression by Modulating the MiR-665/HOXB5 and MiR-873-5p/CADM1 Pathways. Front Oncol 11:714652. https://doi.org/10.3389/fonc.2021.714652

314. Wu S, Wu F, Jiang Z (2018) Effect of HOXA6 on the proliferation, apoptosis, migration and invasion of colorectal cancer cells. Int J Oncol 52:2093–2100. https://doi.org/10.3892/ijo.2018.4352

315. Fu X, Shi L, Zhang W, et al (2014) Expression of Indian hedgehog is negatively correlated with APC gene mutation in colorectal tumors. Int J Clin Exp Med 7:2150–2155, https://doi.org/10.2147/OTT.S139639

316. Ehata S, Miyazono K (2022) Bone Morphogenetic Protein Signaling in Cancer; Some Topics in the Recent 10 Years. Front Cell Dev Biol 10:883523. https://doi.org/10.3389/fcell.2022.883523

317. Wright TA, Gemmell AO, Tejeda GS, et al (2023) Cancer: Phosphodiesterase type 4C (PDE4C), the forgotten subfamily as a therapeutic target. Int J Biochem Cell Biol 162:106453. https://doi.org/10.1016/j.biocel.2023.106453

318. Yang L, Zheng L, Xie X, et al (2021) Targeting PLA2G16, a lipid metabolism gene, by Ginsenoside Compound K to suppress the malignant progression of colorectal cancer. J Adv Res 36:265–276. https://doi.org/10.1016/j.jare.2021.06.009

319. Yun JW, Yang L, Park H-Y, et al (2020) Dysregulation of cancer genes by recurrent intergenic fusions. Genome Biol 21:166. https://doi.org/10.1186/s13059-020-02076-2

320. Endsley MP, Thill R, Choudhry I, et al (2008) EXPRESSION AND FUNCTION OF FATTY ACID AMIDE HYDROLASE IN PROSTATE CANCER. Int J Cancer J Int Cancer 123:1318–1326. https://doi.org/10.1002/ijc.23674

321. Tsai KK, Huang S-S, Northey JJ, et al (2022) Screening of organoids derived from patients with breast cancer implicates the repressor NCOR2 in cytotoxic stress response and antitumor immunity. Nat Cancer 3:734–752. https://doi.org/10.1038/s43018-022-00375-0

322. HT-29 - HTB-38 | ATCC. https://www.atcc.org/products/htb-38. Accessed 13 Dec 2022

323. Daemen A, Griffith OL, Heiser LM, et al (2013) Modeling precision treatment of breast cancer. Genome Biol 14:R110. https://doi.org/10.1186/gb-2013-14-10-r110

324. Yuan Y, Tan C-W, Shen H, et al (2012) Identification of the biomarkers for the prediction of efficacy in first-line chemotherapy of metastatic colorectal cancer patients using SELDI-TOF-MS and artificial neural networks. Hepatogastroenterology 59:2461–2465. https://doi.org/10.5754/hge12127

325. Dorman SN, Baranova K, Knoll JHM, et al (2016) Genomic signatures for paclitaxel and gemcitabine resistance in breast cancer derived by machine learning. Mol Oncol 10:85–100. https://doi.org/10.1016/j.molonc.2015.07.006

326. Fattahi S, Nikbakhsh N, Ranaei M, et al (2021) Association of sonic hedgehog signaling pathway genes IHH, BOC, RAB23a and MIR195-5p, MIR509-3-5p, MIR6738-3p with gastric cancer stage. Sci Rep 11:7471. https://doi.org/10.1038/s41598-021-86946-0

327. Wu Q, Zhang Y, Chen Q (2001) Indian hedgehog Is an Essential Component of Mechanotransduction Complex to Stimulate Chondrocyte Proliferation *. J Biol Chem 276:35290–35296. https://doi.org/10.1074/jbc.M101055200

328. Xu S, Tang C (2022) Cholesterol and Hedgehog Signaling: Mutual Regulation and Beyond. Front Cell Dev Biol 10: https//doi.org/10.3389/fcell.2022.774291

329. Mahon CS, O'Donoghue AJ, Goetz DH, et al (2009) Characterization of a multimeric, eukaryotic prolyl aminopeptidase: an inducible and highly specific intracellular peptidase from the non-pathogenic fungus Talaromyces emersonii. Microbiology 155:3673–3682. https://doi.org/10.1099/mic.0.030940-0

330. Howell S, Kenny AJ, Turner AJ (1992) A survey of membrane peptidases in two human colonic cell lines, Caco-2 and HT-29. Biochem J 284:595–601

331. Tannert A, Pohl A, Pomorski T, Herrmann A (2003) Protein-mediated transbilayer movement of lipids in eukaryotes and prokaryotes: the relevance of ABC transporters. Int J Antimicrob Agents 22:177–187. https://doi.org/10.1016/s0924-8579(03)00217-6

332. Astrada S, Fernández Massó JR, Vallespí MG, Bollati-Fogolín M (2018) Cell Penetrating Capacity and Internalization Mechanisms Used by the Synthetic Peptide CIGB-552 and Its Relationship with Tumor Cell Line Sensitivity. Molecules 23:801. https://doi.org/10.3390/molecules23040801

333. Nessler S, Friedrich O, Bakouh N, et al (2004) Evidence for activation of endogenous transporters in Xenopus laevis oocytes expressing the Plasmodium

falciparum chloroquine resistance transporter, PfCRT. J Biol Chem 279:39438–39446. https://doi.org/10.1074/jbc.M404671200

334. Sung H, Ferlay J, Siegel RL, et al (2021) Global Cancer Statistics 2020: GLOBOCAN Estimates of Incidence and Mortality Worldwide for 36 Cancers in 185 Countries. CA Cancer J Clin 71:209–249. https://doi.org/10.3322/caac.21660

335. Sanchez-Vega F, Mina M, Armenia J, et al (2018) Oncogenic Signaling Pathways in The Cancer Genome Atlas. Cell 173:321-337.e10. https://doi.org/10.1016/j.cell.2018.03.035

336. Dickens E, Ahmed S (2018) Principles of cancer treatment by chemotherapy. Surg Oxf 36:134–138. https://doi.org/10.1016/j.mpsur.2017.12.002

337. Sun Y, Liu Y, Ma X, Hu H (2021) The Influence of Cell Cycle Regulation on Chemotherapy. Int J Mol Sci 22:6923. https://doi.org/10.3390/ijms22136923

338. Blagosklonny MV (2023) Selective protection of normal cells from chemotherapy, while killing drug-resistant cancer cells. Oncotarget 14:193–206. https://doi.org/10.18632/oncotarget.28382

339. Rao KV, Faso A (2012) Chemotherapy-Induced Nausea and Vomiting: Optimizing Prevention and Management. Am Health Drug Benefits 5:232

340. Debela DT, Muzazu SG, Heraro KD, et al (2021) New approaches and procedures for cancer treatment: Current perspectives. SAGE Open Med 9:20503121211034366. https://doi.org/10.1177/20503121211034366

341. Karami Fath M, Babakhaniyan K, Zokaei M, et al (2022) Anti-cancer peptide-based therapeutic strategies in solid tumors. Cell Mol Biol Lett 27:33. https://doi.org/10.1186/s11658-022-00332-w

342. Felício MR, Silva ON, Gonçalves S, et al (2017) Peptides with Dual Antimicrobial and Anticancer Activities. Front Chem 5:. https://doi.org/10.3389/fchem.2017.00005

343. Huan Y, Kong Q, Mou H, Yi H (2020) Antimicrobial Peptides: Classification, Design, Application and Research Progress in Multiple Fields. Front Microbiol 11: https//doi.org/10.3389/fmicb.2020.58277

344. Rani P, Kapoor B, Gulati M, et al (2022) Antimicrobial peptides: A plausible approach for COVID-19 treatment. Expert Opin Drug Discov 17:473–487. https://doi.org/10.1080/17460441.2022.2050693

345. Jin Y, Hammer J, Pate M, et al (2005) Antimicrobial Activities and Structures of Two Linear Cationic Peptide Families with Various Amphipathic β-Sheet and α-Helical Potentials. Antimicrob Agents Chemother 49:4957–4964. https://doi.org/10.1128/aac.49.12.4957-4964.2005

346. Baltutis V, O'Leary PD, Martin LL (2022) Self-Assembly of Linear, Natural Antimicrobial Peptides: An Evolutionary Perspective. ChemPlusChem 87:e202200240. https://doi.org/10.1002/cplu.202200240

347. Lombard J (2014) Once upon a time the cell membranes: 175 years of cell boundary research. Biol Direct 9:. https://doi.org/10.1186/s13062-014-0032-7

348. Gaus K, Gratton E, Kable EPW, et al (2003) Visualizing lipid structure and raft domains in living cells with two-photon microscopy. Proc Natl Acad Sci 100:15554–15559. https://doi.org/10.1073/pnas.2534386100

349. Levental KR, Levental I (2015) Giant Plasma Membrane Vesicles: Models for Understanding Membrane Organization. In: Current Topics in Membranes. Elsevier, pp 25–57

350. Alvares DS, Wilke N, Ruggiero Neto J, Fanani ML (2017) The insertion of Polybia-MP1 peptide into phospholipid monolayers is regulated by its anionic nature and phase state. Chem Phys Lipids 207:38–48. https://doi.org/10.1016/j.chemphyslip.2017.08.001

351. Lefevre F (1997) Alanine-stretch scanning mutagenesis: a simple and efficient method to probe protein structure and function. Nucleic Acids Res 25:447–448. https://doi.org/10.1093/nar/25.2.447

352. Torres MDT, Pedron CN, Higashikuni Y, et al (2018) Structure-function-guided exploration of the antimicrobial peptide polybia-CP identifies activity determinants and generates synthetic therapeutic candidates. Commun Biol 1:1–16. https://doi.org/10.1038/s42003-018-0224-2

353. Andrews JM (2001) Determination of minimum inhibitory concentrations. J Antimicrob Chemother 48 Suppl 1:5–16. https://doi.org/10.1093/jac/48.suppl_1.5

354. Migoń D, Jaśkiewicz M, Neubauer D, et al (2019) Alanine Scanning Studies of the Antimicrobial Peptide Aurein 1.2. Probiotics Antimicrob Proteins 11:1042–1054. https://doi.org/10.1007/s12602-018-9501-0

355. Zamora-Carreras H, Strandberg E, Mühlhäuser P, et al (2016) Alanine scan and 2H NMR analysis of the membrane-active peptide BP100 point to a distinct carpet mechanism of action. Biochim Biophys Acta BBA - Biomembr 1858:1328–1338. https://doi.org/10.1016/j.bbamem.2016.03.014

356. Sarabipour S, Chan RB, Zhou B, et al (2015) Analytical characterization of plasma membrane-derived vesicles produced via osmotic and chemical vesiculation. Biochim Biophys Acta BBA - Biomembr 1848:1591–1598. https://doi.org/10.1016/j.bbamem.2015.04.002

357. Almeida C, Maniti O, Pisa MD, et al (2019) Cholesterol re-organisation and lipid de-packing by arginine-rich cell penetrating peptides: Role in membrane translocation. PLOS ONE 14:e0210985. https://doi.org/10.1371/journal.pone.0210985

358. Martinez-Hernandez C, Del Carmen Aguilera-Puga M, Plisson F. Deconstructing the Potency and Cell-Line Selectivity of Membranolytic Anticancer Peptides. Chembiochem. 2023 Jul 17;24(14):e202300058. doi: 10.1002/cbic.202300058

359. Nayak C, Singh SK (2022) Integrated Transcriptome Profiling Identifies Prognostic Hub Genes as Therapeutic Targets of Glioblastoma: Evidenced by Bioinformatics Analysis. ACS Omega 7:22531–22550. https://doi.org/10.1021/acsomega.2c01820

360. Duconseil P, Gilabert M, Gayet O, et al (2015) Transcriptomic Analysis Predicts Survival and Sensitivity to Anticancer Drugs of Patients with a Pancreatic Adenocarcinoma. Am J Pathol 185:1022–1032. https://doi.org/10.1016/j.ajpath.2014.11.029

361. Niveditha D, Sharma H, Majumder S, et al (2019) Transcriptomic analysis associated with reversal of cisplatin sensitivity in drug resistant osteosarcoma cells after a drug holiday. BMC Cancer 19:1045. https://doi.org/10.1186/s12885-019-6300-2

362. Yang S-T, Kreutzberger AJB, Kiessling V, et al (2017) HIV virions sense plasma membrane heterogeneity for cell entry. Sci Adv 3:e1700338. https://doi.org/10.1126/sciadv.1700338

363. Dey M, Dhanawat G, Gupta D, et al (2023) Giant Plasma Membrane Vesicles as Cellular-Mimics for Probing SARS-CoV-2 Binding at Single Particle Level. ChemistrySelect 8:e202302608. https://doi.org/10.1002/slct.202302608

364. Schafmeister CE, Po J, Verdine GL (2000) An All-Hydrocarbon Cross-Linking System for Enhancing the Helicity and Metabolic Stability of Peptides. J Am Chem Soc 122:5891–5892. https://doi.org/10.1021/ja000563a

365. Yang M, Liu S, Zhang C (2023) Antimicrobial peptides with antiviral and anticancer properties and their modification and nanodelivery systems. Curr Res Biotechnol 5:100121. https://doi.org/10.1016/j.crbiot.2023.100121

366. Steinkuehler J, Sezgin E, Urbancic I, et al (2019) Mechanical properties of plasma membrane vesicles correlate with lipid order, viscosity and cell density. Commun Biol 2:UNSP 337. https://doi.org/10.1038/s42003-019-0583-3

367. Gray EM, Díaz-Vázquez G, Veatch SL (2015) Growth Conditions and Cell Cycle Phase Modulate Phase Transition Temperatures in RBL-2H3 Derived Plasma Membrane Vesicles. PloS One 10:e0137741. https://doi.org/10.1371/journal.pone.0137741

368. Alter CL, Detampel P, Schefer RB, et al (2023) High efficiency preparation of monodisperse plasma membrane derived extracellular vesicles for therapeutic applications. Commun Biol 6:1–17. https://doi.org/10.1038/s42003-023-04859-2

369. Théry C, Witwer KW, Aikawa E, et al (2018) Minimal information for studies of extracellular vesicles 2018 (MISEV2018): a position statement of the International Society for Extracellular Vesicles and update of the MISEV2014 guidelines. J Extracell Vesicles 7:1535750. https://doi.org/10.1080/20013078.2018.1535750

370. Zachowski A (1993) Phospholipids in animal eukaryotic membranes: transverse asymmetry and movement. Biochem J 294:1–14

371. van Engeland M, Nieland LJ, Ramaekers FC, et al (1998) Annexin V-affinity assay: a review on an apoptosis detection system based on phosphatidylserine exposure. Cytometry 31:1–9. https://doi.org/10.1002/(sici)1097-0320(19980101)31

372. Walrant A, Sachon E (2021) Photolabeling Strategies to Study Membranotropic Peptides Interacting with Lipids and Proteins in Membranes. Bioconjug Chem 32:1503–1514. https://doi.org/10.1021/acs.bioconjchem.1c00291

373. Jiao C-Y, Alves ID, Point V, et al (2010) Comparing lipid photo-cross-linking efficacy of penetratin analogues bearing three different photoprobes: dithienyl ketone, benzophenone, and trifluoromethylaryldiazirine. Bioconjug Chem 21:352–359. https://doi.org/10.1021/bc900466q

374. Chakrabarti P, Khorana G (1975) A new approach to the study of phospholipid-protein interactions in biological membranes. Synthesis of fatty acids and phospholipids containing photosensitive groups. Biochemistry 14:5021–5033. https://doi.org/10.1021/bi00694a001

375. Latorre R, Miller CG, Quay S (1981) Voltage-dependent conductance induced by alamethicin-phospholipid conjugates in lipid bilayers. Biophys J 36:803–809

376. Jo E, Blazyk J, Boggs JM (1998) Insertion of magainin into the lipid bilayer detected using lipid photolabels. Biochemistry 37:13791–13799. https://doi.org/10.1021/bi980855c

377. Brunner J, Richards FM (1980) Analysis of membranes photolabeled with lipid analogues. Reaction of phospholipids containing a disulfide group and a nitrene or carbene precursor with lipids and with gramicidin A. J Biol Chem 255:3319–3329

378. Levental I, Byfield FJ, Chowdhury P, et al (2009) Cholesterol-dependent phase separation in cell-derived giant plasma-membrane vesicles. Biochem J 424:163–167. https://doi.org/10.1042/BJ20091283

Appendix 1

Representative Certificate of Analysis

BIOSYNTHESIS

Post Office Box 28
Lewisville, Texas 75067-0028
800.227.0627 | 972.420.8505 (Intl.)
972.420.0442 (f)
www.biosyn.com

Certificate of Analysis

Peptide Sequence (N-terminus to C-terminus):

[NH2]ADWKKLLDAAKQIL[Amide.HCl]

Peptide Name:	MP1 I1A	**Lot No.:**	**A1274-1**
Client Project No.:	N/A		
Modification(s):	N/A	**Qty:**	8 mg
Additional Instructions(s):	N/A	**Counter-ion:**	Chloride Salt

Quality Control Specifications

Format: White Powder

Mass Spectrometry Analysis: Voyager-DE RP

Calculated Mass: MW = 1611.94

Purity Level Analysis: RP-HPLC

Guaranteed Purity: >95%

Observe Purity: >97%

Amino Acid Analysis: No

Endotoxin Services:

Endotoxin Testing: No

Endotoxin Removal: No

Solubility Test: No

Other Information: No

General Solubility Guidelines

Peptides shorter than 5 residues are usually soluble in water or aqueous buffer, unless the entire sequence consists of hydrophobic amino acids such as W, L, I, F, M, V, Y.

Hydrophilic peptides containing >25% charged residues like D, K, R, H, E and <25% hydrophobic amino acids are usually soluble in water or aqueous buffer.

Hydrophobic peptides containing ≥50% hydrophobic residues may be insoluble or only partly soluble in aqueous solutions. In this case, we recommend using organic solvents like DMSO. In such cases dissolve the peptide in the smallest possible volume of 100% DMSO and subsequently add water/buffer until the desired concentration is achieved. If DMSO interferes with your experimental system, DMF (dimethylformamide) or acetonitrile can serve as alternative solvents.

Peptides containing a very high (>75%) proportion of D, E, H, K, N, Q, R, S, T, Y are capable of building intermolecular hydrogen bonds (cross-linking), thus forming gels in aqueous solutions. These peptides should either be treated according to instructions for hydrophobic peptides (see above) or by changing the pH value if possible.

Note: Peptides containing the amino acids Cys, Met, and Trp are susceptible to oxidation; therefore, oxygen-free solvents should be used.

Handling Storage

All Bio-Synthesis peptides are supplied lyophilized. Peptide containing vial should be tightly capped at all time. Repeated freeze-thaw cycles should be avoided for lyophilized peptides or peptide in solutions.

The lyophilized peptide and peptide solutions should be stored at –20 °C when not in use. For long-term storage (over one year), it is recommended that peptides be stored at –80 °C.

Prepared by: Lan Nguyen **Approved by:** Mousa Bazzaz **Date:** 2/18/2019

Liability Disclaimer: All peptides sold by Bio-Synthesis, Inc. are intended solely for laboratory and research use and should not be used in or on human subjects. User assumes all risk of patent infringement by reason of use of material provided by Bio-Synthesis. Bio-Synthesis will not be responsible for damages arising from misuse of any product and is not responsible for the results of research using our products. For additional information, please contact us at info@biosyn.com

Bio-Synthesis, a provider of reliable and innovative products and services to the Life-Science, Diagnostic and Pharmaceutical community.

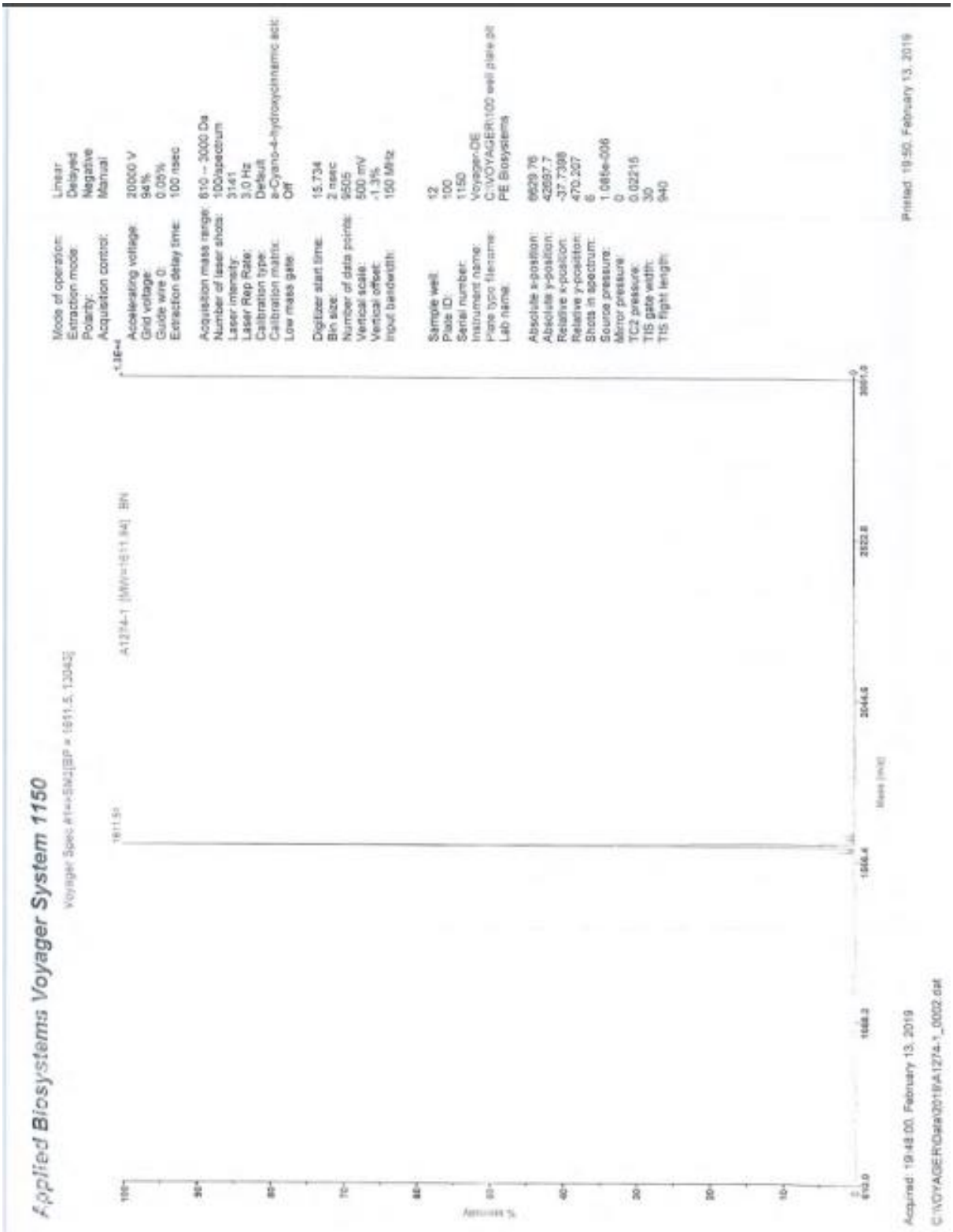
Applied Biosystems Voyager System 1150
Voyager Spec #1=>SM2[BP = 1611.5, 13043]
A1274-1 [MW=1611.84] BN
1611.50
Mode of operation: Linear
Extraction mode: Delayed
Polarity: Negative
Acquisition control: Manual
Accelerating voltage: 20000 V
Grid voltage: 94%
Guide wire 0: 0.05%
Extraction delay time: 100 nsec
Acquisition mass range: 610 – 3000 Da
Number of laser shots: 100/spectrum
Laser intensity: 3141
Laser Rep Rate: 3.0 Hz
Calibration type: Default
Calibration matrix: a-Cyano-4-hydroxycinnamic acid
Low mass gate: Off
Digitizer start time: 15.734
Bin size: 2 nsec
Number of data points: 9505
Vertical scale: 500 mV
Vertical offset: -1.3%
Input bandwidth: 160 MHz
Sample well: 12
Plate ID: 100
Serial number: 1150
Instrument name: Voyager-DE
Plate type filename: C:\VOYAGER\100 well plate.sit
Lab name: PE Biosystems
Absolute x-position: 6629.76
Absolute y-position: 42697.7
Relative x-position: -37.7398
Relative y-position: 470.207
Shots in spectrum: 6
Source pressure: 1.085e-006
Mirror pressure: 0
TC2 pressure: 0.02216
TIS gate width: 30
TIS flight length: 940
Printed: 19:50, February 13, 2019
Acquired: 19:48:00, February 13, 2019
C:\VOYAGER\Data\2019\A1274-1_0002.dat
Mass (m/z)
Abundance %

HPLC REPORT

Sample ID: A1274-1
Method: D:\32Karat\Methods\EMonolithic_2.met
File Name: D:\32Karat\Projects\Default\Data\A1274-1
Column: Monlithic C18, 100x3mm, 120A, Flow Rate: 1ml min.
Wavelength: 220nm
HPLC ID# CD-070/EQ-023

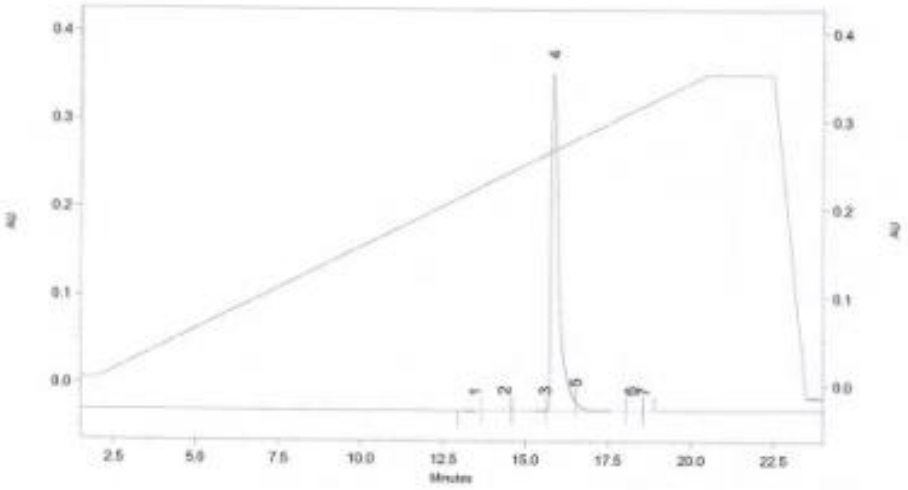

Pk #	Retention Time	Area	Area Percent
1	13.483	1069	0.017
2	14.383	3415	0.054
3	15.600	8372	0.133
4	15.867	6146508	97.938
5	16.550	113576	1.810
6	18.233	2580	0.041
7	18.600	427	0.007
Totals		6275947	100.000

Appendix 2

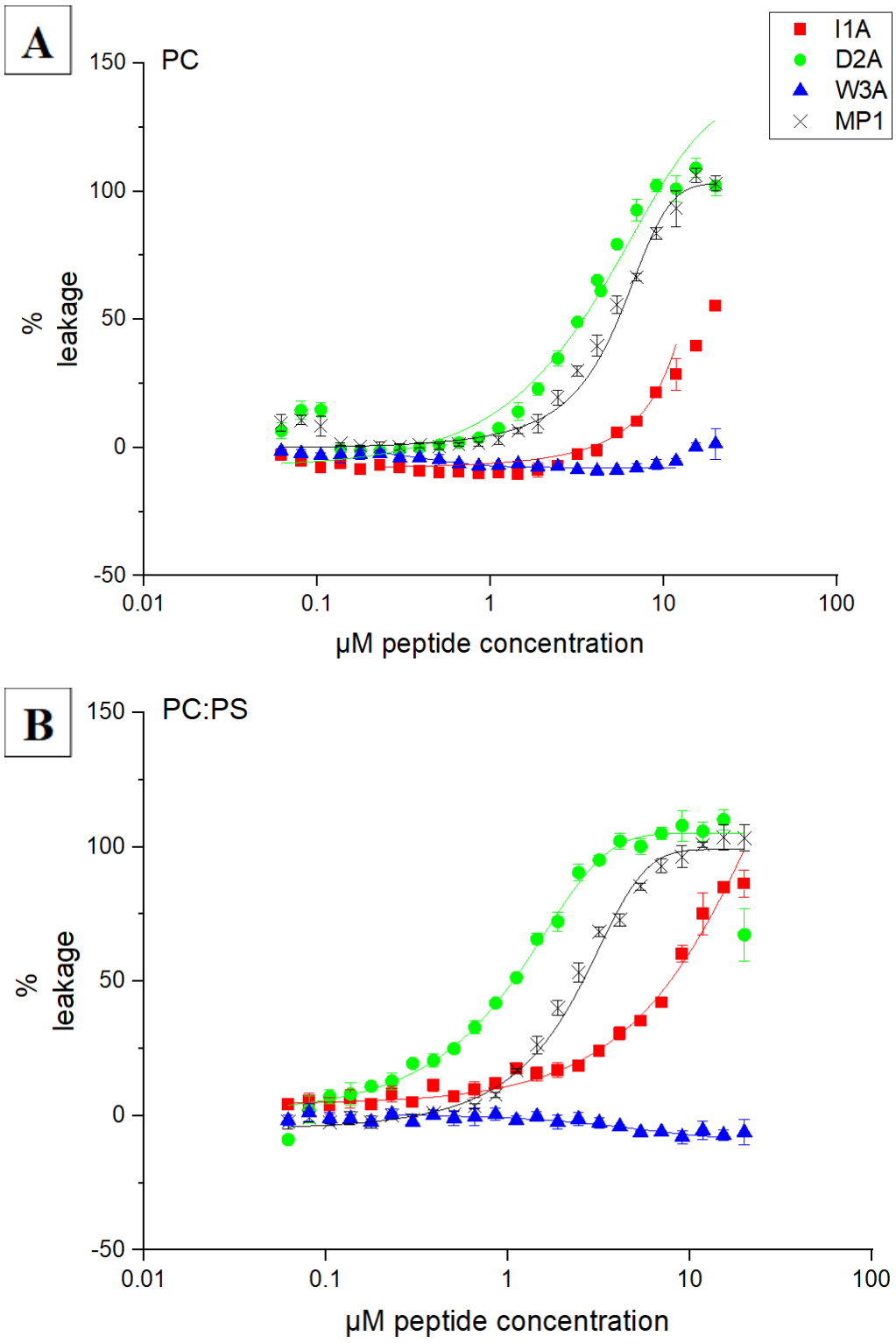

Figure 57 Raw leakage assay data. I1A, D2A and W3A mutants along with MP1 were tested in PC (A) and PC:PS (B) lipid systems. Peptide concentration is shown along the X-axis, the percentage of dye leakage of each peptide is represented on the Y-axis. The curve fitting was conducted with an exponential growth function which indicates that after the initial lag phase, the fluorescence intensity increases at an exponential rate and slows down to eventually reach a plateau. Error bars represent ±SEM from three replicate measurements.

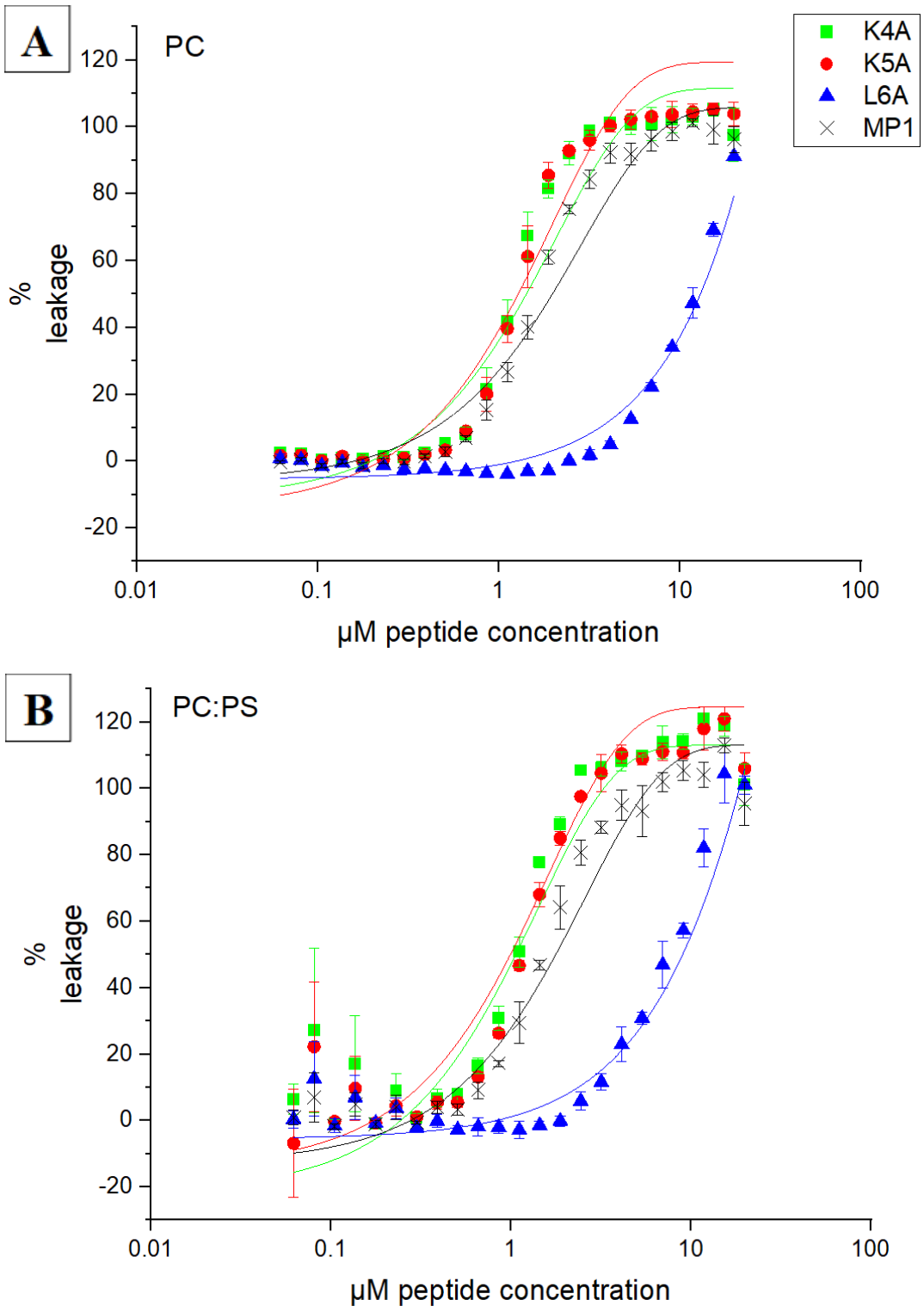

Figure 58 Raw leakage assay data. K4A, K5A and L6A mutants along with MP1 were tested in PC (A) and PC:PS (B) lipid systems. Peptide concentration is shown along the X-axis, the percentage of dye leakage of each peptide is represented on the Y-axis. The curve fitting was conducted with an exponential growth function which indicates that after the initial lag phase, the fluorescence intensity increases at an exponential rate and slows down to eventually reach a plateau. Error bars represent ±SEM from three replicate measurements.

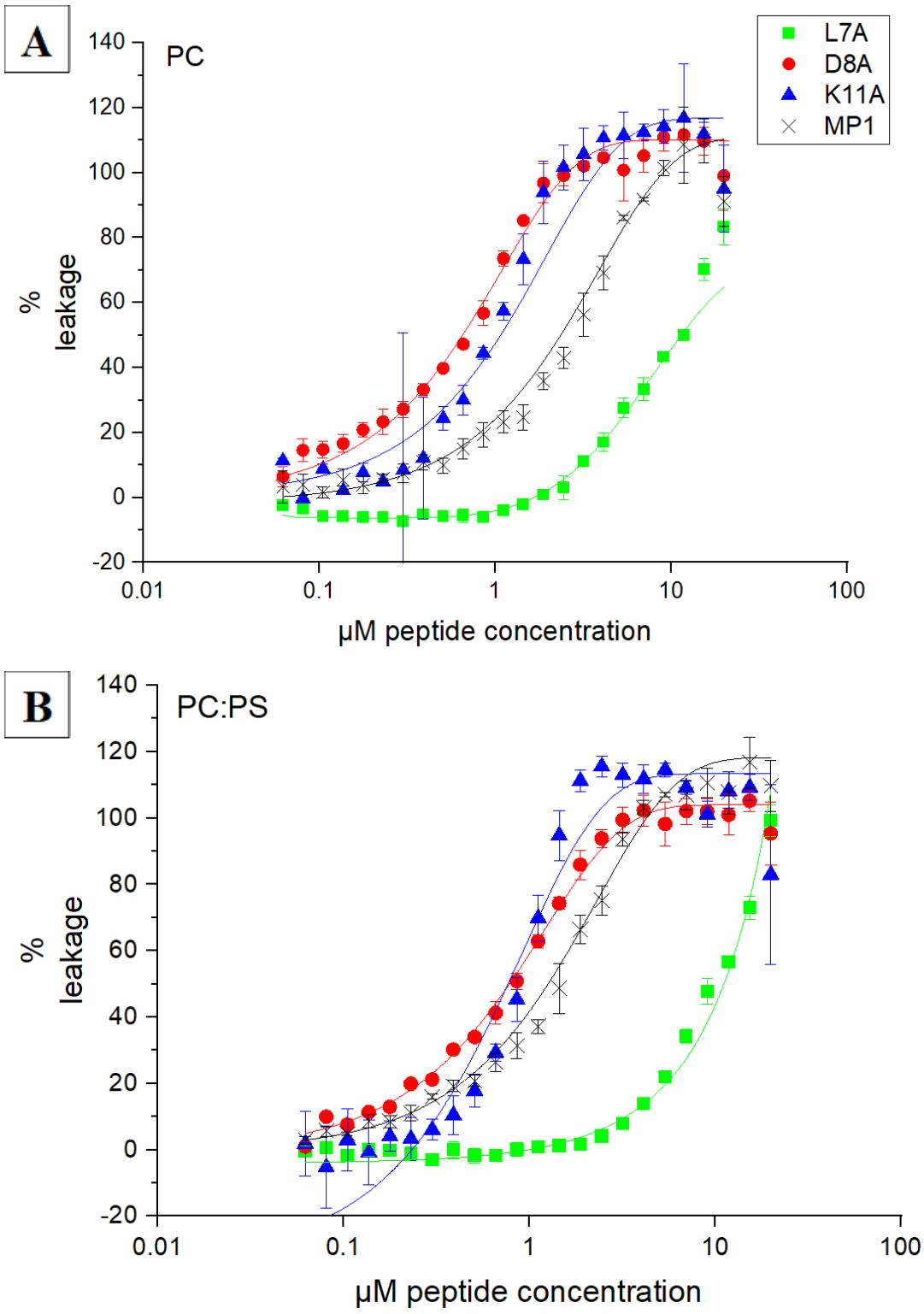

Figure 59 Raw leakage assay data. L7A, D8A and K11A mutants along with MP1 were tested in PC (A) and PC:PS (B) lipid systems. Peptide concentration is shown along the X-axis, the percentage of dye leakage of each peptide is represented on the Y-axis. The curve fitting was conducted with an exponential growth function which indicates that after the initial lag phase, the fluorescence intensity increases at an exponential rate and slows down to eventually reach a plateau. Error bars represent ±SEM from three replicate measurements.

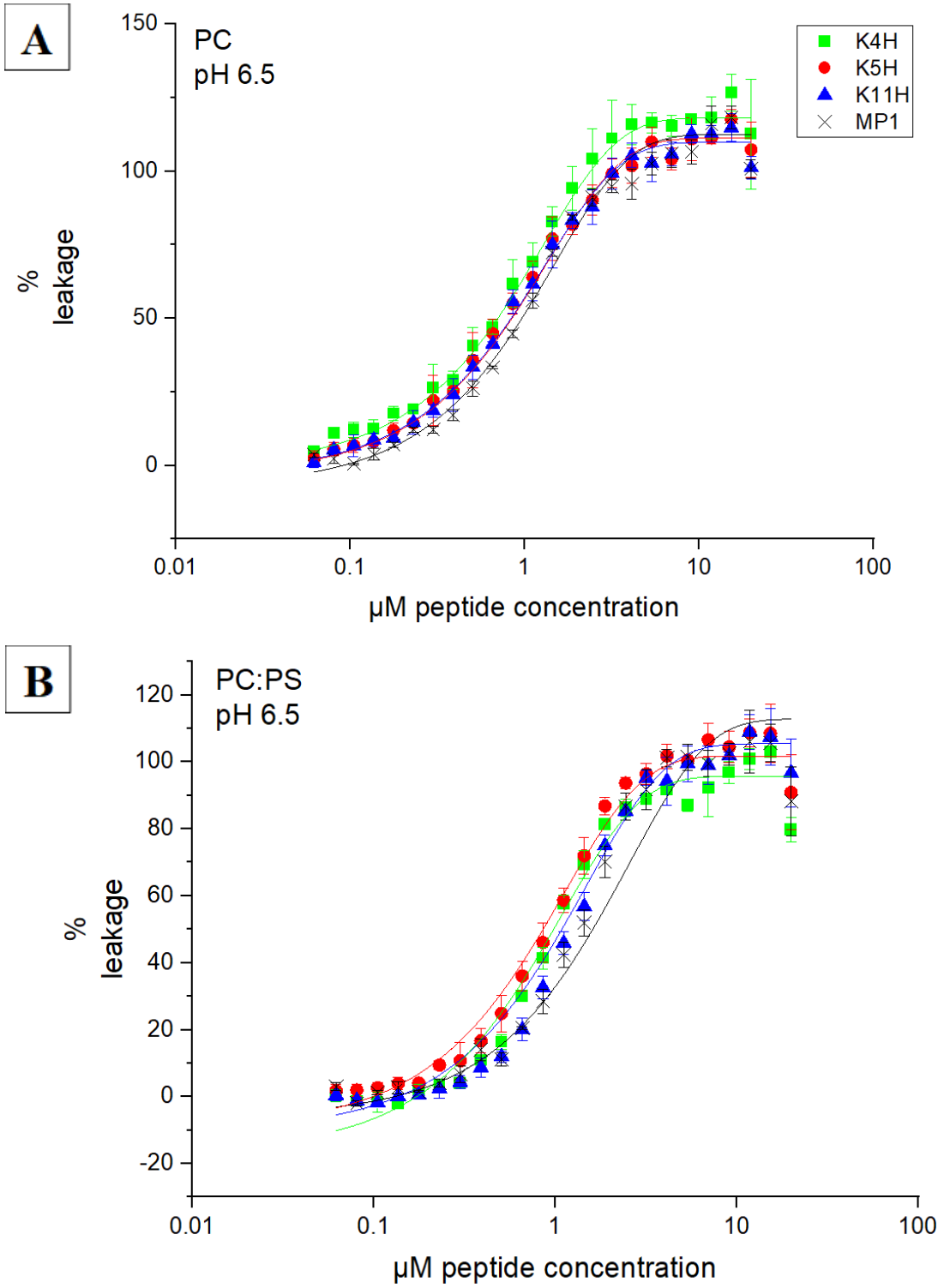

Figure 4 Raw leakage assay data. K4H, K5H and K11H mutants along with MP1 were tested in PC (A) and PC:PS (B) lipid systems at pH 6.5. Peptide concentration is shown along the X-axis, the percentage of dye leakage of each peptide is represented on the Y-axis. The curve fitting was conducted with an exponential growth function which indicates that after the initial lag phase, the fluorescence intensity increases at an exponential rate and slows down to eventually reach a plateau. Error bars represent ±SEM from three replicate measurements.

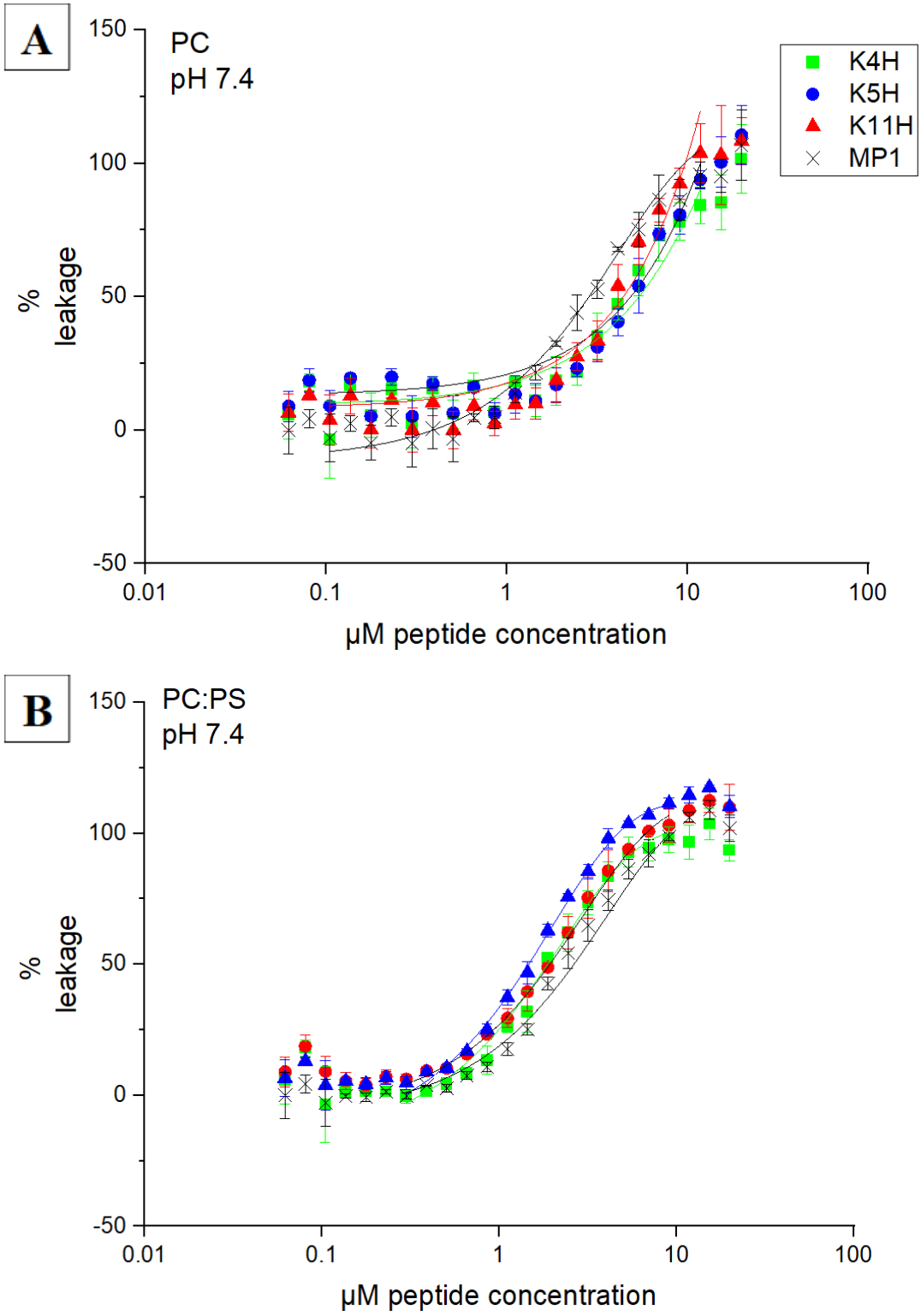

Figure 5 Raw leakage assay data. K4H, K5H and K11H mutants along with MP1 were tested in PC (A) and PC:PS (B) lipid systems at pH 7.4. Peptide concentration is shown along the X-axis, the percentage of dye leakage of each peptide is represented on the Y-axis. The curve fitting was conducted with an exponential growth function which indicates that after the initial lag phase, the fluorescence intensity increases at an exponential rate and slows down to eventually reach a plateau. Error bars represent ±SEM from three replicate measurements.

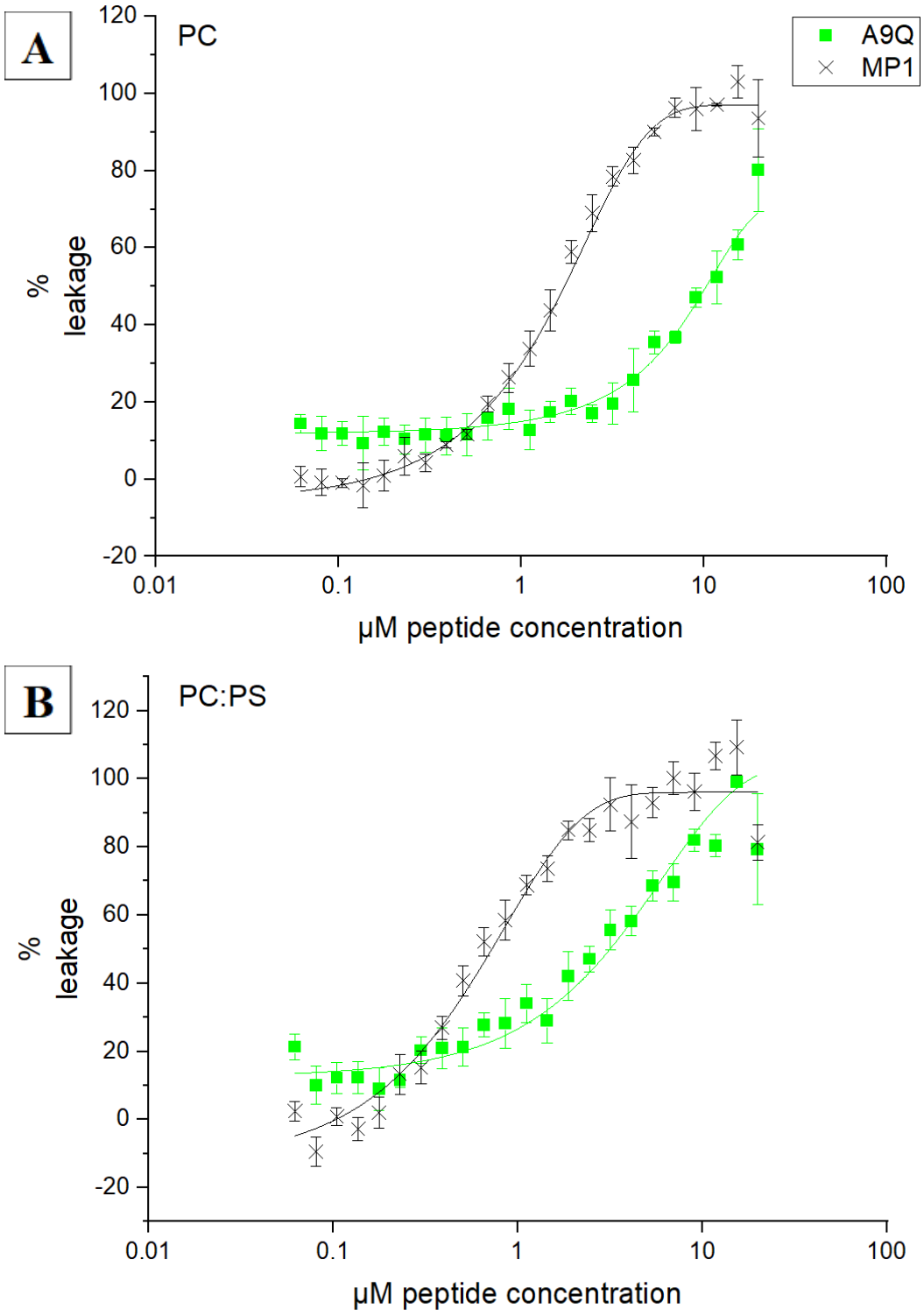

Figure 6 Raw leakage assay data. A9Q mutants along with MP1 were tested in PC (A) and PC:PS (B) lipid systems. Peptide concentration is shown along the X-axis, the percentage of dye leakage of each peptide is represented on the Y-axis. The curve fitting was conducted with an exponential growth function which indicates that after the initial lag phase, the fluorescence intensity increases at an exponential rate and slows down to eventually reach a plateau. Error bars represent ±SEM from three replicate measurements.

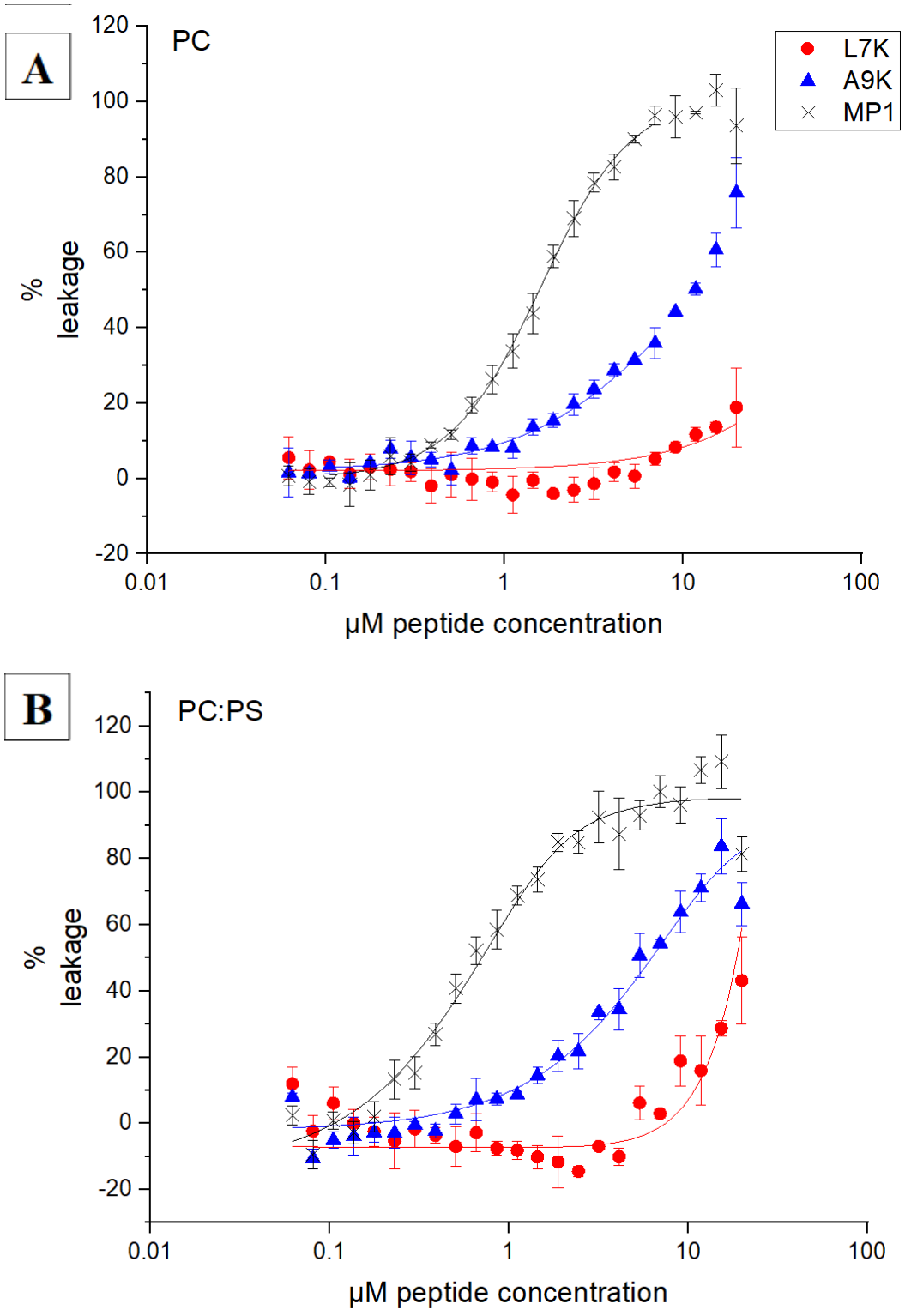

Figure 7 Raw leakage assay data. L7K and A9K mutants along with MP1 were tested in PC (A) and PC:PS (B) lipid systems. Peptide concentration is shown along the X-axis, the percentage of dye leakage of each peptide is represented on the Y-axis. The curve fitting was conducted with an exponential growth function which indicates that after the initial lag phase, the fluorescence intensity increases at an exponential rate and slows down to eventually reach a plateau. Error bars represent ±SEM from three replicate measurements.

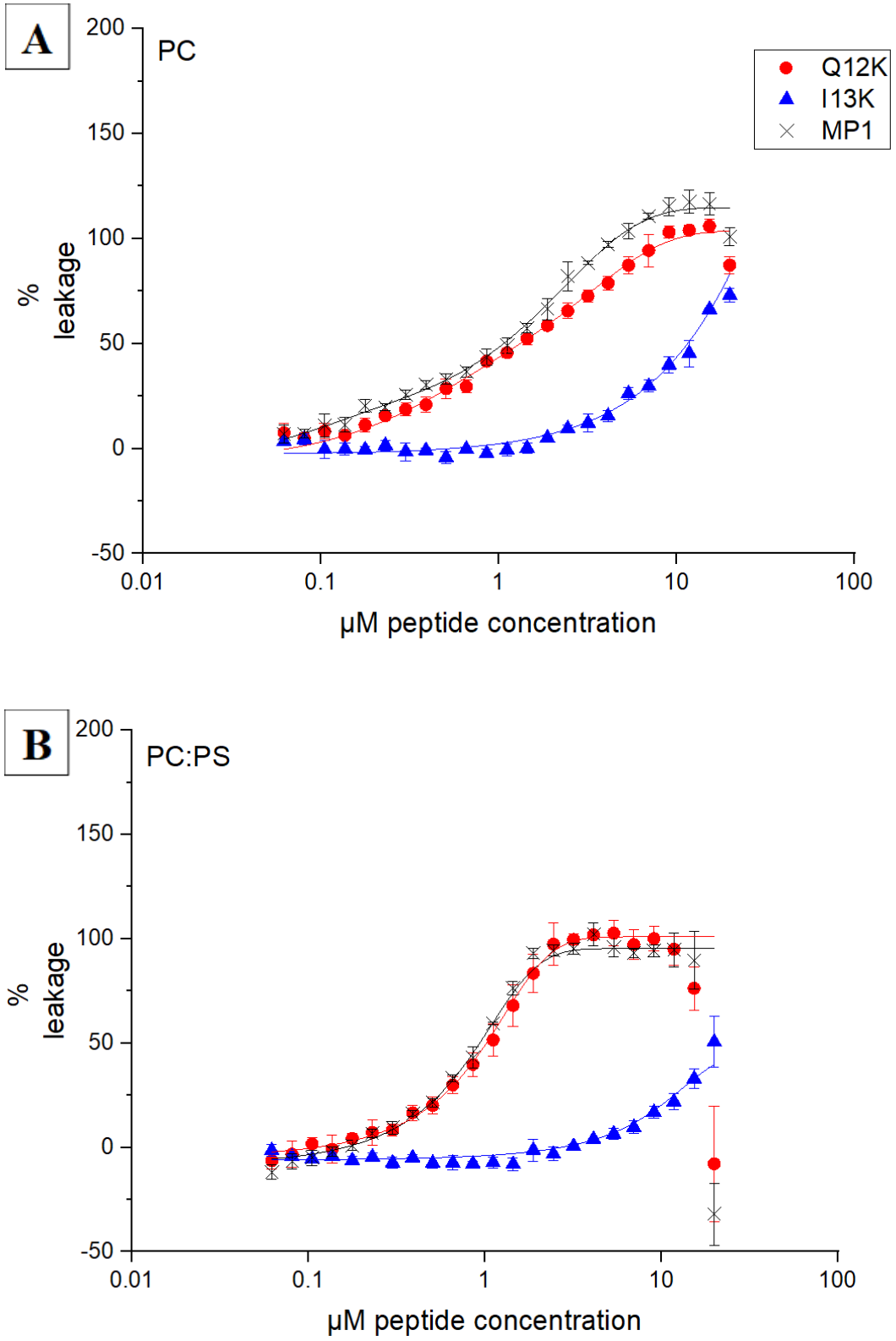

Figure 8 Raw leakage assay data. Q12K and I13K mutants along with MP1 were tested in PC (A) and PC:PS (B) lipid systems. Peptide concentration is shown along the X-axis, the percentage of dye leakage of each peptide is represented on the Y-axis. The curve fitting was conducted with an exponential growth function which indicates that after the initial lag phase, the fluorescence intensity increases at an exponential rate and slows down to eventually reach a plateau. Error bars represent ±SEM from three replicate measurements.

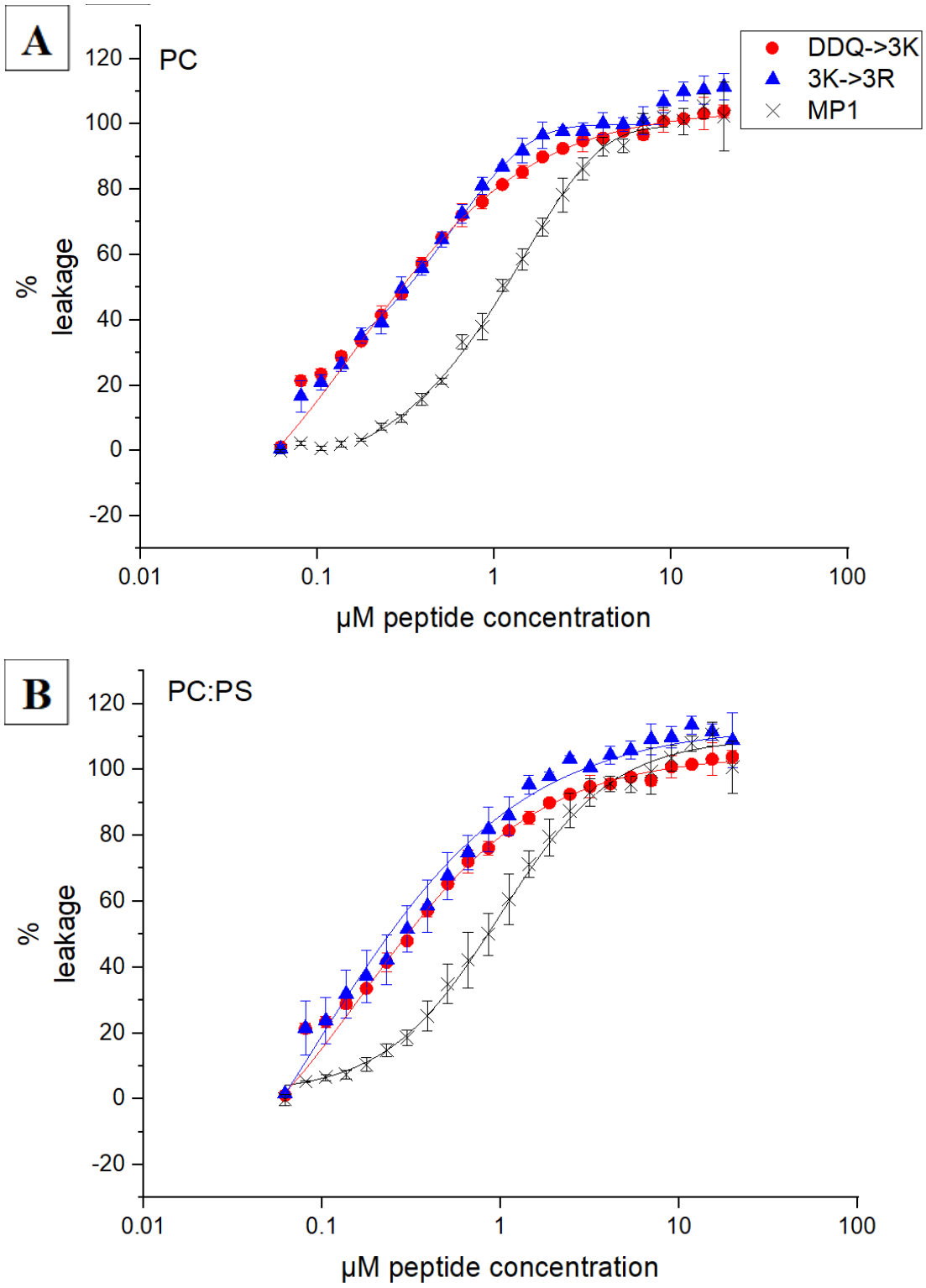

Figure 9 Raw leakage assay data. DDQ->3K and 3K->3R mutants along with MP1 were tested in PC (A) and PC:PS (B) lipid systems. Peptide concentration is shown along the X-axis, the percentage of dye leakage of each peptide is represented on the Y-axis. The curve fitting was conducted with an exponential growth function which indicates that after the initial lag phase, the fluorescence intensity increases at an exponential rate and slows down to eventually reach a plateau. Error bars represent ±SEM from three replicate measurements.

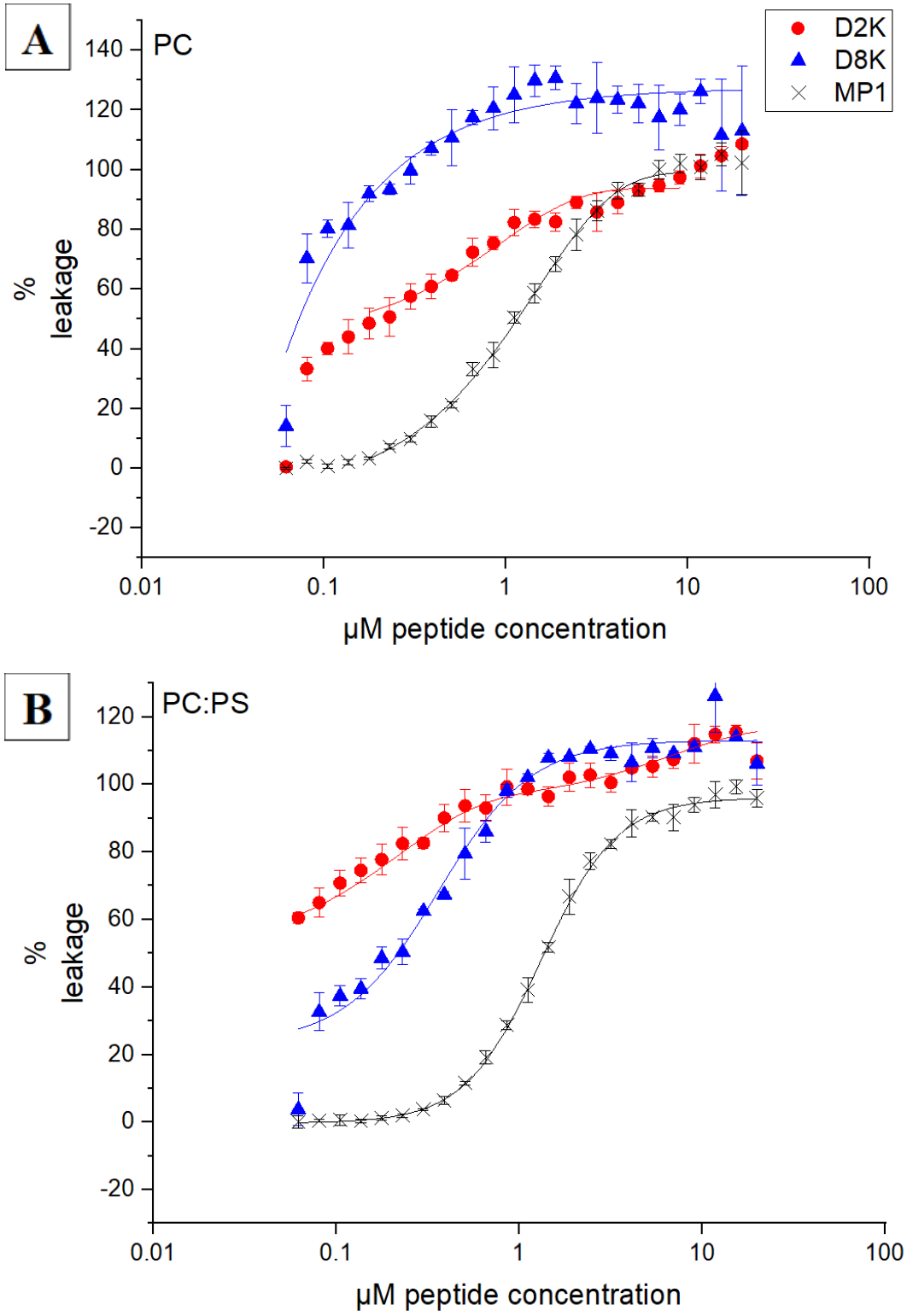

Figure 10 Raw leakage assay data. D2K and D8K mutants along with MP1 were tested in PC (A) and PC:PS (B) lipid systems. Peptide concentration is shown along the X-axis, the percentage of dye leakage of each peptide is represented on the Y-axis. The curve fitting was conducted with an exponential growth function which indicates that after the initial lag phase, the fluorescence intensity increases at an exponential rate and slows down to eventually reach a plateau. Error bars represent ±SEM from three replicate measurements.

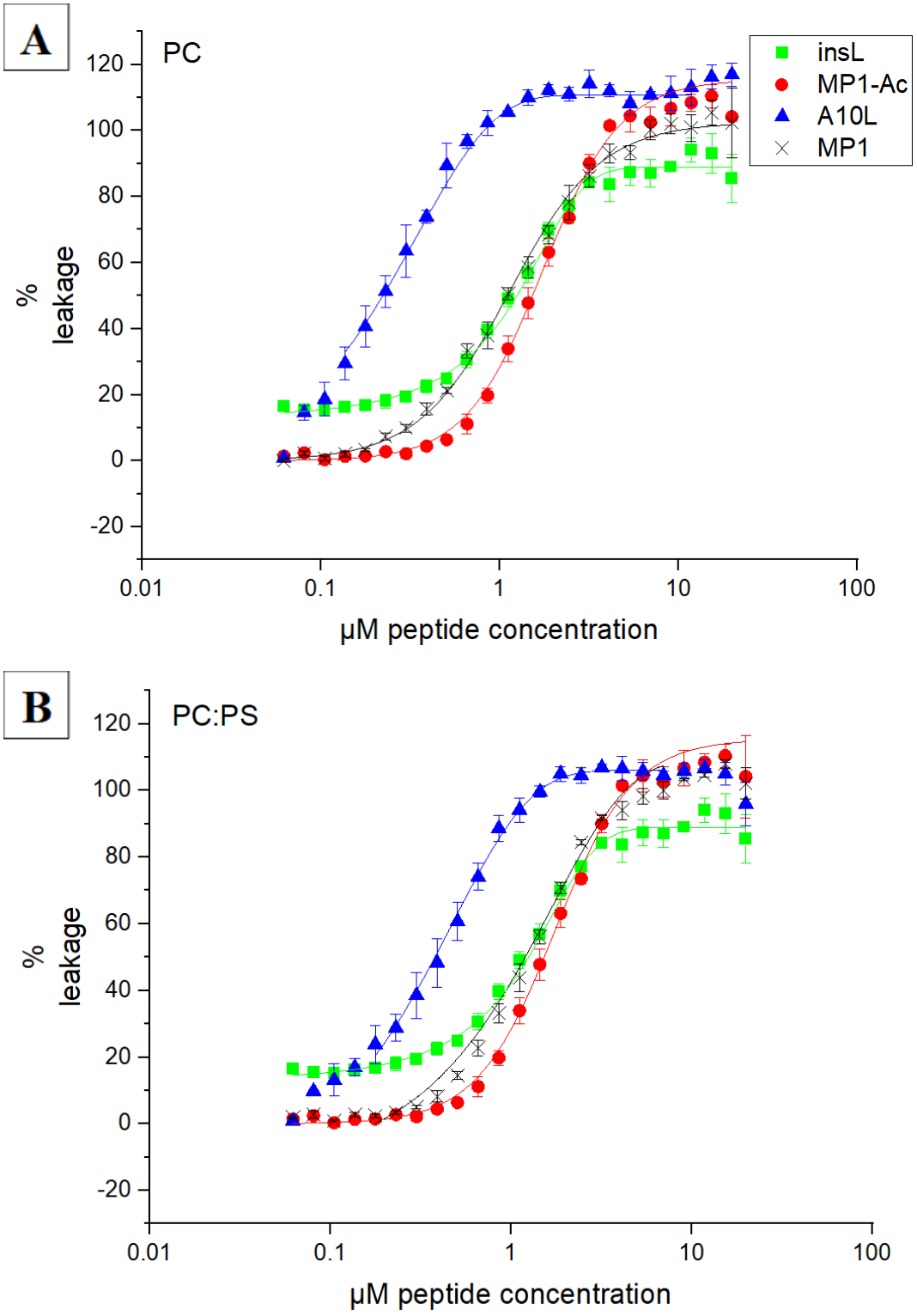

Figure 11 Raw leakage assay data insL, MP1-Ac and A10L mutants along with MP1 were tested in PC (A) and PC:PS (B) lipid systems. Peptide concentration is shown along the X-axis, the percentage of dye leakage of each peptide is represented on the Y-axis. The curve fitting was conducted with an exponential growth function which indicates that after the initial lag phase, the fluorescence intensity increases at an exponential rate and slows down to eventually reach a plateau. Error bars represent ±SEM from three replicate measurements.

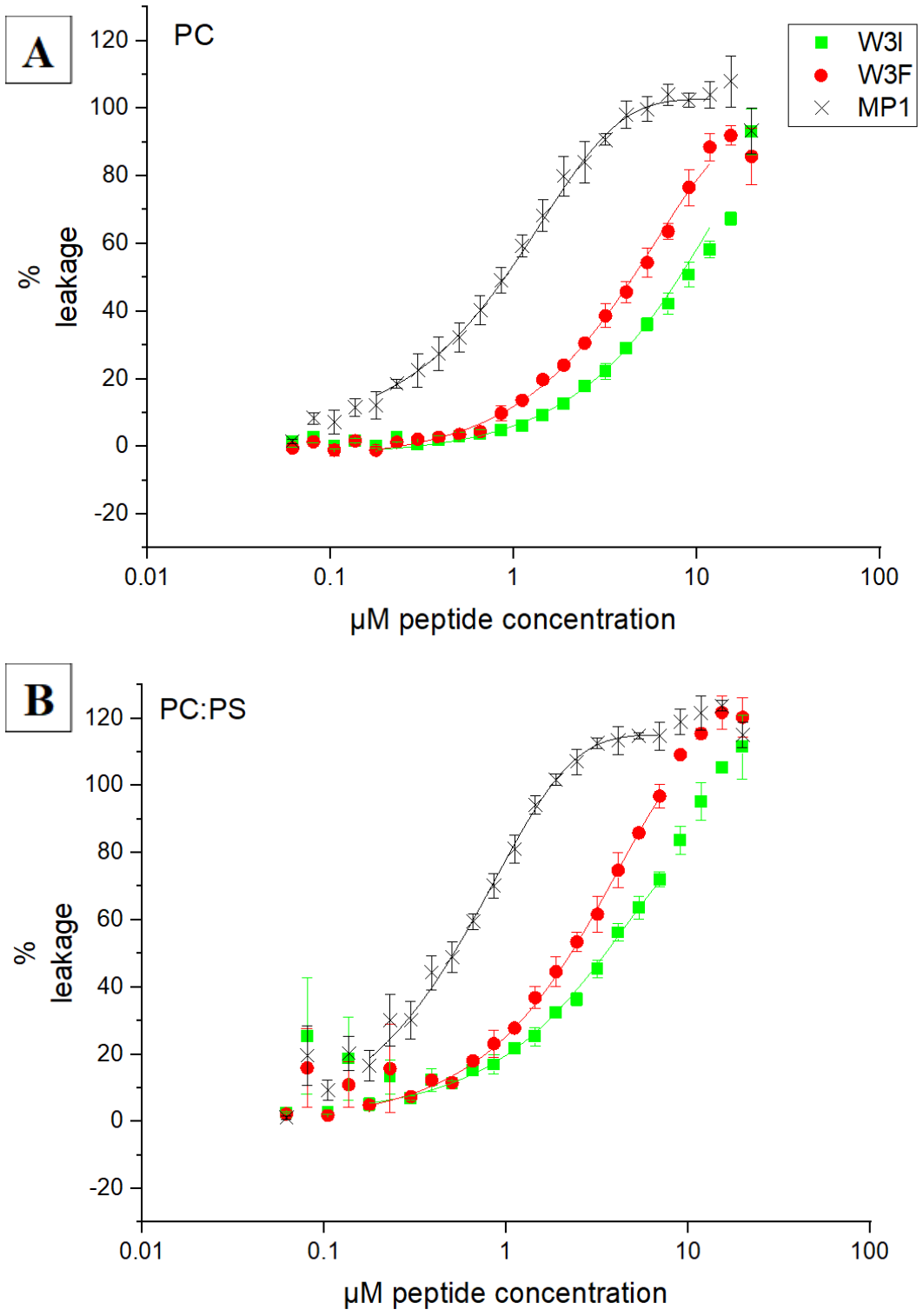

Figure 12 Raw leakage assay data. W3I and W3F mutants along with MP1 were tested in PC (A) and PC:PS (B) lipid systems. Peptide concentration is shown along the X-axis, the percentage of dye leakage of each peptide is represented on the Y-axis. The curve fitting was conducted with an exponential growth function which indicates that after the initial lag phase, the fluorescence intensity increases at an exponential rate and slows down to eventually reach a plateau. Error bars represent ±SEM from three replicate measurements.

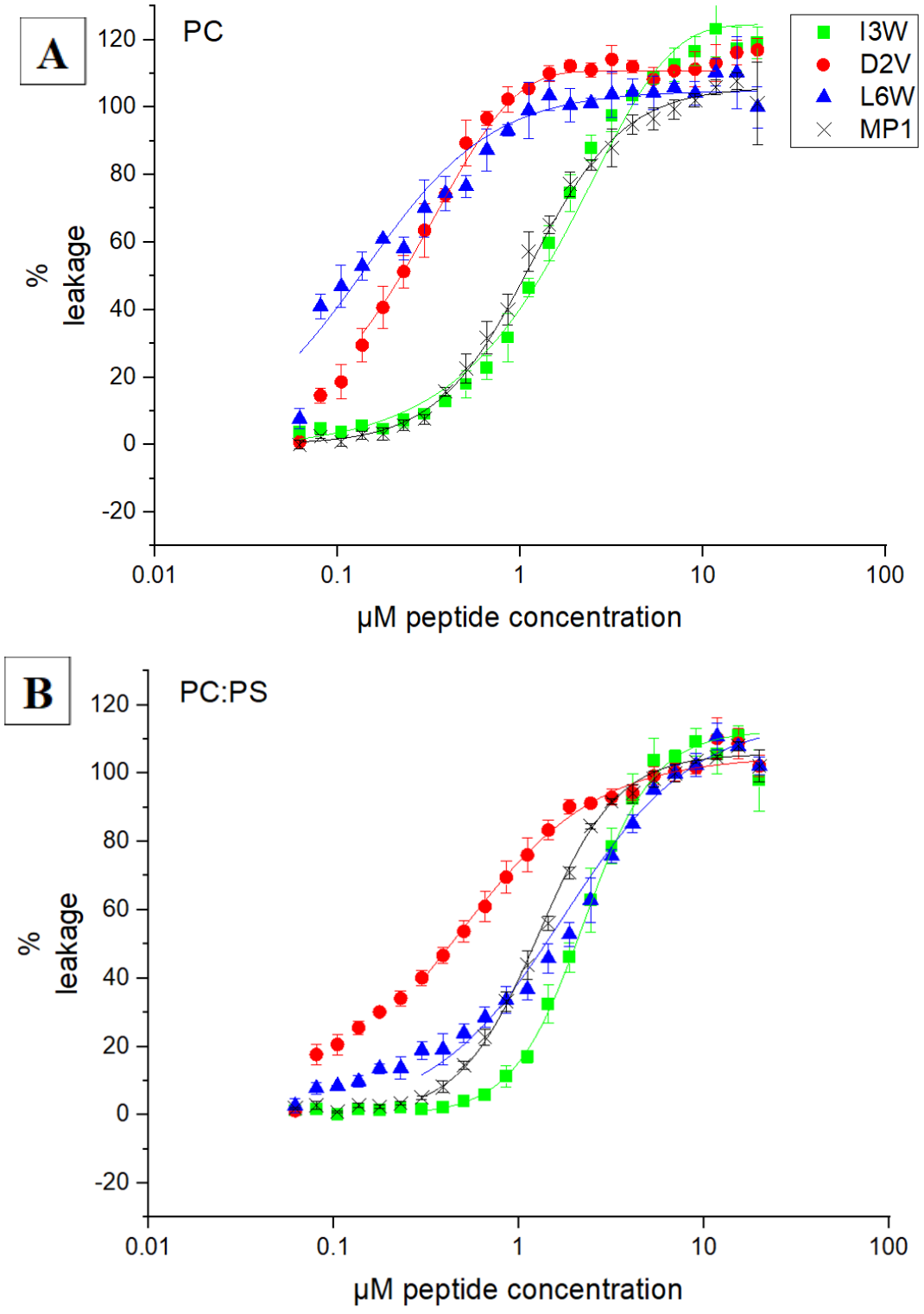

Figure 13 Raw leakage assay data. I3W, D2V and L6W mutants along with MP1 were tested in PC (A) and PC:PS (B) lipid systems. Peptide concentration is shown along the X-axis, the percentage of dye leakage of each peptide is represented on the Y-axis. The curve fitting was conducted with an exponential growth function which indicates that after the initial lag phase, the fluorescence intensity increases at an exponential rate and slows down to eventually reach a plateau. Error bars represent ±SEM from three replicate measurements.

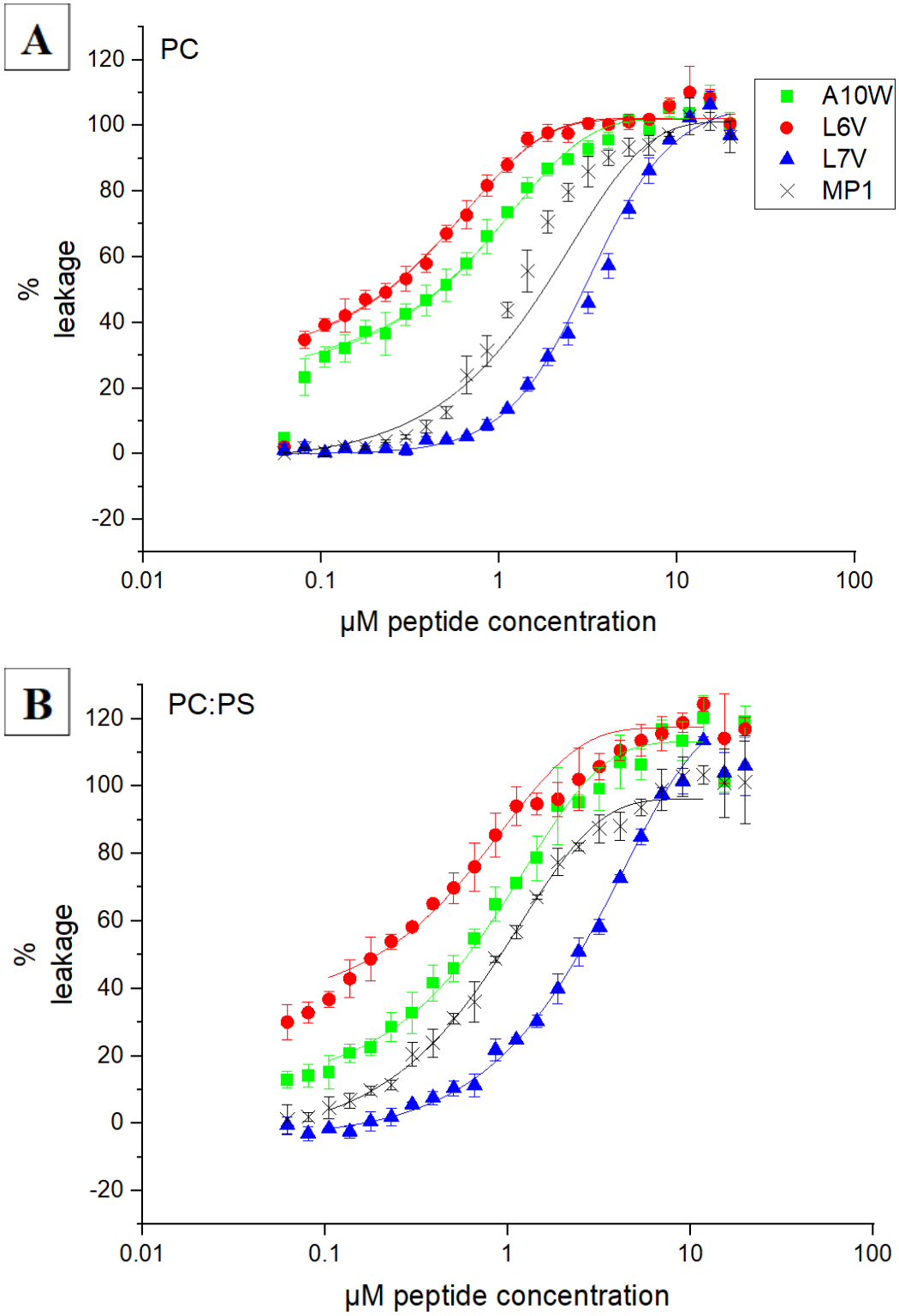

Figure 14 Raw leakage assay data. A10W, L6V and L7W mutants along with MP1 were tested in PC (A) and PC:PS (B) lipid systems. Peptide concentration is shown along the X-axis, the percentage of dye leakage of each peptide is represented on the Y-axis. The curve fitting was conducted with an exponential growth function which indicates that after the initial lag phase, the fluorescence intensity increases at an exponential rate and slows down to eventually reach a plateau. Error bars represent ±SEM from three replicate measurements.

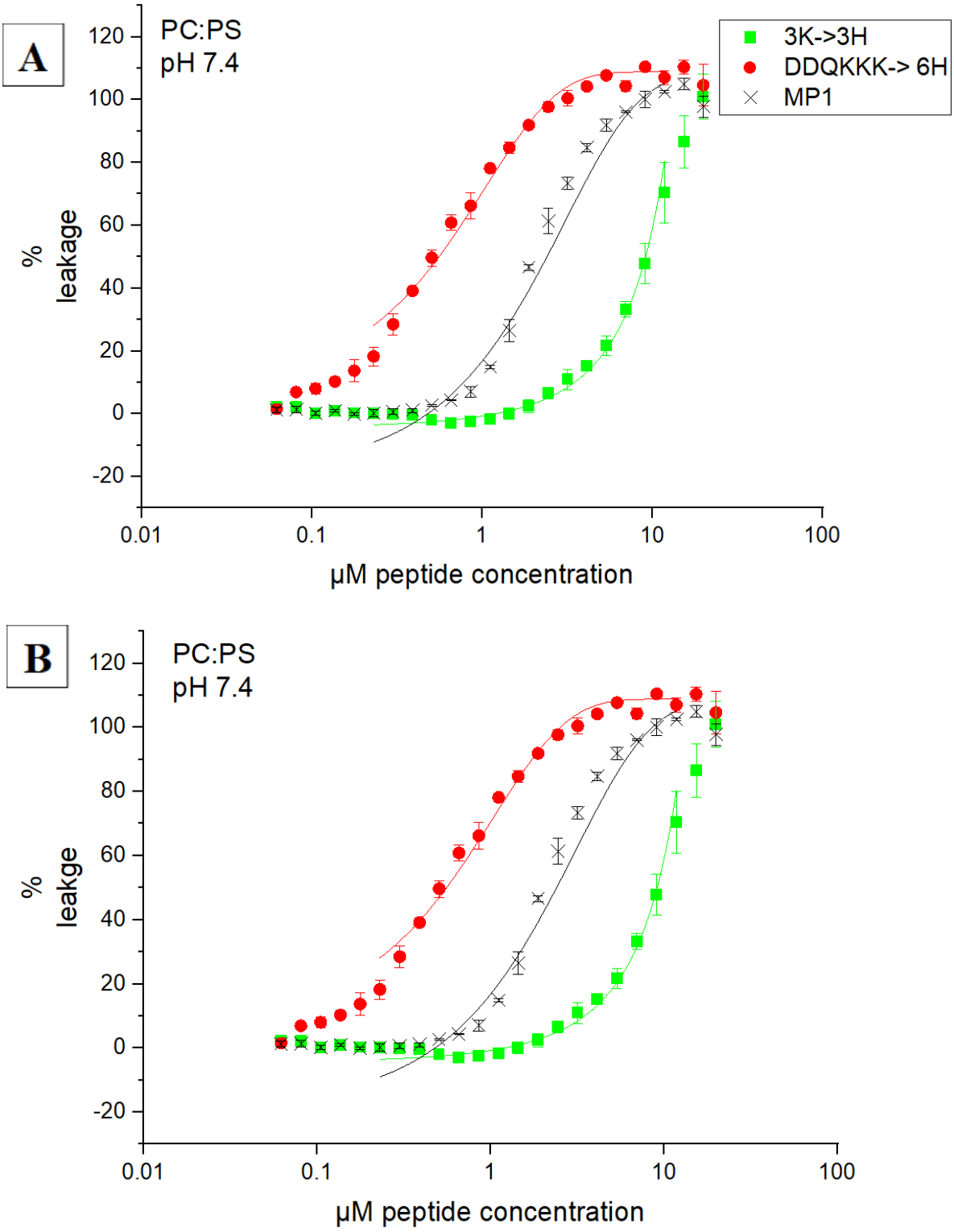

Figure 15 Raw leakage assay data. 3K->3H and DDQKKK->6H mutants along with MP1 were tested in PC (A) and PC:PS (B) lipid systems at pH 7.4. Peptide concentration is shown along the X-axis, the percentage of dye leakage of each peptide is represented on the Y-axis. The curve fitting was conducted with an exponential growth function which indicates that after the initial lag phase, the fluorescence intensity increases at an exponential rate and slows down to eventually reach a plateau. Error bars represent ±SEM from three replicate measurements.

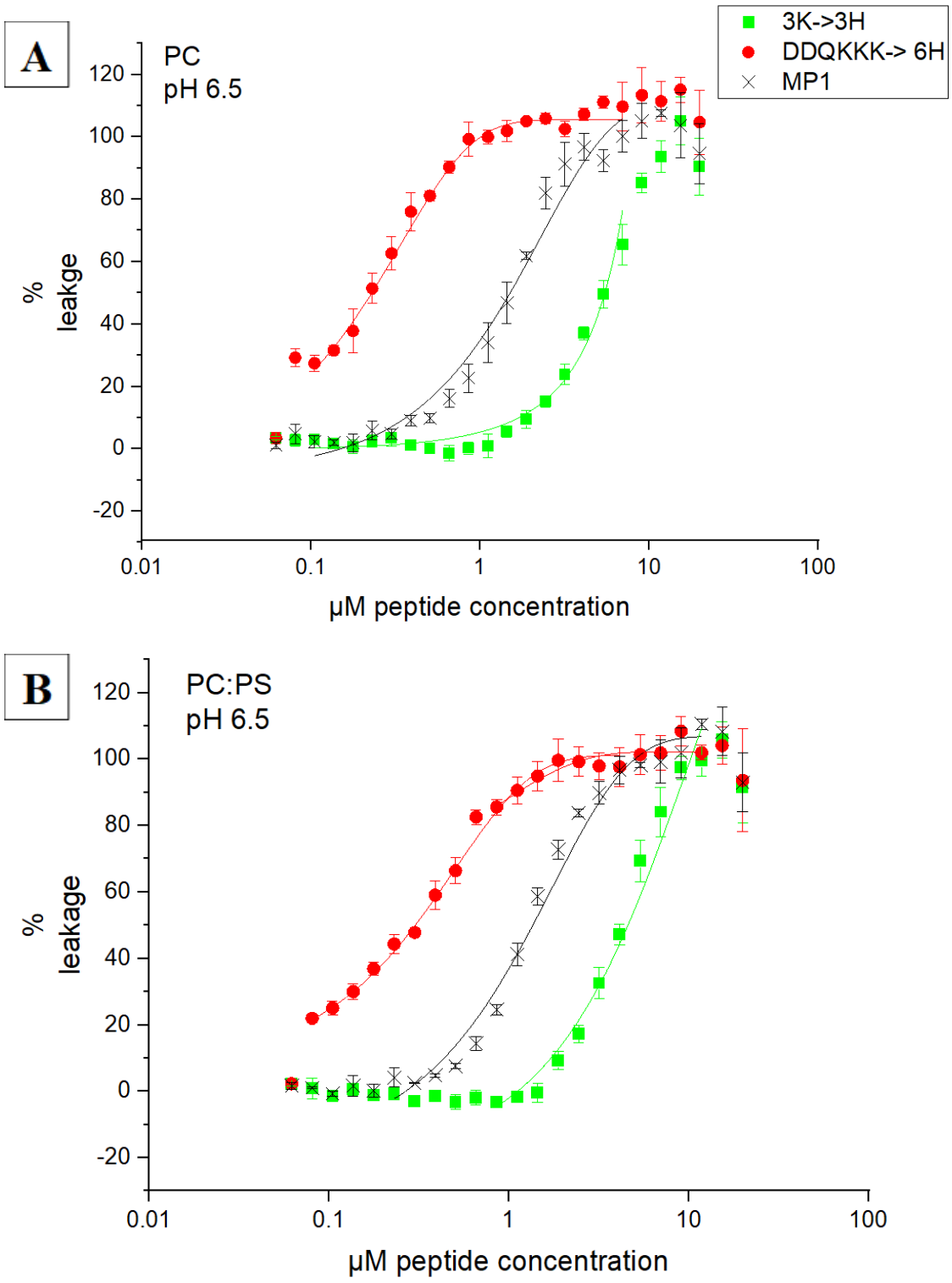

Figure 16 Raw leakage assay data. 3K->3H and DDQKKK->6H mutants along with MP1 were tested in PC (A) and PC:PS (B) lipid systems at pH 6.5. Peptide concentration is shown along the X-axis, the percentage of dye leakage of each peptide is represented on the Y-axis. The curve fitting was conducted with an exponential growth function which indicates that after the initial lag phase, the fluorescence intensity increases at an exponential rate and slows down to eventually reach a plateau. Error bars represent ±SEM from three replicate measurements.